Development of a Novel Single-Phase Auto-Reclosing Scheme for Distribution Network with Integrated Distributed Generation

TAN SOCK FUA

The thesis is submitted in partial fulfillment of the
requirement of
The Robert Gordon University
for the degree of Doctor of Philosophy

June 2010

Abstract

According to G59 recommendation, the common practice adopted by utilities in the UK is to disconnect Distributed generators (DGs) immediately once a network fault is detected to prevent islanding operation and disruption of the operation of conventional auto-reclosing schemes. However, with the continuous increase of penetration of DGs into existing distribution networks, it is becoming increasingly important that DGs must support power networks during steady-state and fault conditions. It has been recognised that 80% of faults in distribution networks are temporary and most of them are single-line-to-ground (SLG) faults. This should give a strong incentive to find ways for maintaining DGs in service during temporary SLG faults as far as possible which would benefit utilities, DG developers and customers. The literature survey shows that no research work has been carried out to investigate a fault identification and phase selection algorithm suitable to be used in a novel single-phase auto-reclosing (SPAR) scheme, specifically suitable to distribution networks with DGs, for maintaining the continued operation of DGs during fault conditions.

The work in this PhD has focused on investigating feeder protection requirements for continued operation of DGs in radial and ring overhead distribution networks with DGs, particularly the new requirements for operating an auto-reclosing scheme in networks with DGs. Simulation results obtained from this investigation have revealed that it is a possible to maintain continued operation of DGs that are based on DFIG and FSIG during temporary SLG faults in radial and ring operated networks. This is followed by investigating the development of an adaptive fault identification and phase selection algorithm suitable for a SPAR scheme in a power system with DGs. The proposed fault identification and phase selection algorithm uses only the three line currents measured at the relay point. The waveform pattern of phase angle and symmetrical components of the three line currents during the transient period following a fault condition is analysed using IF-THEN condition-based rules in order to determine the type of SLG fault. The verification test results have revealed that the proposed method can correctly detect the faulty phase within one cycle in a distribution network with DGs under various network operating and fault conditions. The work in this PhD has resulted in publication of papers (see Appendix I).

Acknowledgements

This research project has been carried out at The School of Engineering, The Robert Gordon University. I would like to thank The Robert Gordon University for providing facilities and financial support to undertake this research project

I owe my deepest gratitude to my PhD supervisor Prof. S. K. Salman, for his consistent encouragement, skilled supervision and guidance, invaluable comments during this research project.

I would to make a special reference to Mr. Chan Y.S for useful discussion the course of software developments.

I am heartily thankful to my husband, my mother, my sister and Mr. David MacPherson and family for their love and support.

Lastly, I offer my regards and blessings to Mr. Martin Simpson from The Robert Gordon University and those who supported me in any respect during the completion of this research project.

SockFua Tan
Aberdeen, June 2010.

Contents

Figures

List of Tables

List of Abbreviation

ANN	artificial neural network
ARC	automatic recloser
CCT	critical clearing time
CHP	combined heat and power
CSG	conventional synchronous generator
DC	direct current
DFIG	doubly-fed induction generator
DG	distributed generation
DLG	double-line-to-ground
EG	embedded generation
FFT	Fast Fourier Transform
FSIG	fixed speed induction generator
GSC	grid side power converter
GUI	graphical user interface
HV	high voltage
IG	Induction generator
KV	kilo voltage
LL	line-line
LOM	Loss of mains
LV	low voltage
MLP	multilayer perceptron
MV	medium voltage
PFFC	power frequency fault components
PV	photo-voltaic
PWM	pulse width modulated
ROCOF	rate of change of frequency
RSC	rotor side power converter
RMU	ring main unit
SG	synchronous generator
SLG	single-line-to-ground
SMMG	series multiresolution morphological gradient
SPAR	single-phase auto-reclosing
TCC	time current characteristic
WTG	wind turbine generator

Chapter 1 Introduction

1.1 Research Challenge

In the UK, a typical rural distribution network has a partially looped network configuration [1-3] and is designed to operate in radial operation mode without having to accommodate any generation unit. It is estimated that 80% of network faults are temporary single-line-to-ground (SLG) faults [3-4]. Thus, automatic restoration of electric supply after a network fault event is required to improve overall network reliability. The auto-reclosing scheme can be used to clear temporary faults and isolate the permanent faults to allow automatic restoration of the electric power supply. Under an auto-reclosing scheme the source circuit breaker, with auto-reclosing at the primary substation or pole mounted automatic recloser along the main feeder, carry out a variable sequence of tripping and closing to check the protected feeder and clear the fault, or isolate the faulty feeder, if necessary, with the coordination of an automatic sectionaliser, fuse and relay [3-5].

The continued increase of distributed generation (DG) or embedded generation (EG) penetration into existing distribution networks in recent years has resulted in (i) changes in the direction and magnitude of power flow and (ii) changes in the network voltage profile [6-11]. Consequently, these have an important impact on network protection [7-8, 12-21]. The protection issues that have been identified are: (i) increase of network fault level which makes costly upgrading protection devices a necessity (ii) disruption of the operation of feeder protection, which causes miscoordination between protective devices, unnecessary tripping of healthy feeders and prevention of successful reclosing of circuit breakers, (iii) introduction of new protection requirements such as loss of mains (LOM) protection to avoid the unintentional islanding condition and high speed relaying to trip network faults while retaining the transient stability of DGs. Substantial research work has been done to resolve these protection issues [14, 22-32]. However, only a limited number of publications [28-30] have considered maintaining the operation of DGs during network fault conditions. With increased penetration of DGs into distribution

networks and customer demand for a highly reliable power supply, it is significant to maintain the operation of DGs during fault conditions as far as possible.

In order to maximise the integration capacity of DGs, future distribution network is very likely to operate in ring operating mode, compared to existing radial operating mode [24, 33-35]. Ring operation mode increases the reliability of electric power supplies and, in the context of DGs, it eases the issues of voltage regulation and change of power flow. However, ring operation mode might complicate the feeder protection issue that has been stated previously, caused by DGs interconnection in radial networks [35-37]. Thus, further research work should be carried out to indentify the protection requirements in ring operated networks with DGs. In this context, comprehensive study on factors which influence the transient stability of DGs during fault condition in ring operated network is necessary. Transient stability of DGs should be taking into consideration when developing a potential protection scheme that has the capability to ensure the continued operation of DGs during fault condition in a ring operated network. Additionally, only limited research work has been carried out to develop a potential protection scheme that is suitable for use in ring operated distribution networks with DGs [35].

The penetration of wind power based DGs into power system network has increased significantly. The total installed wind power capacity reached 159.2GW worldwide at the end of 2009[38] and it is expected that 12% of world's electricity production will be from wind power by the year 2020[39]. In recent years, the technology of wind generation has been switched from fixed speed to variable speed and the advantages of variable speed operation of wind generators are reported in [40-44].The impact of fixed speed induction generator (FSIG) based wind power plant on the operation of auto-reclosing scheme has been investigated in [16]. The variable speed induction generator, doubly fed induction generator (DFIG) has a different operational characteristic and transient response compared to FSIG [44-45]. It appears that no study has been conducted so far to investigate the impact of DFIG on the network protection issue, particularly on the operation of auto-reclosing schemes.

According to G59 recommendation [46] the common practice adopted by utilities in the UK is to disconnect DGs immediately, once a network fault is detected,

irrespective of any type of fault, to prevent islanding operation and disruption of the operation of conventional auto-reclosing scheme [16]. However, with increased penetration of DGs into existing distribution networks, it is increasingly becoming important that DGs must support power networks during steady-state and fault conditions. It has been reviewed above that 80% of faults which occur in distribution networks are temporary and most of them are SLG. This should give a strong incentive to find ways for maintaining DGs in service during temporary SLG faults as far as possible, which is to the benefit of utilities, DG developers and customers.

Investigation into the sustainability of different DG technologies during temporary faults on overhead distribution network should be carried out to (i) assess the possibility of preserving DGs in services as far as possible to optimise electric supply continuity and (ii) identify the requirements of auto-reclosing schemes in distribution networks with high penetration of DGs. By adapting a single-phase auto-reclosing (SPAR) scheme [47-50] used in a transmission network, DGs would be ensured to remain connected to the grid in the SLG fault event while only the faulty phase is tripped. The impact of the implementation of a SPAR scheme in distribution networks with distributed synchronous generators has been reported in reference [51]. DG based on induction generators whether FSIG or DFIG, were not covered in this research study. Substantial research has been done in the past to develop a novel fault identification and phase selection algorithm in conventional transmission lines [52-56] to address the various limitations of conventional phase selector [47-50]. It appears that no research work has been carried out to investigate a fault identification and phase selection algorithm in existing overhead distribution networks that takes into consideration the operation of DGs during fault conditions.

Another consideration is related to the adaptation of an appropriate dynamic DG model to thoroughly asses the transient performance of DGs during various network fault conditions which then facilitates the development of the adaptive fault identification and phase selection algorithm proposed in this research study. The importance of dynamic modelling of DGs in simulation studies related to network protection has been highlighted in [16, 27].

1.2 Research Objectives

The aim of this research work is to examine the development of a new protection technique in distribution networks with DGs in dealing with the protection issues with particular emphasis on identifying new requirements for operating auto reclosing schemes in distribution networks with DGs that operated in radial and ring modes. This is followed by an investigation into the development of an adaptive fault identification and phase selection algorithm to be used in a novel SPAR scheme in a power system with DG.

1.3 Thesis Chapter Outline

The structure of the thesis is arranged to reflect the order of the activities that have been undertaken in this research work. Following is a brief description of the contents of each chapter.

Chapter 2 presents a literature review on DG with particular emphasis on wind generation and on studying the characteristic of feeder protection in conventional rural distribution networks. It also examines the general topic of network protection issues due to interconnection of DGs and existing proposed solutions. The requirement for an auto-reclosing scheme in a distribution network with high penetration of DG has been indentified.

Chapter 3 presents a comprehensive study into the factors that influence the transient stability of FSIG in the investigated medium voltage (MV) overhead distribution network that is operated in ring mode. It also presents the study to asses the sustainability of both FSIG and DFIG during temporary fault conditions in the investigated network. Moreover, the impact of both FSIG and DFIG on the operation of a SPAR scheme in the investigated network has been studied.

Chapter 4 presents a study on the development of an adaptive fault identification and phase selection algorithm to be used in a SPAR scheme with DG. Comprehensive simulation analysis has been presented in this chapter to demonstrate how different types of SLG fault that occur in the investigated MV overhead distribution network

with DFIG can be indentified and then isolated from the network with the proposed method.

Chapter 5 presents the details of the overall process of digital data processing and analysis. The whole process includes fault data analysis and fault data optimisation followed by the process of rule-based fault identification and a phase selection algorithm development and finally the process of verification that aims to check the robustness of the developed algorithm in all possible network operating conditions.

Chapter 6 concludes with the scope of the research work that has been done and the contribution of the research project, followed by suggestions of possible future research work.

Chapter 2 Analysis of Distribution Network Protection Issues Due to Interconnection of Distributed Generation

2.1 Introduction

This chapter describes DG technologies, with particular emphasis on wind power generators, and a review of the protection arrangements in conventional rural distribution networks. The main distribution network protection issues due to interconnection of DG and existing proposed solutions are then outlined. The impact of DG on the operation of conventional auto-reclosing schemes is examined. A new requirement for an auto-reclosing scheme, in order to maintain the operation of DG during network temporary fault condition, is indentified.

2.2 Distributed Generation Technologies

Distributed Generation (DG) or Embedded Generation (EG) refers to electric power generation embedded in a power network at distribution voltage levels and not centrally planned by utilities [7, 57-58]. DG can be categorised as renewable DG, Combined Heat and Power (CHP) DG and storage based DG, according to the different type of generation technologies and energy resources used. Renewable energy based DG, such as medium and small hydro turbines with less than 10MW capacity, on-shore wind farms, biomass based generators, photo-voltaic (PV) systems and geothermal plant that can be found in high renewable energy resource sites [59]. Combined heat power (CHP) based DG or cogeneration refers to the power plant where either electricity or heat is generated as a by-product and they are mostly found in industrial sites. CHP power plants use biomass, geothermal and conventional fossil fuel as energy resources. Storage based DG or fuel cell technologies are systems where electricity is generated from electrochemically combining hydrogen and oxygen.

The penetration of wind power based DG particularly in distribution networks, has increased significantly. The total installed wind power capacity reached 159.2GW worldwide at the end of 2009[38] and it is expected that 12% of world electricity production will be from wind power by the year 2020[39]. The development of this

new generation is driven by, (i) government environmental commitment to tackle climate change by generating electric power from renewable energy resources, (ii) advances in new power generation and storage technologies and (iii) liberalization of the electricity market where the electricity customers are looking for the most reliable electricity supply. [57-58, 60-61]

2.3 Configuration of Wind Turbine Generator (WTG)

Detailed descriptions of different types of DG technologies can be found in the literature [7, 40-44]. This research focuses on the investigation of a novel protection algorithm in a distribution network with wind power generation. An emphasis will be placed on the common type of wind generators to understand the strengths and weaknesses of each of them. Generally, both synchronous and asynchronous (induction) generators can be adopted as wind generators and can be operated either as fixed speed (by being directly connected to the grid bus) or variable speed (by connecting to the grid bus bar via the power electronic converters). The advantages of operating a generator with variable speed in wind power generation includes increased wind energy capture, improved system efficiency, improved power quality, improved transient response, reduced acoustic noise and reduced mechanical stress of the wind turbine generator (WTG) [44-45]. Most of the installed wind power plants are based on one of the following three types of WTG systems (i) fixed speed wind turbine with directly coupled induction generator, (ii) variable speed wind turbine with double fed induction generator and (iii) variable speed wind turbine with direct driven synchronous generator.

2.3.1 Fixed Speed Wind Turbine with Directly Coupled Induction Generator

Figure 2.1 shows the configuration of a fixed speed wind turbine with directly coupled induction generator [44]. This type of wind turbine uses a squirrel cage induction generator with the stator winding directly connected to the grid. The generator speed varies between 1% and 2% of the rated speed. There is a gear box between the wind turbine and generator. This type of generator is robust and cheap because of the simple and relatively low cost construction. However, squirrel cage based FSIG demand reactive power from the grid and this is undesirable in a weak grid. Furthermore, the turbine is heavier and will sustains higher mechanical stress

because the energy from a gust of wind must be absorbed by the gear box and coupling. An additional capacitor bank is required for reactive power compensation.

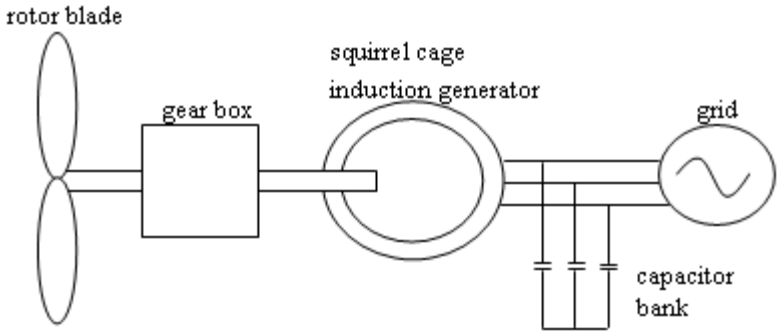

Figure 2.1 Configuration of fixed speed wind turbine with directly coupled induction generator.

2.3.2 Variable Speed Wind Turbine with Doubly Fed Induction Generator

Figure 2.2 shows the configuration of a variable speed wind turbine with a doubly fed induction generator (DFIG) [44]. This type of variable speed wind turbine uses a wound rotor induction generator with the stator winding connected directly to the grid and the rotor is fed by a power electronic converter that enables the rotor frequency to vary within a designed range. The power electronic converter of DFIG only consumes 20% to 30% of the generator rated power compared to full rated conventional power electronic converter that is used in a variable speed wind turbine with direct drive synchronous generator. The turbine is lighter and sustains lower mechanical stress compared to a fixed speed wind turbine. The weakness of this variable speed type of wind turbine compared to a synchronous generator is the requirement of the gear box. Moreover, the power electronic converter of the DFIG is complex and expensive compared to a fixed speed wind turbine type.

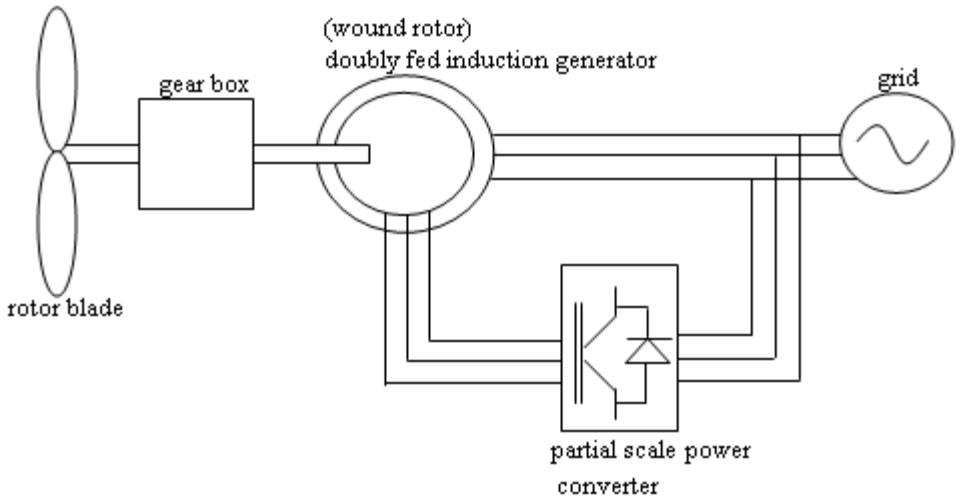

Figure 2.2 Configuration of variable speed wind turbine with doubly fed induction generator.

2.3.3 Variable Speed Wind Turbine with Direct Driven Synchronous Generator

Figure 2.3 shows the configuration of variable speed wind turbine with direct driven synchronous generator [44]. This type of variable speed wind turbine uses a direct drive synchronous generator and the total generator power output is fed to the grid through a power electronic converter that provides a wide range of operating speed. The varying generator frequency is converted to constant grid frequency. This turbine type does not require any gear box. The weakness of this variable speed type of wind turbine is that a complex power converter and generator construction are required compared to the variable speed wind turbine with DFIG.

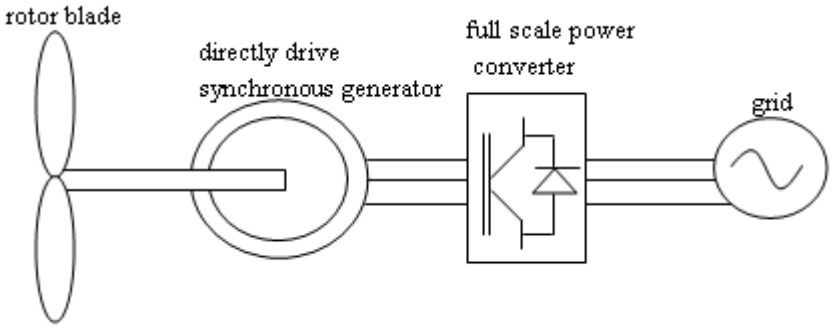

Figure 2.3 Configuration of variable speed wind turbine with direct drive synchronous generator.

2.4 Network Configuration in Radial Distribution Network

The configuration, operation and management of existing distribution networks are based on passive networks. The role of such networks is confined to transferring electricity from generation and transmission system to the load centres [1-3]. Under this situation, the main function of a distribution network is delivering good quality electricity with minimum amount of network control to the load centres at different voltage levels. Most distribution networks, particularly in rural areas are mainly designed to operate in radial mode without any accommodation for generating units.

Figure 2.4 shows the schematic diagram of typical rural distribution network including wind power plant in the UK [1-5]. The 132 kV high voltage (HV) network is supplied from a bulk generation point. Load connected at the medium voltage (MV) level at 33 and 11 kV are supplied from the HV network via 132/33 kV and 33/11 kV distribution substations respectively. Both 132/33 kV and 33/11 kV distribution substations are equipped with two transformers, each of which are supplied from an independent circuit. In order to form a parallel connection the busbar disconnector between them would be closed. This arrangement improves the overall system reliability when one transformer breaks down, the busbar disconnector would be opened and the MV load can still be fully supplied from another circuit. Loads at low voltage (LV) 0.400 kV are connected along 11 kV primary feeder through pole mounted transformers at rating of 11/0.400 kV. The renewable type DGs such as wind power plants are mostly located in rural areas and usually embedded into distribution networks at medium voltage levels as shown in Figure 2.4. The wind power plant is connected at the end of the 11 kV feeder through a 0.690/11 kV transformer.

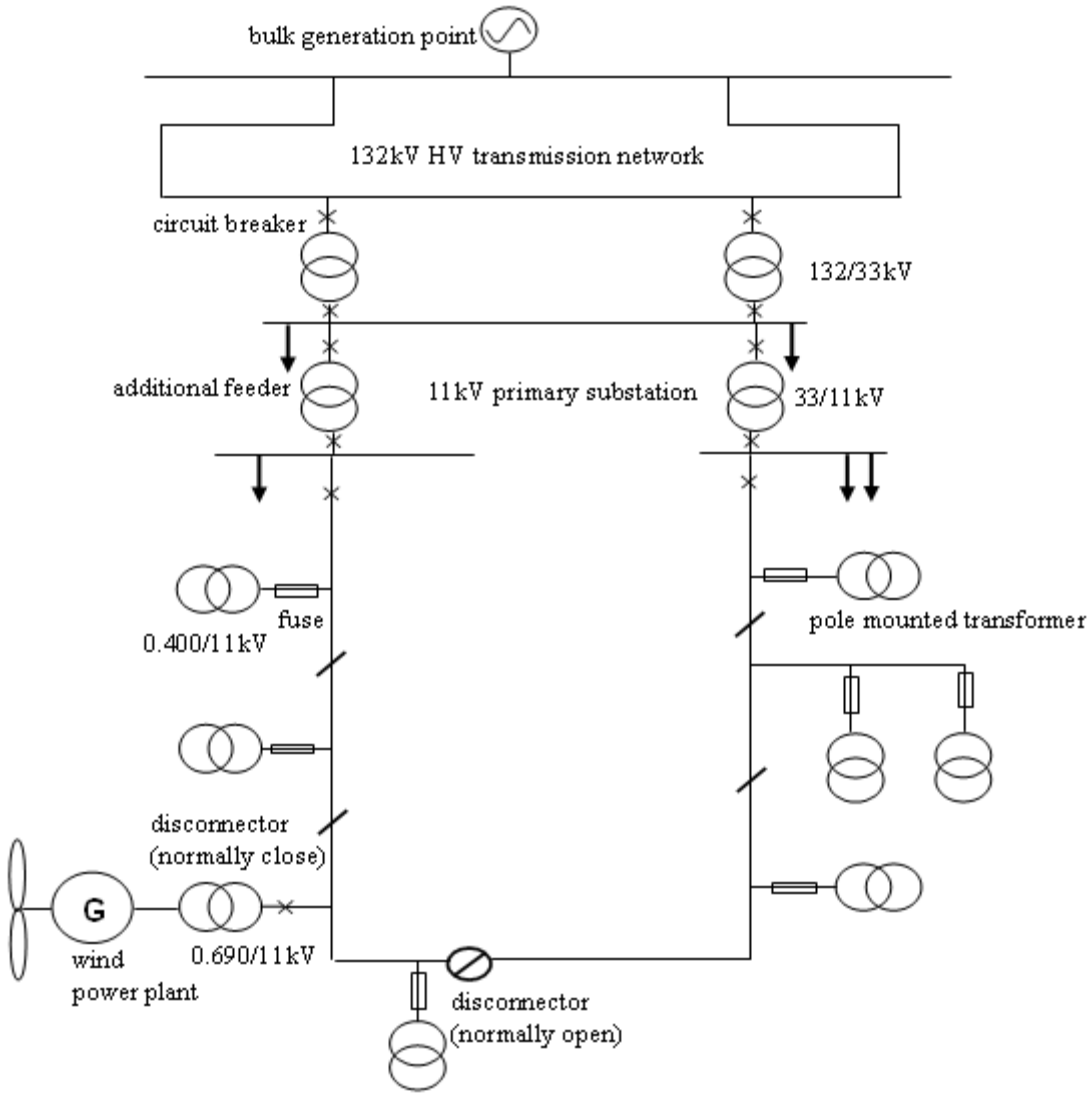

Figure 2.4 MV rural distribution network including wind power plant in the UK.

The rural overhead network has a partially looped network configuration and interconnects with other networks supplied from adjacent primary substations [1,3]. During normal network conditions, the network is operated in radial mode by opening a disconnector at the appropriate point to improve system reliability and simplify system protection [1,3]. The remotely controlled disconnector is distributed along the 11 kV feeders. It is used along with protective devices such as circuit breakers and auto reclosers to improve the period of fault outage. After the circuit breaker at the substation is tripped and locked out, disconnectors located at both sides of the fault are instructed to open and isolate the fault section. The disconnector at the normally open point and substation circuit breaker are then ordered to close to restore power supplies to healthy sections.

In addition to network configuration, the system earthing arrangement affects the system protection. There are four methods of system earthing arrangements, isolated neutral, resonant earthing, impedance neutral earthing and solid earthing. The 132 kV network has a mesh network configuration therefore multiple earthing points are needed and a solid earthing arrangement has been used. 33 kV networks in the UK use a different type of impedance earthing where neutral of the source transformer or the earthing transformer of the source transformer has a delta connection at 33 kV, the winding is earthed either via resistance, tuned arc suppression coil or reactor. 11 kV networks use solid or neutral impedance earthing. 0.400 kV networks use the solid earthing method and there are multiple earthing points to ensure that individual exposure to minimum overvoltage levels dealing faults on electric appliances. [1, 62-64]

2.5 Overcurrent Protection Arrangement in MV Feeder

The MV overhead feeder is protected using phase overcurrent fault and earth fault protection [3]. In a radial overhead feeder, power flows in one direction from the only power supply source to the loads tapped along the feeder section. During an overcurrent fault condition, the protective devices only need to sense the flow of overcurrent in one direction. The distance measurement and direction elements are not required in radial network protection, compared to transmission networks and heavy loaded urban distribution networks, where the flow of fault current is multidirectional, with more than one fault current supply source. Therefore, generally, radial feeders can be effectively protected from network faults with a non directional, time graded overcurrent protection scheme. In the MV networks with solid and low impedance earthing, the earth fault protection element can be integrated into a phase overcurrent protection device. In contrast, for a network earthed with a tuned arc suppression coil or isolated earthed, directional earth fault protection is required to detect the residual fault current, which is much lower than the load current.

In radial distribution networks with overhead feeders, 80% of faults are temporary and most of them are single-line-to-ground (SLG) [2-3]. Thus, automatic restoration of electric supply after a network fault event is required to improve overall network reliability. The auto-reclosing scheme can be used to clear temporary faults and

isolate permanent ones to allow automatic restoration of the electrical power supply. Under the auto-reclosing scheme, a source circuit breaker with auto-reclosing or a pole mounted automatic recloser coordinated with a fuse, sectionliser and relay are used to clear temporary faults and isolate permanent faults to allow the automatic restoration of the electrical power supply [2-4].

A fuse is a protective device that can be installed at the main feeder or lateral feeder in overhead networks. It operates when the fault current heats up and melts the fuse link where TCC (time current characteristic) curves are used to describe the fuse link melting time. A fuse interrupts the fault current only once before it needs to be replaced. Thus, it is used in conjunction with automatic recloser to prevent damage during the event of a temporary fault and the extended time period of fault outages. [3, 65]

A pole mounted automatic recloser is a compact protective device equipped with mechanism that can detect and interrupt the fault by carrying out a predetermined tripping and closing sequence to clear a temporary fault or isolate the permanent faulty section [1-4, 47]. It is used at a substation instead of a source circuit breaker with auto-reclosing for primary network protection. It can also be installed at a specific location at the main feeder for sectioning the long overhead line in order to coordinate with the source circuit breaker, to isolate the fault occurring towards the end of the feeder. Sufficient opening time or dead time setting is required to allow extinction of fault arc. The opening time before high-speed or instantaneous reclosing attempts varies from 0.2 s to 0.5 s [1]. In most of European countries, the opening time of 0.3 s had been used [66]. The opening time before time-delayed reclosing attempt can be more than 10 s [1]. Multiple reclosing attempts are required to ensure a fault is completely cleared from the network and it normally would be two high-speed follow by two time-delayed reclosing. Figure 2.5 shows an example of a high speed reclosing operation of an automatic recloser with single reclose attempt. The fault inception is at t = 3 s and circuit breaker opens at t = 3.4 s and recloses successfully at t = 3.7 s, after which current goes back to normal load condition.

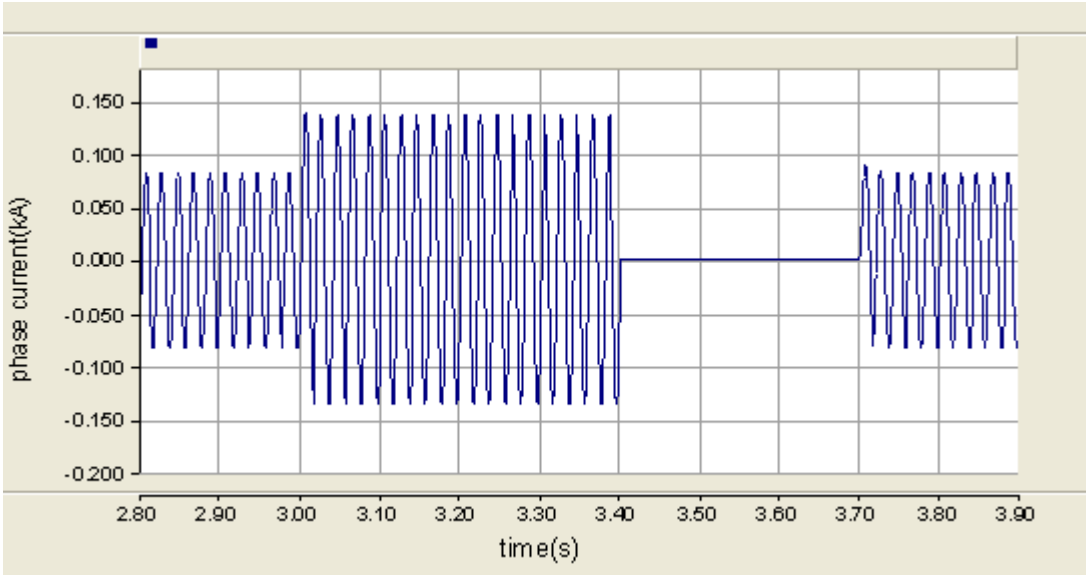

Figure 2.5 Operation principle of automatic recloser with high speed reclosing.

Figure 2.6 shows an example of a common arrangement of automatic recloser and fuse at a radial network feeder [1, 65]. The automatic recloser (ARC) is located at the beginning of the main feeder and fuse F is located at the lateral feeder. The operation of ARC is based on a preset switching strategy. Coordination between ARC and F are used to clear the temporary fault and isolate permanently downstream of F. High-speed reclosing of automatic recloser clears temporary fault and prevent the fuse link from melting. Time-delayed reclosing allows sufficient time for the fuse link to melt to isolate a permanent fault.

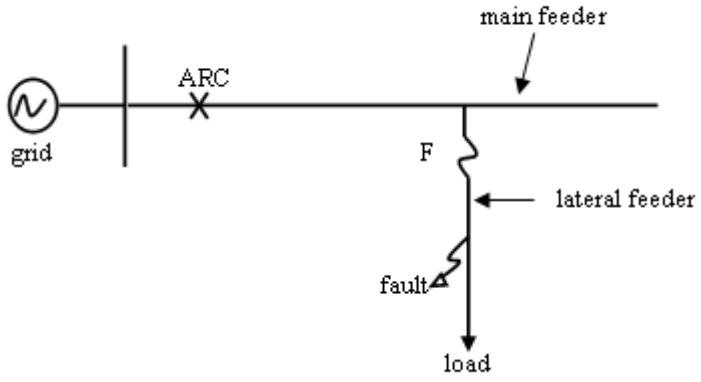

Figure 2.6 Common arrangement of automatic recloser and fuse at radial network feeder.

A Sectionaliser is a protective device that does not interrupt the fault current. It is normally used to coordinate with the automatic recloser in order to isolate faulty

sections in the feeder. The sectionaliser will automatically isolate the faulty sections in the feeder, once the automatic recloser, upstream, has interrupted the fault current. After a preset number of open and reclose operations of the recloser, the sectionaliser will then open during the dead time of the automatic recloser. After the faulty section is isolated, the recloser closes and restores the power supply to the rest of the network. For a temporary fault, the sectionliser would reset once the automatic recloser is reclosed. [3, 65]

2.6 Development of New Protection Technique in Distribution Network with DGs

Traditionally, a distribution network is a passive and radially operated system. It is designed to mainly provide a good power delivery service with minimum network control and without accommodation of any generation unit. Continued penetration of DGs into existing distribution networks in recent years has resulted in bi-directional power flow and changes in the network voltage profile [6-11]. This in turn has an important impact on the operation of conventional feeder protection schemes that are designed based on the assumption of simple radial network operation. Typical network protection issues due to interconnection of DGs have been indentified and existing proposed solutions to these protection issues were reviewed. The impact of DGs on these protection issues is determined by the penetration level, the connection point in the distribution network and the DG technology being employed [8, 17].

The interconnection of DGs may cause a significant increase in network fault levels and consequently makes upgrading protection devices with higher fault interrupting capacity a necessity and such devices are normally expensive. Alternatively, this issue can be solved by a solid state fault current limiter [22] or a superconducting fault current limiter [23]. During a three phase fault condition, synchronous generators provide a substantial fault current and increase the network fault level. In contrast, induction generators only contribute to network fault level during the short period immediately following the fault. The fault current contribution from DGs that are connected to the grid through a power electronic interface, e.g. fuel cells, can be limited by suitable control on the power electronic switches [7-8, 20].

The fault current contribution from DGs also disrupts the time grading coordination on feeder protection, e.g., miscoordination between fuse-fuse [8, 20] or fuse-recloser [12, 14, 21]. Thus in reference [14], a procedure to achieve coordination between fuse-recloser in a network with DG has been suggested based on the application of a microprocessor-based recloser. Moreover, fault contribution from DGs may also cause the unnecessary tripping of healthy feeders [12, 15, 18, 21]. Non-directional overcurrent relays are mostly used in existing radial feeder protection [1-2]. In the case where the fault and DG are located at different feeders, the relay at the beginning of the DG's feeder would trip as a significant amount of fault current flows to the faulty feeder. Thus, it is also suggested in [13-14] that directional elements are a necessity in protecting a distribution network with DG.

Apart from that, maximum fault clearing time is also a concern in a distribution networks with DG. It is reported in [20, 27] that the critical clearing time (CCT), which determines the transient stability of the DG, is far less than the tripping time setting of conventional feeder protective devices. Therefore, to retain transient stability of DGs, the maximum fault clearing time needs to be reduced. The speed of fault clearance in existing distribution networks is not an important factor as it is in transmission networks where the system stability is involved. However, future distribution network will be expected to accommodate a significant proportion of DGs. The DGs need to remain in service as far as possible during a network fault condition in order to improve the system stability and reliability of power delivery. Thus, recently, intensive research activities have been carried out in the development of high speed protection techniques in distribution networks with DGs [24, 25-26].

Bo et al. [24] proposed a non communication, accelerated protection technique that can be used in a power system with two end power sources, for instance a distribution network with DGs. Superimposed and sequence current signals are used to speed up the fault detection operation for faults that occur within the protected section and consequently initiate a trip signal to the circuit breakers at both ends of the section.

Development of a high speed fault transient based-directional overcurrent protection method has been suggested in [25]. Each of the overcurrent relays in the network

detects the fault current transient directional signal during fault condition. The signals are then exchanged via a communication link between each of these relays to confirm the exact fault location so that the faulty section can be isolated from the rest of the network.

In [26] it is proposed to replace conventional overcurrent relays with a high speed distance protection scheme in the urban distribution network to improve transient performance of DGs during network fault condition. Upgrading of the existing ring main unit (RMU) in the substation and replacing of existing relays with new microprocessor based-relays are needed for the proposed protection scheme. Renewable type of DGs, like wind power plant are mostly connected to rural networks. However, distance protection in rural networks with DGs is unfeasible due to (i) the requirement of additional voltage transformers to be installed in the network for voltage measurement which will add a financial burden and (ii) overhead network has long distribution lines and distance protection has low accuracy in protecting long network lines.

Apart from the solutions proposed above, research work has also been carried out to develop a novel network protection scheme that is intended to maintain the continued operation of DGs during fault conditions [28-30]. Under the adaptive protection scheme proposed in [28], the network is divided into different protection zones with a reasonable balance of load and DGs. Each protection zone is separated by a circuit breaker which is equipped with a communication channel to check synchronization and auto-reclosing functions. A computer based-relay is installed at the main power distribution substation, to monitor power and current flow and control operation of the circuit breaker at each network protection zone. A fault location and protection scheme based on a multilayer perceptron (MLP) has been proposed in [29]. In this research work, the zone protection approach as suggested in [28] has been implemented in the investigated system. The fault type and fault location are determined at the main power substation using a MLP neural network approach. After that, a signal will be issued from the substation to isolate the faulty zone from the rest of the system. Under the protection schemes proposed in [28-29], the DG units located at other protected zones that are different than the faulty zone can continue the operation throughout the fault condition. However, implementation of

the proposed protection schemes in [28-29] can be costly because of the installation cost of a communication link between DGs and the distribution substation is expensive. A conventional circuit breaker and recloser needs to be upgraded to a microprocessor based-type, to allow intensive signal communication process. An adaptive network protection scheme based on wavelet transformation has been proposed in [30]. In SLG fault conditions, the wavelet coefficients of the transient fault currents that are measured at the main significant points of the network are analysed in order to determine the faulty section in the investigated network. The faulty section can be then isolated from the rest of the network. Due to the high fault detection speed, the DG units that are located at other sections other than the fault section, can remain in service as far as possible throughout the fault condition. The proposed method can be implemented in a distribution network with DG, without any communication medium.

Unintentional islanding is another major issue in addition to the feeder protection issues stated above. Unintentional islanding refers to a condition where part of the public load becomes islanded with DGs caused by fault clearance upstream of the distribution feeder. Unintentional islanding is undesired due to its impact on the islanded load; personnel safety and islanded DGs [7-8, 66]. Loss of mains (LOM) protection refers to the protection relay which automatically detects such a condition and disconnects DGs from islanding operation [7-8, 19]. In the UK, a LOM protection scheme is a requirement for all grid connected DGs as stated in Association's Engineering Recommendations G59/1[46]. LOM can be detected through passive, active and telecommunication based methods. Passive techniques are based on measuring and monitoring the system state, e.g significant changing in generator frequency and voltage. Rate of change of frequency (ROCOF) is a typical passive based LOM detection method [7]. However this passive method may cause nuisance tripping or can be fooled particularly for the islanding condition, where the local load almost matches the local DGs generation [7, 67]. An ANN based LOM relay is reported in [31]. This is the result of continuous research in this field aiming to improve the accuracy of existing passive techniques.

The active techniques are based on actively interacting with the generator relay and utility system to get an indication of islanding operation, e.g., monitoring the

generator frequency. If the frequency drifts beyond a certain preset value, it is taken as an indication that islanding condition has occurred. [19- 20]

A telecommunication based method i.e., intertripping scheme [19, 32] is superior compared to passive and active methods. But, installation of the intensive communication channels to be used for intertripping is far more expensive, compared to a LOM relay used in passive and active methods [32].

Meanwhile, future distribution network are very likely to change from radial to ring in order to maximise the integration capacity of DGs [24, 33-35]. In a ring operated network, power flow through each feeder is more even compared to a radial network, power losses are reduced and the voltage rise due to connection of DGs can be limited [33-35].The ring operation mode can be realised by closing the ring connector that is normally opened at the end of two radial feeders [68]. There are advantages in adopting ring mode operation in future distribution networks but it could complicate the protection system of networks with integrated DGs [35-37]. For instance, the fault clearance speed, which is already an issue with regard to the connection of DGs in radial mode, might be more significant when the network is switched to operate in ring mode. Special consideration is required for feeder protection when operated in ring mode, particularly, the coordination between the relays that are installed on the ring feeders and the ring connector when a DGs is located at ring feeder. There is a possibility that the operating time of protective devices installed at such feeders may exceed the CCT limits of DGs which determine its stability. The consequence of exceeding the CCT would lead to unnecessary tripping of DGs. The factors influence the transient stability of DGs during fault condition in distribution network has been reported in [69], but mainly for radial operating mode and ring operating mode is not included in the research work.

It can be concluded from the literature review that significant research has been carried out to tackle the protection issues due to interconnection of DGs. This include high speed transient based directional overcurrent protection [25], development of new protection algorithms, e.g., the adaptive zone protection scheme [28-29] and an ANN based LOM detection method [31]. However, only a few potential protection solutions proposed in [28-30] allow the continued operation of DGs during fault

condition as far as possible. In other research works reported above, the DGs connected downstream of the protective devices need to be disconnected before the 1st reclose takes place to prevent islanding operation and disruption of the operation of conventional auto reclosing scheme [16].

Additionally, it has been concluded from the literature review that further research work needs to be conducted to identify factors which influence transient stability of DGs in ring networks and accordingly develop a new protection scheme. Such scheme should have the capability to ensure the continued operation of DGs during fault conditions, in both radial and ring network.

2.7 Impact of DGs on Operation of Conventional Auto-Reclosing Scheme

Interconnection of DGs has significant impact on the operation of auto-reclosing scheme in a conventional distribution network. Apart from causing protection coordination problems between recloser and fuse as reviewed above, DGs also prevent successful reclosing by turning a temporary fault into a permanent one during the recloser opening time. This could cause the deterioration of reliability of the power supply. Besides that, DGs might cause out of phase reclosing between the islanded part and the network during the power restoration period and cause detrimental impact on DGs itself and network components. Under current utility practices, DGs must be tripped before the 1st attempt to reclose, (instantaneous reclosing) so that the usual fault clearance procedure can be carried out as before DG connection [46, 66]. There are also operating conflicts that may a rise between the auto reclosing scheme and LOM protection. The dead time setting might be too short and may not allow enough time for DGs to disconnect from the network [66]. Thus, high speed LOM detection is required to ensure proper coordination between LOM protection and the network auto reclosing scheme in order to trip DGs before the 1st reclose takes place.

In recent years, the technology of wind generator has been switched from fixed speed to variable speed and the advantages of variable speed operation of wind generator are reported in [40-44]. The impact of fixed speed induction generator (FSIG) based wind power plant on the operation of an auto-reclosing scheme has been investigated

in [16]. The variable speed induction generator, doubly fed induction generator (DFIG), has different operational characteristics and transient response compared to FSIG [44-45]. It appears that no study has been conducted so far to investigate the impact of DFIG on the network protection issue, particularly on the operation of an auto-reclosing scheme.

2.8 The Implementation of Single Phase Auto Reclosing (SPAR) Scheme in Distribution Network with DGs

With increased penetration of DGs and customers demand for highly reliable power supply, the existing protection procedure of tripping DGs from the grid during all possible network fault conditions should be revised for the benefits of the utility as well as customers. Having in mind that 80% of these faults are temporary and extinguish themselves without external intervention [3-4], it becomes increasingly important that DGs remain in service during temporary fault events as far as possible in order to (i) improve overall system security by preventing loss of significant power caused by tripping of multiple DGs and (ii) improve the reliability of the power delivery system especially where DGs supply a load centre at the remote end of the feeder. In this perspective, investigation into the sustainability of different DGs technologies during temporary faults on overhead distribution networks should be carried out to (i) assess the possibility of preserving DGs in services as far as possible to optimise electric supply continuity and (ii) identify the new requirements of auto-reclosing schemes in distribution networks with DGs for effective temporary fault clearing.

The detailed comparative analysis reported in [45, 70] shows that different DG technology types, which include DFIG, FSIG and conventional synchronous generator (CSG) have their own unique operational characteristic which affect their transient response during network fault conditions. These need to be taken into consideration in deciding the fault detection time and dead time settings in auto-reclosing scheme. On the other hand, improvement in the existing auto-reclosing scheme in distribution network is required. Due to the fact that most temporary faults are unsymmetrical SLG, the single-phase auto-reclosing (SPAR) scheme which is currently used in transmission networks should be adapted in distribution networks

[47-50]. 3 phase auto reclosers are widely used in existing MV rural distribution network to prevent unbalanced loading on the network [1, 4]. The drawback of three-phase reclosing is the temporary disconnection of all three phases of the faulted feeder from the rest of the network during all fault condition regardless of the type of fault. In the context of DG connection, the application of 3 phase auto reclosing in a conventional overhead distribution network will affect the operation of DGs during a temporary SLG fault condition. It would cause unnecessarily isolation of DGs from the grid. In contrast, a single pole recloser trips only the phase subjected to SLG fault conditions and initiates three pole reclosure for other types of network faults. The conventional phase selection relays used in both transmission and distribution networks are distance relay and relay based on voltage and current operation [47-48]. The development of an adaptive phase selection technique in existing transmission and distribution lines is reported in [52-56] to address the limitation of conventional phase selector [47-50] that are susceptible to the variation in operating system parameters, such as fault resistance, mutual coupling from adjacent parallel lines, etc.

A phase selection technique based on fault generated high frequency noise and an ANN network has been proposed in [52]. The high frequency noise is obtained from a conventional capacitor voltage transformer in the transmission line. This approach will be costly to adapt in a power distribution network as a voltage transformer is not always available and furthermore the computational training of the ANN learning process is time consuming. A fuzzy logic based-fault phase selector that utilises the information of the magnitude of sequence components and angle between fault current phasors has been proposed in [53] to be used in a transmission network. The proposed method mainly determines the phase involved in SLG faults either involving the ground or not. Reference [54] proposes a phase selector based on series multiresolution morphological gradient (SMMG) transformation in the transmission network. In the proposed method, the power frequency fault components (PFFC) of the modular currents are extracted using an SMMG filter in order to indentify the faulty phase in the investigated system [54].

A fault identification technique based on a combination of a hybrid cause-effect network and fuzzy logic has been proposed in [55]. Under the proposed scheme, each of the fault events occurring in the investigated system are classified into one of five

groups as follows: SLG fault, double-line-to-ground (DLG) fault, line-line (LL) fault, three-line-to-ground fault and three-line fault. A fuzzy logic based-fault identification technique solely based on an analysis of the sequence components of the fault current phasors has been proposed in [56] for a conventional unbalanced distribution network. In the proposed method, the input parameters to the fuzzy based-fault classification module are (a) the phase angle between positive, negative and zero sequence components of the fault current phasors and (b) the ratio of the magnitudes of the sequence components of fault current phasors. The proposed method can indentify the phase or phases involved in an SLG fault, DLG fault, LL fault, three-line-to-ground fault and three-line fault.

The literature review shows that no research work has been carried out to investigate fault identification and phase selection algorithms in existing overhead distribution networks that take into consideration the operation of DGs during fault conditions. Although earth fault (SLG fault) detection elements had been included in modern integrated protection devices used in existing distribution networks for a number of years, for instance modern pole mounted auto-recloser [71-72], the operation of DGs during fault conditions has not been taken into consideration when the settings of these protection devices are determined. The presence of multiple fault current sources in distribution networks poses difficulty in indentifying the fault type and location. Continued investigation into the development of a novel fault identification phase selection algorithm is essential to facilitate a high speed and accurate single-phase operation in rural overhead networks with auto-reclosing scheme and DGs while maintaining the continued operation of DGs throughout the temporary SLG fault event. Therefore, this research project presents the development of an adaptive single phase fault identification and phase selection algorithm based on the analysis of symmetrical components and the phase angle of three-phase line currents measured at the relay point. Additionally, adaption of an appropriate dynamic model of a wind turbine drive induction generator is necessary in this research project, to thoroughly asses the transient response of DGs in various network fault conditions in order to examine the possibility of preserving the operation of DGs in fault conditions. Moreover, the accurate transient response of DGs during post fault condition is essential to facilitate the development of the proposed high speed, accurate fault identification and phase selection algorithm.

Chapter 3 Protection Requirements for Maintaining Continued Operation of Integrated DG in Overhead Distribution Networks

3.1 Introduction

Nowadays, international standards and national grid codes specify requirements for DGs interconnection to distribution networks [73]. Examples of such include (i) IEEE Standard 1547 that provides a uniform standard for interconnecting DGs with electric power system [74] and (ii) Australian Standard AS 4777.1—2005 that specifies the installation requirement for interconnecting inverter based DGs into the power grid in Australia [75]. According to the G59 recommendation [46] the common practice adopted by utilities in the UK is to disconnect DGs immediately once a network fault is detected to prevent islanding operation and disruption of the operation of conventional auto reclosing schemes [16]. However, with increased penetration of DGs into the existing power distribution networks and customer demand for a highly reliable power supply, it is significant for DGs to support the power network during steady-state and fault conditions. This chapter is therefore concerned with an investigation into the protection requirements for maintaining continued operation of DGs in a distribution network following fault condition.

In order to increase the installation capacity of DGs, future distribution networks will be operated in ring operation mode compared to radial [24, 33-35]. Thus, an investigation is presented in this chapter to identify factors that influence the transient stability of DGs in overhead networks that are operated in ring mode. The study is intended to indentify the protection requirement for the continued operation of DGs during fault condition in a distribution network that is operated in ring mode. It is well known that 80% of faults on distribution networks are temporary which extinguish themselves without external intervention and most of them are single-line-to-ground (SLG) faults [3-4]. Also included in this chapter is an investigation into the sustainability of different DG technologies during temporary faults, particularly SLG faults. The study is intended to indentify the protection requirements that allow

continued operation of DGs during fault conditions in a distribution network with an auto-reclosing scheme.

3.2 Power System Model under Consideration

The investigation presented in this chapter is based on modelling and simulation of a portion of a MV overhead distribution network with integrated DG under different system operating conditions using computational power systems simulation tool, PSCAD/EMTDC.

3.2.1 PSCAD/EMTDC Simulation Tool

EMTDC is a well-established power system analysis tool dedicated to simulation of transient and dynamic events [76-78]. EMTDC (Electromagnetic Transients including DC) represents and solves differential equations (for both electromagnetic and electromechanical systems) in the time domain [76-78]. PSCAD is a graphical user interface (GUI) for EMTDC. PSCAD allows the user to graphically assemble the circuits, run the simulations, analyse the results and manage the data in a completely integrated environment [79].

The PSCAD/EMTDC component library has an extensive range of models for power system fault transient analysis purposes. These include programmable network faults and various network components such as transformer (with or without saturation effect). The dynamic behaviour of the DG can be simulated in detail using a torsional shaft model (multi mass model) with up to five individual masses. Moreover, the power electronic model facilitates the design of a power electronic converter, which is used in certain types of DG technologies, such as DFIG. A brief comparison of the most widely used power system simulation tools in transient fault analysis can be found in [80]. Other than that, the following models in the PSCAD/EMTDC component library have been found very useful in this research work.

a. Basic protective component such as relay with different characteristics and circuit breakers with optional pre-insertion of resistance to simulate time delay for closing the breaker.

b. Digital signal processing components such as an online frequency scanner based on Fast Fourier Transform (FFT) that can determine the harmonic magnitude and phase of the input signal e.g., the current or voltage in the time domain. The component contains functions for both an anti aliasing filter and digital signal sampling in one block. A 6^{th} order Butterworth low pass filter acts as an anti-aliasing filter.

c. Various models of transmission line to represent cable and overhead lines. It includes the Bergeron line model with distributed parameters and PI section with lumped parameters. PI section is suitable for short line modeling and it can be adapted to model an overhead distribution line.

d. Multiple numbers of squirrel cage induction machines with the same rating and characteristic can be modeled as a single unit by adjusting the machine parameters called "number of coherent machine" in the squirrel cage machine model. Simulating multiple machines coherently speeds up the simulating time.

The users are also allowed to rewrite the source code of an existing library model or build a new model with the users' own graphics and source code using FORTAN or C languages [76, 78]. The availability of extensive library components and advantage of creating customers own models facilitate the design of the fault identification and phase selection algorithm in this research work.

3.2.2 Model of Wind Turbine Driven Induction Generator

In this research project, adaption of an appropriate dynamic model of the wind turbine driven induction generator is necessary to thoroughly assess the transient response of DGs in various network fault conditions in order to examine the possibility of preserving the operation of DGs under fault conditions. Moreover, accurate simulation of the transient response of DGs during post fault conditions is essential to facilitate the development of the high speed and accurate fault identification and phase selection algorithm that will be presented in Chapter 4. The

importance of dynamic modelling of DG in simulation studies related to network protection issues has been highlighted in [16, 27].

3.2.2.1 Fixed Speed Induction Generator (FSIG)

A 0.6 MW wind turbine based-FSIG model has been developed to investigate factors that influence transient stability of DGs in ring operated networks. The generator is modelled using a squirrel cage induction machine component. The single cage induction generator was implemented using the double cage induction machine model in PSCAD/ EMTDC component library, by setting the impendence value of the second cage at a very large value of 10 p.u. The machine parameters of the 0.6 MW FSIG can be found in Appendix A1.

2.0 MW wind turbine based FSIG has been developed to compare the sustainability of two types of wind turbine driven induction generators during network temporary fault. In order to compare the transient response of both DFIG and FSIG during fault condition in the study, both FSIG and DFIG are modelled using a wound rotor induction machine component. The machine parameter for 2.0 MW FSIG and DFIG can be found in Appendix A2.

3.2.2.2 Doubly Fed Induction Generator (DFIG)

The dynamic model of a 2.0 MW wind turbine driven DFIG developed in [81] has been adapted in this work. The machine parameter for the 2.0 MW DFIG can be found in Appendix A2. For the 2.0 MW DFIG model, a partial scale power converter that consists of the grid side power converter (GSC) and rotor side power converter (RSC) with their respectively control schemes, together with a DC link component are modelled appropriately. Figure 3.1 shows the schematic diagram of the 2.0 MW DFIG model. It consists of 2.0 MW wound rotor induction generator. The generator stator is connected directly to the grid. The generator rotor is connected to the network via back-to-back Pulse Width Modulated (PWM) power converters with a control scheme and an intermediate DC link capacitor.

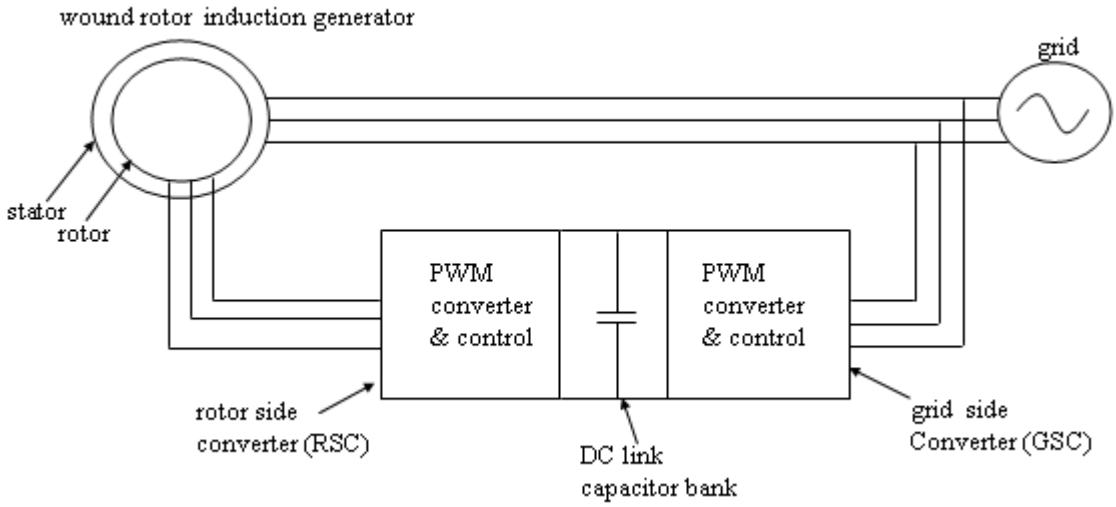

Figure 3.1 Schematic diagram of doubly fed induction generator.

Both the stator and rotor side power converters are controlled using a vector control technique, which allows decoupled control of both generator active and reactive power. The aim of the vector control scheme of the rotor side converter (RSC) is to control independently the active power and reactive power flow into the grid. The aim of vector control scheme of the grid side converter (GSC) is to keep the DC link voltage constant at a preset value regardless of the magnitude and direction of rotor power flow and control reactive power flow between the GSC and the grid. The detailed description of the vector control structure for RSC and GSC of the 2.0 MW DFIG is beyond the scope of this thesis and it can be found in [81]. The control strategy of the 2.0 MW DFIG is that at steady state condition, the generator absorbs modest reactive power from the grid while the generator terminal voltage is kept close to 1.0 pu.

3.2.2.3 Mechanical Driven Train

The actual mechanical driven train of the wind turbine consists of the rotor blade, high speed shaft, gear box, low speed shaft and generator rotor. As stated in [44] a two mass model or a system with two degree of freedom (2-DOF) is sufficient to represent the mechanical driven train of a wind turbine for power system transient study purposes. In the two mass model, the gear box and high speed shaft are assumed to be infinitely stiff and only the low speed shaft is modelled due to its softness [44]. Moreover, it has been reported [69] that the single mass model of the

FSIG introduces significant error in the value of the critical clearing time (CCT), whereby the single mass model results in greater CCT compared with the two mass model. In this research project, the mechanical driven train of the wind turbine is modelled using two masses $J_1$and J_2 are that connected by one spring element, K, as illustrated in Figure 3.2. J_1 is the total mass of the wind turbine, low speed shaft and gear box, J_2 is the mass of the generator rotor and K is the stiffness of the low speed shaft. The mechanical driven train of the wind turbine is modelled using the multimass component in the PSCAD/EMTDC component library.

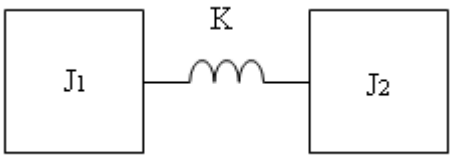

Figure 3.2 Two mass model of mechanical driven train of wind turbine.

3.2.2.4 Capacitor Bank

The inclusion of a capacitor bank acts as a local source of reactive power for the FSIG. This reduces the need for the reactive power consumed by the generator to be sourced from the grid. In this research project, the capacitor bank for both 0.6 MW and 2.0 MW FSIGs are rated at 30% of generator capacity as suggested in [45]. Both of the capacitor banks are modelled using the fixed value capacitor component in the PSCAD/EMTDC library. For the 2.0 MW DFIG, the reactive power is controlled by the integrated power converter, thus the need for the capacitor bank is eliminated.

3.2.3 Simplified Model of Medium Voltage Distribution Overhead Network

The power system model used in this study is shown in Figure 3.3 and it represents a typical medium voltage rural overhead distribution network in the UK [1-5]. The FISG or DFIG, is assumed to be connected at the end of feeder 1 to represent the interconnection of DG at the remote end of the distribution network.

The grid is modelled by a voltage source with short circuit level of 1800 MVA and a distribution substation represented by a 10 MVA, 33/11 kV star/delta transformers. Each of the 0.5 MVA loads supplied by feeders 1 and 2 is connected to their

corresponding feeders though 0.5 MVA, 0.415/11 kV delta/star transformer. Other loads connected to other feeders in the system are lumped together and represented by a single load of 3MVA at feeder 3. It is assumed to be connected at the end of a feeder though a 3.0MVA, 0.415/11 kV delta/star transformer.

The length of distribution lines 1 to 6 are assumed to be 5km and distribution line 7 is 10km. The parameter of the distribution line $Z_L = 0.3664\angle 59.50°\ \Omega$ per km. R_{f1} and R_{f2} are relays installed at the sources of feeder 1 and feeder 2 respectively. A ring connector, R_{ring}, is installed at the end of feeder 2. Radial operation mode is implemented by opening connector R_{ring}, whereas ring operation mode is implemented by closing it.

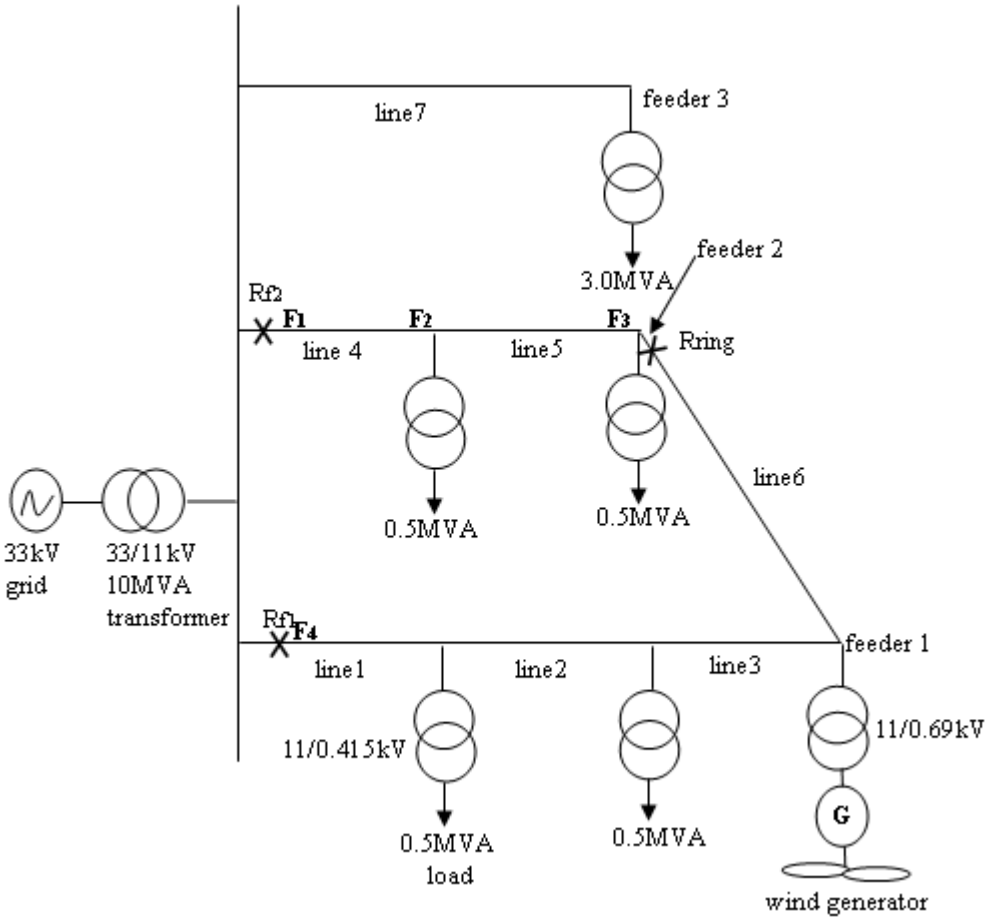

Figure 3.3 Schematic diagram of investigated distribution network with wind generator.

3.2.4 Determine Zero Sequence Line Impedance in the Investigated Power Distribution Network

The importance of zero sequence impendence to determine unsymmetrical network fault has been reported in [82-84]. In this research work, the positive sequence impedance, Z_{L1} and negative sequence impedance, Z_{L2} of the distribution line are identical and $Z_L = Z_{L1} = Z_{L2} = 0.3664\angle 59.50°\ \Omega$ per km. In the absence of detailed information about zero sequence impedance, Z_0 the ratio of $Z_0/Z_1=2$, as suggested in reference [84], has been used in the research work.

3.3 Investigation into Factors affecting the Transient Stability of DG during Fault Condition in Distribution Network with Ring Operating Mode

In the UK, the voltage rise issue has been identified as the main factor limiting the penetration level of DGs into distribution network in rural areas [9]. This issue however can be eased by operating the distribution network in ring mode rather than radial mode, with an appropriate protection strategy and voltage control [37, 68]. In this section, the impact of 0.6 MW wind turbine based FSIG on protective device settings in a ring feeder is reported. The factors influencing the generator CCT in a ring feeder during a three phase fault condition has been investigated. The aim of the study is to determine the feeder protection requirements in a ring network with FSIG in order to ensure proper coordination between protective devices in the ring feeder, so that the fault clearing time does not exceed the CCT, which ensures continued operation of FSIG after the faulted line section bas been detected and isolated. Similar studies the on factors which influence the CCT of FSIG in radial networks have been reported in [27, 69].

The CCT of a DG can be defined as the maximum fault duration that a fault can remain a power network without having that DG loss its transient stability. The concept of CCT applied at synchronous generators (SG) and induction generators (IG) are different. In the case of SG, during fault condition, the electrical power output, *Pe* reduces and leads to the acceleration of SG and the rotor angle, δ increases. After fault clearance, the SG is said to remain stable, if δ increase below a maximum rotor angle that is known as critical clearing angle. Otherwise, if the δ continue to increase above the critical clearing angle, then the SG become unstable and the time

corresponding to the critical clearing angle is known as CCT of the SG. In the case of IG, during fault condition, the electromagnetic torque, *Te* reduces and leads to the acceleration of IG and rotor speed increases. After fault clearance, if the rotor speed slow down and generator retains its prefault condition, then the IG is said to remain stable. Otherwise, if the rotor speed continues to increase with the generator terminal experience sustained voltage dip, then the generator become unstable. Therefore the maximum fault clearing time required for the IG to retain to its prefault condition is known as CCT of IG. [27, 69, 85-86]

3.3.1 Determination of FSIG's CCT in Radial and Ring Mode Operations

In order to determine the CCT of the installed FSIG, a three-phase-to-ground fault is applied at point F_1 which is 1km from the 33 kV grid on feeder 2 (see Figure 3.3), once when the network is operated in radial mode and then in ring mode. The fault is assumed at t = 15 s into the simulation for a duration of 130 ms. The 0.6 MW FSIG is connected at the end of feeder 1 through a 1.0 MVA, 0.69/11 kV step up transformer.

Figures 3.4 (a) to (g) show the variations of the machine parameters of the 0.6 MW FSIG following the fault condition in a radial network. Immediately after fault inception at t = 15 s, the terminal voltage dropped to less than 0.1 p.u as shown in Figure 3.4(a). This has caused the stator and rotor fluxes to drop, which results in reduction of active power as shown in Figure 3.4(b). The electromagnetic torque decreases upon the fault initiation as shown in Figure 3.4(c) and this can be explained using equation (3.1) as shown below [85-86].

$$T_e = KsV^2 \qquad (3.1)$$

K is a constant value that depends on the machine parameters and *s* is machine slip, which can be either –s or +s. The negative and positive signs indicate that, the machine is used as a generator and a motor respectively. *V* is the machine terminal voltage. The exact value of slip and terminal voltage prior to and during fault condition determines whether the electromagnetic torque is increased or decreased during fault conditions. As shown in Figure 3.4(d) the induction generator accelerates from -1.0% slip to about -13% slip while the terminal voltage falls from

96% to about 0.06%. Employing (3.1) the maximum value of electromagnetic torque during the fault condition can be calculated as below.

$$\frac{Te_2}{Te_1} = \left(\frac{-0.13}{-0.01}\right) x \left(\frac{0.06}{0.96}\right)^2$$

$_1$ and $_2$ indicate prior and during fault conditions respectively. T_{e1} and V_1 being chosen are -1.0 p.u and 0.96 p.u respectively, so the calculated T_{e2} is -0.051 p.u. The maximum electromagnetic torque obtained from the time domain simulation is -0.045p.u (see Figure 3.4(c)). Figure 3.4(e) shows the variation of stator current following the fault inception. Figure 3.4(f) is the magnification of Figure 3.4(e) for the time period started from t = 14.9 s to t = 16 s. During fault condition, the initial fault current contribution from the 0.6 MW generator to the considered network fault at F_1 reached 300% of full load current as shown in Figure 3.4(f).

As shown in Figure 3.4(g), after fault clearance a high inrush current is drawn from the grid to re-establish the generator's entire magnetic field which causes a significant amount of reactive power to be absorbed from the grid compared to the prefault condition. The initial fault current reaches 200% of full load current after fault clearance as shown in Figure 3.4(f). It was observed from Figure 3.4(b) to (e) and (g) that active power, electromagnetic torque, rotor speed, stator current and reactive power exhibit obvious decaying oscillation after fault clearance. This is because the exchange of power does not occur instantaneously due to the inductance in the machine winding and the inertia of the rotating mass [27, 85]. All of these parameters have successfully regained their pre-fault values after the clearance of the fault. This result shows that the transient stability of the wind generator is maintained which means the CCT of the generator has not been exceeded.

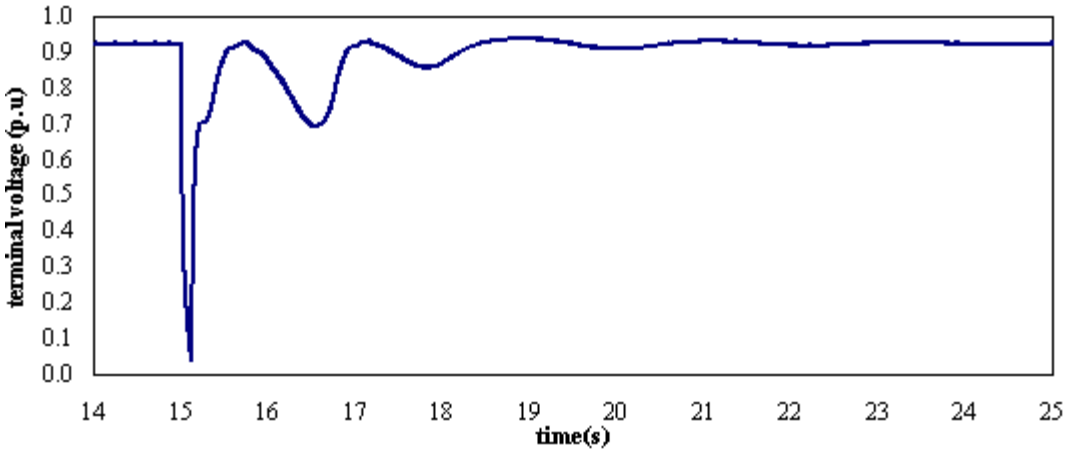
terminal voltage (p.u)
1.0
0.9
0.8
0.7
0.6
0.5
0.4
0.3
0.2
0.1
0.0
14 15 16 17 18 19 20 21 22 23 24 25
time(s)

(a)

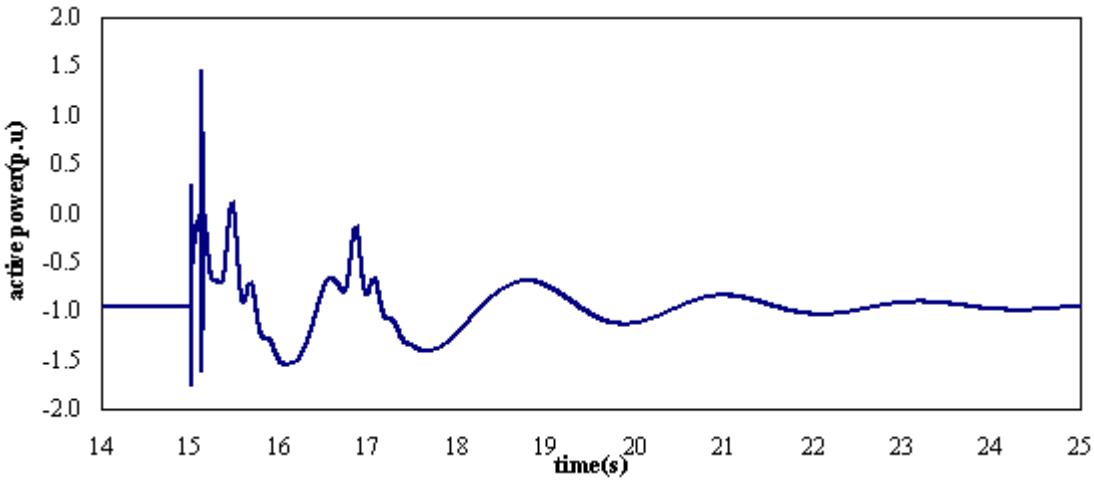
active power(p.u)
2.0
1.5
1.0
0.5
0.0
-0.5
-1.0
-1.5
-2.0
14 15 16 17 18 19 20 21 22 23 24 25
time(s)

(b)

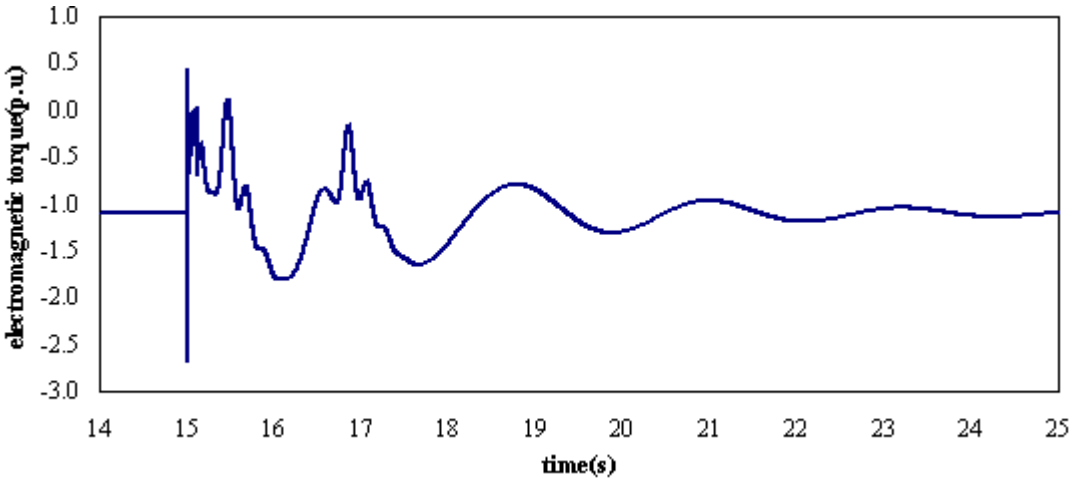
electromagnetic torque(p.u)
1.0
0.5
0.0
-0.5
-1.0
-1.5
-2.0
-2.5
-3.0
14 15 16 17 18 19 20 21 22 23 24 25
time(s)

(c)

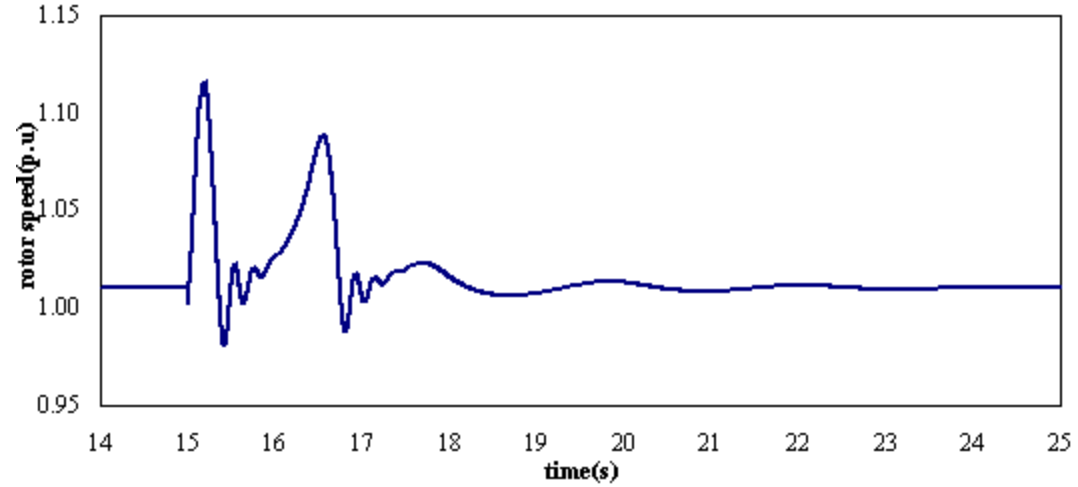
1.15
1.10
1.05
1.00
0.95
rotor speed(p.u)
14
15
16
17
18
19
20
21
22
23
24
25
time(s)

(d)

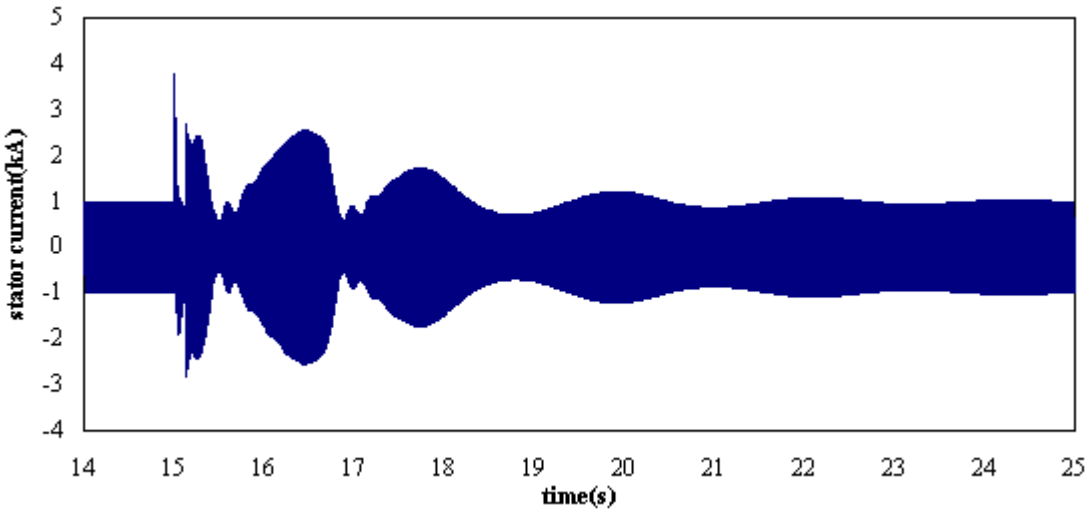
5
4
3
2
1
0
-1
-2
-3
-4
stator current(kA)
14
15
16
17
18
19
20
21
22
23
24
25
time(s)

(e)

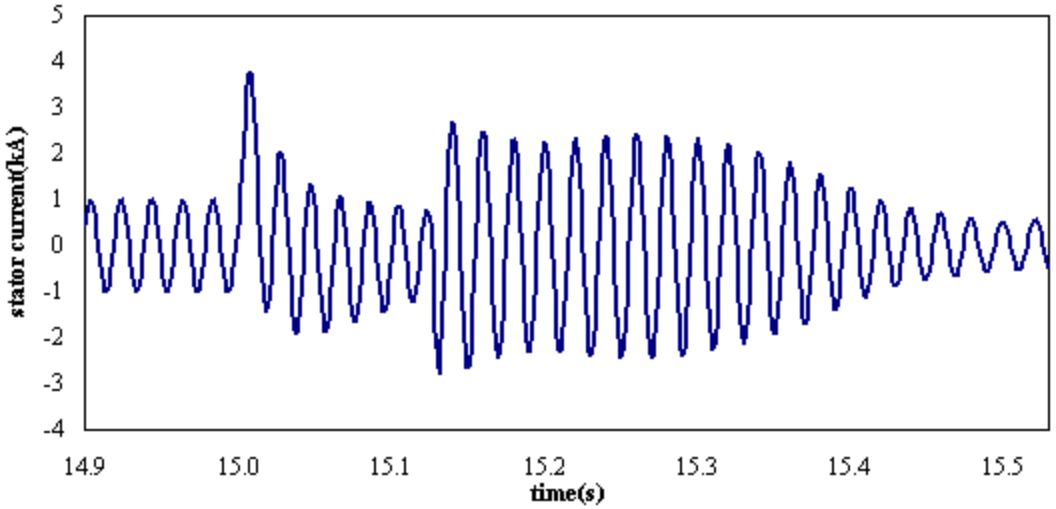
5
4
3
2
1
0
-1
-2
-3
-4
stator current(kA)
14.9
15.0
15.1
15.2
15.3
15.4
15.5
time(s)

(f)

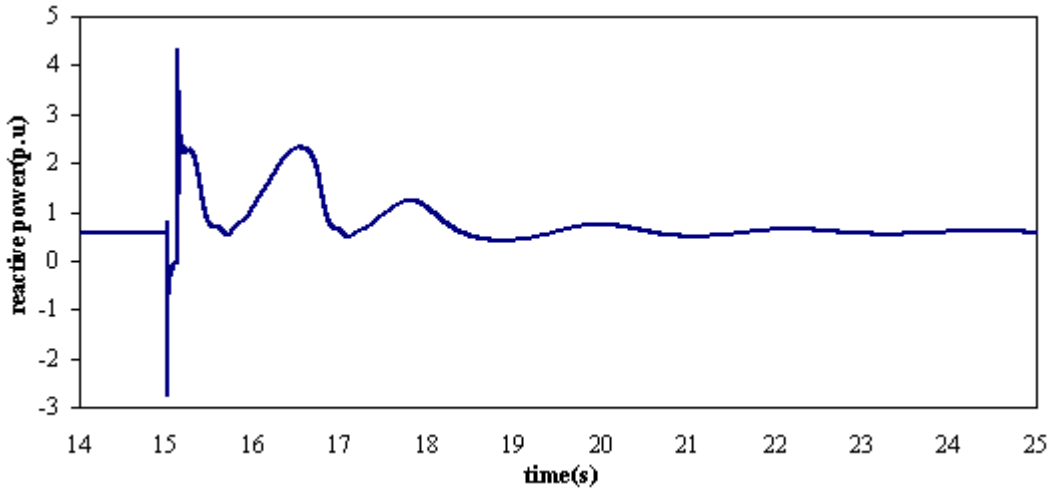

(g)

Figure 3.4 Transient performance of 0.6 MW FSIG following a three phase network fault with duration of 130 ms in radial network: (a) terminal voltage (b) active power (c) electromagnetic torque (d) rotor speed (e) stator current (f) stator current (magnification of figure (e)) and (g) reactive power.

Figures 3.5(a) and (b) show variations of the generator's terminal voltage and rotor speed in radial and ring networks. It was found that, the peak of rotor speed acceleration during fault condition in the ring network is slightly higher than the radial network; that is 1.130 p.u compared to 1.116 p.u. However, for the above network fault, the dynamic behaviour of DG after fault clearance is significantly better in the ring network compared to the radial network. The decay of oscillation in the terminal voltage and rotor speed is less significant in the ring network compared to the radial network. The machine parameters restore their prefault condition sooner in the ring network compared to the radial network. It was also found from this investigation that the generator can not retain its pre-fault condition when the fault duration is greater than 141 ms and 145 ms when the network operated as radial and ring respectively. These values are therefore considered as the generator's CCT for their respective network of operation. This investigation has also shown that in order to prevent the tripping of the considered FSIG which is connected at the end of feeder 1, the fault at F_1 must be cleared not greater than 141 ms and 145 ms for radial and ring network respectively.

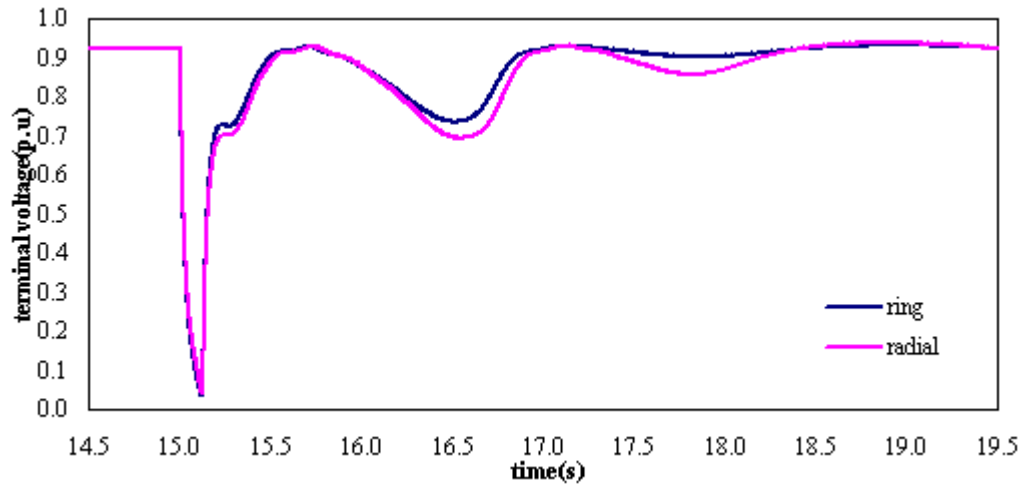

(a)

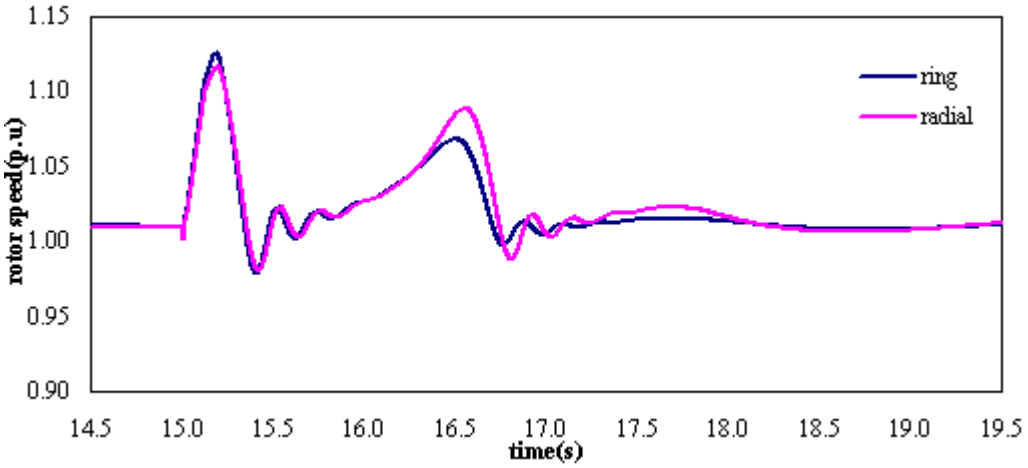

(b)

Figure 3.5 Variation of (a) terminal voltage and (b) rotor speed of 0.6 MWFSIG following a three-phase-to-ground fault with duration of 130ms in ring and radial network.

3.3.2 Effect of Network Operating Mode on the Generator's CCT

The objective of this study is to examine the effect of network configuration on the magnitude of the generator's CCT. Radial and ring configurations have been considered in this study. The generator is connected at the end of feeder 1(see Figure 3.3). A three-phase-to-ground fault is applied to three locations, F_1, F_2 and F_3, which are 1km, 5km and 10km from the 33 kV grid on feeder 2. The generator's CCT at each of these fault locations has been determined. The corresponding results are summarised in Figure 3.6. This figure shows the values of generator's CCT for the assumed faults at F_1, F_2 and F_3 in ring mode operation compared to radial mode operation. This figure shows that the values of the generator's CCT in ring mode at

the three different fault locations are not much different from each other. In contrast, in the case of radial operation, the value of the CCT related to each fault location is significantly different from one fault location to another. This is because the power flow in feeders operated in ring configuration is more evenly distributed compared the power flow when the feeders are operated in radial mode. Thus, this effect shows on the flow of fault current.

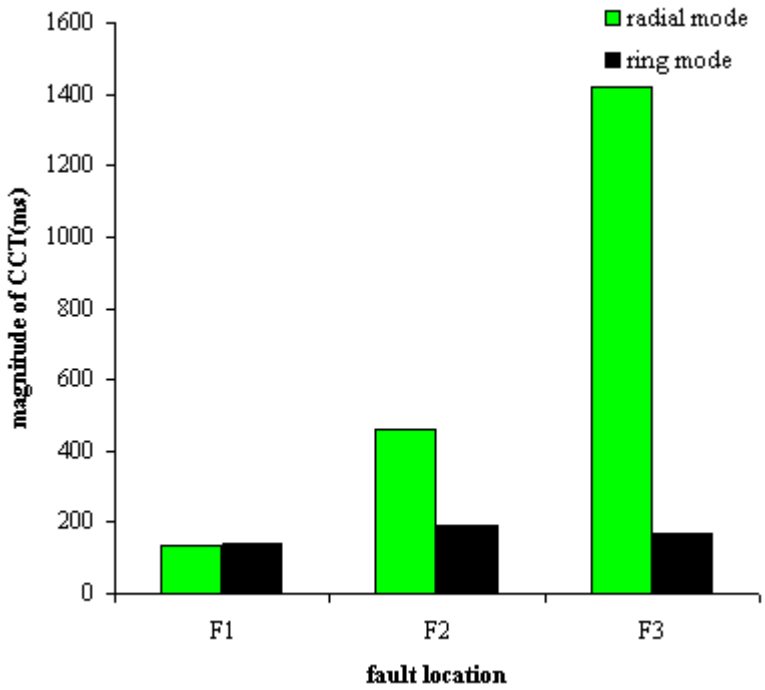

Figure 3.6 Effects of network operating mode on generator's CCT.

3.3.3 Effect of Generator's Location on Its CCT value in Ring Network

The objective of this study is to examine the effect of connecting generator at different locations along a network feeder, in a ring operated network, on the value of the generator CCT. Two locations have been considered, the first is 5km from 33 kV grid on feeder 1 while the other is 15km from 33 kV grid on feeder 1. The corresponding results are summarised in Figure 3.7.

This figure shows that generator's CCT value increases as the generator's location moves along feeder 1 from the 33kV grid. This observation is found to be true for all the considered fault locations at F_1, F_2 and F_3. The figure also shows that the values of the generator's CCT due to faults along feeder 2 varies over a wide range when

the generator is located at the beginning of feeder 1, which is 5km from 33 kV grid on feeder 1 compared to its location at the end of the same feeder, which is 15km from 33 kV grid on feeder 1.

This can be explained with reference to Figure 3.8 and Table 3.1. Although the investigated system is operated in ring network operation, where the power flow is evenly distributed within the ring feeder, the current flow from the DG is divided into two currents I_{DG1} and I_{DG2} (see Figure 3.8 (a) and (b)). These currents are divided evenly during normal and fault network conditions when the DG is located at the end of the feeder compared to its location at the beginning of feeder. Table 3.1 shows the average values of I_{DG1} and I_{DG2} current through phase a before and during a fault condition for fault at location F2 with fault duration of 120 ms. I_{DGN1} and I_{DGN2} are I_{DG1} and I_{DG2} currents through phase a before fault condition respectively. I_{DGF1} and I_{DGF2} are I_{DG1} and I_{DG2} currents through phase a during fault condition respectively. It has been found that, the magnitudes of I_{DGN1} and I_{DGN2} are the same when the DG is connected at the end of the feeder compared to its connection at the beginning of the feeder. The difference between magnitudes of I_{DGF1} and I_{DGF2} is significantly less when the DG location is at end of the feeder compared to the DG location at the beginning of the feeder.

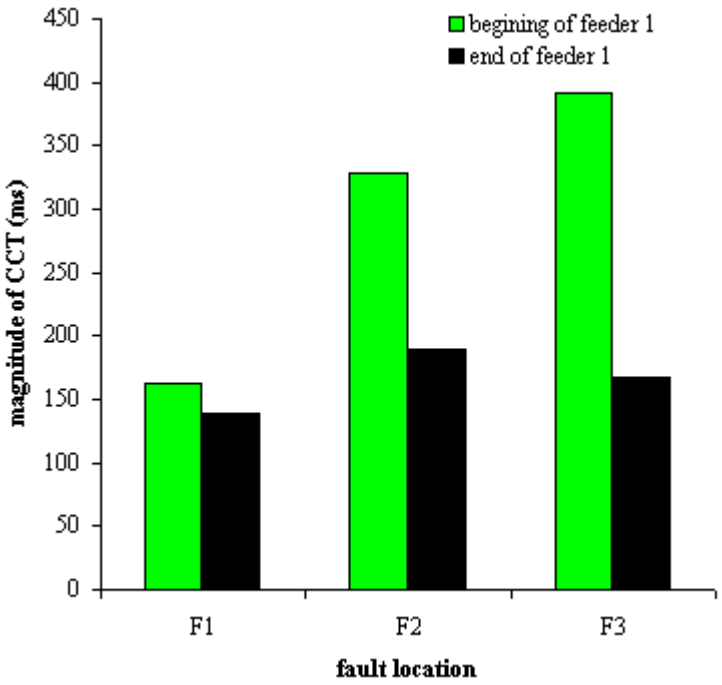

Figure 3.7 Effects of tripping sequence on generator's CCT in ring network.

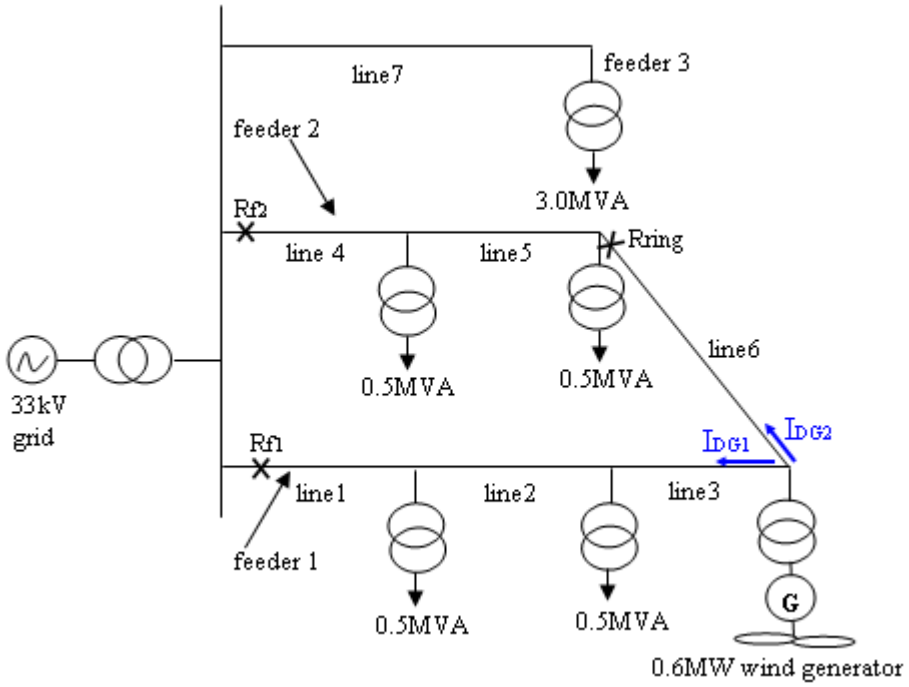

(a)

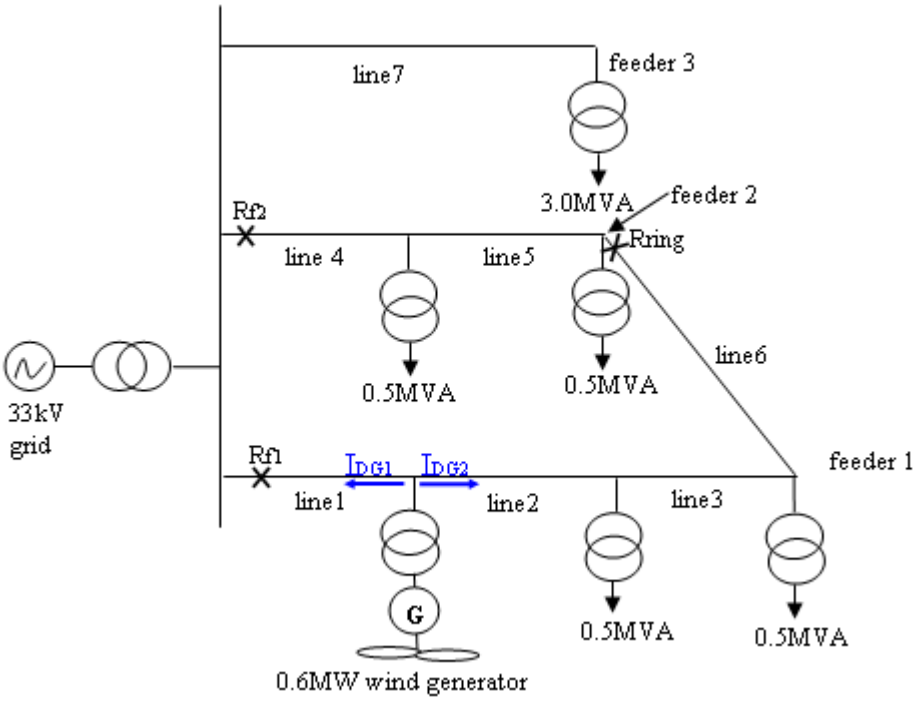

(b)

Figure 3.8 Schematic diagram of investigated distribution network with two different DG locations: (a) end of feeder 1and (b) beginning of feeder1.

Table 3.1

Average value of phase a of I_{DG1} and I_{DG2} during normal and fault conditions for two different DG locations: (a) end of feeder 1and (b) beginning of feeder1.

DG location	I_{DG1} and I_{DG2} flow through phase a during normal and fault condition			
	I_{DGN1}(A)	I_{DGN2}(A)	I_{DGF1}(A)	I_{DGF2}(A)
(a) end of feeder 1(15km from 33 kV grid)	21	21	499	508
(b) beginning of feeder 1 (5km from 33 kV grid)	31	49	465	502

3.3.4 Effect of Multi-Generator and Their Equivalent on the CCT in Ring Network

The objective of this study is to examine the effect of connecting more than one generator located at different network locations on the CCT of the generators under consideration. Two case studies have been considered. The first case study involves two generators G1 and G2 with rated values of 0.6 MW and 1.8 MW respectively. The first generator is connected at the end of the feeder through a 0.69/11 kV transformer while the second generator is connected directly at the 11 kV bus at the substation. In the second case study an equivalent generator, G3, with total rating of 2.4 MW is connected directly to the 11 kV bus.

G2 and G3 are represented in the model as 3 coherent machines and 4 coherent machines respectively. G2 and G3 is modelled using the machines parameters of G1. G2 is 3 times G1 and G3 is 4 times G1. Both G2 and G3 can be derived using the facilities within the PSCAD/EMTDC software call “modelling coherent machines” (see 3.2.1(d)). It is used to find the parameters of the generator based on another generator with known parameters. Table 3.2 shows the inertia constants of the wind turbine and generator rotor, H_T and H_G respectively for G1, G2 and G3.

Table 3.2

Inertia constant of wind turbine and generator rotor for G1, G2 and G3.

Generator	Inertia constant of wind turbine and generator rotor	
	H_T(s)	H_G(s)
G1	3.2	0.5
G2	3.2	1.5
G3	3.2	2.0

The corresponding results are summarised in Figure 3.9. This figure shows according to the results from the first case study that the CCT of G2 increases significantly with the fault location from F_1 to F_3 compared to that related to G1. This is because the current component I_{DG1} and I_{DG2} from G1 are more evenly divided compared to those associated with G2 (see figure 3.8(a) and figure 3.10). The second case study, on the other hand reveals the CCT of G3 is generally greater than those due to G1 and G2. This is because the significant increase in the value of the inertia constant of the generator rotor has an appreciable effect on the CCT [69]. By increasing the value of H_G from 0.5s to 1.5s, the CCT of G3 has increased significantly compared to those due to G1 and G2 at fault location F_2 and F_3. The CCT of the three generators G1, G2 and G3 due to a fault at F_1 are the lowest and they are close to each other.

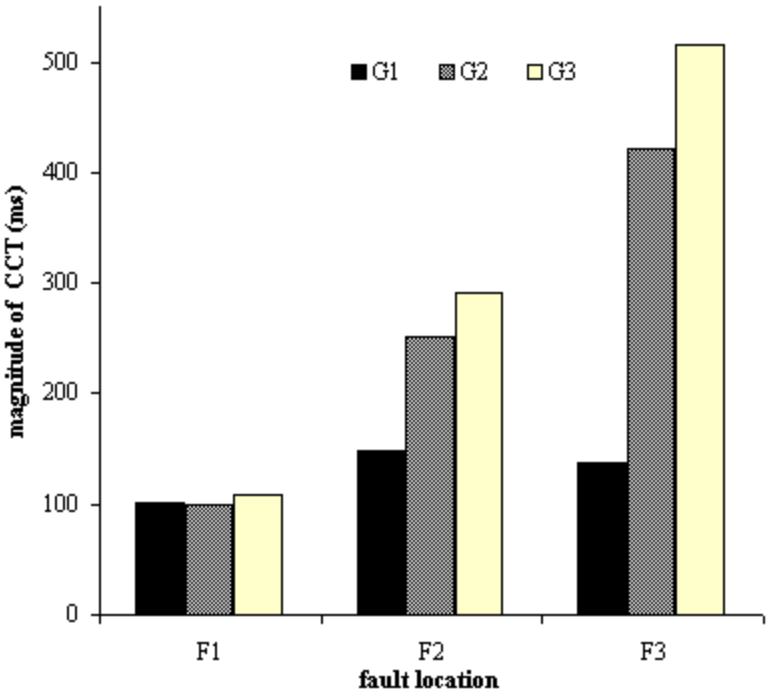

Figure 3.9 Effect of different generator location at generator's CCT on ring network.

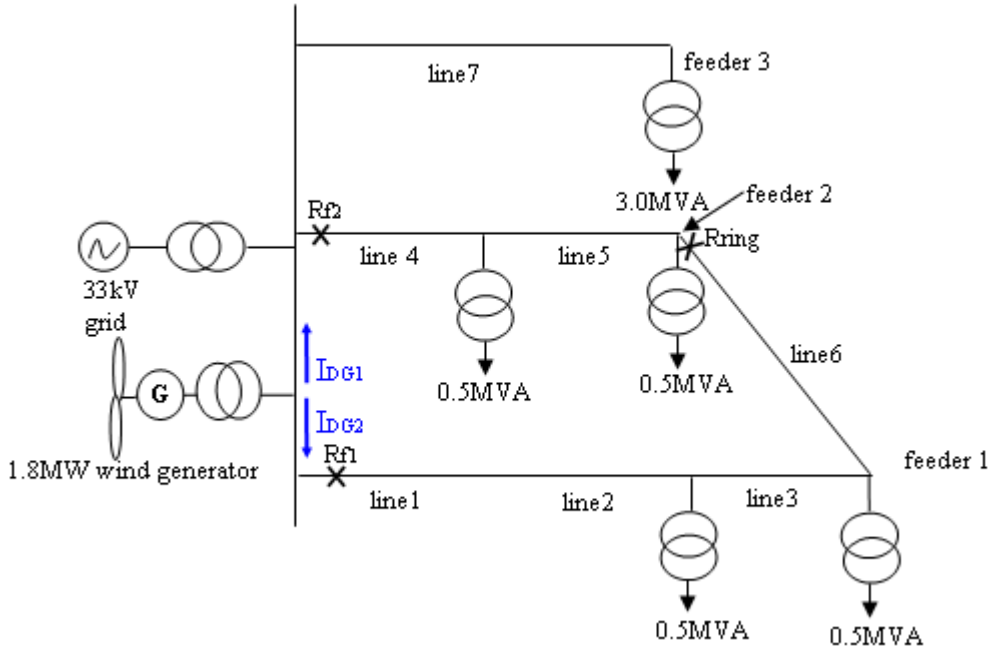

Figure 3.10 Schematic diagram of investigated distribution network with DG connected directly to 11 kV bus.

3.3.5 Effect of Tripping Sequence of Protective Devices on Generator's CCT in Ring Network

The objective of this study is to examine the effect of the tripping sequence of the protective devices on the generator's CCT in a ring network. Ring connector R_{ring} and either feeder relay R_1 or R_2 should be tripped to isolate the faulted feeder from the rest of the network for any fault that occurs within the ring. A 2000 ms duration three-phase-to-ground fault, i.e., sustained fault, is assumed at F_1 on feeder 2. R_{ring} and R_2 are required to open their associated circuit breakers to ensure (i) the isolation of the assumed fault on feeder 2 and (ii) the prevention of the tripping of the wind generator connected to feeder 1. Values t_{ring} and t_{F2} refer to tripping times of R_{ring} and R_2 respectively. R_{ring} and R_2 are operated according to two different tripping sequences; (a) t_{ring} greater than t_{F2} and (b) is t_{ring} lower than t_{F2}. The same investigation is repeated for fault locations F_2 and F_3 on feeder 2. The corresponding results are summarised in Figure 3.11. This figure shows that the tripping in sequence (a) causes a decrease in the magnitude of the generator's CCT with the fault location as it moves from F_1 (beginning of Feeder 2) to F_3 (end of Feeder 2), while the tripping sequence (b) causes an increase in generator CCT with fault location.

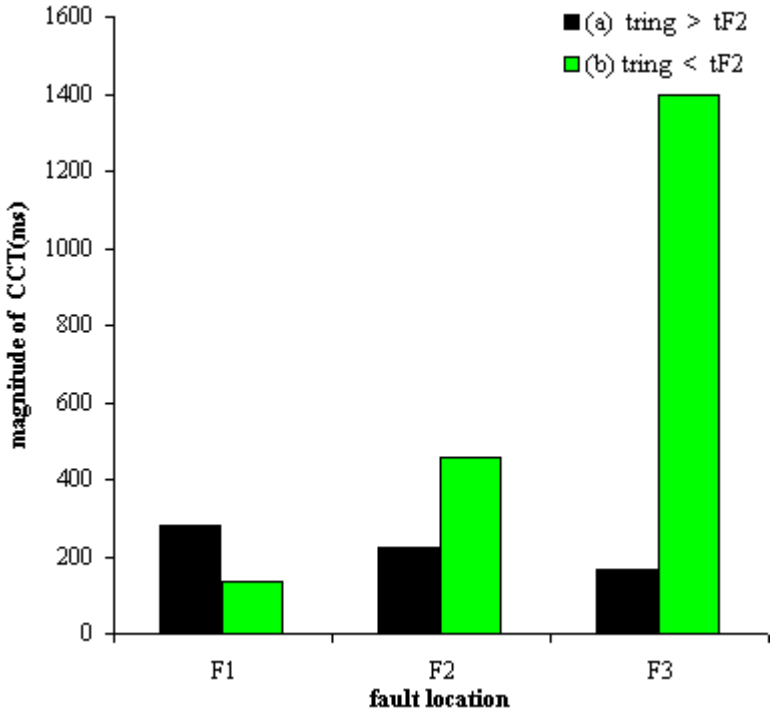

Figure 3.11 Effects of the tripping sequence on generator's CCT in ring network.

3.3.6 Effect of Opening the Ring at Different Locations on Generator' CCT value in Ring Network

The objective of this study is to examine the effect of opening the ring at different locations on the generator's CCT. For the purpose of comparison two case studies have been considered. In case study 1 three circuit breakers $R_{Ring1,}$ R_{Ring2}, R_{Ring3} are installed at three different locations in the ring feeder as shown in Figure 3.12. R_2 and R_{Ring1}, R_{Ring1} and R_{Ring2}, R_{Ring2} and R_{Ring3} are tripped to clear faults at F_1, F_2 and F_3 respectively. However, in case study 2 only R_{Ring3} is installed at line 6 (see Figure 3.3) and consequently R_2 and R_{Ring3} need to be tripped to clear all faults at the three considered fault locations. F_1 and F_2 refer to 1km and 5km at feeder 2 while F_3 refer to 1km at line 6. The corresponding results are summarised at Figure 3.13. This figure shows that the value of the generator's CCT in each fault location is significantly different from each other when the system under investigated is operated as described in case study 1 compared to case study 2. Besides, the magnitude of the generator's CCT increases with the fault location when system is operated according to case study 1. Figure 3.13 also reveals that for faults at F1, the value of the generator CCT in both case studies are very close to each other. It is also shown in this figure that longer fault clearance time can be allowed for faults

occurring at F_2 and F_3 when lines 5 and 6 are protected using ring connectors that are located at both ends of each line section.

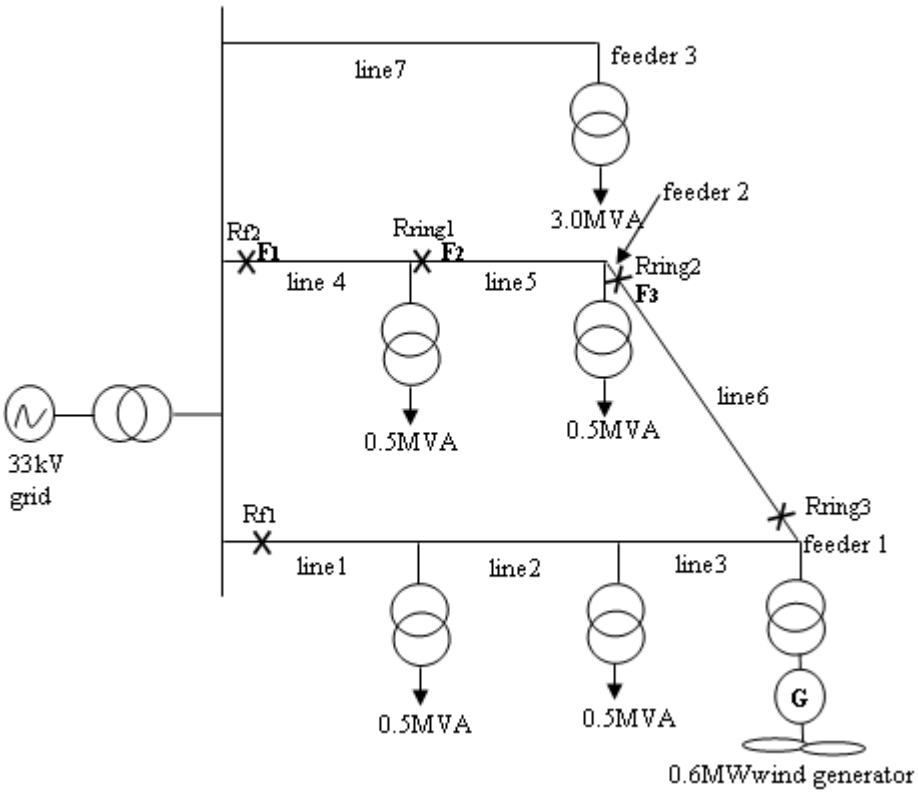

Figure 3.12 Schematic diagram of the investigated distribution network with ring connectors located at 3 locations in network.

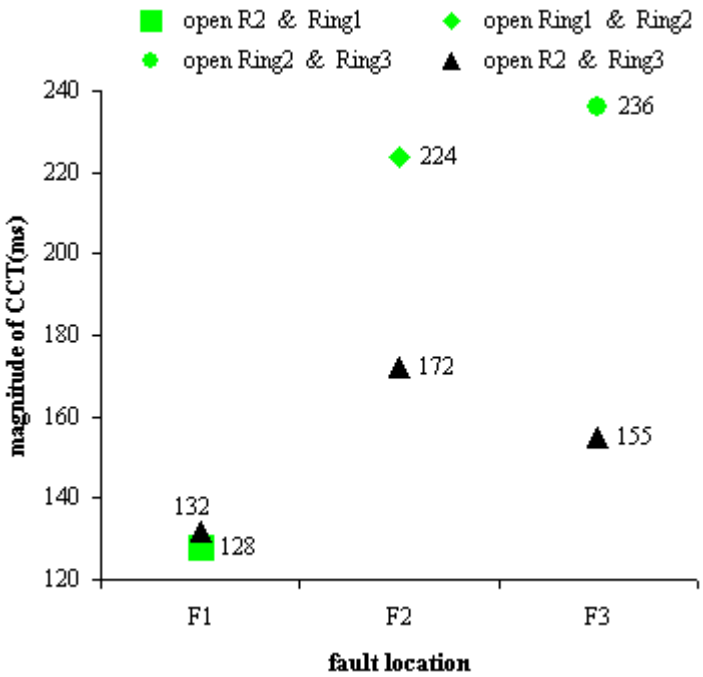

Figure 3.13 Effect of opening the ring connector at different network location on generator CCT.

The following can be concluded from the simulation results obtained in this investigation:

a. The value of the generator's CCT obtained and the overall response of the main machine parameters after fault clearance show that the transient stability of DG is improved in a ring network compared to a radial network.

b. For fault events on the MV network with DGs located at an adjacent healthy feeder from the faulty feeder, the required fault tripping time of the protective relay on the faulty feeder to preserve the operation of DGs at healthy feeder during fault condition is significantly different between ring and radial mode of operations, for certain fault location e.g., F_3 (see section 3.3.2). Thus, time graded protection coordination based on conventional directional overcurrent in ring network [3] might become incompatible with presence of DGs in a ring network. Apart from that, it was found in the case study whereby the feeder is divided into several line sections by installation of additional circuit breakers in the ring feeder, a longer time can be allowed to detect and isolate the faulty section during fault condition while maintaining the stability of the DG.

c. Furthermore, optimisation of the generator location and tripping sequence needs to be taken into consideration when developing novel protection in a ring network with DGs in order to maintain the stability of DG, so that the operation of DG can be continued during fault condition.

3.4 Investigation into the Sustainability of Different DG Technologies during Temporary Fault

Due to the continued increase of penetration of DGs, it has become increasingly important that the DG remain in service during network temporary fault events as far as possible in order to maximise the benefits of interconnection of DGs and increase the overall power delivery reliability. Investigation into the sustainability of

different DG technologies during temporary faults in overhead distribution network should be carried out to (i) assess the possibility of preserving DGs in service as far as possible to optimise electric supply continuity and (ii) identify the requirements of auto-reclosing scheme in distribution networks with high penetration of DGs. In this section, the dynamic behaviour of two different type of wind generation technologies, FSIG and DFIG, during various type of temporary fault in radial and ring operated networks has been assessed. This is followed by an investigation into the application of a Single-Phase Auto-Reclosing (SPAR) scheme in a distribution network with DG.

3.4.1 Transient Performance of DFIG under Network Fault Condition

In this section, the dynamic behaviour of 2.0 MW DFIG during network fault condition is evaluated. The power system under investigation is shown in Figure 3.3. In this study, the grid is represented by a voltage source with short circuit level of 40 MVA to simulate a weak distribution network. The 2.0 MW DFIG is connected at the end of feeder 1 through a 2.5 MVA, 0.69/11 kV step up transformer. The detail of the other network parameters can be found in section 3.2.3. A three-phase-to-ground fault is assumed at fault point F_4 which is 1km (from the grid) on feeder 1 when the network is operated in radial mode and then in ring mode. The fault is assumed at t = 35 s for a duration of 200 ms. Figure 3.14(a) to (g) show the variation of main generator output parameters following the fault condition in the radial network.

Immediately after the fault occurs at t = 35 s the generator terminal voltage drops as shown in Figure 3.14(a), and this causes the corresponding stator and rotor flux to drop, which results in a significant reduction in generator active powers as shown in Figure 3.14(b). The active power reduction activates the control scheme at the RSC and after approximately t = 35.1s, the magnitude of active power has been maintained at a fixed level. Meanwhile, as shown in Figure 3.14(c) and (d), changes in both electromagnetic torque and reactive power due to fault inception also activate the control scheme at the RSC. As the results of that, both of these parameters had been controlled at fixed level after t = 35.1 s. Due to the decoupling control of active and reactive power, variation of rotor speed will not be transferred to active power and electromagnetic torque. As shown in Figure 3.14(e), the rotor speed kept

increasing after fault inception while the active power and machine torque have been retained at a fixed level after t = 35.1 s, as shown respectively in Figure 3.14(b) and (c).

The variation of rotor speed causes a rise of 40% in the magnitude of the DC link voltage as shown in Figure 3.14(f). This can be explained as follows: the DC link act as a storage element to provide the machine with the required reactive power so that the DFIG can generate sufficient active power [44-45]. In doing so, the current may be supplied or drawn from the rotor side converter and increase the DC voltage value [44-45]. As shown in Figure 3.14(g) after fault inception, a high transient rotor current is produced and flows towards the DC link. Because the generator terminal voltage drops immediately after the fault, the exchange of power between the DC link capacitor and the grid has been limited. Thus, the additional energy goes to charge the DC link capacitor and increase the DC link voltage to 40% of its prefault value, as shown in Figure 3.14(f).

After the fault is cleared, the terminal voltage rises instantly. Both generator active power and electromagnetic torque regain their prefault value immediately. The rotor speed is restored to the prefault value approximately 10 seconds after fault clearance, as shown in Figure 3.15.

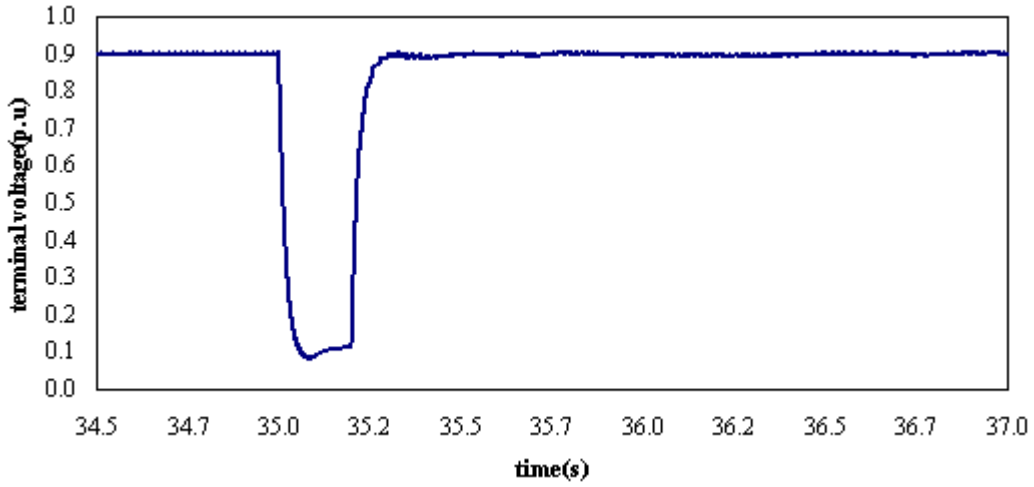

(a)

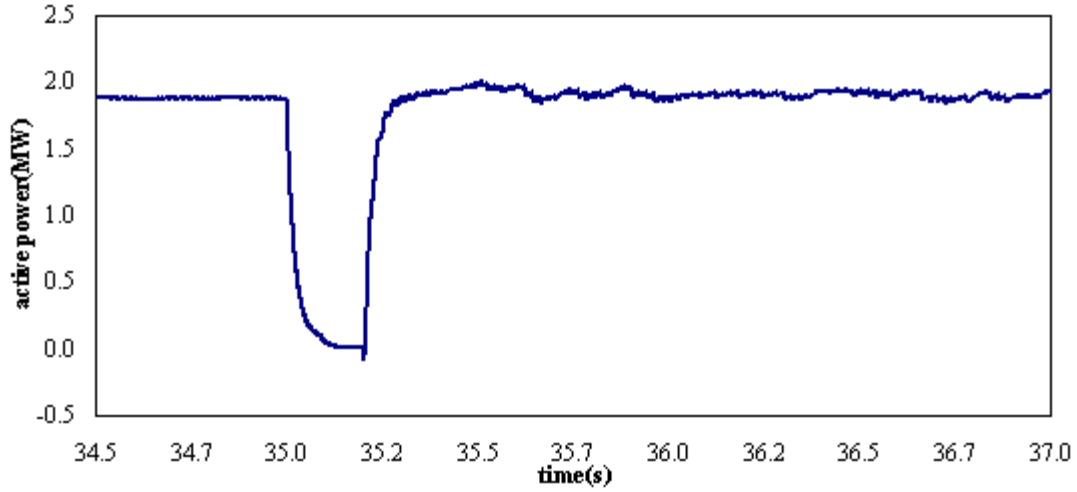
active power(MW)
2.5
2.0
1.5
1.0
0.5
0.0
-0.5
34.5
34.7
35.0
35.2
35.5
35.7
36.0
36.2
36.5
36.7
37.0
time(s)

(b)

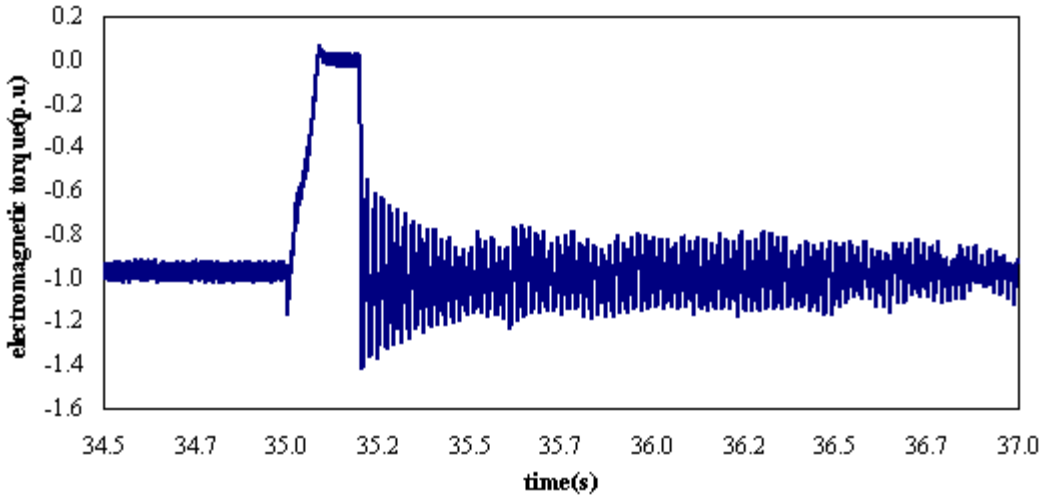
electromagnetic torque(p.u)
0.2
0.0
-0.2
-0.4
-0.6
-0.8
-1.0
-1.2
-1.4
-1.6
34.5
34.7
35.0
35.2
35.5
35.7
36.0
36.2
36.5
36.7
37.0
time(s)

(c)

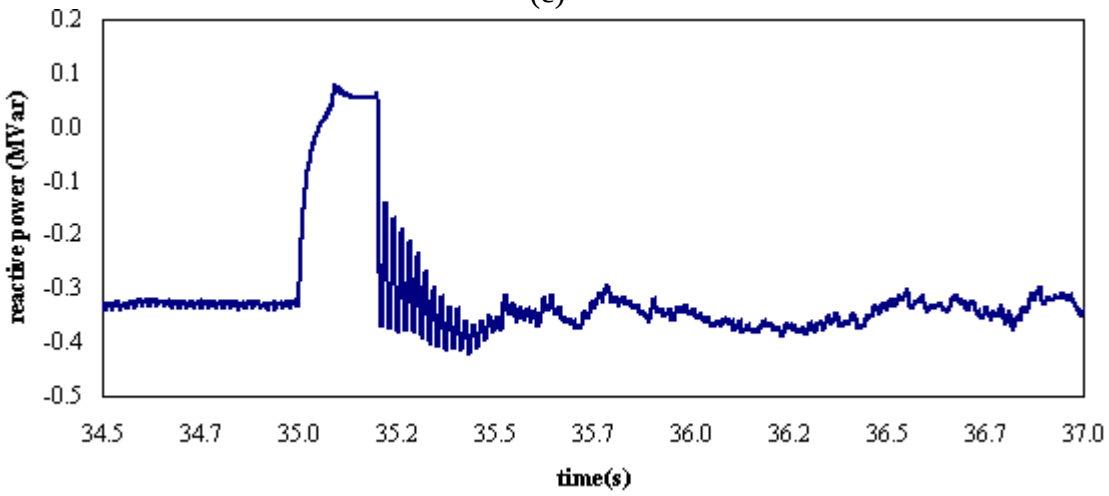
reactive power (MVar)
0.2
0.1
0.0
-0.1
-0.2
-0.3
-0.4
-0.5
34.5
34.7
35.0
35.2
35.5
35.7
36.0
36.2
36.5
36.7
37.0
time(s)

(d)

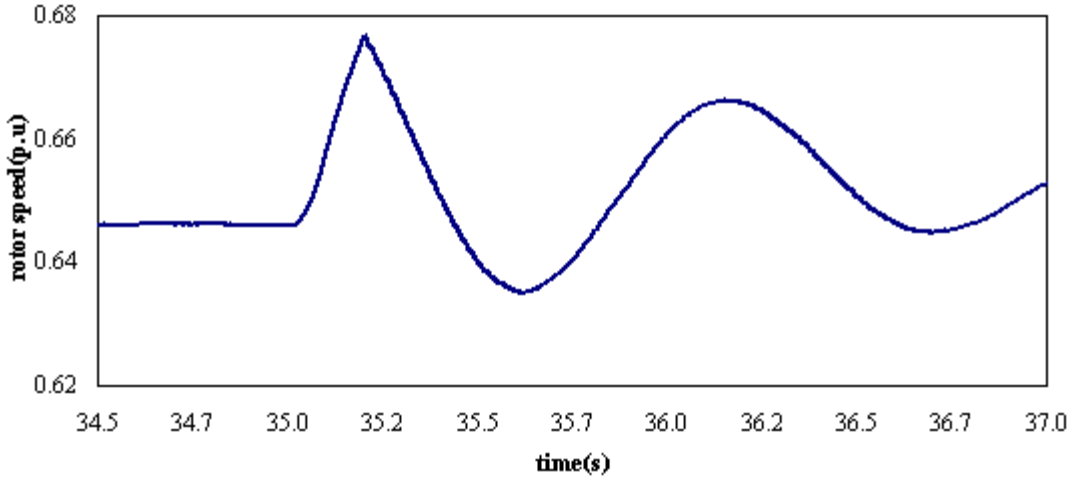

(e)

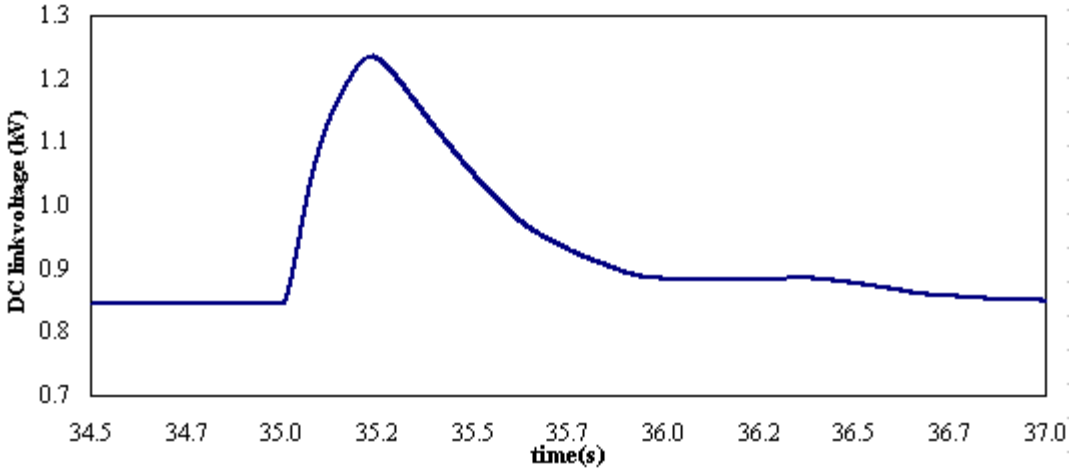

(f)

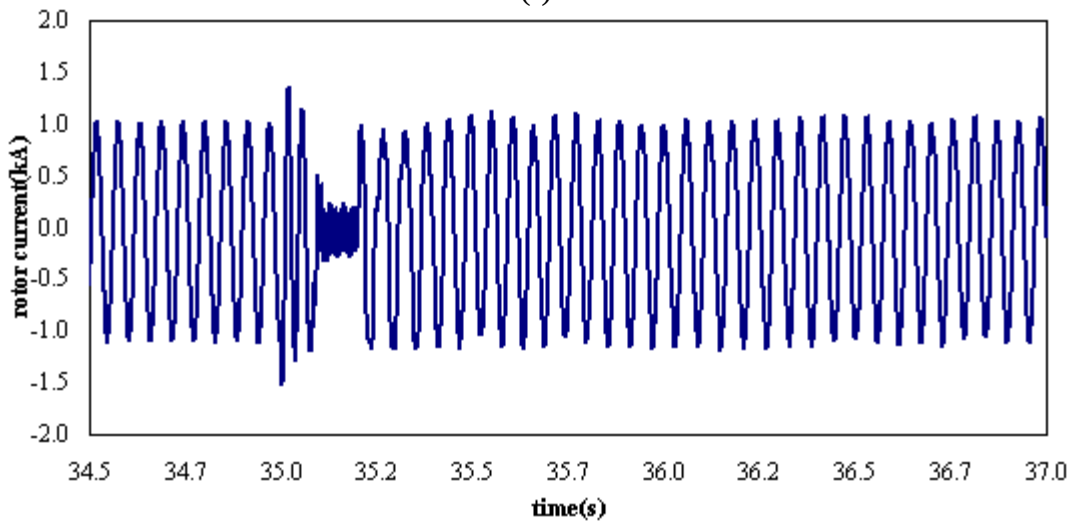

(g)

Figure 3.14 Transient performance of 2.0 MW DFIG following a three phase network fault with a duration of 200 ms in radial network: (a) terminal voltage (b) active power (c) electromagnetic torque (d) reactive power (e) rotor speed (f) DC link voltage and (g) rotor current .

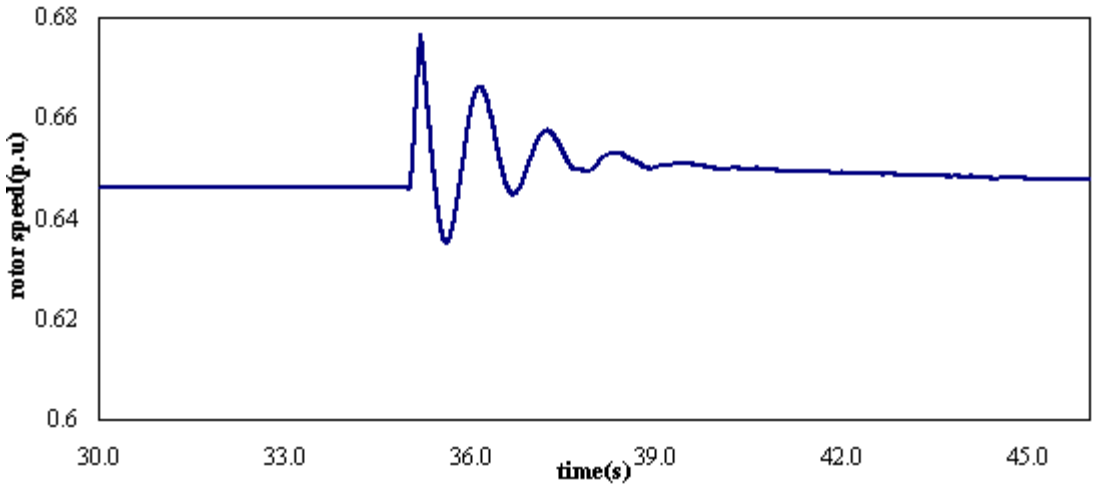

Figure 3.15 Variation of generator rotor speed before and after fault inception.

3.4.2 Comparison between Transient Performance of FSIG and DFIG in Radial and Ring Operated Network

In order to compare the transient performance of 2.0 MW FSIG and DFIG for the considered network fault condition in section 3.4.1, the 2.0 MW DFIG, which is located at the end of feeder 1 in the investigated system shown in Figure 3.3, is replaced with the 2.0 MW FSIG. Figure 3.16(a) to (c) show the variation of generator's terminal voltage, active power and rotor speed of the 2.0 MW DFIG in radial and ring network after fault inception. Figure 3.17(a) to (c) show the variation of generator's terminal voltage, active power and rotor speed of the 2.0 MW FSIG in radial and ring network after fault inception.

It can be seen from Figure 3.16(a) and (b) that, for the considered network fault, during fault inception period (from t = 35 s to t = 35.2 s), the dynamic behaviour of the DFIG is slightly better in the ring network compared to the radial network. The magnitude of voltage drop and active power after fault inception is slightly less in the ring network compared to the radial network. By contrast, it is shown in Figure 3.17(a) and (b) that, the magnitude of voltage drop and active power for FSIG after fault inception has no significant difference in both ring and radial networks.

During post fault period (from t = 35.2 s onward), it is shown in Figure 3.16(a) to (c) that, the dynamic behaviour of the DFIG in both radial and ring network has no significant difference. Figure 3.16(c) shows that oscillation pattern in the rotor speed

after fault clearance is similar both ring and radial operation modes. In contrast, it is shown in Figure 3.17(a) to (c) that, the dynamic behaviour of the FSIG after fault clearance is significantly better in the case of the ring network compared to the radial network. The rate of oscillation in terminal voltage, active power and rotor speed is less significant in the ring network compared to the radial network. The machine parameters restore their prefault conditions faster in the ring network compared to the radial network.

Apart from that, it can be seen from Figures 3.16 and 3.17 that, for the considered network fault, the active power of the DFIG is considerably improved compared to that related to the FSIG in ring network. The minimum active power drop of the DFIG and FSIG during fault in the ring network is 0.3 p.u and 0.01 p.u respectively. After fault clearance, due to the action of the vector control scheme installed at the DFIG, the machine parameters restore their prefault conditions sooner for the DFIG, compared to the FSIG, in both ring and radial networks.

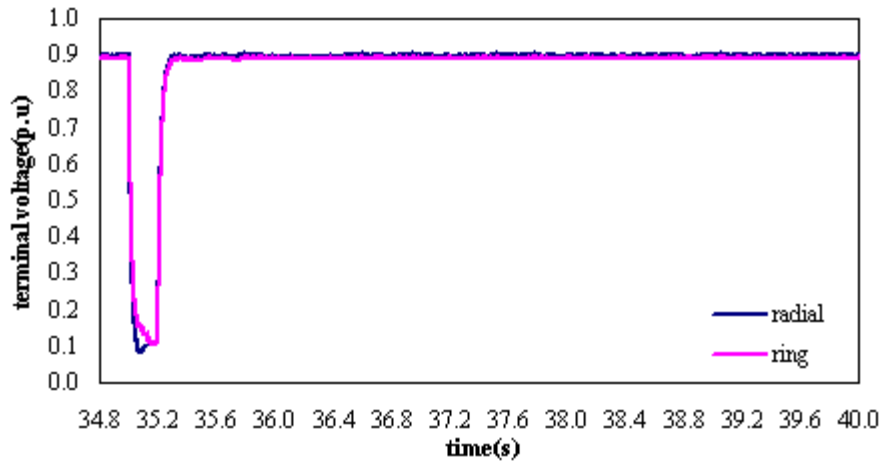

(a)

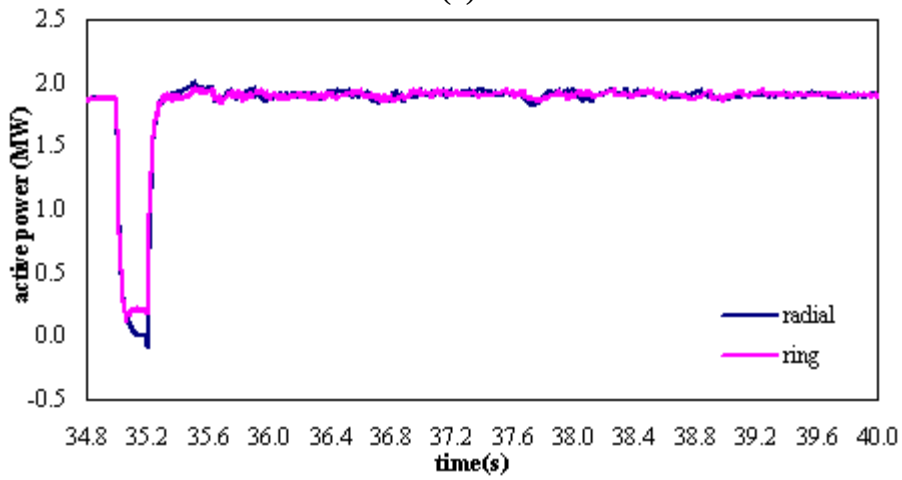

(b)

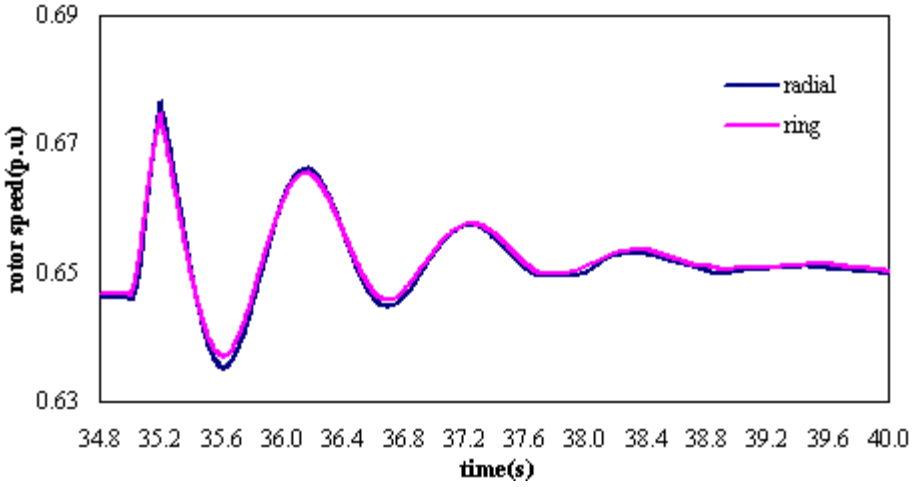

(c)

Figure 3.16 Variation of (a) terminal voltage, (b) active power and (c) rotor speed of 2.0 MW DFIG following a three-phase-to-ground fault with duration of 200 ms in ring and radial network.

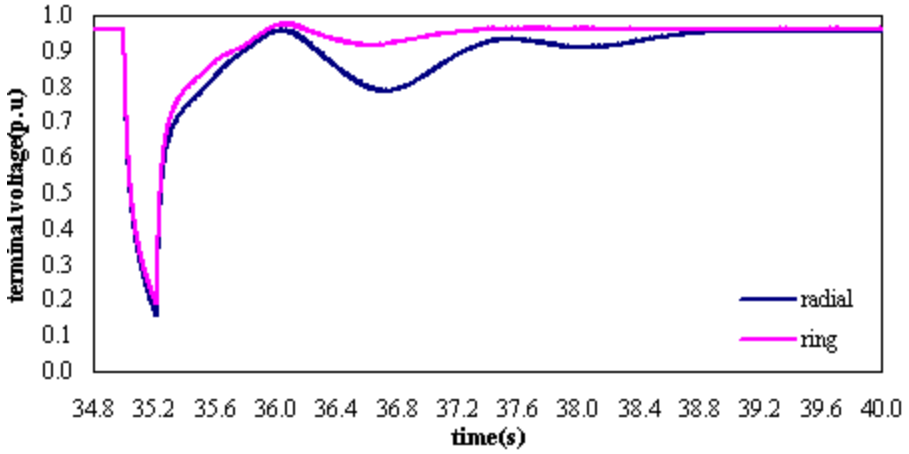

(a)

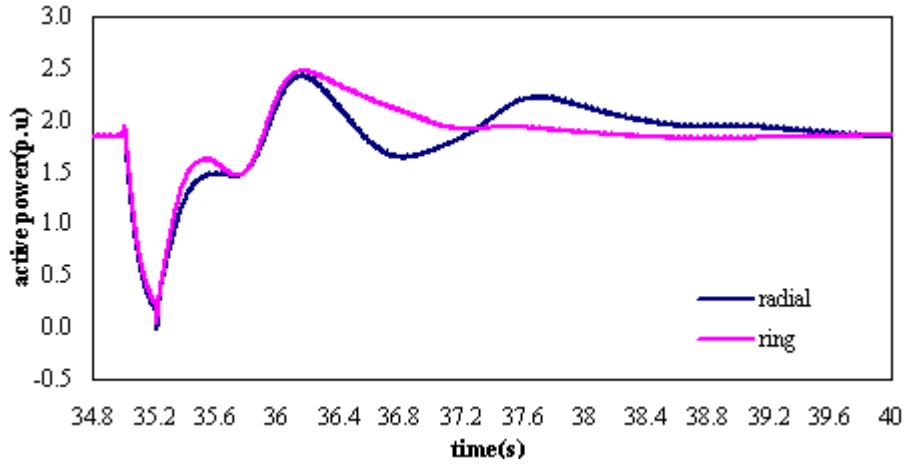

(b)

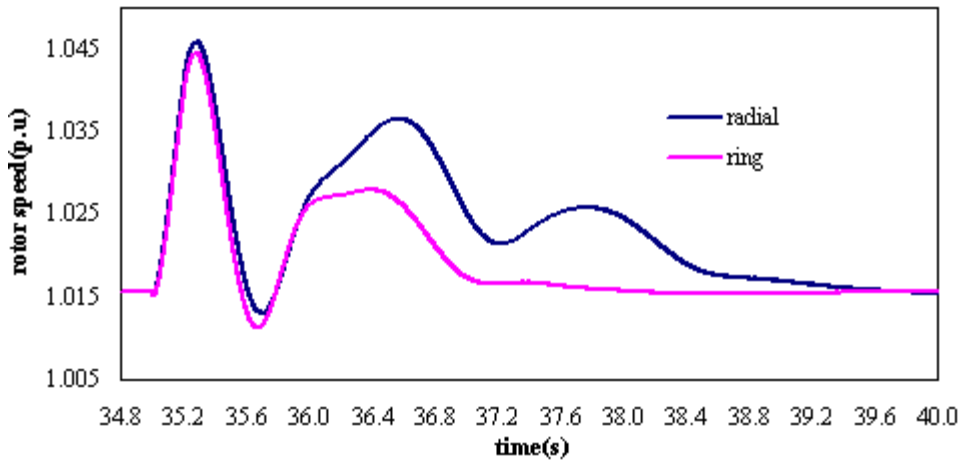

(c)

Figure 3.17 Variation of (a) terminal voltage, (b) active power and (c) rotor speed of 2.0 MW FSIG following a three-phase-to-ground fault with duration of 200 ms in ring and radial network.

It has been found in this investigation that, for the above fault condition, the DFIG can not retain pre-fault values when the fault duration is greater than 510 ms and 587 ms in radial and ring respectively. On the other hand, FSIG can not retain its pre-fault values when fault duration is greater than 229 ms and 278 ms. These values are therefore considered as the generator's CCT for the DFIG and FSIG in radial and ring networks respectively.

It can be concluded from the simulation results obtained in this investigation that, for a fault event located at the DG feeder, the transient performance of both the DFIG and FSIG is considerably improved in a ring network compared to a radial network. Furthermore, a longer fault clearance time is allowed while maintaining the transient stability, of both the DFIG and FSIG in a ring network compared to a radial network. It has been observed that, the DFIG has a better transient performance following a three-phase-to-ground fault condition, compared to the FSIG, in both radial and ring operated networks. The operation of DGs should be continue in fault condition to maximise the benefits of the DG interconnection. Operating FSIG in a network with radial mode will be considered as the worst case scenario in deciding the tripping time setting of circuit breakers.

3.4.3 Effect of Unsymmetrical Single-Line-to-Ground Fault Event on the Transient Stability of DG and Operation of G59 Protection

Considering that 80% of faults on distribution networks are temporary and most of them are unsymmetrical single-line-to-ground (SLG) faults [3-4], it is becoming increasingly important that the DG should remain in service during temporary SLG faults as far as possible for the benefit of utilities, DG developers and customers. Meanwhile, the requirement in technical recommendation G59 [46] states that DGs need to be protected against over/under voltage during any abnormal network conditions to prevent islanding operation. Phase voltage fluctuation of DGs outside the limits of +/-10% for over 0.5 seconds is not permitted. The effect of unsymmetrical network faults on the transient stability of DGs and consequence operation of G59 has been reported in reference [87] for Conventional Synchronous Generator (CSG). Induction generators whether FSIG or DFIG, were not covered in this research study. The detailed comparative analysis reported in [45, 70] shows that different DG technology types have their own unique operational characteristics which will affect their transient response during network faults. These need to be taken into consideration when assessing the possibility of maintaining operation of DGs during unsymmetrical faults. Therefore, in this section, the effect of temporary SLG faults on the transient stability of FSIG and DFIG and the operation of G59 protection is reported. The aim of this study is to investigate the sustainability of FSIG and DFIG during temporary SLG fault conditions, while complying with the under/over voltage protection requirements of G59.

A three-phase symmetrical fault, phase a-b-c-to-ground fault (ABCG) and SLG fault, phase a-to-ground fault (AG) have been considered in this investigation to compare the effects of symmetrical and unsymmetrical faults on the dynamic behaviour of both FSIG and DFIG. The fault is assumed at the fault point F_4, which is 1km (from the grid) on feeder 1 of the investigated power system (see Figure 3.3), when the network is operated in radial mode and then in ring mode. The fault is assumed at t = 35 s for a duration of 200 ms. The variation of terminal voltage, generator active power and rotor speed of the 2.0 MW DFIG following AG and ABCG faults in a radial network and a ring network are shown in Figure 3.18 and 3.19 respectively. The variation of terminal voltage, generator active power and rotor speed of the 2.0

MW FSIG following AG and ABCG faults in radial network and ring network are shown in Figure 3.20 and 3.21 respectively.

It is shown in Figures 3.18 to 3.21 that, the transient performance of both FSIG and DFIG for the AG fault is much better compared to the ABCG fault condition. The terminal voltage and active power drop is less and the rotor speed increases less during the AG fault compared to the ABCG fault condition. It can be observed from Figure 3.18(a) and 3.19(a) for the 2.0MW DFIG in both radial and ring network, the average voltage drop in AG fault condition is 33% of the generator terminal voltage prior to fault. It also shows in 3.20(a) and 3.21(a) that for 2.0MW FSIG in both radial and ring network, the average voltage drop in AG fault condition is 33% of the generator terminal voltage prior to the fault.

Apart from that, it can be seen from Figure 3.18 and 3.19 that, due to the action of the vector control scheme installed at the DFIG, the observed machine parameters restore their prefault conditions immediately after fault clearance in both AG and ABCG fault events. By contrast, it can be seen from Figure 3.20 and 3.21 that significantly less time is needed for the observed parameters of FSIG to restore their prefault condition in the case of an AG fault compared to an ABCG fault condition.

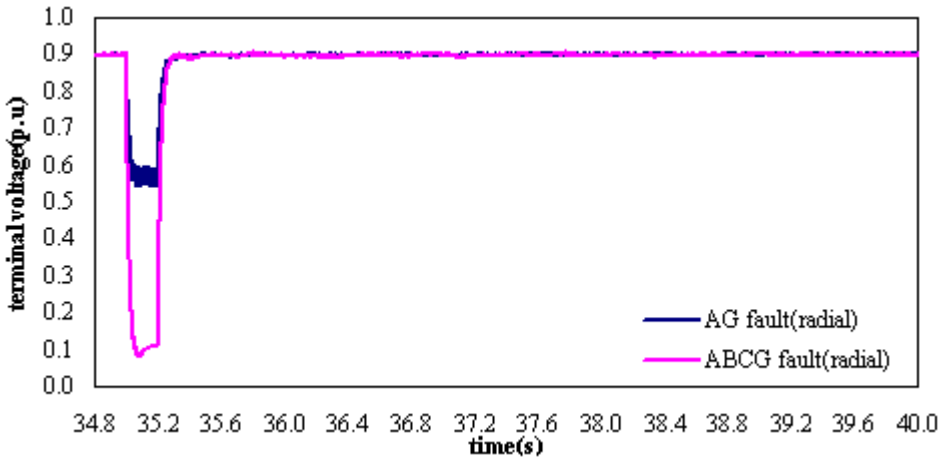

(a)

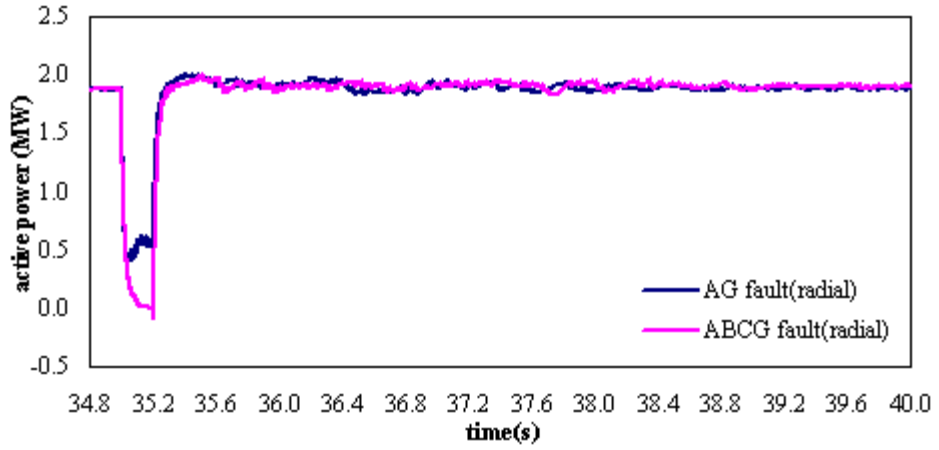

(b)

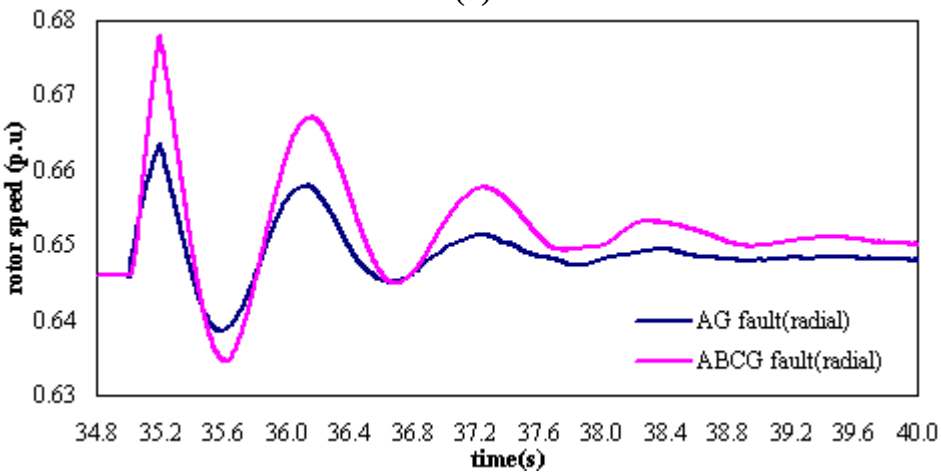

(c)

Figure 3.18 Variation of (a) terminal voltage, (b) active power and (c) rotor speed of 2.0 MW DFIG following a AG and ABCG fault with duration of 200 ms in radial network.

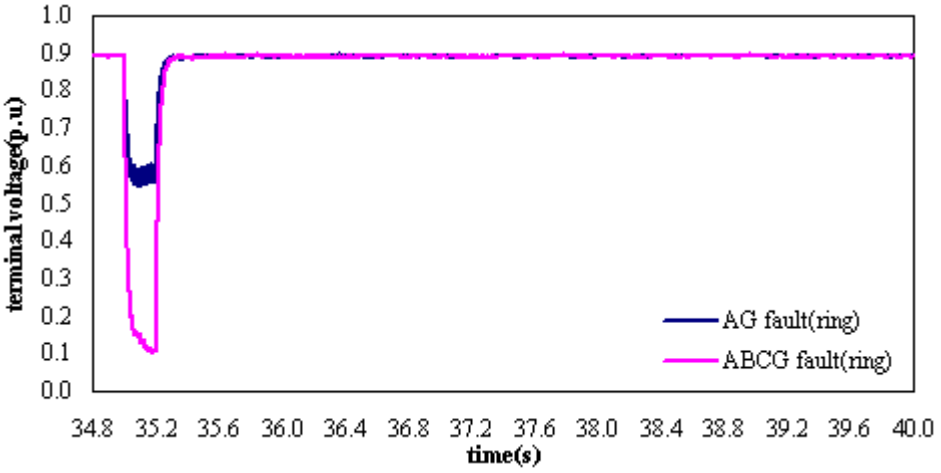

(a)

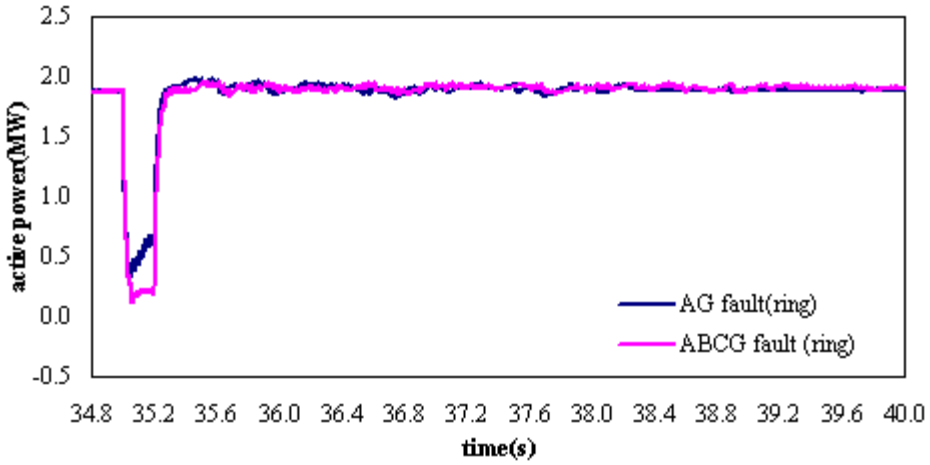

(b)

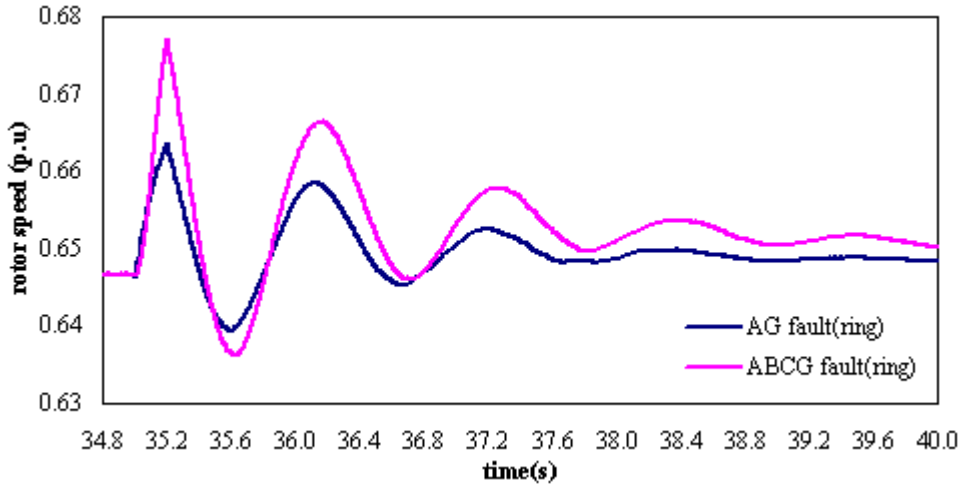

(c)

Figure 3.19 Variation of (a) terminal voltage, (b) active power and (c) rotor speed of 2.0 MW DFIG following a AG and ABCG fault with duration of 200 ms in ring network.

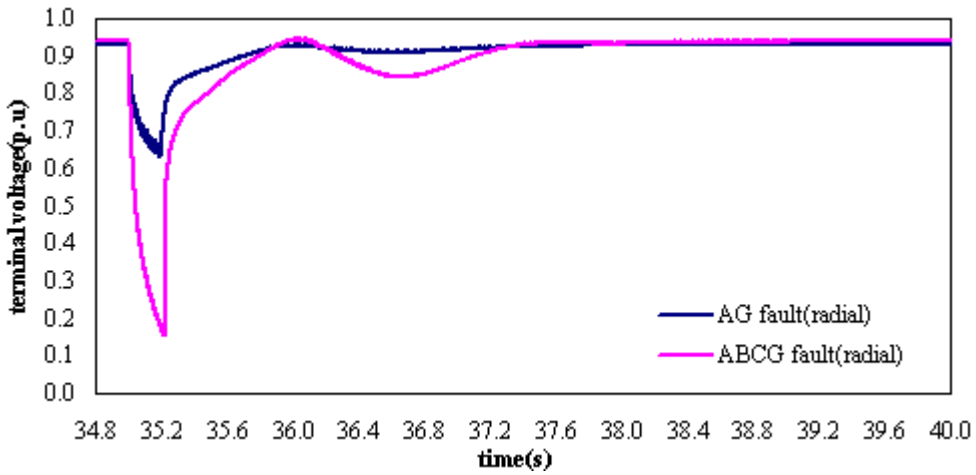

(a)

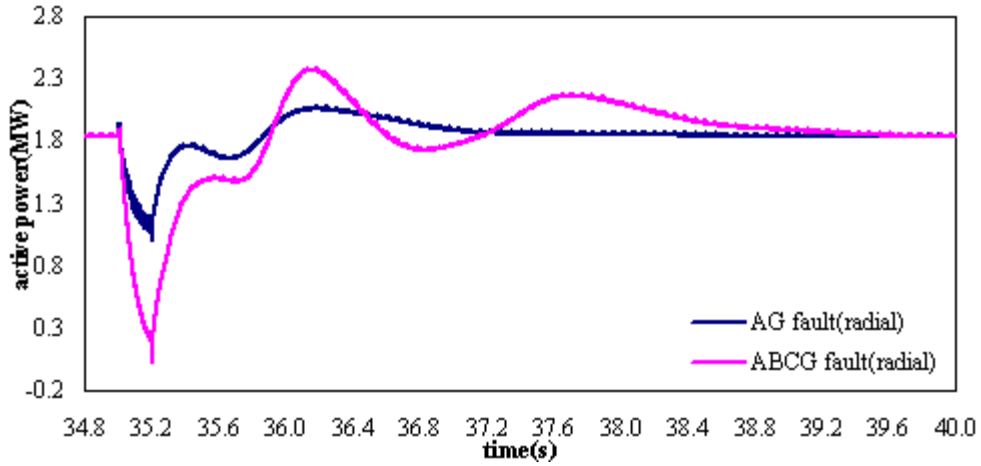

(b)

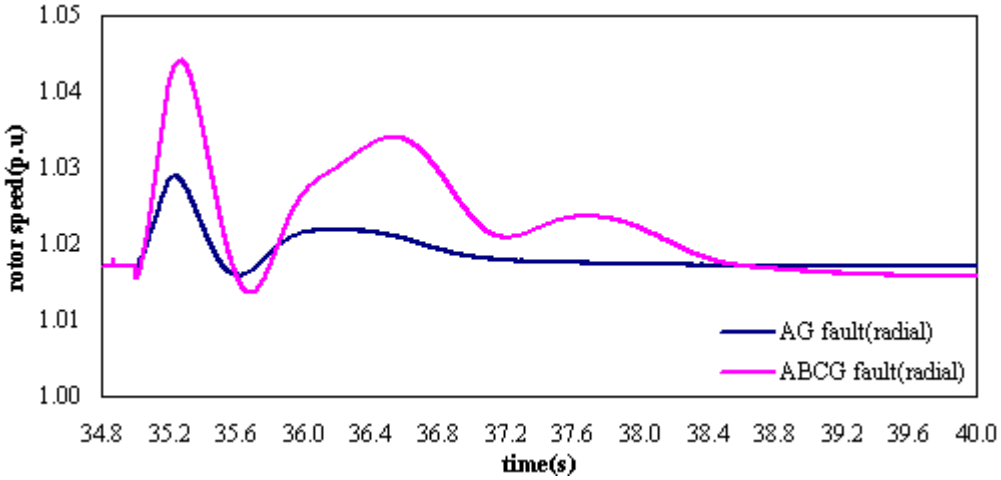

(c)

Figure 3.20 Variation of (a) terminal voltage, (b) active power and (c) rotor speed of 2.0 MW FSIG following a AG and ABCG fault with duration of 200 ms in radial network.

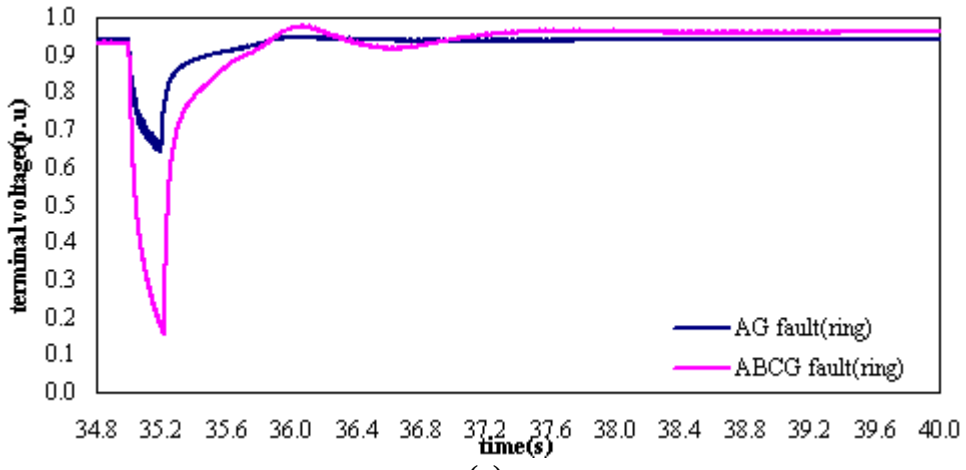

(a)

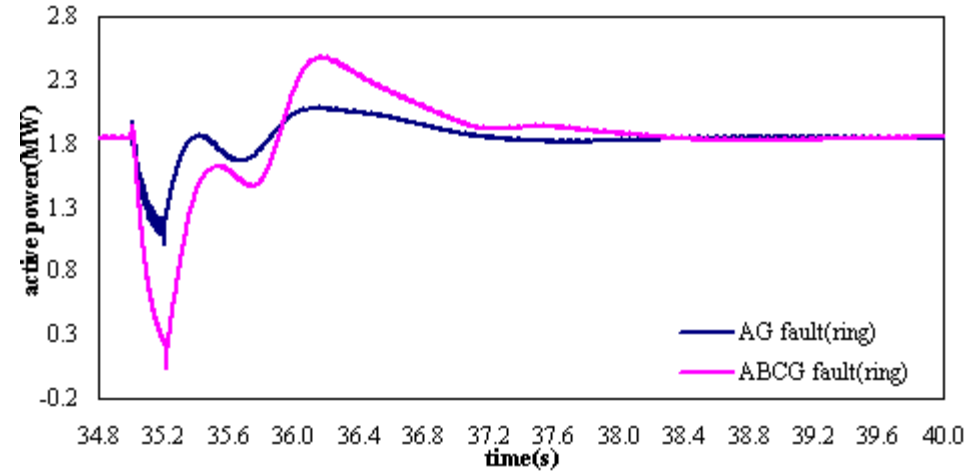

(b)

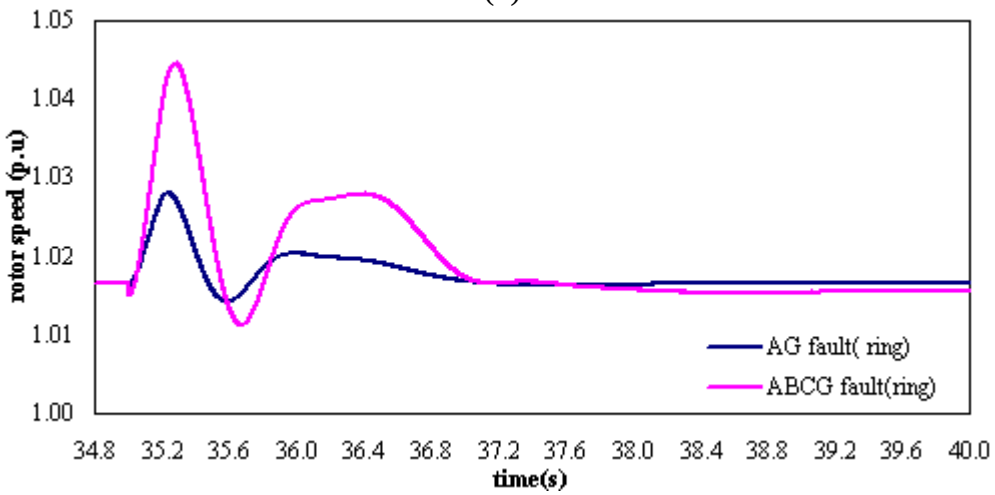

(c)

Figure 3.21 Variation of (a) terminal voltage, (b) active power and (c) rotor speed of 2.0 MW FSIG following a AG and ABCG fault with duration of 200 ms in ring network.

It can be concluded from the simulation results obtained in this investigation that a SLG fault is not critical compared to three phase symmetrical faults. Both FSIG and DFIG remain stable during a SLG fault condition although the voltage dip during a fault condition drops below the voltage limits specified in G59. It is significance to continue operate DGs in SLG fault condition, although the voltage drop under the Thus, if the operation of DG during fault conditions is permitted in the future, then, the current voltage limits of under/over voltage protection specified in G59 need to be justified. It has also been found in this investigation that the action of the control scheme installed on the DFIG has apparently improved the transient performance of DFIG compared to FSIG, particularly after fault clearance.

3.4.4 Impact of operation of SPAR on the Transient Performance of DG

Most faults on distribution networks are temporary SLG faults [3-4] and not critical for DG's transient stability according to the investigations reported in section 3.4.3. In this section, the impact of operation of SPAR as assessed based on the transient performance of DG following a SLG fault event is reported. As shown in Figure 3.22, the DG feeder, which is feeder 1 in the investigated power system, is divided into protection zones such that when a fault occurs at a certain protection zone it is cleared by the pair of circuit breakers that are located at the two ends of the line section defining the considered protection zone. For instance, an internal fault which occurs within line 1 is isolated by tripping both circuit breakers associated with $R_1$and R_{11}. It is assumed that there is no time delay between the tripping time of these circuit breakers. Apart from that, it is assumed that SPAR scheme is applied at feeder 1 in the investigated power system. R_1 to R_{33} are assumed to be relays equipped with a complex protection function that includes fault classification and phase selection schemes. R_1 to R_{33} trips the phase subjected to SLG fault condition and initiates three phase reclosure for other types of network faults. Under this protection scheme, a DG connected at the end of feeder 1 will continue to operate during any SLG fault condition that occurs within line1, line 2 and line 3.

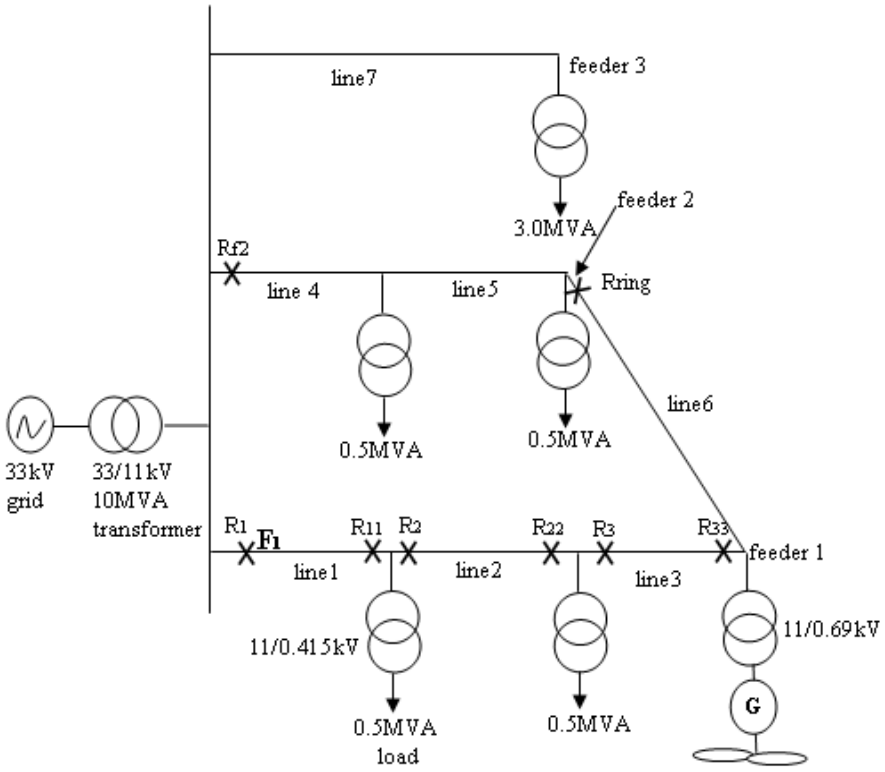

Figure 3.22 Power system under consideration with DG feeder is protected using zone protection scheme.

3.4.4.1 Effect of Recloser Opening Time (T_o) on Dynamic Behaviour of DG during Temporary Fault Conditions

In order to investigate the effect of recloser opening time (T_o) on the transient performance of DG, a SLG fault, phase-a-to-ground (AG) fault is assumed at F_1 1km along feeder 1, (see Figure 3.22) when the investigated system is operated in radial mode and then ring mode. The fault inception instant (FIT) is t = 35 s into the simulation for a fault duration of 0.6s.

Three recloser opening times, T_o, for high speed reclose attempts have been considered in this investigation, being 0.5s, 1.0s and 2.0 s. Values of T_o were selected according to reference [1, 66]. The operating time sequence of circuit breakers associated with both R_1 and R_{11} are shown in Table 3.3. Note that the circuit breakers take 0.2s to trips after fault inception. T_{o1} indicates circuit breaker opening time before 1st reclosing attempt. Note that $T_{o1} = T_o$ in this simulation study. $CBOT_1$ indicates the circuit breaker opening time instant before 1st reclosing attempt. $CBRT_1$ indicates the circuit breaker closing time instant for 1st reclosing attempt. The 1st reclosing attempt is assumed to be high speed reclosing. Figure 3.23 illustrates the operating time sequence of these circuit breakers.

Table 3.3

Operating time sequence of circuit breaker associated with both R_1 and R_{11} for AG fault at 1km along feeder 1 for different T_{o1}.

Fault duration	FIT	T_{o1}	$CBOT_1$	$CBRT_1$
0.6 s	35 s	0.5 s	35.2 s	35.7 s
0.6 s	35 s	1.0 s	35.2 s	36.2 s
0.6 s	35 s	2.0 s	35.2 s	37.2 s

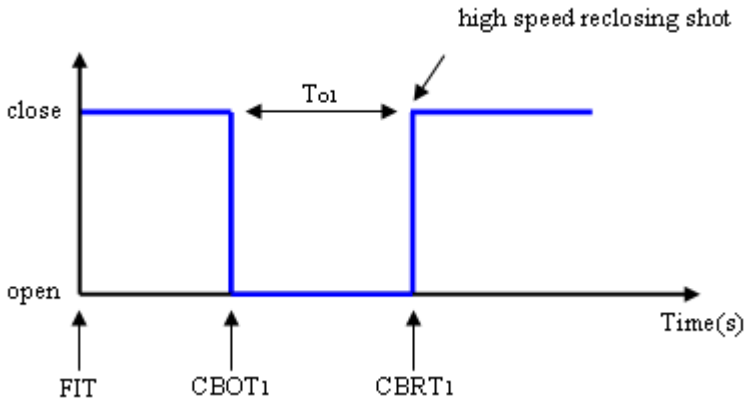

Figure 3.23 Illustration of the operating time sequence of circuit breaker associated with both R_1 and R_{11}.

The simulation results are summarised in Figure 3.24 to 3.27. The effect of circuit breaker opening time setting, T_{o1}, on the dynamic behaviour of the 2.0 MW DFIG following an AG fault in radial and ring network are shown in Figure 3.24 and 3.25 respectively. The effect of circuit breaker opening time setting T_{o1} on the dynamic behaviour of 2.0 MW FSIG following an AG fault in radial and ring networks is shown in Figure 3.26 and 3.27 respectively.

Figures 3.24 and 3.25 show that circuit breaker opening time setting, T_{o1} has clear impact on the transient performance of the DFIG in a radial network compared to a ring network. It can be seen from Figures 3.24(a) and (b) that, when the investigated system is operated in radial mode, the generator terminal voltage and active power have reduced to 0.85 p.u and 1.7 MW respectively, during the circuit breakers opening time period, following fault isolation at t = 35.2 s, compared to their pre fault values of 0.9 p.u and 1.9 MW. Both of these parameters regain their prefault values only after reclosing of circuit breakers. The reclose time depends on $T_{o1.}$ In contrast, it can be seen from Figure 3.25(a) that when the investigated system is operated in ring mode, during the circuit breaker open time period, after the fault is isolated, the drop of terminal voltage is not as bad as Figure 3.24(a). Figure 3.25(b) also shows that during the circuit breakers' opening time period, following fault isolation, the generator active power recovered to prefault value immediately. It can be seen from Figures 3.24 (c) and 3.25(c) that, during the circuit breakers' open time period, following fault isolation, the oscillation pattern of the rotor speed for the

three different values of T_{o1} is significantly different in the case of radial operating mode compared to that related to the ring network.

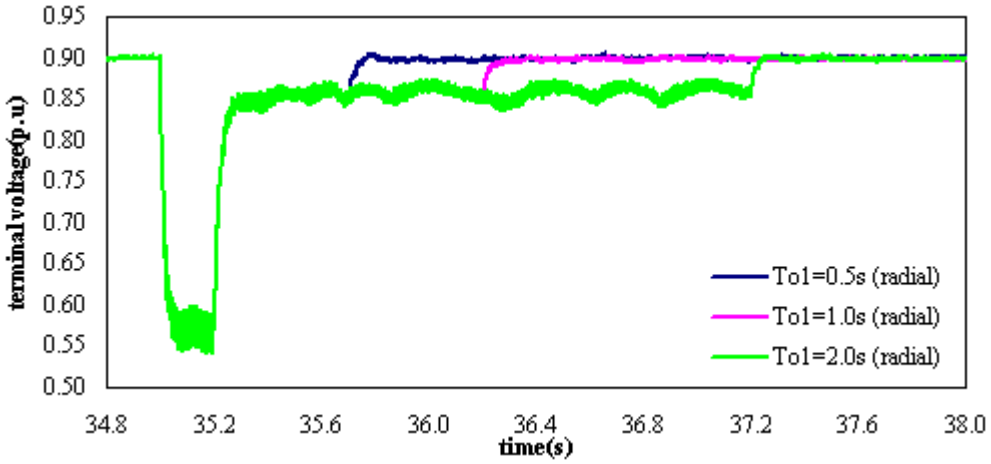

(a) terminal voltage

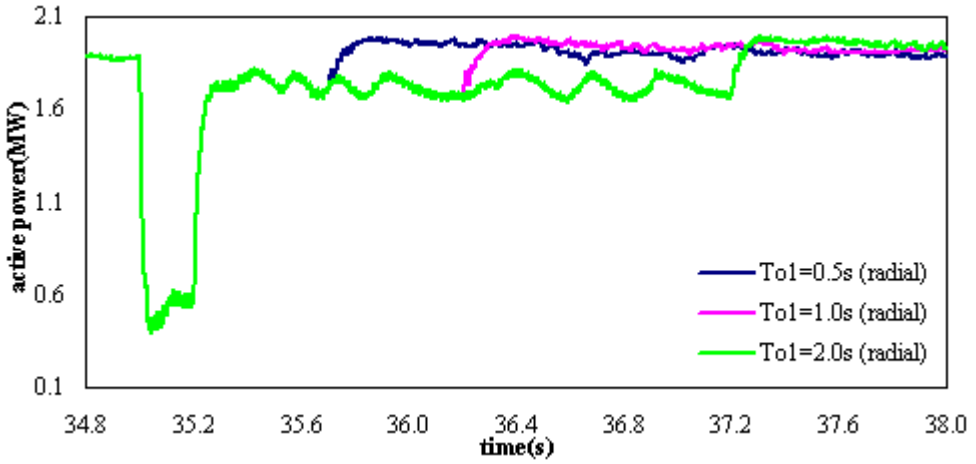

(b) active power

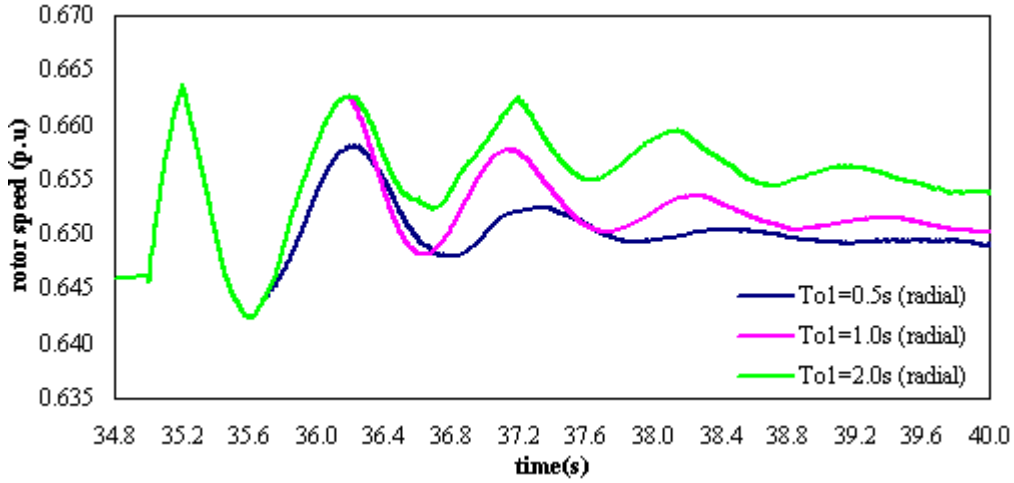

(c) rotor speed

Figure 3.24 Effect of circuit breaker opening time setting T_{o1} on the dynamic behaviour of 2.0 MW DFIG following a AG fault in radial network.

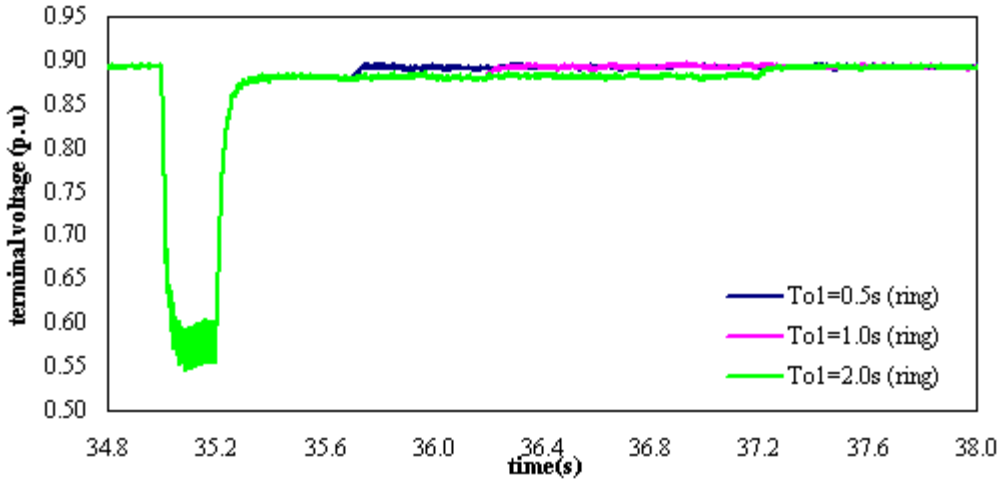

(a) terminal voltage

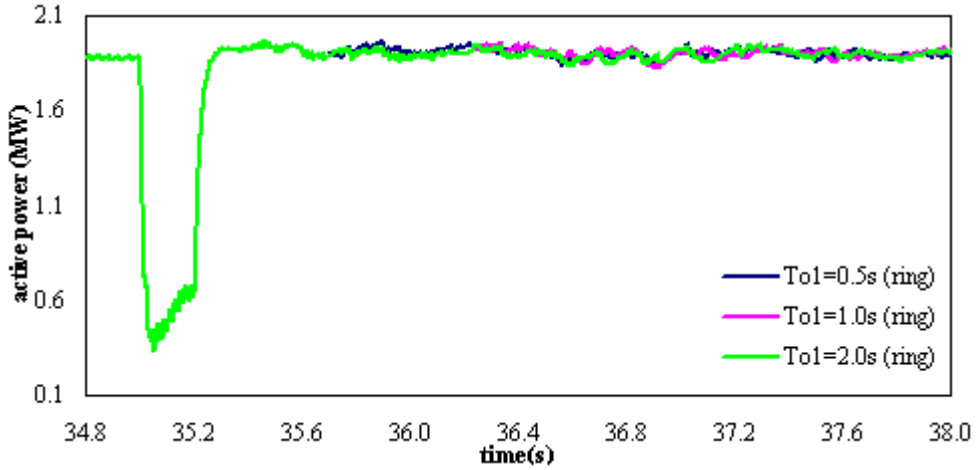

(b) active power

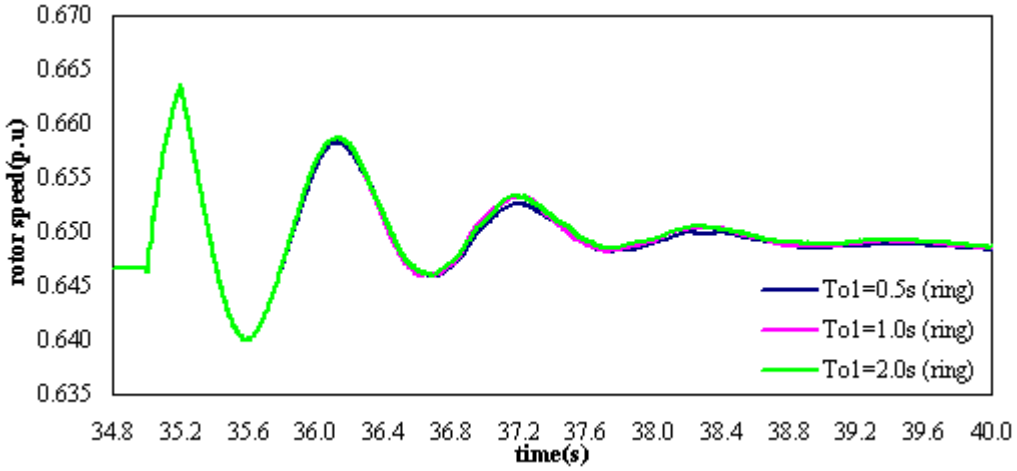

(c) rotor speed

Figure 3.25 Effect of circuit breaker opening time setting T_{o1} on the dynamic behaviour of 2.0 MW DFIG following a AG fault in ring network.

It can be seen from Figure 3.26 and 3.27 that, the effect of T_{o1} on the transient behaviour of the FSIG for the considered fault is significant in the radial network compared to the ring network. Figure 3.26(a) shows that when the investigated system is operated as a radial network the magnitude of generator terminal voltage drop during the circuit breaker opening time after the fault isolation depends on the T_{o1} setting. The worst case is when T_{o1} = 2.0 s, where the voltage dropped from 0.98 p.u prior to the fault to minimum 0.8 p.u. In contrast, Figure 3.27(a) shows that when the investigated system is operated as a ring network the terminal voltage drop during the opening time of circuit breaker is less significant compared to the radial network. The terminal voltage drops of different values of T_{o1} are comparable to each other. Other then that, it can be seen from Figure 3.26 (c) and 3.27(c) that, the oscillation pattern of rotor speed at the three different values of T_{o1} during the circuit breaker open time period, after fault isolation, are significantly different in the radial network compared to that related to the ring network operating mode.

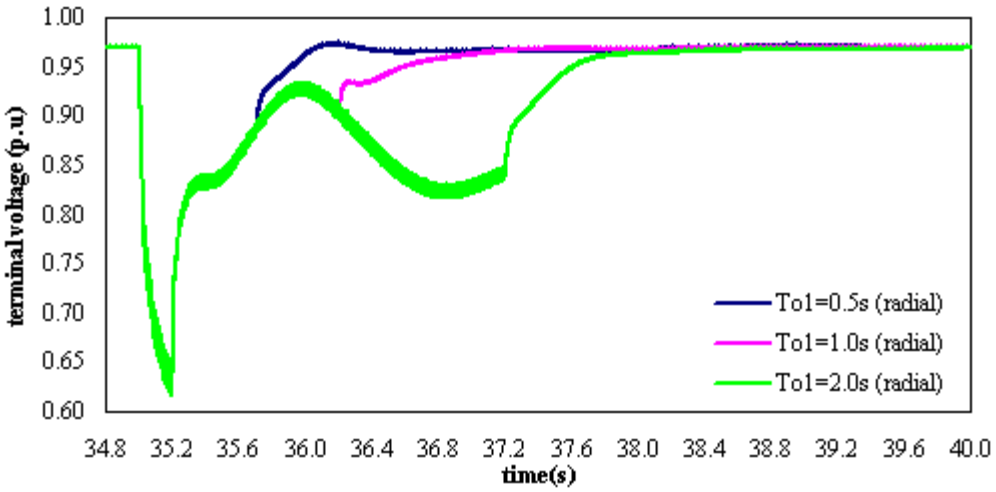

(a) terminal voltage

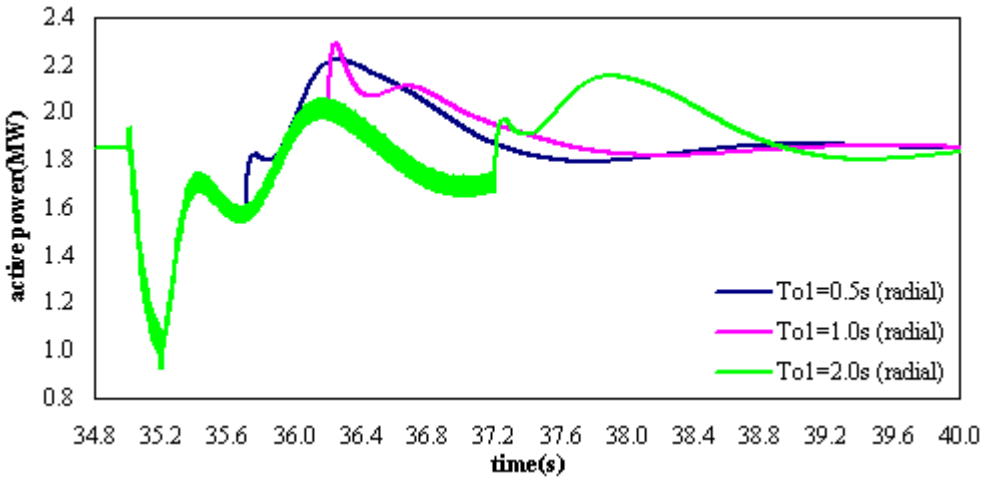

(b) active power

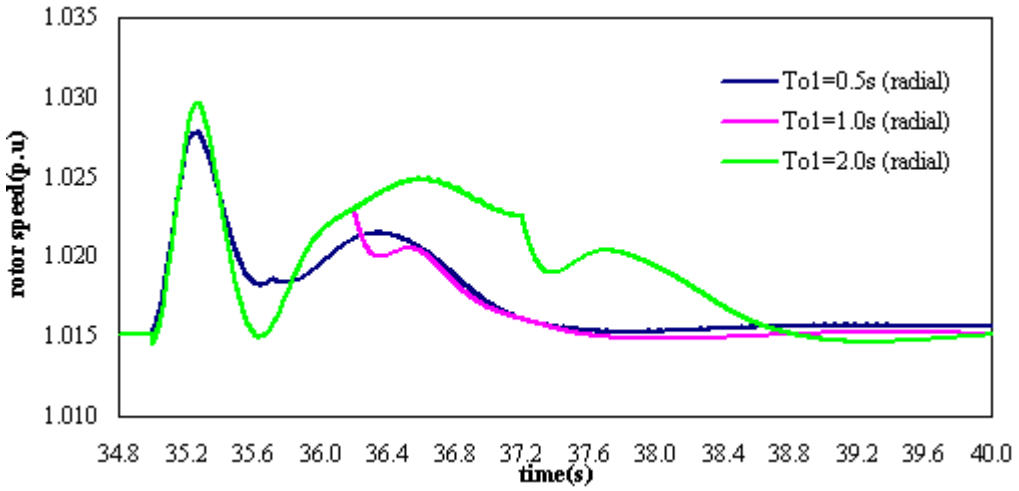

(c) rotor speed

Figure 3.26 Effect of circuit breaker opening time setting T_{o1} on the dynamic behaviour of 2.0 MW FSIG following AG fault in radial network.

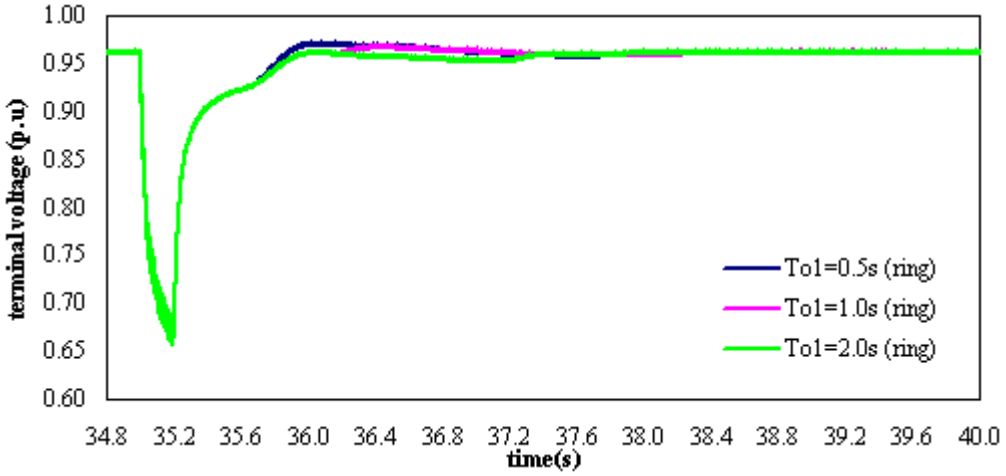

(a) terminal voltage

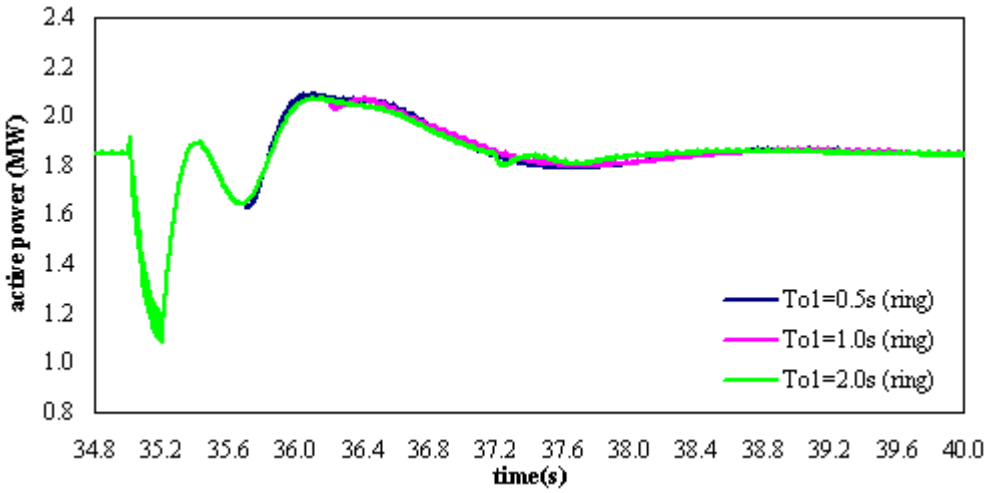

(b) active power

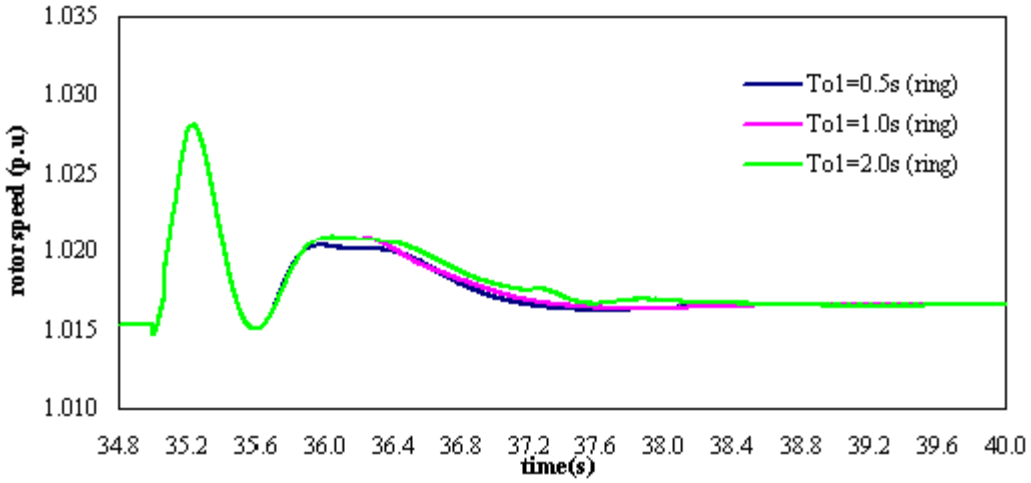

(c) rotor speed

Figure 3.27 Effect of circuit breaker opening time setting T_{o1} on the dynamic behaviour of 2.0 MW FSIG following AG fault in ring network.

It can be concluded from the simulation results obtained from this investigation that the effect of the recloser opening time (T_o) on the dynamic behaviour of FSIG is more significant compared to DFIG, particularly when the investigated system is operated in radial operating mode.

3.4.4.2 Effect of Recloser Opening Time (T_o) on Transient Stability of DG

In this simulation, the transient stability of DG is determined by assessing the main parameters of DG such as terminal voltage, active power and rotor speed. If these parameters regain their prefault values during the recloser opening time, after the fault is isolated, the generator will be considered as stable, otherwise it is unstable. In order to determine the effect of the recloser opening time (T_o) on the transient stability of DG for the considered network fault condition in section 3.4.4.1, an AG fault is applied at a further two fault locations of 7.5km and 14km which are located within line 2 and line 3 respectively on feeder 1. The operating time sequence of circuit breakers associated with R_2 to R_{33} are identical to R_1 and R_{11} and can be found in Table 3.3 in section 3.4.4.1.

The simulation results are summarised in Table 3.4 where S indicates the generator is stable and U indicates the generator is unstable. It can be found in Table 3.4 that the 2.0 MW DFIG remains stable throughout the fault and recloser opening time at all

fault locations and under different T_{o1} setting both in radial and ring networks. In contrast, FSIG become unstable in radial network at certain locations and T_{o1} settings as follows: (i) fault located at 7.5km and T_{o1} = 2.0 s, (ii) fault located at 14km and T_{o1} = 1.0 s and 2.0 s. This can be explained as follows: grid connected FSIG demand a certain amount of reactive power from the network [40, 44]. When the investigated system is operated in radial operation mode, reactive power flows only in one direction from the 33 kV grid to the 2.0 MW FSIG through feeder 1(see Figure 3.22). With phase *a* of the faulty section along feeder 1 become isolated from the network during an AG fault condition, the amount of reactive power received by the generator becoming not sufficient. Eventually, this affects the transient stability of the DG. In contrast, when the investigated power system is operated in ring operation mode, the reactive power flows in two directions, one from the 33 kV grid to the 2.0 MW FSIG through feeder 1 and the second one through feeder 2. With a single phase of the faulty section along feeder 1 being isolated from the network, the reactive power that flows from the 33 kV grid to the generator through feeder 1 ensures sufficient reactive power to keep the generator stable during the reclosing opening time. Apart from that, the action of the control scheme installed at the DFIG has the capability of controlling the reactive power demand during network fault conditions [40, 44]. Therefore, it is more robust and able to ride through the opening time of the recloser.

Table 3.4
The state of transient stability of 2.0 MW FSIG and DFIG (S : generator is stable and U : generator is unstable) : Different values of To_1 for AG fault at fault locations 1km, 7.5km and 14km along feeder 1.

Fault Location	To_1	radial		ring	
		FSIG	DFIG	FSIG	DFIG
1km	0.5 s	S	S	S	S
	1.0 s	S	S	S	S
	2.0 s	S	S	S	S
7.5km	0.5 s	S	S	S	S
	1.0 s	S	S	S	S
	2.0 s	U	S	S	S
14km	0.5 s	S	S	S	S
	1.0 s	U	S	S	S
	2.0 s	U	S	S	S

The operating time sequence in Table 3.3 represents the successful reclosing shots due to a temporary fault event, where the fault is self-cleared before the high speed reclose attempt (before $CBRT_1$). Therefore, the following simulation study is concerned with the successful reclosing due to a temporary fault event where the fault is self-cleared before the time delayed reclose attempt. Table 3.5 shows the operating time sequence of the circuit breaker associated with R_1 to R_{33}. $CBOT_2$ is the instant at which the circuit breaker opens before the 2nd reclosing attempt takes place. $CBRT_2$ is the instant at which the circuit breaker closes at the 2nd reclosing attempt. Figure 3.28 illustrates the operating time sequence of the circuit breaker associated with R_1 to R_{33}.

The 2nd reclosing attempt is assumed to be times delayed reclose. The opening time T_{o1} for high speed reclose attempt being chosen in this simulation is 2.0 s and according to references [1, 66] this value represent the worst case for high speed reclose attempt. The Three values for the opening time T_{o2} of 10 s, 30 s and 60 s for time delayed reclose attempt have been considered. According to simulation results shown in Table 3.4, the 2.0 MW FSIG is unstable at certain fault locations and values of T_{o1} while the 2.0 MW DFIG remain stable at all considered fault locations and values of T_{o1}, therefore only the DFIG is considered in this simulation study.

Table 3.5

Operating time sequence of circuit breaker associated with R_1 to R_{33} for AG fault at 1km, 7.5km and 14km along feeder 1 for different T_{o1} and T_{o2}.

Fault duration	To_1	To_2	FIT	$CBOT_1$	$CBRT_1$	$CBOT_2$	$CBRT_2$
10 s	2.0 s	10 s	35 s	35.2 s	37.2 s	37.4 s	47.2 s
10 s	2.0 s	30 s	35 s	35.2 s	37.2 s	37.4 s	67.2 s
10 s	2.0 s	60 s	35 s	35.2 s	37.2 s	37.4 s	97.2 s

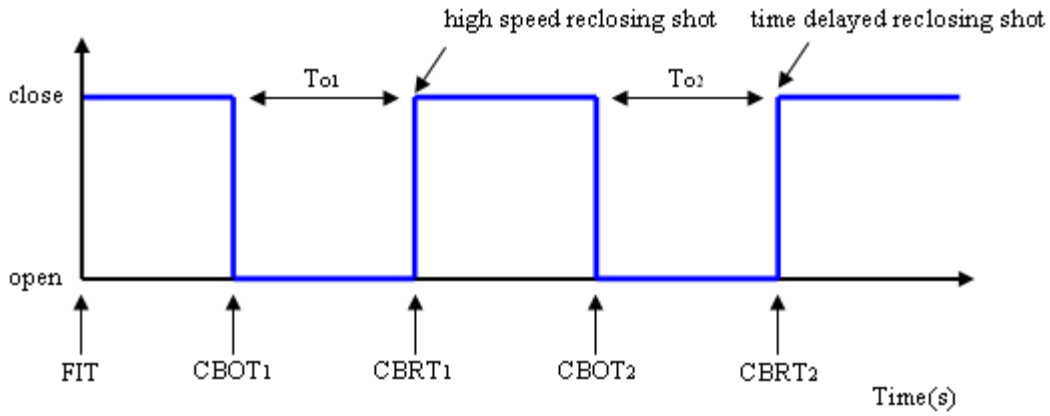

Figure 3.28 Illustration of the operating time sequence of circuit breaker associated with R_1 to R_{33}.

The simulation results are summarised in Table 3.6, where S indicates generator is stable and U indicates generator is unstable. It was found that, the 2.0 MW DFIG remained stable at all fault locations and values of T_{o2} in both radial and ring network operation mode.

Table 3.6

The state of transient stability of 2.0 MW DFIG (S : generator is stable and U : generator is unstable): Different value of To_2 for AG fault at fault location of 1 km, 7.5 km and 14km along feeder 1.

Fault Location	To_1	To_2	DFIG	
			Radial	Ring
1 km	2.0 s	10 s	S	S
	2.0 s	30 s	S	S
	2.0 s	60 s	S	S
7.5km	2.0 s	10 s	S	S
	2.0 s	30 s	S	S
	2.0 s	60 s	S	S
14km	2.0 s	10 s	S	S
	2.0 s	30 s	S	S
	2.0 s	60 s	S	S

The following can be concluded from the simulation results obtained in this investigation:

a. DFIG is more robust compared to FSIG. With the action of the control scheme installed, the DFIG remains stable under different recloser opening time settings for high speed and time delayed attempts.

b. With DGs permitted to operate in SLG fault condition, the type of DG technology and network operation mode need to be taken into consideration when deciding the recloser opening time. For instance, in the radial network with grid connected FSIG, if the faulty section is located far from the generator, then a longer recloser opening time setting can be applied.

Chapter 4: Development of the proposed Adaptive Rule-based Fault Identification and Phase Selection Algorithm for Maintaining the Continued Operation of DG

4.1 Introduction

Due to continued penetration of DGs into existing distribution networks, the tripping of DGs during network fault condition may affect the network stability and reliability. Operation of DGs should be maintained during network temporary faults as far as possible, in order to maximise the benefits of the interconnection of DGs and increase the reliability of the power supply service to consumers. Conventional three phase auto reclosers in distribution networks have become incompatible with the presence of DGs, because they interrupt the operation of the DG during network temporary single-line-to-ground (SLG) fault events and cause unnecessary disconnection of the DG. Therefore the application of a single-phase auto-reclosing (SPAR) scheme as been used in transmission networks should be considered in distribution networks with DG. In this context, the phase selection technique needs to be reliable to ensure the correct tripping of the faulty phase, to avoid the DG losing its transient stability. Other than that, the operating speed of the phase selector is also important. The phase selection process is required to be completed immediately in the post fault period before the tripping of the associated circuit breaker [49]. High speed operation of the phase selector can significantly reduce the tripping time of the circuit breaker, which will eventually minimise the possibility of having a DG lose its transient stability.

This chapter presents the development of a high speed adaptive rule-based fault identification and phase selection algorithm to be used in the implementation of a SPAR scheme in power distribution networks with DG. The emphasis in this chapter will be placed on presenting the fault identification strategy and phase selection procedure. The fault identification strategy makes use of only the three line currents measured at the relay point. The waveform pattern of phase angle and symmetrical components of the three line currents during the transient period of the fault condition is analyzed using condition based-rules with an IF-THEN structure, in

order to determine the type of SLG fault. The phase selection procedures are outlined as follows: if a fault condition is detected and it is a SLG fault then the fault type will be indentified and the output signal of phase selector will indicate type the type of fault as SLG. Accordingly the tripping signal that ensures the tripping of only the faulty phase of the protected distribution line section is issued. Otherwise, if a fault condition is detected and subsequently indentified as a double-line-to-ground (DLG) or line to line (LL) and three phase symmetrical fault, then the output signal of the phase selector indicates the existence of a fault condition that requires the tripping of all three phases and subsequently a three-phase tripping signal is issued. The fault identification strategy and phase selection procedure are implemented and verified in the PSCAD/EMTDC power system software.

4.2 Power System under Investigation

The investigation presented in this chapter is based on the modelling and simulation of a portion of a MV overhead distribution network with integrated DG under different system operating conditions using the computational power systems simulation tool, PCAD/EMTDC. The detailed description of PSCAD/EMTDC can be found in section 3.2.1.

4.2.1 Dynamic Model of 2.0MW Wind Turbine Driven DFIG

The adaptation of an appropriate dynamic DG model is essential to thoroughly asses the transient response of DGs during various network fault conditions which then facilitate the development of the adaptive fault identification and phase selection algorithm proposed in this research study.

As discussed in Chapter 3, an investigation has been carried out to asses the possibility of preserving DGs in service during network temporary faults. Both fixed FSIG and DFIG are modelled in detail to thoroughly understand the transient response of the two different types of wind-driven generators during network temporary faults. It has been concluded from the investigation that DFIG has a better transient performance compared to FSIG during a network temporary fault. Consequently for the work that will be reported in this chapter, a 2.0MW DFIG model will be used to represent DGs that are interconnected to existing distribution

networks. In this research work a simulation model of DG based on doubly fed induction generator (DFIG) was adopted using PSCAD/EMTDC [81]. The detailed description of the DFIG generator can be found in section 3.2.2.2 and the machine parameters of the 2.0MW DFIG can be found in Appendix A2.

4.2.2 11kV Rural Distribution Network Model

The power system under investigation is shown in Figure 4.1.The grid is represented by a voltage source with short circuit level of 40MVA. The 2.0MW DFIG is connected at the end of feeder 1 through a 2.5MVA, 0.69/11kV step up transformer. The length of distribution line sections 1 to 6 is assumed to be 5km and distribution line section 7 is 10km. The parameter of the distribution line Z_L = 0.3664∠59.50° Ω per km. The details of other network parameters can be found in section 3.2.3.

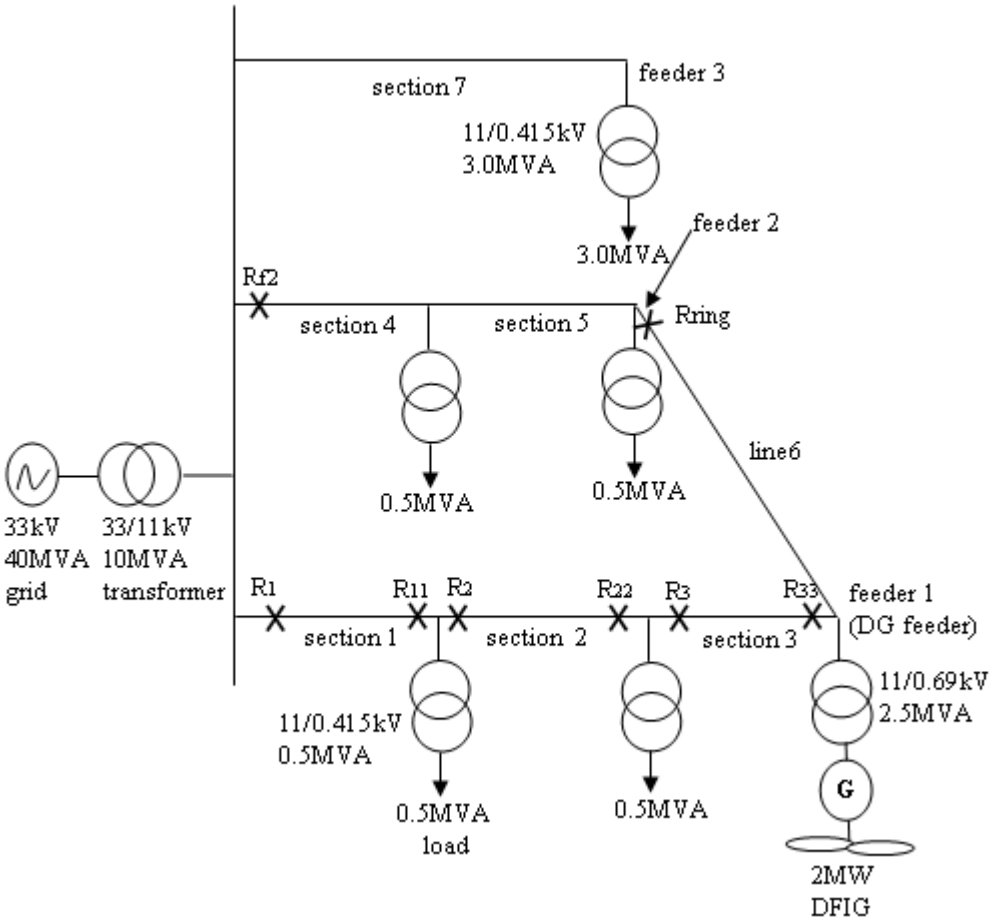

Figure 4.1 Network configuration of investigated 11kV overhead network with DG.

4.2.3 Proposed Zone Protection Approach

In order to preserve the operation of the DG during temporary fault condition and reduce the costly investment in additional protection devices to the investigated system, it is proposed in this research work to protect the feeder with DG using a zone protection approach and the feeder with load using an already existing conventional approach e.g., non directional overcurrent protection.

As shown in Figure 4.1, the DG feeder which is feeder 1 is divided into protection zones such that when a fault occurs in a certain protection zone, it is cleared by the pair of circuit breakers that are located at the two ends of the line section defining the considered protection zone. For instance, an internal fault which occurs within section 1 is isolated by tripping both circuit breakers associated with $R_1$and R_{11}. Meanwhile, other load feeders, such as feeder 2, are assumed to be protected using only conventional overcurrent relays located at the beginning of the feeder, R_{f2}. Any fault occurred at feeder 2 will cause the isolation of the whole feeder. It is assumed that SPAR is applied at feeder 1 in the investigated system. The phase selection technique proposed in this research work used in the SPAR scheme will be elaborated in the following section. Under the proposed protection scheme, DG connected at the end of feeder 1 can be maintained in service in the event of an SLG temporary fault.

With efficient DG placement and effective new adaption in both network voltage control and network protection, there is a possibility that distribution networks in future will be operated in ring rather than radial mode in order to increase the penetration of DG [24, 33-35]. The proposed protection scheme can effectively be applied in conventional networks that switch from radial to ring operation mode. Once the fault is successfully detected at the DG feeder, the ring connector R_{ring} is opened and then the zone protection approach is applied to isolate the faulty section from the network.

4.3 Fault Identification Strategy

A detailed analysis of the fault current can provide essential information about the nature of the fault. In the proposed method, the following parameters have been used

to identify types of fault (i) the phase angle differences between line currents and (ii) the ratio of sequence components.

4.3.1 Phase Angle Difference between Line Current

The analysis of variation in phase angle difference between line currents I_a, I_b and I_c during fault conditions has been found useful in detecting faulty phase. A phase selection technique based on the phase angle criterion of the line currents has been proposed recently in [53] to identify SLG fault. The phase angle differences between line currents are defined in equation (4.1) to (4.3)

$$\varphi AB = \varphi I_a - \varphi I_b \tag{4.1}$$

$$\varphi BC = \varphi I_b - \varphi I_c \tag{4.2}$$

$$\varphi CA = \varphi I_c - \varphi I_a \tag{4.3}$$

Where φAB = phase difference between I_a and I_b
φBC = phase difference between I_b and I_c
φCA = phase difference between I_c and I_a

4.3.2 Ratio of Sequence Components

Analysis on the sequence components of line currents I_a, I_b and I_c has been found useful for the detection of unbalanced condition in power systems, for instance unsymmetrical fault events [82-84]. Fault classification in relaying, based on the analysis of sequence components, has been proposed in recently published work [53, 56, 89]. Equations (4.4) to (4.6) show the relationship between sequence components and line currents. The derivation of Equations (4.4) to (4.6) can be found in [82].

$$I_1 = \frac{1}{3}(I_a + aI_b + a^2 I_c) \tag{4.4}$$

$$I_2 = \frac{1}{3}(I_a + a^2 I_b + aI_c) \tag{4.5}$$

$$I_0 = \frac{1}{3}(I_a + I_b + I_c) \tag{4.6}$$

Where

(i) $I_1, I_{2,} I_0$ are positive, negative and zero sequence current components with phase a as reference.

(ii) a is an operator which gives a phase shift of 120º so $a = 1\angle 120^\circ$ and $a^2 = 1\angle 240^\circ$.

Ratios of the magnitude of sequence current components are defined in equations (4.7) and (4.8).

$$R_{01} = \left|\frac{I_0}{I_1}\right| \tag{4.7}$$

$$R_{21} = \left|\frac{I_2}{I_1}\right| \tag{4.8}$$

For unsymmetrical line fault, the positive, negative and zero sequence network currents I_1, I_2 and $I_{0,}$ have a particular relationship depending on the type of fault. Equation (4.8) to (4.10) show the relationship between sequence components in SLG fault, DLG and LL respectively. The derivation of Equations (4.8) to (4.10) can be found in [82].

$$I_1 = I_2 = I_0 \tag{4.8}$$

$$I_1 + I_2 + I_0 = 0 \tag{4.9}$$

$$I_1 = -I_2,\ I_0 = 0 \tag{4.10}$$

The presence of positive, negative and zero sequence components in a particular fault event indicate that it is either a SLG or a DLG fault. The simulation work conducted in [88] shows that the ratio of sequence component I_0/I_1 and I_2/I_1 is higher for a SLG fault compared to a DLG fault in a transmission network.

4.3.3 Preprocessing of Line Current Measurements

In general, the three phase line current measurements generated during fault condition are non-sinusoidal. They contain harmonic components and an exponentially decaying DC component, in addition to the current signal at the fundamental frequency [90]. Thus, the Fast Fourier Transform (FFT) algorithm can be used to remove higher harmonic components and to attenuate the DC component in the generated line currents. The application of the FFT algorithm in digital protection for a power system has been reported in [91].

In this research project, the FFT algorithm has been used to extract the three phase line currents signals at the fundamental frequency and the sampling rate chosen for the FFT is 64 sample/cycle. The symmetrical components of the three phase line currents at the fundamental frequency are then obtained based on the simple transformation equations shown in (4.4) to (4.6). The component called the on-line frequency scanner (FFT) in the PSCAD/EMTDC library [79] is used to preprocess the current signals before conducting a detailed analysis on the line currents and symmetrical components to demonstrate how the proposed fault identification algorithm can be used to identify SLG faults.

4.3.4 Simulation Test and Result

Intensive simulation tests were carried out to demonstrate how equations (4.1) to (4.3) and (4.7) to (4.8) are used to identify the type of SLG fault. Firstly, a simulation test was conducted to analyse the variation of φAB, φBC, φCA and the ratios R_{01} and R_{21} for different types of SLG faults. Then, a sequence of simulation tests were conducted to (a) distinguish between fault and normal network conditions, (b) distinguish between SLG and DLG faults and (c) identify SLG from LL and symmetrical three phase faults. Finally, development of the relevant condition rule-based table was undertaken based on the simulation results.

4.3.4.1 Determine Variation of φAB, φBC, φCA, Ratios R_{01} and R_{21} during SLG Faults

A phase-a-to-ground (a-g) fault is assumed at 1km from the grid in the investigated power system (see Figure 4.1) which is initiated at t = 34.998s for a period of one cycle. Since the fault occurred within section 1 that is protected by relays R_1 and R_{11}, the current measurements of relay R_1 and R_{11} are collected. The test was repeated with phase-b-to-ground (b-g) and phase-c-to-ground (c-g).

Figure 4.2(a) to (c) show variation of φAB, φBC and φCA, for a-g, b-g and c-g faults respectively based on the derivation of line current measured at relay R_{11}. Note that φAB, φBC and φCA are represented by the blue, green and red colours respectively in Figure 4.2(a) to (c).

The variation of φAB, φBC and φCA in these figures during transient period following assumed fault conditions are then analyzed to find the relationship between the type of SLG fault and phase angle differences between line currents. The value of φAB, φBC and φCA, prior to fault occurrence are approximately 120°, -240° and 120° respectively. However, depending on the type of SLG fault these values deviate from their pre-fault values, i.e., either increase or decrease immediately after fault inception. The maximum and minimum value of φAB, φBC and φCA in these figure are significantly different when compared to each other, e.g., it is shown in Figure 4.2(a) that the maximum value of φCA is approximately 300° while in both of Figure 4.2(b) and (c) the maximum value of φCA are approximately 130° and 120° respectively. Additionally these figures reveal that, depending on the type of SLG fault, each of the φAB, φBC and φCA waveforms may cross the 0°-axis at a particular time instant, e.g., it can be seen from Figure 4.2(a) under a-g fault condition that, φAB, φBC and φCA have all crossed the 0°-axis. However, it is shown in Figure 4.2(c) that, only φCA has crossed the 0°-axis.

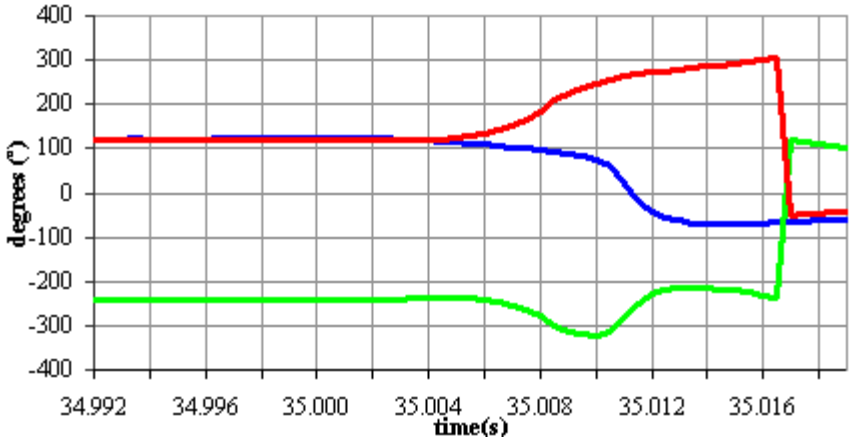

(a) a-g fault

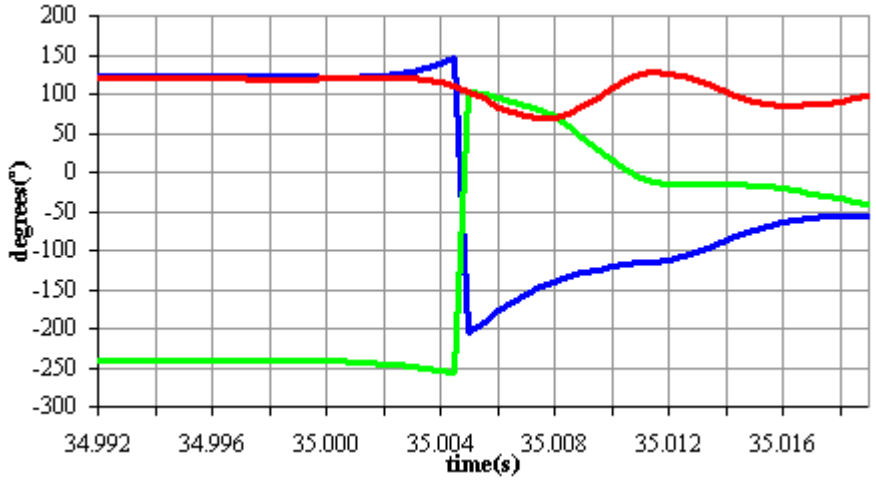

(b) b-g fault

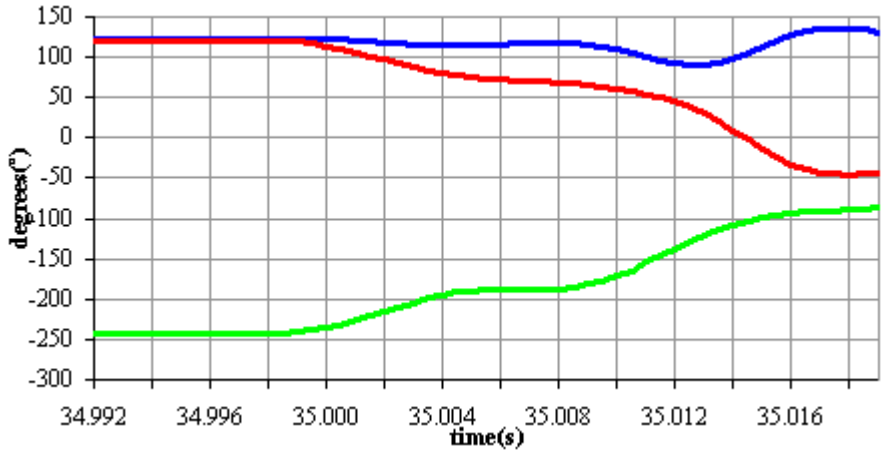

(c) c-g fault

Figure 4.2 Variation of φAB(blue waveform), φBC (green waveform)and φCA (red waveform) in SLG faults (based on line current measurement of relay R_{11}).

The analysis of the three parameters φAB, φBC and φCA can be done more precisely with better accuracy from the data table. Table 4.1 shows the data points of φAB, φBC and φCA versus time corresponding to a-g fault in Figure 4.2(a) from t = 34.996 s to t = 35.016 s. The minimum data point of parameters φAB, φBC and φCA can be used as one of the criterion to identify the type of SLG fault. As shown in Table 4.1, in this fault case, the exact minimum point of φBC, $min_{\varphi BC}$ =-321.4750° occurred at t = 35.0095 s. Note that the data points of φAB, φBC and φCA at t = 35.0095 s are highlighted in Bold in Table 4.1. The data points of φAB and φCA, $datapoint_{\varphi AB}$ and $datapoint_{\varphi CA}$ corresponding to $min_{\varphi BC}$ are 73.2498° and 248.2252° respectively, and $datapoint_{\varphi CA} > datapoint_{\varphi AB} > min_{\varphi BC.}$. Therefore the following statement has been concluded from analysis of the data point in Table 4.1 : φBC= -321.4750° and $\varphi CA > \varphi AB > \varphi BC$ at t = 35.0095 s .Note that, the values of φAB, φBC and φCA shown in Table 4.1 have been derived from values of φI_a, φI_b and φI_c that shown in Table 1 in Appendix B. φAB, φBC and φCA has been derived from φI_a, φI_b and φI_c using equations (4.1) to (4.3). φI_a, φI_b and φI_c are the phase angles of the line current a, b and c obtained from relay R_{11} in the investigated system shown in Figure 4.1.

Table 4.1

The value of φAB, φBC and φCA prior and following a-g fault corresponding to figure 4.2(a) from t = 34.996 s to t = 35.016 s.

Time (s)	Phase angle difference between line currents		
	φAB (°)	φBC (°)	φCA (°)
34.9960	122.0805	-242.3458	120.2653
34.9965	122.1788	-242.2745	120.0958
34.9970	122.2769	-242.2341	119.9572
34.9975	122.3637	-242.2124	119.8487
34.9980	122.4536	-242.1904	119.7368
34.9985	122.4150	-242.1452	119.7302
34.9990	122.3183	-242.0902	119.7719
34.9995	122.3945	-242.0879	119.6934
35.0000	122.6797	-242.1549	119.4752
35.0005	123.2159	-242.3086	119.0927
35.0010	123.3624	-242.1529	118.7904
35.0015	123.1483	-241.6541	118.5058
35.0020	122.5603	-240.8628	118.3026
35.0025	121.6108	-239.8946	118.2838
35.0030	120.0445	-238.7762	118.7317
35.0035	118.5880	-238.2587	119.6707
35.0040	116.7709	-238.0437	121.2727

35.0045	114.6435	-238.2917	123.6482
35.0050	112.3451	-239.4160	127.0709
35.0055	108.9679	-242.9527	133.9848
35.0060	106.1902	-247.7355	141.5453
35.0065	103.2221	-255.0889	151.8668
35.0070	100.0721	-265.7603	165.6882
35.0075	96.6973	-279.8658	183.1684
35.0080	91.6398	-300.2819	208.6421
35.0085	87.1135	-312.4270	225.3134
35.0090	81.3837	-319.7414	238.3576
35.0095	**73.2498**	**-321.4750**	**248.2252**
35.0100	59.7563	-315.5290	255.7728
35.0105	21.2514	-284.6766	263.4252
35.0110	-18.8066	-249.1866	267.9932
35.0115	-43.7256	-228.2165	271.9421
35.0120	-56.2936	-219.1930	275.4866
35.0125	-63.1738	-215.5935	278.7673
35.0130	-68.1173	-214.8372	282.9545
35.0135	-70.0299	-216.0273	286.0572
35.0140	-70.9036	-218.2743	289.1779
35.0145	-70.9575	-221.4180	292.3755
35.0150	-70.3570	-225.3403	295.6973
35.0155	-68.7866	-231.5130	300.2996
35.0160	-67.2444	-236.5470	303.7914

Figure 4.3(a) to (c) show the variation of ratios R_{01} (blue waveform) and R_{21}(green waveform) for a-g, b-g and c-g faults based on line currents measured at relay R_{11}. Note that ratios R_{01} and R_{21} are illustrated as blue and green curves in Figure 4.3(a) to (c). The values of both ratio R_{01} and R_{21} prior to fault are 0. After fault inception, the values of both ratios R_{01} and R_{21} increase significantly regardless of the type of SLG fault. The existence of ratios R_{01} and R_{21} in a-g, b-g and c-g faults indicates that the considered faults are unsymmetrical and involve the ground.

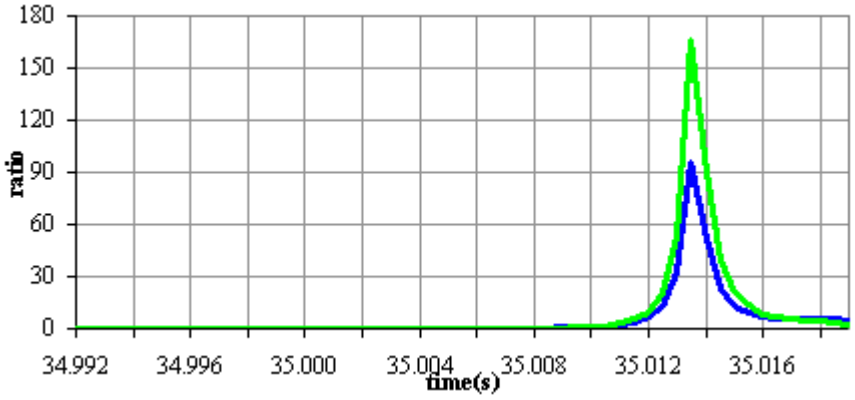

(a) a-g fault

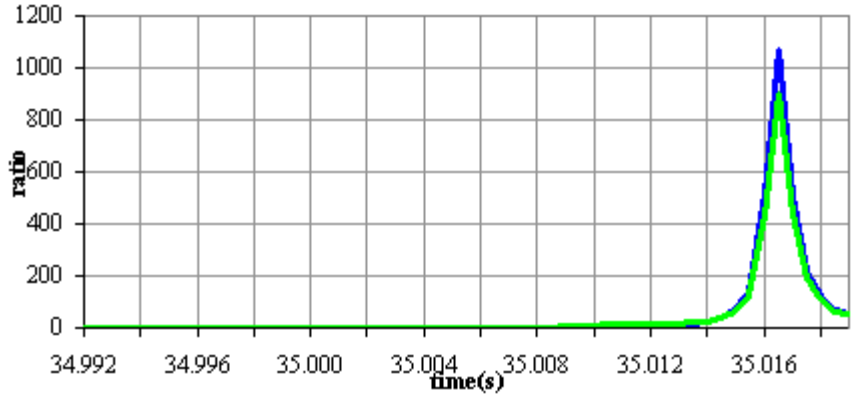

(b) b-g fault

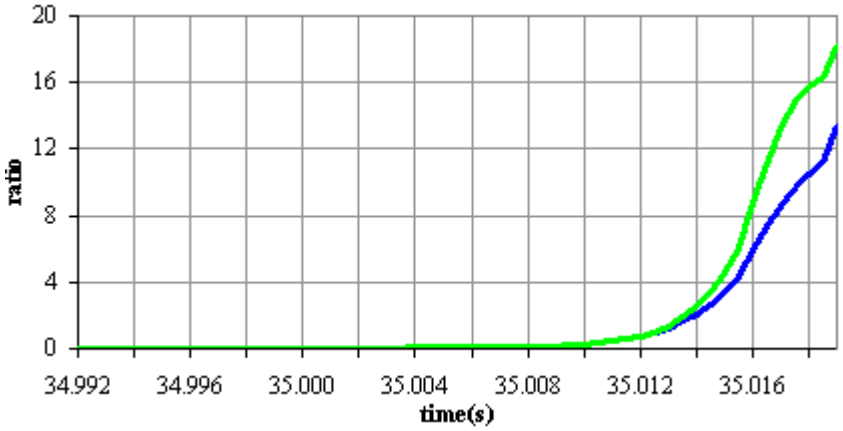

(c) c-g fault

Figure 4.3 Variation of ratios R_{01}(blue waveform) and R_{21}(green waveform)in SLG faults (based on line current measurement of relay R_{11}).

4.3.4.2 Determination Variation of φAB, φBC , φCA and Ratios R_{01} and R_{21} during DLG Faults

In this section, the variation of φAB, φBC and φCA and ratios R_{01} and R_{21} for DLG are assessed in order to distinguish between (i) fault and normal conditions and (ii) SLG and DLG faults. This is important because other type of faults such as LL faults and three phase symmetrical faults can be easily determined using R_{01} defined by equation (4.7). Phases a and b to ground (a-b-g) fault is assumed at 1km from the grid and the fault is initiated at t = 34.998s for a duration of 1 cycle. The test was repeated with phases b and c to ground (b-c-g) and phases c and a to ground (c-a-g) faults. Figures 4.4 (a) to (c) show the variation of φAB, φBC and φCA for a-b-g, b-c-g and c-a-g faults based on the three phase currents measured at relay $R_{11.}$ It was found from these figures that, after fault inception, the value of φAB, φBC and φCA deviate from their values prior to the fault. The variation of φAB, φBC and φCA for a-b-g, b-

c-g and c-a-g faults are significantly different when compared to the a-g , b-g and c-g faults shown in Figure 4.2. Thus, by analysing the difference between the variation of φAB, φBC and φCA during the transient period for SLG and DLG fault cases, SLG faults can be distinguished from DLG faults.

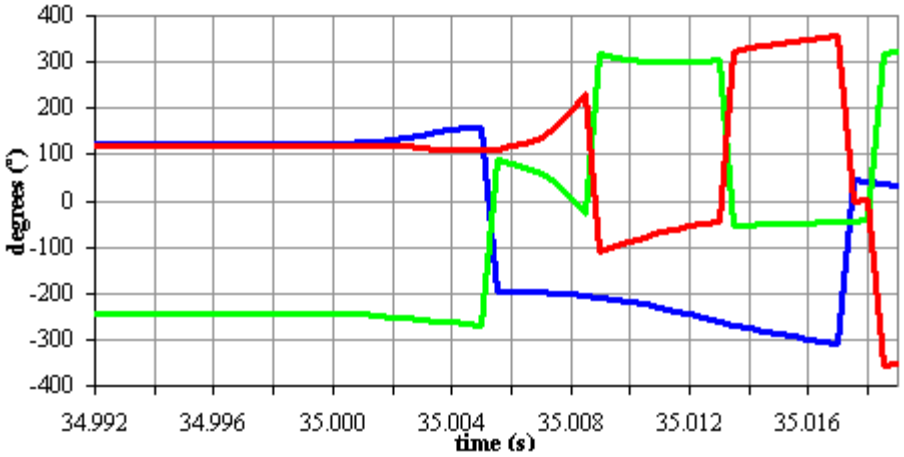

(a) a-b-g fault

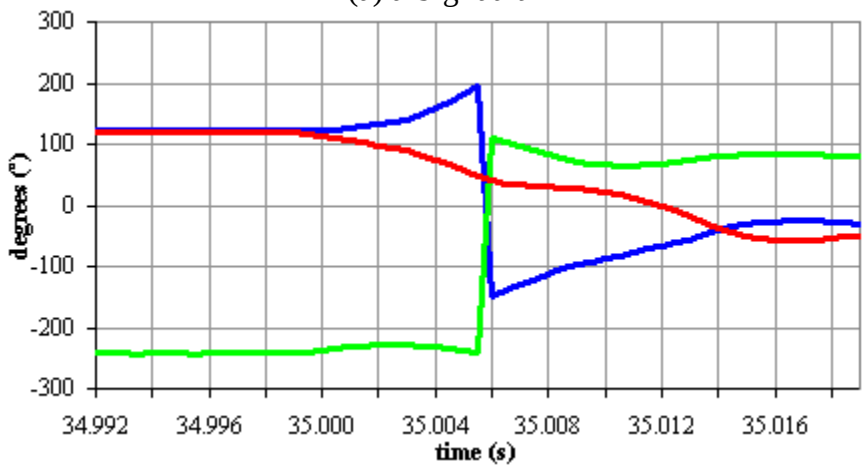

(b) b-c-g fault

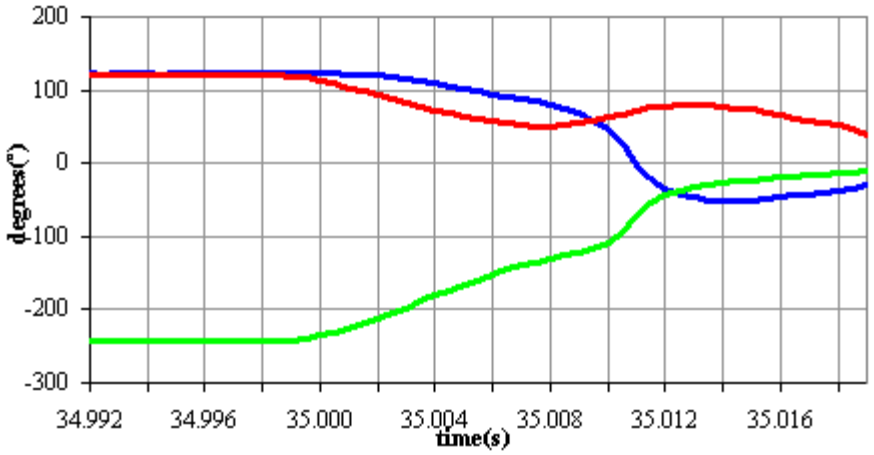

(c) c-a-g fault

Figure 4.4 Variation of φAB (blue waveform), φBC (green waveform) and φCA (red waveform) in DLG faults (based on line current measurement of relay R_{11}).

Figures 4.5(a) to (c) show the variation of ratios R_{01} (blue waveform) and R_{21} (green waveform) for a-b-g, b-c-g and c-a-g fault. The existence of ratios R_{01} and R_{21} in the case of a-b-g, b-c-g and c-a-g faults indicate that the considered faults are unsymmetrical and involve ground. It will be concluded in Figures 4.5 and 4.3 the following: The values of ratio R_{01} and R_{21} for both SLG and DLG do not remain constant during the transient period of fault condition. Furthermore, the waveform pattern of ratio R_{01} and R_{21} in both SLG and DLG are very similar to each other during the transient period in fault condition. Therefore it is not considered as an effective parameters to distinguish between SLG and DLG during the transient period of the fault condition. However, according to research work reported in [88], if current measurement is collected during steady state of fault condition, i.e., a couple of cycles after fault inception, then the magnitude of ratio R_{01} and R_{21} is generally higher in SLG than DLG, so it can be used to distinguish between SLG and DLG cases.

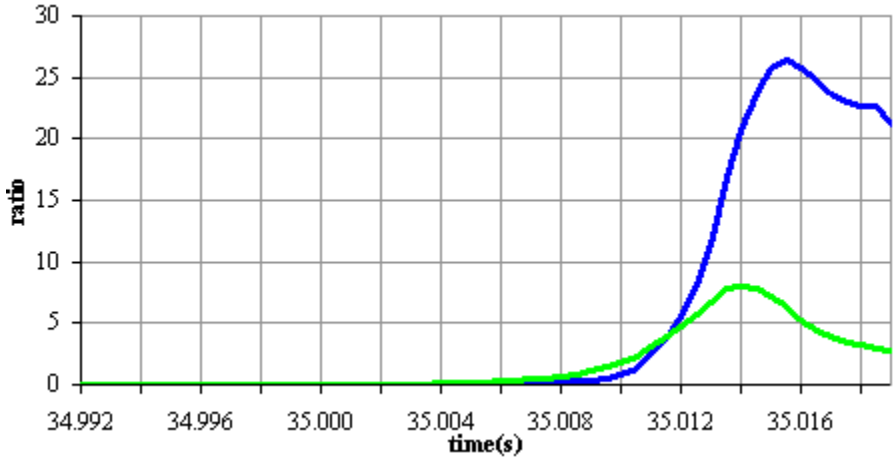

(a) a-b-g fault

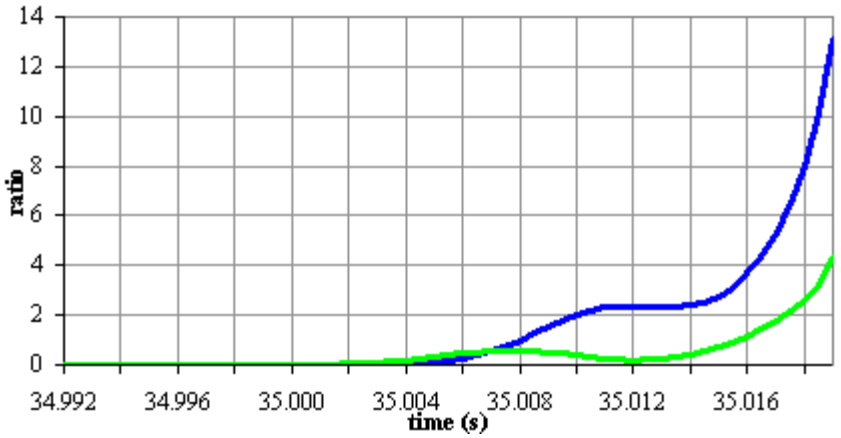

(b) b-c-g fault

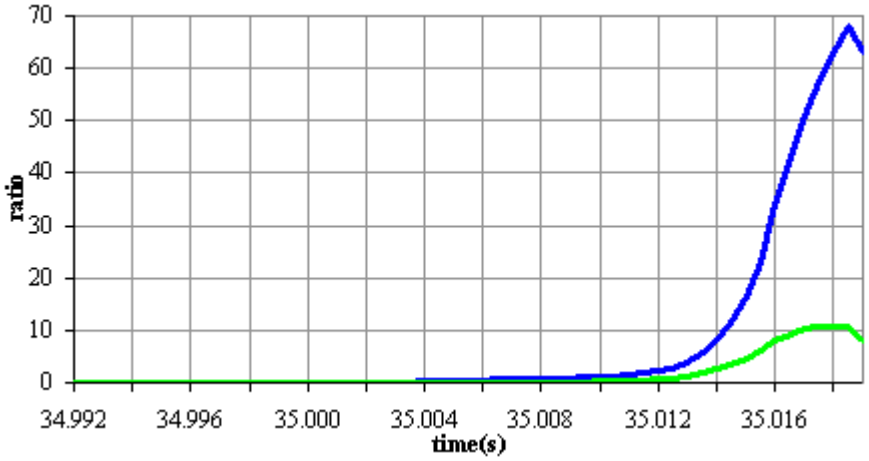

(c) c-a-g fault

Figure 4.5 Variation of R_{01}(blue waveform) and R_{21}(green waveform)in DLG faults (based on line current measurement of relay R_{11}).

4.3.4.3 Determination Variation of *φAB, φBC, φCA,* Ratios R_{01} and R_{21} during LL and Symmetrical Three Phase Faults

In this section, the variation of *φAB*, *φBC*, *φCA* and ratios R_{01} and R_{21} for LL and symmetrical three phase faults are assessed in order to (i) distinguish between fault and normal network conditions and (ii) indentify SLG from LL and symmetrical three phase faults. A simulation test is conducted whereby a phase a and b and c (a-b-c) fault is assumed at 1km from the grid. The fault is initiated at t = 34.998s with a duration of 1 cycle. The test was repeated with three types of LL fault, which are phase a to b (a-b), phase b to c (b-c) and phase c to a (c-a).

Figures 4.6 (a) to (d) show the variation of *φAB* (blue curve), *φBC* (green curve)and *φCA* (red curve) for a-b, b-c, c-a and a-b-c faults based on the three phase currents measured at relay $R_{11.}$ These figures reveal that the values of *φAB*, *φBC* and *φCA* prior to fault are approximately 120°, -240° and 120° respectively. Depending on the type of fault, these values deviate from their pre-fault values, i.e., either increase or decrease immediately after fault inception.

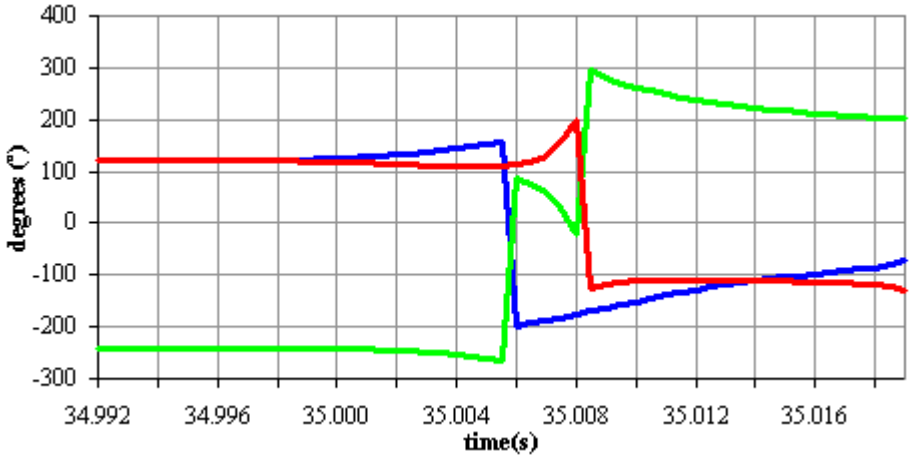

(a) a-b fault

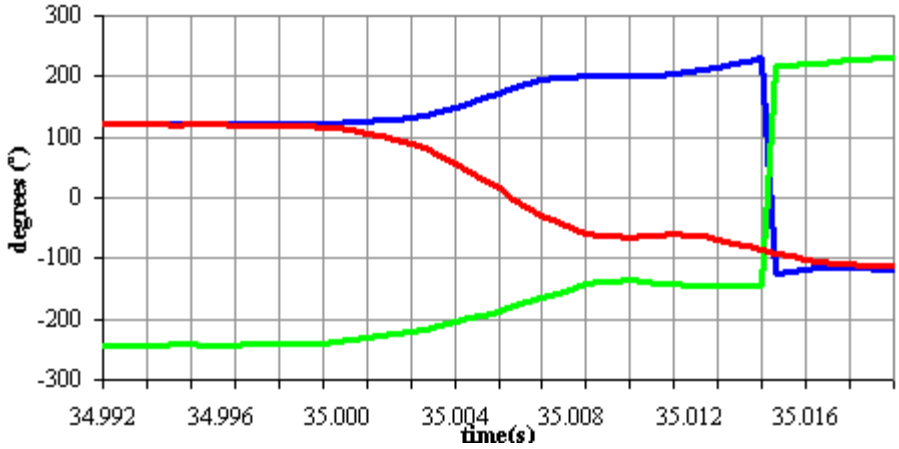

(b) b-c fault

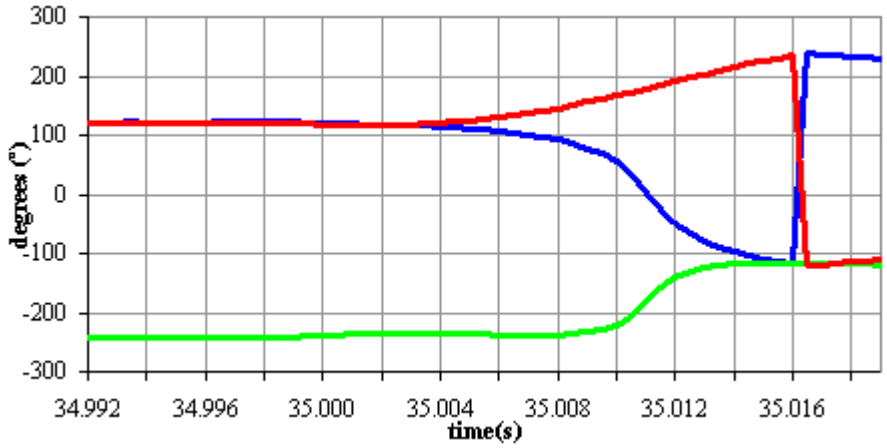

(c) c-a fault

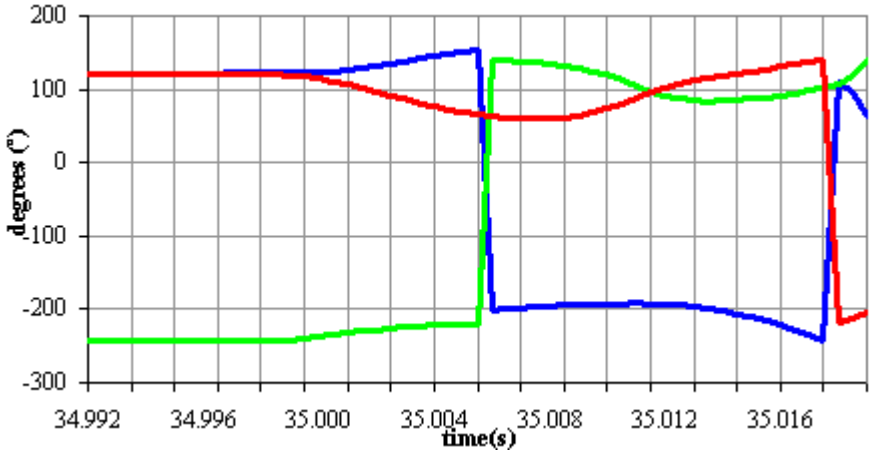

(d) a-b-c fault

Figure 4.6 Variation of φAB (blue waveform), φBC (green waveform)and φCA (red waveform) in LL and three phase systematical faults (based on line currents measurement of relay R_{11}).

Figures 4.7(a) to (d) show the variation of ratios R_{01} (blue waveform)and R_{21}(green waveform) for a-b, b-c, c-a and a-b-c faults based on the three phase currents measured at relay $R_{11.}$ It can be seen from these figures that the magnitude of the ratio R_{01} remains approximately equal to zero prior to and after the occurrence of a fault in all type of fault condition. The value of the ratio R_{21} in a three phase symmetrical fault is less than 1 and it can be negligible compared to LL faults which continue to increase after fault inception.

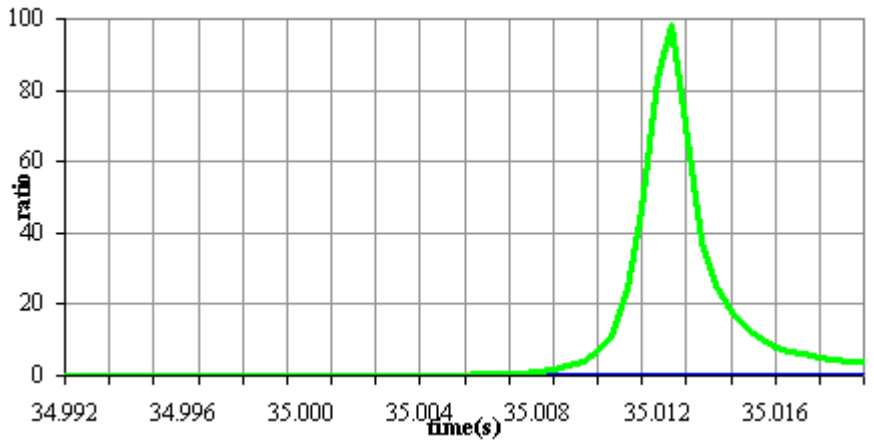

(a) a-b fault

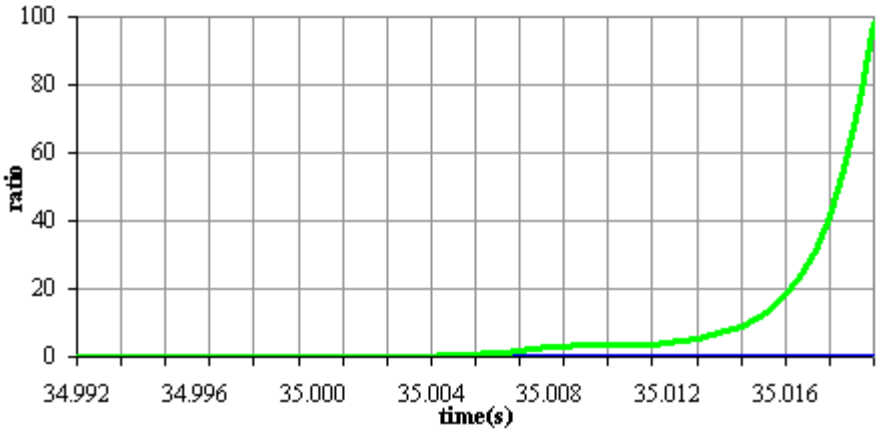

(b) b-c fault

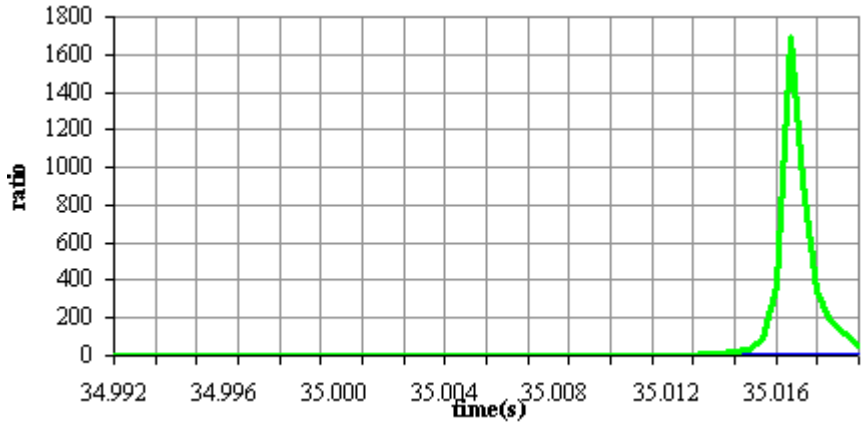

(c)c-a fault

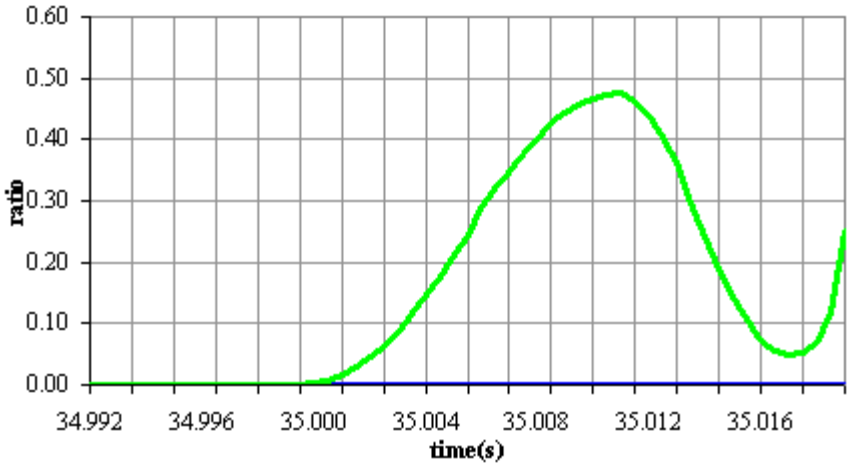

(d) a-b-c fault

Figures 4.7 Variation of ratios R_{01}(blue waveform)and R_{21} (green waveform)in LL and three phase symmetrical faults (based on line current measurement of relay R_{11}).

The following can be concluded from the analysis of the five considered parameters φAB, φBC, φCA and the ratios R_{01} and R_{21} presented in Figures 4.2 to 4.7:

a. After fault inception, the values of φAB, φBC and φCA deviate from their pre-fault values of approximately 120°, -240° and 120° respectively by a magnitude which depend on the type of fault. Therefore, parameters φAB, φBC and φCA can be used to differentiate between normal and fault conditions for all types of faults.

b. By anlaysing the variations of φAB, φBC and φCA after fault inception distinctive characteristic can be indentified for each fault type. The maximum and minimum values of φAB, φBC and φCA in each fault case together with the existence of zero-crossing point (0°-axis crossing) of φAB, φBC and φCA can be used as a useful criterion to indentify the type of fault. Finally, parameters φAB, φBC and φCA can be used to differentiate SLG and DLG fault.

c. The existence of ratios R_{01} or R_{21} after the occurrence of fault conditions can be used as a useful criterion to indentify faults that involve of the ground. Ratio R_{01} can be used, in conjunction with φAB, φBC and φCA, to indentify LL and three phase symmetrical faults.

4.3.5 Construction of Condition-Based Rules for SLG Fault Identification

Table 4.2 shows the condition-based rules that have been constructed to indentify the type of SLG. The "IF-THEN" condition-based rules are constructed based on the analysis of the five waveforms of the five parameters, φCA, φAB, φBC and the ratios R_{01} and R_{21} obtained from each of the fault cases shown in Figures 4.2 to 4.7 and the data points of these five parameters in each of these fault cases.

Table 4.2

Conditional rules based on analysis of waveforms in Figures 4.2 to 4.7.

Fault type	Rule
a-g	If ($\varphi CA > \varphi AB > \varphi BC$) and ($\varphi BC < -300^{\circ}$) and (R_{01} and $R_{21} > 1$) then (output = a-g)
b-g	If ($\varphi CA > \varphi BC > \varphi AB$) and ($\varphi BC < 0^{\circ}$) and (R_{01} and $R_{21} > 1$) then (output = b-g)
c-g	If ($\varphi AB > \varphi CA > \varphi BC$) and ($\varphi CA < 0^{\circ}$) and (R_{01} and $R_{21} > 1$) then (output = c-g)
fault exist	If ($\varphi AB < 115^{\circ}$ or $\varphi AB > 125^{\circ}$) and ($\varphi BC < -245^{\circ}$ or $\varphi BC > -235^{\circ}$) and ($\varphi CA < 115^{\circ}$ or $\varphi CA > 125^{\circ}$) then (output = fault exist)
no fault	If ($115^{\circ} \leq \varphi AB \leq 125^{\circ}$) and ($-245^{\circ} \leq \varphi BC \leq -235^{\circ}$) and ($115^{\circ} \leq \varphi CA \leq 125^{\circ}$) then (output = no fault)

As shown in Table 4.2, both of the input statements in the 'IF-THEN' condition-based rules i.e, ($\varphi CA > \varphi AB > \varphi BC$) and ($\varphi BC < -300^{\circ}$) used to indentify a-g fault, are constructed based on the analysis of the criterion of the minimum value of φBC. It can be seen in Figure 4.2, that the minimum value of φBC is definitely less than -300° and the exact minimum value found in the datapoints for φBC in a-g fault case is -327.7450° (see table 4.1). The value of -300° has been used in "IF-THEN" rule in Table 4.2 instead of -327.4750° . This is because the fault detection time of a-g can be improved slightly using the value of -300° instead of -327.4750° . As shown in Table 4.1, the first data point of φBC after -300° is -300.2819° which is recorded at t = 35.008 s and the minimum data point of φBC, -327.4750° recorded at t = 35.0095 s. Therefore at t = 35.008 s, both of the input statements: ($\varphi CA > \varphi BC > \varphi AB$) and ($\varphi BC < -300^{\circ}$)in 'IF-THEN' rules should be fulfilled to classify the fault as a-g and consequently the output statement (output = a-g) is executed.

It is also shown in Table 4.2 that one of the two input statements in the 'IF-THEN' condition-based rules i.e., ($\varphi BC < 0^{\circ}$) used to indentify a b-g fault, is based on the analysis of criterion of 0°-axis crossing point that was found on the φBC waveform in the case of a b-g fault. It can be seen in Figure 4.2(b) that φBC cross 0°-axis at

approximately t = 35.01 s and according to the data points for fault case b-g shown in Table 4.3 below whereby the first data point that corresponds to the 0°-axis crossing by φBC for b-g fault case is -8.6495° which occurred at t = 35.0105 s. Note that the data points for φAB, φBC and φCA at t = 35.0105 s are highlighted in bold in Table 4.3. Therefore, at t = 35.0105 s, the two input statements i.e., ($\varphi CA > \varphi BC > \varphi AB$) and ($\varphi BC < 0°$) in 'IF-THEN' condition-based rule should be fulfilled to classify the fault as a b-g fault which leads to the execution of the output statement (output = b-g). The criterion of 0°-axis crossing point has also been used to identify a c-g fault as shown in Table 4.2.

Table 4.3

Data point of φAB, φBC and φCA corresponding to b-g fault in Figure 4.2(b) from t = 35.004 s to t = 35.016 s.

Time (s)	Phase angle difference between line current		
	φAB (°)	φBC(°)	φCA(°)
35.0040	146.3764	-255.7650	109.3886
35.0045	-204.2915	101.6654	102.6261
35.0050	-193.2623	98.7673	94.4950
35.0055	-177.3043	94.2073	83.0969
35.0060	-165.9593	90.0032	75.9560
35.0065	-155.9866	84.9242	71.0624
35.0070	-147.2754	78.8524	68.4230
35.0075	-140.0352	71.2558	68.7794
35.0080	-132.4550	57.7155	74.7395
35.0085	-128.0355	44.5139	83.5216
35.0090	-124.4746	29.4175	95.0571
35.0095	-121.5938	14.5811	107.0127
35.0100	-119.2232	2.2792	116.9440
35.0105	**-116.5118**	**-8.6495**	**125.1612**
35.0110	-114.4143	-12.9366	127.3509
35.0115	-111.7766	-15.0543	126.8309
35.0120	-108.1065	-15.8089	123.9155
35.0125	-103.0018	-15.7716	118.7734
35.0130	-94.1079	-15.3808	109.4887
35.0135	-86.8996	-15.3749	102.2745
35.0140	-79.9836	-15.8511	95.8347
35.0145	-73.8260	-16.8902	90.7162
35.0150	-68.7098	-18.5019	87.2117
35.0155	-63.5231	-21.4986	85.0217
35.0160	-60.7179	-24.3044	85.0223

Since the rules in Table 4.2 are mainly constructed to indentify SLG type faults, other type of faults such as LL, DLG and three phase symmetrical faults are all classified as 'fault exist'. They have been indentified using the common characteristics of φCA, φBC and φAB during normal and fault condition for all fault types considered in this investigation,. It can be seen from Figure 4.2 to 4.7 that, during normal network condition, φCA, φBC and φAB are approximately 120°, -240° and 120° and after fault inception, these values will either increase or decrease depending on the type of fault. After careful analysis of the data points related to each type of fault under consideration, it has been noticed that, the variation of values of φCA, φBC and φAB during normal condition is between $\pm$ 5° of the average values of 120°, -240° and 120° respectively. In order to discriminate the normal network operating condition from network fault condition accurately, the upper and lower tolerance limits of $\pm$ 5° added to each of these values, as shown in the three statements in 'IF-THEN' rules to identify other faults type i.e., (φAB < 115° or φAB > 125°) and (φBC <-245° or φBC > -235°) and (φCA <115° or φCA >125°).

4.4 Phase Selection Procedure of Adaptive Rule-based Phase Selector

The condition-based rules shown in Table 4.2 are transformed into Fortran source code [92-94] and then integrated into a new component model built in PSCAD/EMTDC to test the validity of the rules.

Figure 4.8 shows schematic diagram of the adaptive phase selector module built with the PSCAD library blocks and Fortran source code based on the condition-based rules in Table 4.2. The adaptive phase selector module has three input current signals I_a, I_b and I_c , which constitute the line currents measured at the protective device in the power system under consideration. After preprocessing these three input current signals, five parameters φAB, φBC and φCA and the ratios R_{01} and R_{21} are derived. The task of preprocessing the input current signals is carried out using the on-line frequency scanner (FFT) in the PSCAD library. The five parameters are then fed into the block with Fortran source code based on the condition-based rules shown in Table 4.2. The output signals from the module are assigned the values '1', '2', '3', '4'and '5' which corresponding to a-g, b-g, c-g, fault exist and no fault conditions.

The phase selection procedure can be outlined as follow: the proposed phase selector firstly indentifies ‘fault exist’ and ‘no fault’ conditions by issuing ‘4’ or ‘5’. This can be achieved by assessing the φAB, φBC and φCA and the ratios R_{01} and R_{21} that are derived from the input current signals, I_a, I_b and I_c . Later on, if input current signal into the phase selector is obtained from the SLG fault case, the output signal will turn from ‘4’ or ‘5’ to ‘1’, ‘2’or ‘3’ depending on the type of SLG fault. Otherwise, if the input current signals are due to other fault condition such as DLG, LL and three phase symmetrical fault, then the output signal will remain at ‘4’.

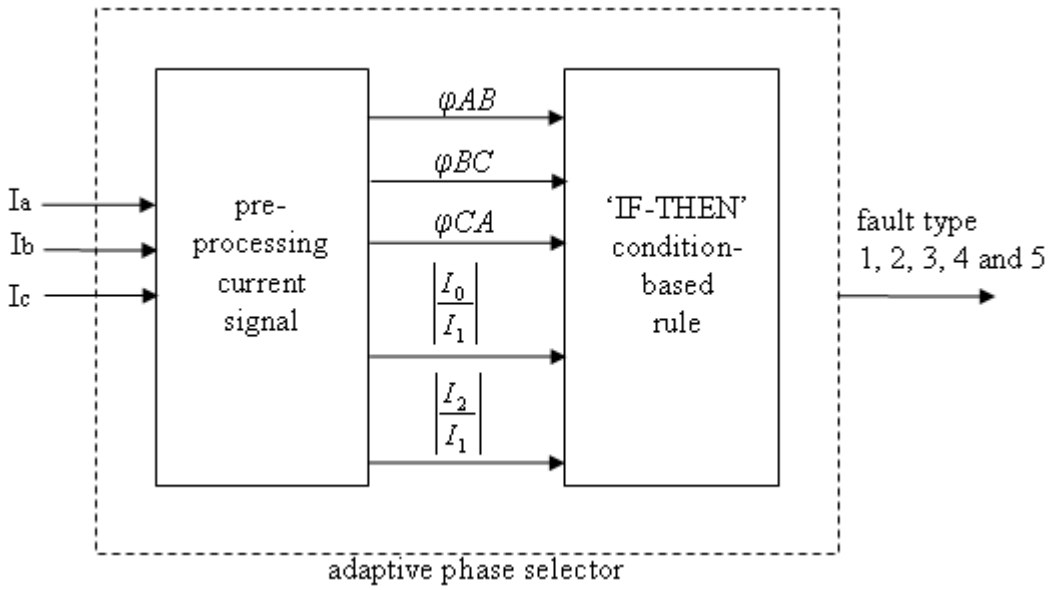

Figure 4.8 Schematic diagram of adaptive rule based phase selector.

Figures 4.9 (a) to (d) illustrate the output tripping signals of the adaptive phase selector module corresponding to a-g, b-g, c-g and b-c-g fault cases. It was found in these figures that the output signal after fault inception at t = 34.998 s drops from ‘5’ corresponding to ‘no fault’ condition to ‘4’ which corresponds to ‘fault exist’. The output signal then dropped from ‘4’ to ‘1’, ‘2’ and ‘3’ respectively in Figures 4.9(a) to (c) corresponding to a-g, b-g and c-g fault types. Figure 4.9(d) shows that output signal corresponding to b-c-g fault case, because it is not one of the SLG fault, the output signal remains at ‘4’ to indicate fault exist.

Other than that, it can be seen from Figure 4.9(a) to (d) that the time for successful fault detection varies with the type of SLG fault. The speed of fault detection is subjected to the criteria being used to construct the condition-based rules in Table 4.2. The decision whether to trip only the faulty phase or all three phases can then be decided using the output signal of the phase selector at a certain time instant after detecting the 'fault exist' condition. In this investigation, it was found from the simulation results shown in Figure 4.9s (a) to (d) that the type of SLG fault can be successfully detected within a period of one cycle after fault inception, therefore the output signal of the phase selector to either trip a single phase or three phases is decided one cycle after detecting the condition 'fault exist'. In this context, an additional timer is required to count the time of one cycle starting from the time instant where the 'fault exist' condition is detected.

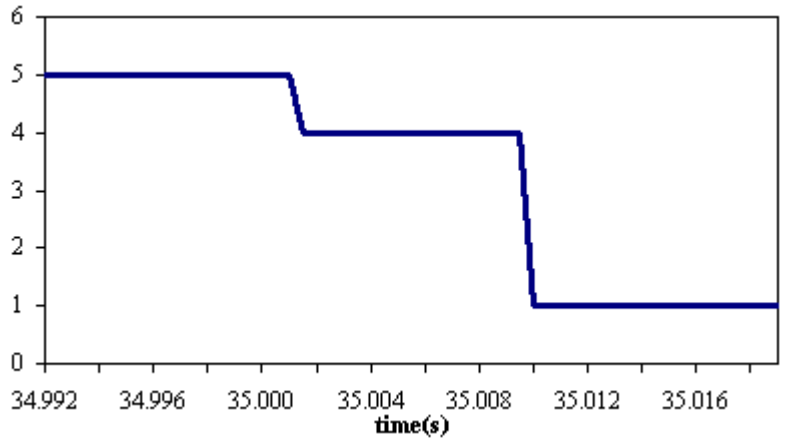

(a) output signal of '1' indicate a-g fault

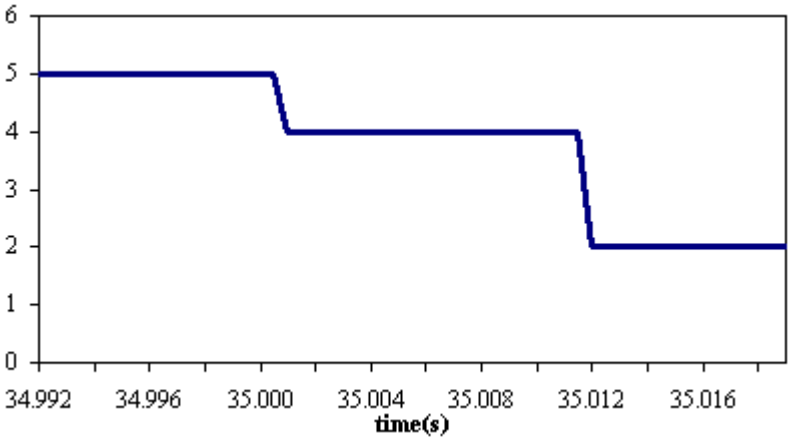

(b) output signal of '2' indicate b-g fault

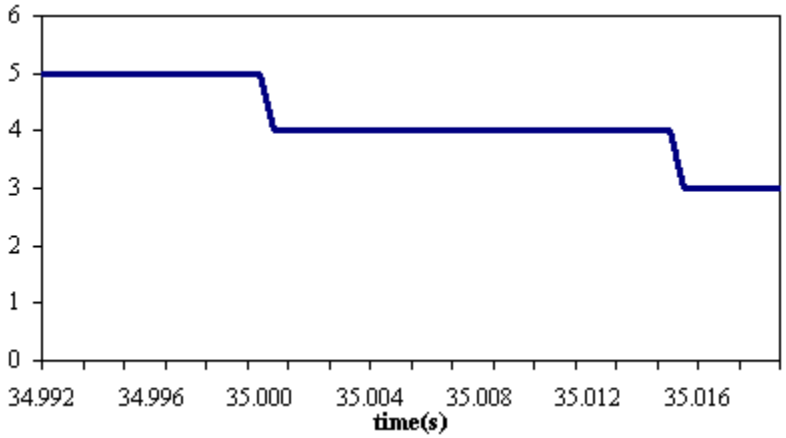

(c) output signal of '3' indicate c-g fault

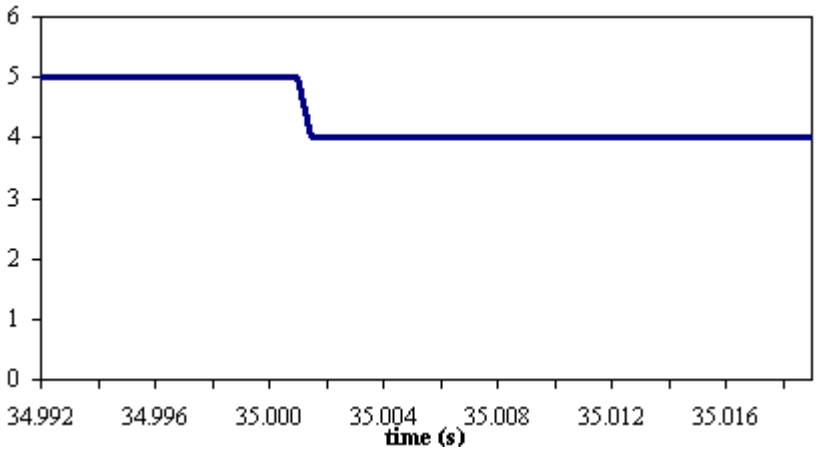

(d) output signal of '4' indicate other fault

Figure 4.9 Output signal of adaptive phase selector after the following fault condition being detected: (a) a-g fault, (b) b-g fault, (c) c-g fault and (d) b-c-g fault.

4.5 Fault Data Generation using PSCAD/EMTDC

The condition-based rules shown in Table 4.2 are valid for a SLG fault with a fault resistance $R_f = 0\Omega$ that occurs within line section 1 from the 33kV grid (see Figure 4.1). Depending upon the network configuration, fault resistance, fault section, fault inception angle (FIA), the variation of the considered five parameters particularly *φAB*, *φBC* and *φCA*, during the transient period might have a significant difference in certain fault cases. Consequently, this will affect the performance of the adaptive rule based phase selector discussed in section 4.4. Figure 4.10 shows variations of *φAB*, *φBC* and *φCA* due to a b-g fault assumed at 2.5km from 33kV grid with a different fault resistance. The variation of *φAB*, *φBC* and *φCA* shown in Figure 4.10(a) and (b) have a distinctive difference when compared to each other. Figure 4.10(a) is due to a b-g fault with $R_f = 0\Omega$ and fault location = 2.5 km from 33kV grid (see Figure 4.1).

φBC crossed 0°-axis at approximately t = 34.012 s and the phase selector discussed in section 4.4 can successfully indentify the fault type as 'b-g'. In contrast, Figure 4.10(b) shows variations of φAB, φBC and φCA due to a b-g fault with $R_f = 5\Omega$ and fault location = 2.5 km from the 33kV grid. Although in this case, the fault is also assumed within line section 1, the figure clearly shows that φBC does not cross the 0°-axis. Thus, the fault type of this fault case has been classified by phase selector as 'fault exist', due to the fact that the criterion of 0°-axis crossing point of φBC used to construct the statement in the 'IF-THEN' condition-based rules to identify a b-g fault (see section 4.3.5) does not exist in this particular fault case. In this context, the classification of 'fault exist' by the phase selector is incorrect.

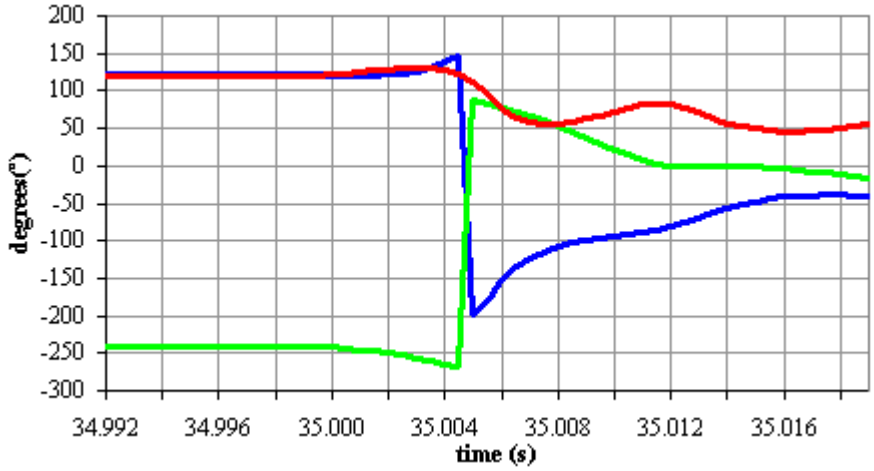

(a) b-g fault at 2.5km from 33kV grid, $R_f = 0\Omega$

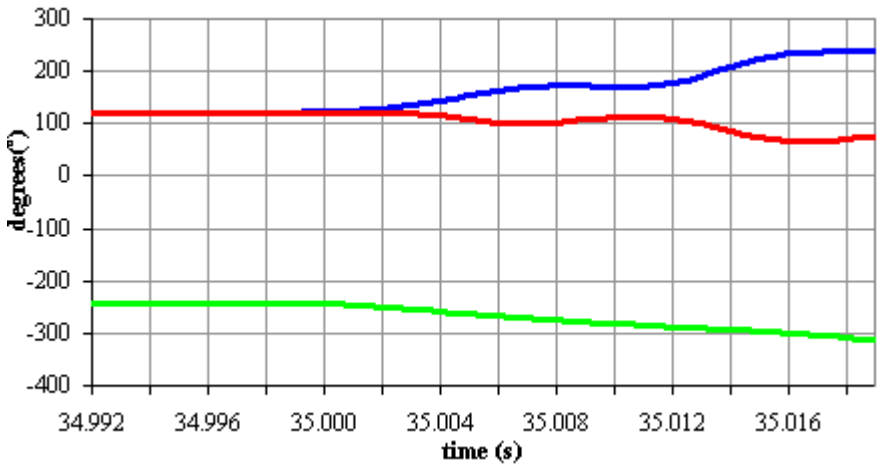

(a) b-g fault at 2.5km from 33kV grid, $R_f = 5\Omega$

Figure 4.10 Variation of waveform φAB (blue waveform), φBC(green waveform) and φCA(green waveform) due to b-g fault assumed at 2.5km from 33kV grid with different fault resistance.

Sufficient fault data is necessary to simulate a practical distribution network with system operating conditions that are varied all the time. Intensive simulation tests were carried out in PSCAD/EMTDC to generate fault data under different system operating conditions. This included different network operating mode (radial and ring), faults at different sections (various locations within sections 1, 2 or 3) , different fault resistances, R_f (0 and 5Ω) , different fault inception angles, FIA (0° and 90°) and network loading level (full load or half load). The scenarios used for generating data are summarized in Table 4.4. A total of 2592 SLG fault cases have been simulated. Note that:

a. FIA has been defined from the positive going zero crossing instant of phase-a current. 0° and 90° fault inception angles are corresponding to t = 34.998 s and t = 35.003 s in the generated fault cases.
b. The term 'full load' indicates the originally loading shown at each feeder in the investigated network (see Figure 4.1 in section 4.2.2). The term 'half load' indicates that the loading of all these feeders have been reduced to 50% of the 'full load' uniformly.

Table 4.4

Scenarios used for generating 2592 of SLG fault cases in PSCAD/EMTDC.

Relay under consideration	R_1 to R_{33} along feeder 1
fault type	a. phase a to ground fault b. phase b to ground fault c. phase c to ground fault
fault location	a. line section 1: 1km, 2.5km and 4km b. line section 2: 6km , 7.5km and 9km c. line section 3: 11km 12.5km and 14km
fault resistance, R_f	a. 0Ω b. 5Ω
fault inception angle, FIA	a. 0° b. 90°
network loading level	a. full load (FL) b. half load (HL)
network configuration	a. radial b. ring

In addition to the requirement of generating sufficient simulation fault data, a more effective method is needed to process and analysis the large volume of fault data, so that the unique characteristic of each investigated SLG fault case can be found and eventually the fault type of each fault case can be indentified correctly. In this context, several software programmes have been developed mainly using C ++, to handle the data processing, analysing and testing, in order to effectively manage the large volume of collected fault data and extract the useful information required for the construction of the proposed rule-based fault identification and phase selection algorithm. The detailed digital data processing followed by the fault identification and phase selection algorithm construction and verification will be elaborated on Chapter 5.

4.6 Conclusion

The simulation results obtained from this investigation indicate that the proposed condition rule-based fault identification and phase selection algorithm can successfully indentify the type of SLG fault during fault condition. It has been found that the fault type can be indentified within a cycle after the fault inception. The detection time depends on the criterion being used to construct the rule-based fault identification algorithm. The high speed capability of fault detection which is characteristic of the proposed algorithm would facilitate high speed operation of the phase selector. This would satisfy the main requirement of maintaining transient stability of a grid connected DG.

Chapter 5: Digital Data Processing and Testing of the Proposed Adaptive Rule-based Fault Identification and Phase Selection Algorithm

5.1 Introduction

This chapter presents the digital data processing and testing adopted in the development of the proposed rule based fault identification and phase selection algorithm, whose aim is to maintain the continued operation of DG during SLG faults. Several software modules have been developed mainly using the C ++ language [95-98] to efficiently handle the massive fault data processing, followed by the fault identification and phase selection algorithm construction and verification. For the convenience of the reader while reading chapter 5, the power system under investigation that was shown in Figure 4.1, Chapter 4, has been reproduced in Figure 5.1. In this figure, the length of distribution line sections 1 to 6 is assumed to be 5km and the distribution line section 7 is 10km.

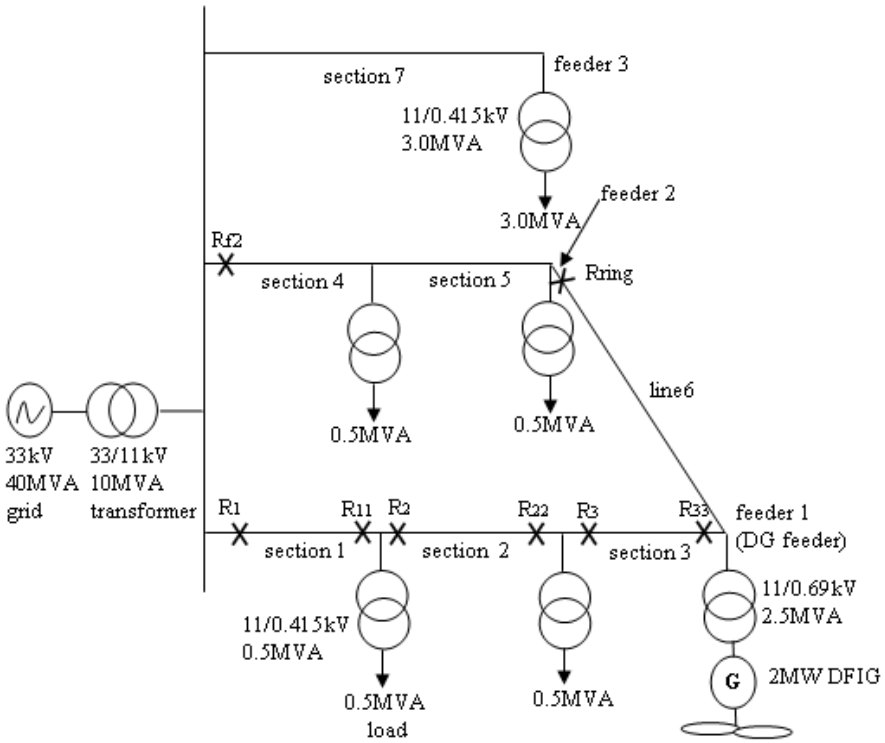

Figure 5.1 Network configuration of investigated 11kV overhead network with DG.(reproduced from Figure 4.1 in section 4.2.2 at Chapter 4)

5.2 Digital Fault Data Processing

As reported in section 4.5 in Chapter 4, a total of 2592 cases of SGL have been simulated using PSCAD/EMTDC to collect sufficient fault data to represent a practical system. These fault cases needed to be analysed accurately so that useful information could be extracted from each of the fault cases for the construction of the fault identification algorithm later on. The data processing of 2592 fault cases poses a certain degree of difficulty if it is handled manually and furthermore the end result can not be guaranteed to be accurate. Therefore, computer intervention in the data processing of 2592 cases is necessary. Several software programmes have been developed using C++ to handle automatically the main tasks of fault data processing. The tasks include: storage and retrieval fault cases, analysis of fault cases to find the key information which characterize the fault case under consideration and finally construction and verification of the fault identification and phase selection algorithm using fault cases.

5.3 Fault Data Storing and Retrieving

Each of the fault cases generated from PSCAD/EMTDC is given unique name e.g., R11-Ra-FL0R0D-AG-12.5km, where 'R11' refers to current measurement obtained from relay R_{11} (see the Figure 5.1), 'Ra' refers to radial network operating mode (while 'Ri' refers to ring network operating mode), 'FL' refers to full load of the network loading level (while 'HL' refers to half load), '0R' refers to $R_f = 0\Omega$ (while '5R' refers to $R_f = 5\Omega$) , '0D' refers to FIA (fault inception angle) = 0° (while '90D' refers to FIA = 90°) and 'AG' refers to a-g fault (while 'BG' refer to b-g fault and 'CG' refer to c-g fault), '12.5KM' refers to the fault location at 12.5km along feeder 1 from 2MW DFIG that is located at the end of feeder 1 (see the Figure 5.1). Fault location 12.5km is in section 1.

Each fault case consists of data points from the five parameters, φAB, φBC, φCA, R_{01} and R_{21} that are used in the proposed fault identification strategy described in section 4.3 in Chapter 4. The data window for each of these parameters consists of 55 data points corresponding to 55 samples which define the window of collected data. The 2592 fault cases are all saved in a Folder called "Case Database A". Then, each of the fault case in this folder was analysed in the fault data analysis process that will be

explained in section 5.4 subsequently. The results of the fault data analysis process are then saved in a File called “Case Database B”. After that, the fault data in this file is subjected to an optimisation process which will be explained in section 5.5 later on. The optimisation process is intended to extract key fault features which can uniquely characterize each of the fault cases after being retrieved from the Case Database B file. The results of fault data optimisation process are then saved in a file called “Case Database C”. The data is saved in Case Databases A, B and C in a text file format type called tab delimited file (.txt) format. The latter is used to ensure easy access of the data fro the analysing processes in the subsequent algorithm development, testing and verification. The process of storage and retrieval fault data from Case Data A, B and C can be summarised in flow chart shown in Figure 5.2

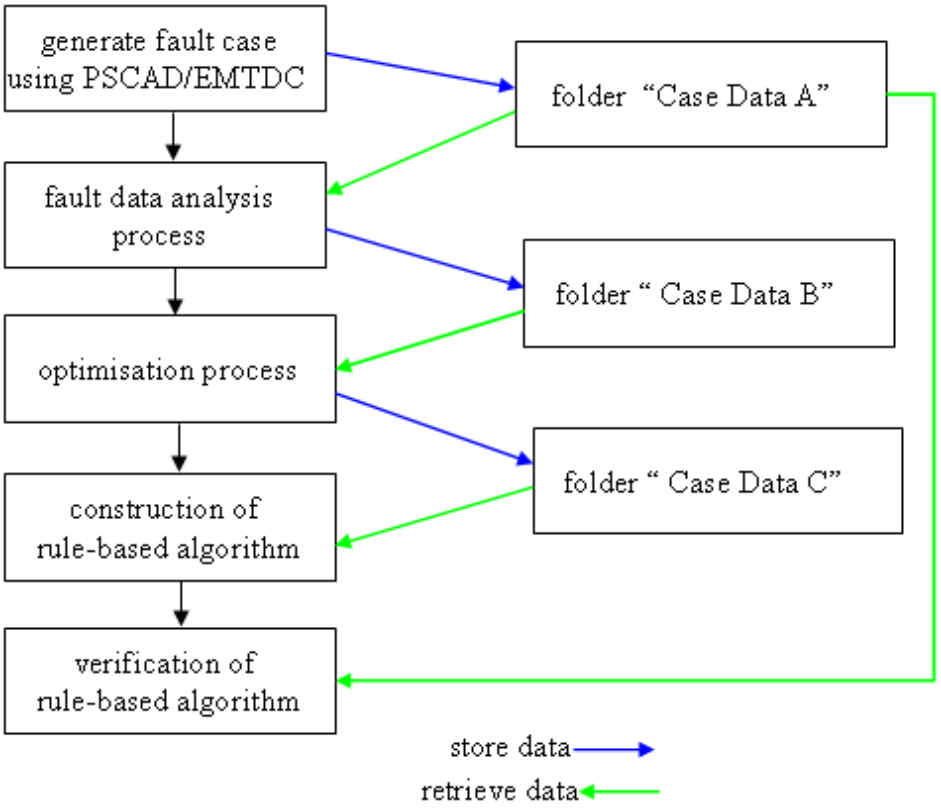

Figure 5.2 Flow chart illustrate the process of storage and retrieval fault data from Case Data A, B and C.

Figure 5.3 (a) to (c) below shows the procedure for transferring the fault data of a fault case generated in the PSCAD environment into a text file form, which is saved in Case Database A. The fault data saved in Case Database B and C will be discussed in sections 5.4 and 5.5 respectively.

As shown in Figure 5.3 (a), firstly the fault data is exported from PSCAD into Excel by copying the data points collected within the required investigated time interval to the clipboard and then pasting them into Excel. As shown in Figure 5.3(b), the fault data is then displayed in comma separated value (.csv) format in the Excel environment so that graphs corresponding to each of the fault cases can be created and included in the thesis. Figure 5.3(c) shows that the data points are finally pasted directly into Notepad, saved as tab delimited file (.txt) format and saved in Case Database A. data points of each of the fault case for the 2592 fault cases under consideration in ".txt" format can be found in Appendix C.

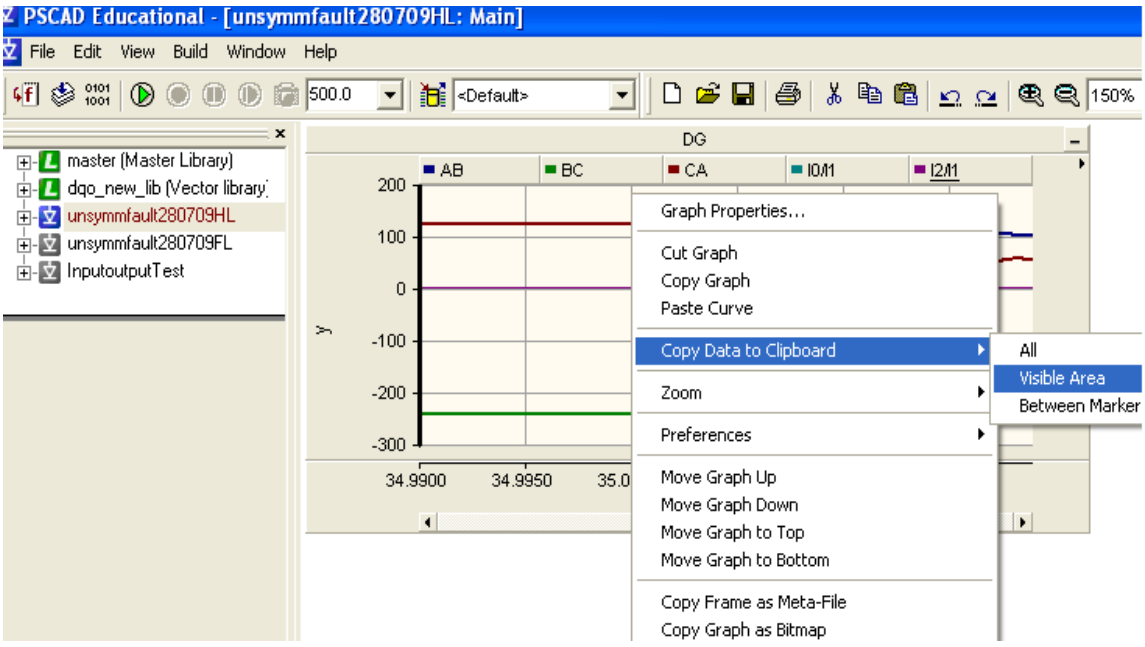

(a) data points within measured data window are copied into clipboard and then exported from PSCAD to Excel.

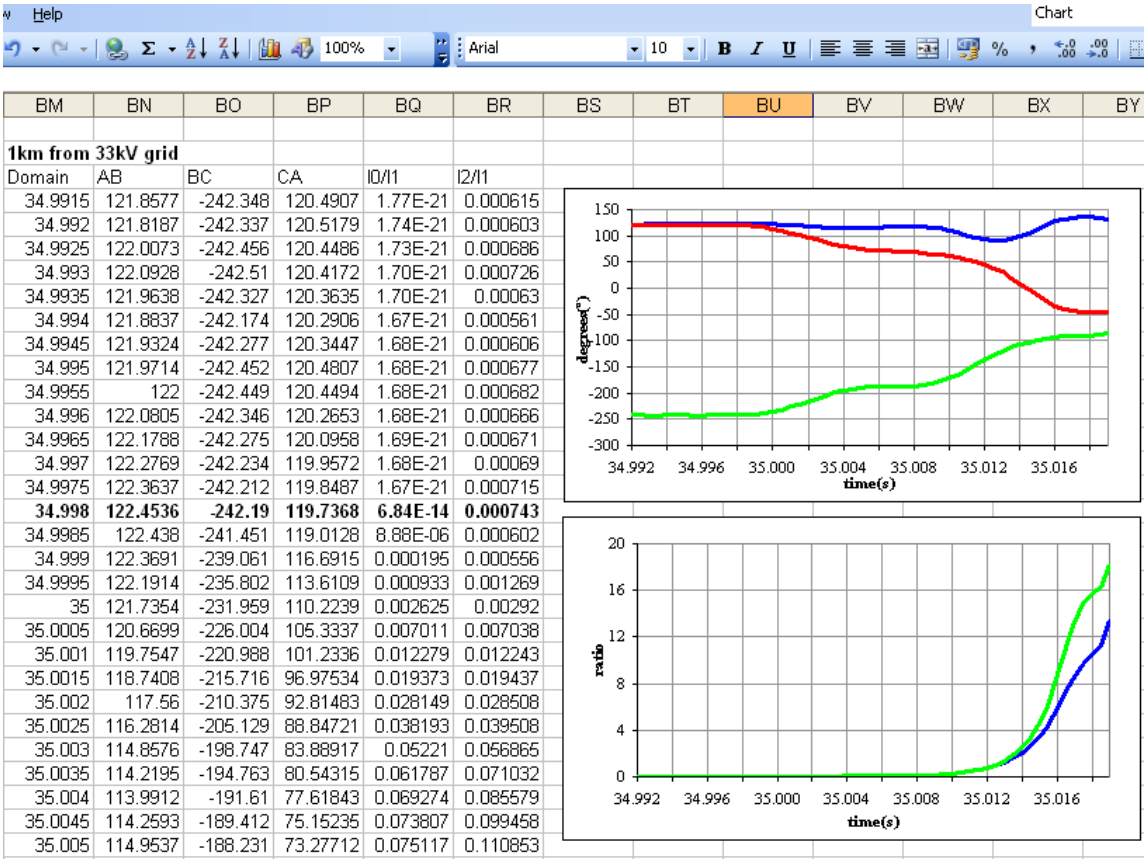

BM	BN	BO	BP	BQ	BR	BS	BT	BU	BV	BW	BX	BY
1km from 33kV grid												
Domain	AB	BC	CA	I0/I1	I2/I1							
34.9915	121.8577	-242.348	120.4907	1.77E-21	0.000615							
34.992	121.8187	-242.337	120.5179	1.74E-21	0.000603							
34.9925	122.0073	-242.456	120.4486	1.73E-21	0.000686							
34.993	122.0928	-242.51	120.4172	1.70E-21	0.000726							
34.9935	121.9638	-242.327	120.3635	1.70E-21	0.00063							
34.994	121.8837	-242.174	120.2906	1.67E-21	0.000561							
34.9945	121.9324	-242.277	120.3447	1.68E-21	0.000606							
34.995	121.9714	-242.452	120.4807	1.68E-21	0.000677							
34.9955	122	-242.449	120.4494	1.68E-21	0.000682							
34.996	122.0805	-242.346	120.2653	1.68E-21	0.000666							
34.9965	122.1788	-242.275	120.0958	1.69E-21	0.000671							
34.997	122.2769	-242.234	119.9572	1.68E-21	0.00069							
34.9975	122.3637	-242.212	119.8487	1.67E-21	0.000715							
34.998	**122.4536**	**-242.19**	**119.7368**	**6.84E-14**	**0.000743**							
34.9985	122.438	-241.451	119.0128	8.88E-06	0.000602							
34.999	122.3691	-239.061	116.6915	0.000195	0.000556							
34.9995	122.1914	-235.802	113.6109	0.000933	0.001269							
35	121.7354	-231.959	110.2239	0.002625	0.00292							
35.0005	120.6699	-226.004	105.3337	0.007011	0.007038							
35.001	119.7547	-220.988	101.2336	0.012279	0.012243							
35.0015	118.7408	-215.716	96.97534	0.019373	0.019437							
35.002	117.56	-210.375	92.81483	0.028149	0.028508							
35.0025	116.2814	-205.129	88.84721	0.038193	0.039508							
35.003	114.8576	-198.747	83.88917	0.05221	0.056865							
35.0035	114.2195	-194.763	80.54315	0.061787	0.071032							
35.004	113.9912	-191.61	77.61843	0.069274	0.085579							
35.0045	114.2593	-189.412	75.15235	0.073807	0.099458							
35.005	114.9537	-188.231	73.27712	0.075117	0.110853							

(b) display of data points in a fault case in (.cvs) format together with corresponding graphs using Excel.

```
File  Edit  Format  View  Help
34.9915 121.8576694     -242.3483746    120.4907052     1.77E-21        0.000614937
34.992  121.8187416     -242.3366328    120.5178912     1.74E-21        0.000603117
34.9925 122.0072819     -242.455838     120.4485561     1.73E-21        0.000686177
34.993  122.0928322     -242.5100338    120.4172016     1.70E-21        0.000726453
34.9935 121.9638405     -242.3273617    120.3635212     1.70E-21        0.000630381
34.994  121.8836623     -242.1742157    120.2905535     1.67E-21        0.000561426
34.9945 121.9323722     -242.277093     120.3447208     1.68E-21        0.000606066
34.995  121.9714499     -242.4521846    120.4807348     1.68E-21        0.000676859
34.9955 122.0000483     -242.4494361    120.4493878     1.68E-21        0.000682172
34.996  122.0804801     -242.3458151    120.265335      1.68E-21        0.000665528
34.9965 122.1787542     -242.2745191    120.0957648     1.69E-21        0.000670782
34.997  122.276853      -242.234085     119.957232      1.68E-21        0.000690396
34.9975 122.3637246     -242.2123964    119.8486718     1.67E-21        0.000714973
34.998  122.4535981     -242.1903795    119.7367814     6.84E-14        0.000743458
34.9985 122.4379772     -241.4507832    119.012806      8.88E-06        0.000601664
34.999  122.3690751     -239.060606     116.6915308     0.000195299     0.000556439
34.9995 122.1914254     -235.8023408    113.6109154     0.000932625     0.001268554
35      121.7354173     -231.9593368    110.2239195     0.002624753     0.002920019
35.0005 120.6698694     -226.0035589    105.3336896     0.007010621     0.007037981
35.001  119.7547097     -220.9882915    101.2335818     0.012279188     0.012243404
35.0015 118.7407872     -215.7161224    96.97533515     0.019372807     0.019436763
35.002  117.5599867     -210.3748195    92.81483283     0.028148548     0.02850843
35.0025 116.2813869     -205.128595     88.84720816     0.038192571     0.039508158
35.003  114.8575844     -198.746759     83.88917453     0.052210114     0.056865395
35.0035 114.2195323     -194.7626831    80.54315082     0.06178747      0.071032082
35.004  113.9911652     -191.6095997    77.61843449     0.0692739       0.085579115
35.0045 114.2592651     -189.4116186    75.15235349     0.073807238     0.099458022
35.005  114.9537233     -188.2308432    73.27711996     0.075116955     0.110853008
```

(c) display of data points in a fault case in (.txt) format using Notepad.

Figure 5.3 The procedure of transferring fault data generated in PSCAD environment into a text file format.

5.4 Fault Data Analysis

The aim of analysing fault data cases is to determine common parameters of interest, i.e., max and min values, and to identify the features of each fault case. A total of 38 elements that represent the features of each fault case have been indentified. These elements are stored in a vector **X** where **X** = {x_1, x_2,…., x_i,….,x_m}, i = 1, 2, 3,…, m. x_i is the i^{th} element in vector **X** and m = 38. They are selected from a total of 275 data points which constitute the total collected data points within a window for a particular fault case.

5.4.1 Selection of x_i^{th} Elements of Vector X

The selection of 38 elements which form the parameters of X are based on several dominant criterions which have been identified after carefully studying each of five variations, *φAB*, *φBC*, *φCA*, R_{01} and R_{21}. The criterion that have been considered are as follows:

a. maximum and minimum data point of *φAB*, *φBC* and *φCA*
b. predefined crossing variations of *φAB*, *φBC* and *φCA* which respect to 0°- axis and 150°-axis.
c. maximum values of ratios R_{01} and R_{21}.

5.4.1.1 Maximum and Minimum Values of *φAB*, *φBC* and *φCA*

The maximum and minimum data points of the three input parameters *φAB*, *φBC* and *φCA* are considered as very powerful criterions that can be used to identify SLG type faults. In each fault case, the maximum and minimum values of each of the input parameters *φAB*, *φBC* and *φCA* have been selected. In addition to that, the values of the other two input parameters corresponding to maximum and minimum values of the considered parameter have also been selected. This can be explained as followed with reference to Table 5.1. The data points of fault case R33-Ra-FL0R90D-CG-1km that are shown in Table 5.1 are taken from t = 35.0035 s to 35.065 s, which is the time period where the maximum value of *φBC* has occurred. The maximum values of *φBC*, $max_{\varphi BC}$ = 100.0703° occurred at t = 35.0065 s. Note that the values of *φAB* , *φBC* and *φCA* at t =35.0065 s are highlighted in Bold in Table 5.1. The values of *φAB* and *φCA*, corresponding to $max_{\varphi BC}$ are -211.5989° and 111.5286°. Accordingly,

the values 100.0703°, -211.5989° and -111.5286° have been included in the vector **X** corresponding to this fault case. Note the considered fault case i.e., R33-Ra-FL0R90D-CG-1km refers to the c-g fault (based on the line current measurement of relay R_{33} in Figure 5.1) assuming the following fault and network operating conditions: $R_f = 0\Omega$, FIA = 90° (corresponding to the fault inception time of 35.003 s), fault location = 1km from the 2MW DFIG (within section 3), network configuration = radial network, loading condition = full load. Figure 5.4 shows the corresponding waveforms *φAB*, *φBC* and *φCA* for the period which cover pre-fault and fault conditions starting from t = 34.9965 s to t = 35.0235 s.

Table 5.1

The data point of *φAB*, *φBC* and *φCA* corresponding to fault case: R33-Ra-FL0R90D-CG-1km, from t = 35.0035 s to t = 35.007 s.

Time (s)	Phase angle difference between line current		
	φAB	*φBC*	*φCA*
35.0035	121.7454	-240.6852	118.9397
35.0040	122.6972	-242.0295	119.3323
35.0045	124.4991	-244.2246	119.7255
35.0050	127.4380	-246.9422	119.5042
35.0055	133.6458	-251.4807	117.8349
35.0060	140.1972	-255.4900	115.2928
35.0065	**-211.5989**	**100.0703**	**111.5286**
35.0070	-201.7983	95.2305	106.5678

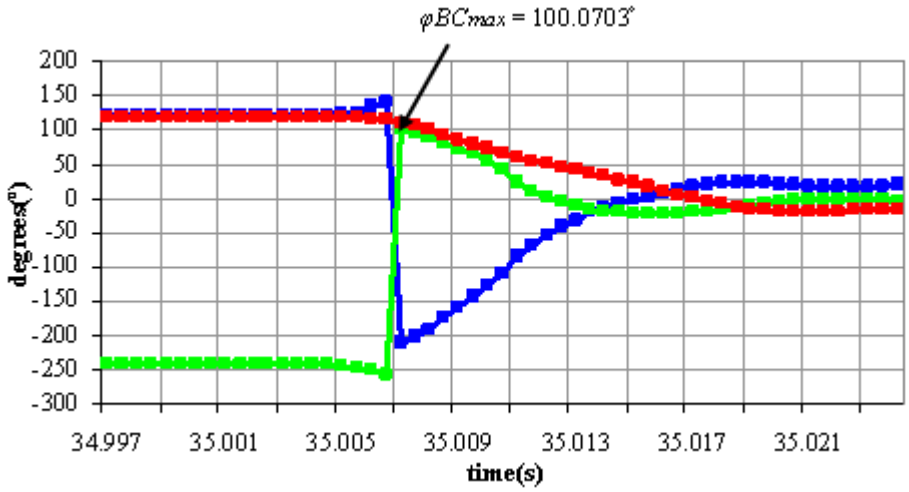

Figure 5.4 Waveforms of *φAB* (blue waveform) , *φBC* (green waveform) and *φCA* (red waveform) corresponding to the fault case: R33-Ra-FL0R90D-CG-1km, stretching from t = 34.9965 s to t = 35.0235 s.

5.4.1.2 The Predefined Crossing Values of φAB, φBC and φCA

The predefined crossing values of φAB, φBC and φCA refer to the 0°-axis crossing and the 150°-axis crossing values of φAB, φBC and φCA.

In the fault data analysis process, 0°-axis crossing values is defined as the first data point, being observed after the input parameters φAB, φBC and φCA cross 0°-axis. For 0°-axis crossing, the first data point can be either a positive or negative value, depending on the oscillation pattern of φAB, φBC and φCA, either from a positive going 0°-axis crossing or negative going 0°-axis crossing. This can be explained with reference Figure 5.5 that shows the fault case R22-Ri-HL5R90D-CG-7.5km, plotted from t = 34.9965 s to t = 35.0235 s . This figure shows that first value of data point of φAB (blue waveform) after it crosses the 0°-axis is -178.9094° as φAB is going from positive to negative at the crossing point. Meanwhile, φBC (green waveform) crosses 0°-axis twice within the considered time interval. At the first crossing, φBC goes from negative to positive at where the 1st data point after a 0°-axis crossing is -128.2861°. At the second crossing, φBC goes from positive to negative where the 1st data point after the 0°-axis crossing is -3.6769°. It is also shown in this figure that, φCA (red waveform) does not cross 0°-axis within the considered time interval, which means that φCA in this fault case does not have a data point that shows the criterion of 0°-axis crossing. Note the considered fault case i.e., R22-Ri-HL5R90D-CG-7.5km refers to c-g fault (based on line current measurement of relay R_{22} in Figure 5.1) assuming the following fault and network operating condition: $R_f = 5\Omega$, FIA = 90° (corresponding to the fault inception time of 35.003 s) , fault location = 7.5km from 2MW DFIG (within section 2) , network configuration = ring network, loading condition = half load.

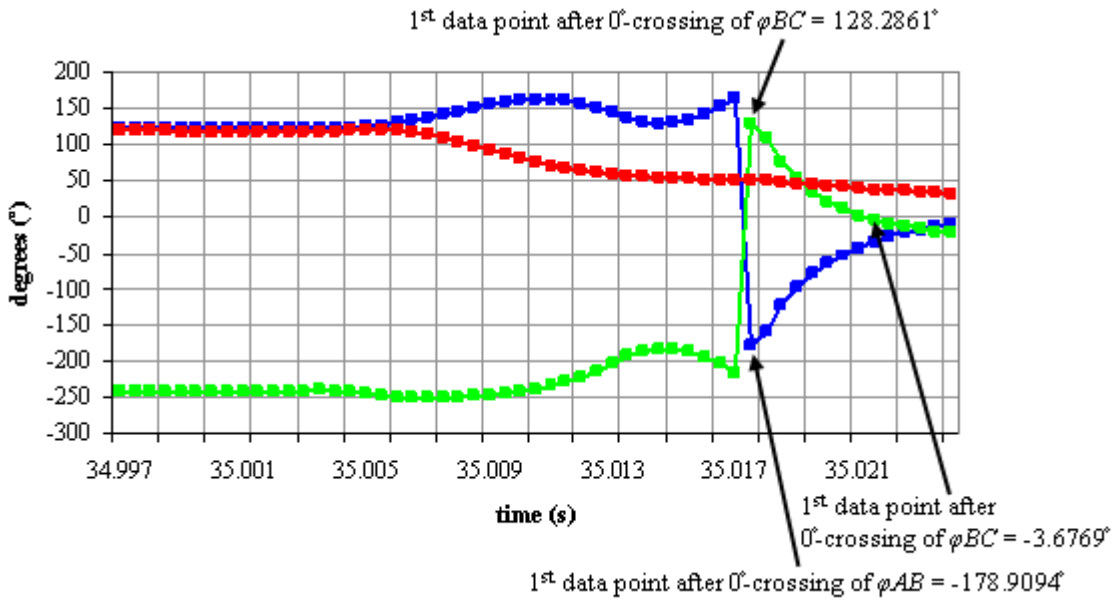

Figure 5.5 Waveforms φAB (blue waveform), φBC (green waveform) and φCA (red waveform) corresponding to the fault case: R22-Ri-HL5R90D-CG-7.5km for the time interval, from t = 34.9965 s to t = 35.0235 s.

Table 5.2 shows the fault data points corresponding to this fault case for the fault time interval from t = 35.0025 s to t = 35.0230 s. Table 5.2 shows that the 1st data point after the 0°-axis crossing by φAB is a negative value which is -178.9094° at t = 35.017 s and the corresponding values φBC, and φCA are 128.2861° and 50.6233°. Note that in table 5.2, the data points of φAB, φBC and φCA at t =35.0170 s are highlighted in Bold. Although φBC crosses the 0°-axis twice within the investigated time interval of this fault case, only its first time 0°-axis crossing has been considered and consequently only the 1st data point after this first crossing point together with corresponding values of φAB and φCA have been considered and therefore used as elements in vector **X**. Therefore the values of -178.9094°, 128.2861° and 50.6233° have been included as elements in vector **X** corresponding to this fault case.

Table 5.2

The data point of φAB, φBC and φCA corresponding to fault case:

R22-Ri-HL5R90D-CG-7.5km, from t = 35.0025 s to t = 35.0230 s.

Time (s)	Phase angle difference between line current		
	φAB	φBC	φCA
35.0025	123.1734	-240.7625	117.5891
35.0030	122.8786	-240.5697	117.6910
35.0035	123.0324	-241.1069	118.0745
35.0040	123.7519	-243.0824	119.3305
35.0045	124.9250	-245.5260	120.6010
35.0050	126.5205	-247.5361	121.0155
35.0055	129.7994	-249.2865	119.4871
35.0060	133.2322	-250.1398	116.9076
35.0065	137.0594	-250.5285	113.4691
35.0070	141.0667	-250.3725	109.3058
35.0075	145.3834	-249.6450	104.2616
35.0080	151.1399	-248.1304	96.9904
35.0085	155.0025	-246.5425	91.5400
35.0090	158.2403	-244.5294	86.2891
35.0095	160.6859	-242.0281	81.3423
35.0100	162.1586	-238.9191	76.7605
35.0105	162.2303	-233.5427	71.3124
35.0110	160.3909	-228.1893	67.7984
35.0115	156.6747	-221.3300	64.6553
35.0120	151.4759	-213.3123	61.8364
35.0125	145.0252	-204.4391	59.4139
35.0130	135.4003	-192.2029	56.8026
35.0135	130.4805	-185.7055	55.2250
35.0140	128.8538	-182.8546	54.0008
35.0145	130.3616	-183.5025	53.1409
35.0150	134.0766	-186.5933	52.5167
35.0155	142.6765	-194.6474	51.9708
35.0160	152.3507	-204.0610	51.7103
35.0165	164.8445	-216.1429	51.2984
35.0170	**-178.9094**	**128.2862**	**50.6233**
35.0175	-157.8343	108.1856	49.6487
35.0180	-123.7470	75.8078	47.9392
35.0185	-99.2917	52.8539	46.4378
35.0190	-79.7075	34.8779	44.8296
35.0195	-64.8728	21.6919	43.1809
35.0200	-53.4831	11.9376	41.5455
35.0205	-41.7519	2.2915	39.4604
35.0210	-34.3753	-3.6769	38.0522
35.0215	-27.7538	-9.0471	36.8009
35.0220	-22.1720	-13.4721	35.6441
35.0225	-17.7309	-16.8420	34.5729
35.0230	-13.1569	-20.1711	33.3280

It has been observed that in certain fault cases none of the variables φAB, φBC and φCA cross the 0°-axis. For example in the fault cases shown in Figures 5.6 and 5.7, it can be seen that none of the three parameters φAB (blue waveform) , φBC (green waveform) and φCA (red waveform) crosses the 0°-axis.

Note that the fault case shown in Figure 5.6 is R22-Ra-FL5R90D-AG-9km which refers to an a-g fault (based on line current measurement of relay R_{22} in Figure 5.1) assuming the following fault and network operating condition: $R_f = 5\Omega$, FIA = 90° (corresponding to the fault inception time of 35.003 s), fault location = 9km from the 2MW DFIG (within line section 2), network configuration = radial network, loading condition = full load. Note that the fault case shown in Figure 5.7 is R11-Ra-FL5R0D-BG-12.5km which refers to a b-g fault (based on line current measurement of relay R_{11} in Figure 5.1) assuming the following fault and network operating condition: $R_f = 5\Omega$, FIA = 0° (corresponding to the fault inception time of 34.998 s), fault location = 12.5km from 2MW DFIG (within section 1), network configuration = radial network, loading condition = full load.

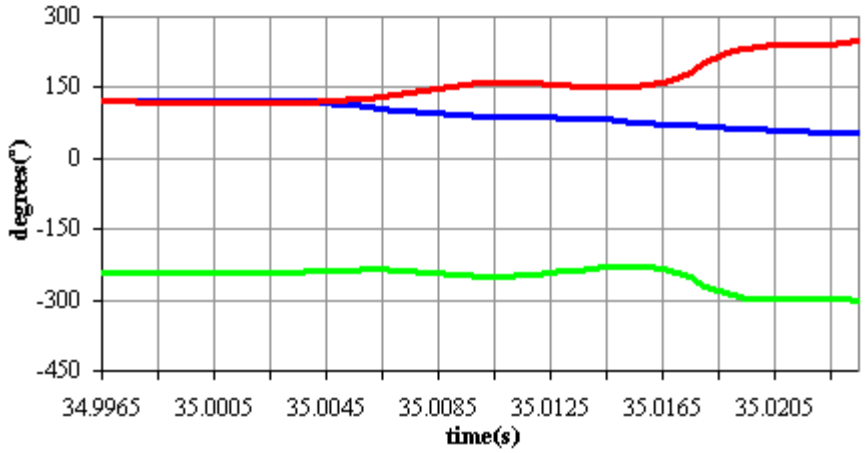

Figure 5.6 Waveforms φAB (blue waveform), φBC (green waveform) and φCA(red waveform) corresponding to fault case: R22-Ra-FL5R90D-AG-9km, for the time interval from t = 34.9965 s to t = 35.0235 s.

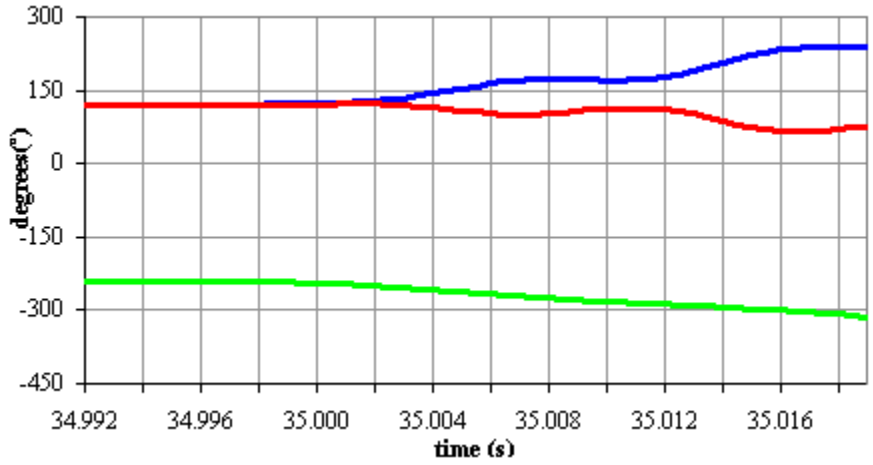

Figure 5.7 Waveforms φAB (blue waveform) , φBC (green waveform) and φCA (red waveform) corresponding to fault case: R11-Ra-FL5R0D-BG-12.5km, for the time interval from t = 34.9915 s to t = 35.0185 s.

After careful study of Figures 5.6 and 5.7, a new α-axis has been identified where α is equal to 150°. Therefore 150°-axis crossing values have been defined as the first data point being observed after the input parameters φAB or φCA have crossed the 150°-axis. This is because, it has been noticed in significant amounts of fault cases with $R_f = 5\Omega$ that either φAB, or φCA crosses 150°-axis instead of the 0°-axis e.g., φCA (red waveform) have crossed 150°-axis in the fault case shown in Figure 5.5 while φAB (blue waveform) have crossed 150°-axis in the fault case shown in Figure 5.6. Table 5.3 shows the fault data points corresponding to the fault case R22-Ra-FL5R90D-AG-9km for the fault period from t = 35.002 s to t = 35.011 s. It is shown in Table 5.3 that the 1st data point immediately after φCA crosses the 150°-axis is equal to 152.7106° at t = 35.009 s and the corresponding values of φAB, and φBC are 92.9024° and -245.6130°. Note that in Table 5.3, the data points of φAB, φBC and φCA at t =35.009 s are highlighted in Bold. Therefore 92.9024°, -245.6130° and 152.7106° have been included as elements in vector **X** related to this fault case.

Table 5.3

The data point of φAB, φBC and φCA corresponding to fault case: R22-Ra-FL5R90D-AG-9km, for the time interval from t = 35.0020 s to t = 35.0110 s.

Time (s)	Phase angle difference between line current		
	φAB (°)	φBC(°)	φCA(°)
35.0020	122.2656	-241.3189	119.0533
35.0025	122.1898	-241.2302	119.0403
35.0030	121.9300	-241.0009	119.0709
35.0035	121.5814	-240.7463	119.1648
35.0040	120.3118	-240.0693	119.7575
35.0045	118.1690	-238.8747	120.7058
35.0050	115.5610	-237.4411	121.8800
35.0055	111.8960	-236.1263	124.2303
35.0060	108.9142	-235.7721	126.8579
35.0065	105.8373	-236.0153	130.1780
35.0070	102.8008	-236.8672	134.0664
35.0075	100.0115	-238.2929	138.2814
35.0080	96.7758	-241.0004	144.2246
35.0085	94.6869	-243.3328	148.6459
35.0090	**92.9024**	**-245.6130**	**152.7106**
35.0095	91.4250	-247.5677	156.1428
35.0100	90.2379	-248.9744	158.7365
35.0105	89.0304	-249.7527	160.7222
35.0110	88.3108	-249.4330	161.1222

Table 5.4 shows the fault data points corresponding to the fault case R11-Ra-FL5R0D-BG-12.5km defined during the interval from t = 34.9970 s to t = 35.006 s. Table 5.4 shows that the 1st data point following the crossing of 150°-axis by φAB is 153.4043° at t = 35.0045 s and the corresponding values of φBC, and φCA are -262.7650° and 109.3607°. Note that in Table 5.4, the data points of φAB, φBC and φCA at t =35.0045 s are highlighted in Bold. Therefore 153.4043°, -262.7650° and 109.3607° have been included as elements in vector **X** related to this fault case.

Table 5.4

The data point of φAB, φBC and φCA corresponding to fault case

: R11-Ra-FL5R0D-BG-12.5km, for time interval from t = 34.9970 s to t = 35.006 s.

Time (s)	Phase angle difference between line current		
	$\varphi AB(^{\circ})$	$\varphi BC\,(^{\circ})$	$\varphi CA(^{\circ})$
34.9970	121.5033	-242.4665	120.9633
34.9975	121.6277	-242.5110	120.8833
34.9980	121.7532	-242.5740	120.8209
34.9985	121.9519	-242.6804	120.7285
34.9990	122.3942	-243.1335	120.7393
34.9995	122.8806	-243.9064	121.0258
35.0000	123.4759	-244.8636	121.3877
35.0005	124.6741	-246.4973	121.8232
35.0010	126.0377	-248.0668	122.0292
35.0015	128.0592	-249.8818	121.8226
35.0020	130.7722	-251.8798	121.1076
35.0025	134.0153	-253.9271	119.9118
35.0030	139.1056	-256.5329	117.4273
35.0035	143.5979	-258.5341	114.9362
35.0040	148.4774	-260.7038	112.2264
35.0045	**153.4043**	**-262.7650**	**109.3607**
35.0050	158.2217	-264.5609	106.3391
35.0055	164.0313	-266.7325	102.7012
35.0060	167.4715	-268.5160	101.0444

5.4.1.3 Maximum Data Point of Ratios R_{01} and R_{21}

The maximum values of ratios R_{01} and R_{21} were found to be useful indicators for confirming that a fault case involves a ground connection. Consequently, the maximum values of ratios R_{01} and $R_{21,}$ R_{01max} and R_{21max} respectively, within the considered time interval of a particular fault case, have been included in the vector **X** that corresponding to that fault case.

It was found in section 4.3, Chapter 4 that in all generated fault cases, prior to fault, values of ratios R_{01} and R_{21} are zero but after fault inception, ratios R_{01} and R_{21} have increased significantly from almost zero to maximum values R_{01max} and R_{21max}. The magnitude of both R_{01max} and R_{21max} were found to vary for the considered fault cases. Figures 5.8 and 5.9 show the variation of ratios R_{01} and R_{21} corresponding to fault cases R33-Ri-HL5R0D-CG-4km and R33-Ra-FL5R90D-CG-4km respectively. As shown in Figure 5.8, R_{01max} (blue waveform) and R_{21max} (green waveform) in fault

case R33-Ri-HL5R0D-CG-4km are 1.2391 and 0.5150 respectively. Therefore 1.2391 and 0.5150 have been included as elements in vector **X** related to this fault case. As shown in Figure 5.9, R_{01max} (blue waveform) and R_{21max} (green waveform) in fault case R33-Ri-HL5R0D-CG-4km are 3.4954 and 0.1596 respectively. Therefore 3.4954 and 0.1596 have been included as elements in vector **X** corresponding to this fault case. It can be concluded from Figures 5.8 and 5.9 that the fault in both of the considered fault cases has a connection between phase c and the ground, i.e., which occurred at the same fault location which is 4km from the 2MW DFIG. However, due to differences in other network parameters such as fault inception time, network configuration and network loading condition, it has been found that the magnitudes of R_{01max} (blue waveform) and R_{21max} (green waveform) are significantly difference for the two fault cases. Note that:

a. R33-Ri-HL5R0D-CG-4km refers to c-g fault (based on line current measurement of relay R_{33} in Figure 5.1) assuming the following fault and network operating condition: $R_f = 5\Omega$, FIA = 0° (corresponding to the fault inception time of 34.998 s), fault location = 4km from the 2MW DFIG (within section 3), network configuration = ring network, loading condition = half load.

b. R33-Ra-FL5R90D-CG-4km is refer to c-g fault (based on line current measurement of relay R_{33} in Figure 5.1) with following fault and network operating condition: $R_f = 5\Omega$, FIA = 90° (corresponding to the fault inception time of 35.003 s), fault location = 4km from the 2MW DFIG (within section 3), network configuration = radial network, loading condition = full load.

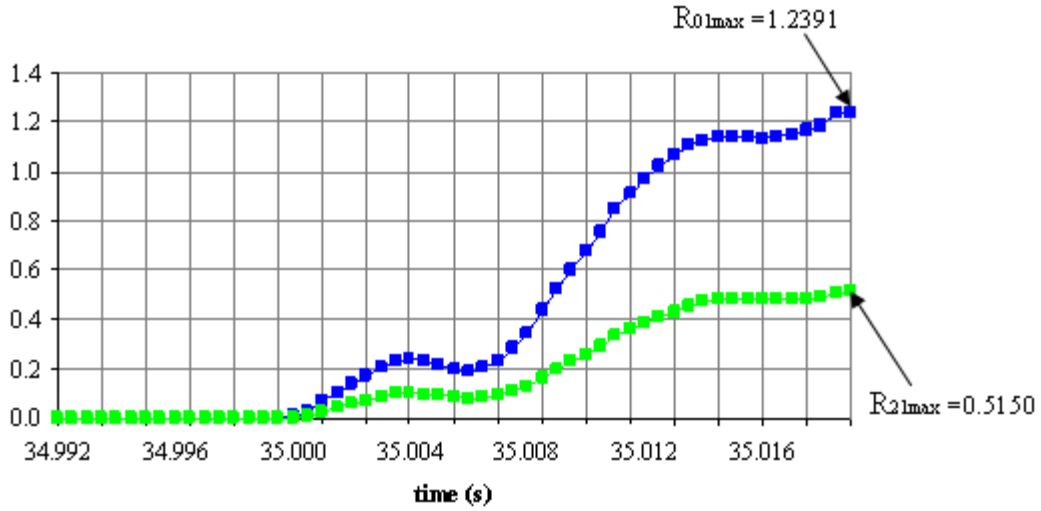

Figure 5.8 Waveform ratio R_{01}(blue waveform) and R_{21} (green waveform) corresponding to fault case: R33-Ri-HL5R0D-CG-4km, for the time interval from t = 34.9915 s to t = 35.0185 s.

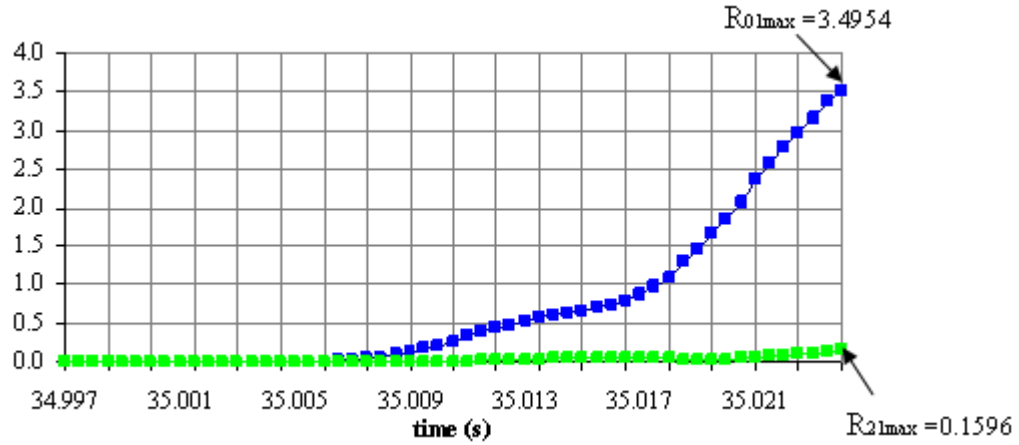

Figure 5.9 Waveform ratio R_{01}(blue waveform) and R_{21} (green waveform) corresponding to fault case: R33-Ra-FL5R90D-CG-4km , for the time interval form t = 34.9965 s to t = 35.0235 s.

5.4.2 Determination of All Elements of Vector X

As explained in section 5.4.1, the considered dominant criterions of φAB, φBC, φCA , R_{01} and R_{21} found in each of the fault cases such as maximum and minimum values of φAB, φBC and φCA are used as elements x_i, of vector **X**. In Table 5.5, each element, x_i^{th} is corresponding to a particular dominant criterion, e.g., element x_1 corresponds to $max\varphi AB$, x_2 corresponds to $\varphi BC_{max\varphi AB}$ etc. The definition of all the dominant criterions given in table 5.5 is detailed below:

1. $max\varphi AB$ = the data point of φAB with a maximum value within the investigated time interval.
2. $\varphi BC_{max\varphi AB}$ = the data point of φBC corresponds to $max\varphi AB$ within the investigated time interval. (which means $\varphi BC_{max\varphi AB}$ is picked at the same time instant as $max\varphi AB$)
3. $\varphi CA_{max\varphi AB}$ = the data point of φCA corresponds to $max\varphi AB$ within the investigated time interval. (which means $\varphi CA_{max\varphi AB}$ is picked at the same time instant as $max\varphi AB$)
4. $max\varphi BC$ = the data point of φBC with a maximum value within the investigated time interval.
5. $\varphi AB_{max\varphi BC}$ = the data point of φAB corresponds to $max\varphi BC$ within the investigated time interval.
6. $\varphi CA_{max\varphi BC}$ = the data point of φCA corresponds to $max\varphi BC$ within the investigated time interval.
7. $max\varphi CA$ = the data point of φCA with a maximum value within the investigated time interval.
8. $\varphi AB_{max\varphi CA}$ = the data point of φAB corresponds to $max\varphi CA$ within the investigated time interval.
9. $\varphi BC_{max\varphi CA}$ = the data point of φBC corresponds to $max\varphi CA$ within the investigated time interval.
10. $min\varphi AB$ = the data point of φAB with a minimum value within the investigated time interval.
11. $\varphi BC_{min\varphi AB}$ = the data point of φBC corresponds to $min\varphi AB$ within the investigated time interval. (which means $\varphi BC_{min\varphi AB}$ is picked at the same time instant with $min\varphi AB$)

12. $\varphi CA_{min\varphi AB}$ = the data point of φCA corresponds to $min\varphi AB$ within the investigated time interval. (which means $\varphi CA_{min\varphi AB}$ is picked at the same time instant with $min\varphi AB$)
13. $min\varphi BC$ = the data point of φBC with a minimum value within the investigated time interval.
14. $\varphi AB_{min\varphi BC}$ = the data point of φAB corresponds to $min\varphi BC$ within the investigated time interval.
15. $\varphi CA_{min\varphi BC}$ = the data point of φCA corresponds to $min\varphi BC$ within the investigated time interval.
16. $min\varphi CA$ = the data point of φCA with a minimum value within the investigated time interval.
17. $\varphi AB_{min\varphi CA}$ = the data point of φAB corresponds to $min\varphi CA$ within the investigated time interval.
18. $\varphi BC_{min\varphi CA}$ = the data point of φBC corresponds to $min\varphi CA$ within the investigated time interval.
19. $0\text{-}crossing\varphi AB$ = the first data point after φAB crosses the 0°-axis within the investigated time interval.
20. $\varphi BC_{0\text{-}crossing\varphi AB}$ = the data point of φBC corresponding to $0\text{-}crossing\varphi AB$ within the investigated time interval. (which means $\varphi BC_{0\text{-}crossing\varphi AB}$ is picked at the same time instant with $0\text{-}crossing\varphi AB$)
21. $\varphi CA_{0\text{-}crossing\varphi AB}$ = the data point of φCA corresponds to $0\text{-}crossing\varphi AB$ within the investigated time interval. (which means $\varphi CA_{0\text{-}crossing\varphi AB}$ is picked at the same time instant with $0\text{-}crossing\varphi AB$)
22. $0\text{-}crossing\varphi BC$ = the first data point after φBC crosses the 0°-axis within the investigated time interval.
23. $\varphi AB_{0\text{-}crossing\varphi BC}$ = the data point of φAB corresponds to $0\text{-}crossing\varphi BC$ within the investigated time interval.
24. $\varphi CA_{0\text{-}crossing\varphi BC}$ = the data point of φCA corresponds to $0\text{-}crossing\varphi BC$ within the investigated time interval.
25. $0\text{-}crossing\varphi CA$ = the first data point after φCA crosses the 0°-axis within the investigated time interval.
26. $\varphi AB_{0\text{-}crossing\varphi CA}$ = the data point of φAB corresponds to $0\text{-}crossing\varphi CA$ within the investigated time interval.

27. $\varphi BC_{0\text{-}crossing\varphi CA}$ = the data point of φBC corresponds to *0-crossing*φCA within the investigated time interval.
28. *150-crossing*φAB = the first data point after φAB crosses the 150°-axis within the investigated time interval.
29. $\varphi BC_{150\text{-}crossing\varphi AB}$ = the data point of φBC corresponds to *150-crossing*φAB within the investigated time interval. (which means $\varphi BC_{150\text{-}crossing\varphi AB}$ is picked at the same time instant with *0-crossing*φAB)
30. $\varphi CA_{150\text{-}crossing\varphi AB}$ = the data point of φCA corresponds to *150-crossing*φAB within the investigated time interval. (which means $\varphi BC_{150\text{-}crossing\varphi AB}$ is picked at the same time instant with *0-crossing*φAB)
31. *150-crossing*φBC = the first data point after φAB crosses the 150°-axis within the investigated time interval.
32. $\varphi AB_{150\text{-}crossing\varphi BC}$ = the data point of φAB corresponds to *150-crossing*φBC within the investigated time interval.
33. $\varphi CA_{150\text{-}crossing\varphi BC}$ = the data point of φAC corresponds to *150-crossing*φBC within the investigated time interval.
34. *150-crossing*φCA = the first data point after φCA crosses the 150°-axis within the investigated time interval.
35. $\varphi AB_{150\text{-}crossing\varphi CA}$ = the data point of φAB corresponds to *150-crossing*φCA within the investigated time interval.
36. $\varphi BC_{150\text{-}crossing\varphi CA}$ = the data point of φBC corresponds to *150-crossing*φCA within the investigated time interval.
37. $maxR_{01}$ = the data point of ratio R_{01} with a maximum value within the investigated time interval.
38. $maxR_{21}$ = the data point of ratio R_{21} with a maximum value within the investigated time interval.

Table 5.5

Element, x_i in predefined parameter vector **X** and the corresponding dominant criterion.

dominant criterion	element x_i	dominant criterion	element x_i
1. $max\varphi AB$	x_1	20. $\varphi BC_{0\text{-}crossing\varphi AB}$	x_{20}
2. $\varphi BC_{max\varphi AB}$	x_2	21. $\varphi CA_{0\text{-}crossing\varphi AB}$	x_{21}
3. $\varphi CA_{max\varphi AB}$	x_3	22. $0\text{-}crossing\varphi BC$	x_{22}
4. $max\varphi BC$	x_4	23. $\varphi AB_{0\text{-}crossing\varphi BC}$	x_{23}
5. $\varphi AB_{max\varphi BC}$	x_5	24. $\varphi CA_{0\text{-}crossing\varphi BC}$	x_{24}
6. $\varphi CA_{max\varphi BC}$	x_6	25. $0\text{-}crossing\varphi CA$	x_{25}
7. $max\varphi CA$	x_7	26. $\varphi AB_{0\text{-}crossing\varphi CA}$	x_{26}
8. $\varphi AB_{max\varphi CA}$	x_8	27. $\varphi BC_{0\text{-}crossing\varphi CA}$	x_{27}
9. $\varphi BC_{max\varphi CA}$	x_9	28. $150\text{-}crossing\varphi AB$	x_{28}
10. $min\varphi AB$	x_{10}	29. $\varphi BC_{150\text{-}crossing\varphi AB}$	x_{29}
11. $\varphi BC_{min\varphi AB}$	x_{11}	30. $\varphi CA_{150\text{-}crossing\varphi AB}$	x_{30}
12. $\varphi CA_{min\varphi AB}$	x_{12}	31. $150\text{-}crossing\varphi BC$	x_{31}
13. $min\varphi BC$	x_{13}	32. $\varphi AB_{150\text{-}crossing\varphi BC}$	x_{32}
14. $\varphi AB_{min\varphi BC}$	x_{14}	33. $\varphi CA_{150\text{-}crossing\varphi BC}$	x_{33}
15. $\varphi CA_{min\varphi BC}$	x_{15}	34. $150\text{-}crossing\varphi CA$	x_{34}
16. $min\varphi CA$	x_{16}	35. $\varphi AB_{150\text{-}crossing\varphi CA}$	x_{35}
17. $\varphi AB_{min\varphi CA}$	x_{17}	36. $\varphi BC_{150\text{-}crossing\varphi CA}$	x_{36}
18. $\varphi BC_{min\varphi CA}$	x_{18}	37. $maxR_{01}$	x_{37}
19. $0\text{-}crossing\varphi AB$	x_{19}	38. $maxR_{21}$	x_{38}

Table 5.6 shows the value of elements of vector **X** extracted from the fault case R22-Ra-FL5R90D-CG-9km. Note that all of the x_i where i = 1,2,3,….,38 are extracted from the 275 data points within the investigated time interval of this fault case as shown in Table 5.7. Figure 5.10(a) shows the variation of φAB (blue waveform), φBC(green waveform), φCA(red waveform) and Figure 5.10(b) shows R_{01} (blue waveform) and R_{21} (green waveform) related to this fault case represented by the data points shown in Table 5.7. Note that fault case R22-Ra-FL5R90D-CG-9km refers to a c-g fault (based on line current measurement of relay R_{22} in Figure 5.1) assuming the following fault and network operating condition: R_f = 5Ω, FIA = 90° (corresponding to the fault inception time of 35.003 s), fault location = 9km from the 2MW DFIG (within section 2), network configuration = radial network, loading condition = full load.

As shown in Table 5.6, for this fault case x_1 = 162.8822, x_2 = -277.8458 and x_3 = 64.9635. According to Table 5.5, x_1 corresponds to dominant criterion $max\varphi AB$, x_2 is corresponding to dominant criterion $\varphi BC_{max\varphi AB}$ and x_3 corresponds to dominant criterion $\varphi CA_{max\varphi AB}$. Therefore, x_1 = 162.8822 means that 162.8822 is the data point of φAB with a maximum value that can be found within the investigated time interval. As shown in Table 5.7, the maximum value of φAB is 162.8822° within the investigated time interval and 162.8822° occurred at t = 35.0165 s (data point no.41). The variable x_2 = -277.8458 means that -277.8458° is the data point of φBC picked at the t = 35.0165 s (data point no.41) when the maximum value of φAB, 162.8822° is found. The variable x_3 = 64.9635 means that 64.9635° is the data point of φCA that picked at t = 35.0165 s (data point no.41) when maximum value of φAB, 162.8822° is found. The other values of x_i shown in Table 5.6 are determined in a similar way.

In addition to that, it is shown in Table 5.6 that for the value of certain elements x_i = 0 e.g., where i = 25, 26 and 27, which means the element has "no value". According to Table 5.5, variable x_{25} = *0°-crossing*φCA, x_{26} = $\varphi AB_{0\text{-}crossing\varphi CA}$ and x_{27} = $\varphi BC_{0\text{-}crossing\varphi CA}$. Thus, x_{25} = 0 means the 1st data point after φCA crosses the *0°*-axis can not be found within the investigated time interval related to this fault case. This is because, as shown in Figure 5.10, in this fault case φCA does not cross the *0°*-axis within the investigated time interval. This also leads to, x_{26} = 0 and x_{27} = 0 due to x_{25} = 0. This is similar for values x_{31} to x_{36}.

It was also found in Figure 5.10(a) that, φBC (green waveform) crosses the 0°-axis twice within the investigated time interval, from t = 34.9965 s to t = 35.0235 s. As explained in the previous section (section 5.4.1) that although in certain fault cases the three parameters φAB, φBC or φCA may cross the 0°-axis more than once within the investigated time interval, only the first crossing is considered. Therefore, in this fault case, only the 1st data point after the first 0°-axis by φBC and the corresponding φAB and φCA are considered as elements of vector **X** related to this fault case.

Table 5.6

Elements of vector **X** for fault case R22-Ra-FL5R90D-CG-9km: element ith x and the corresponding data point.

x_i	data point	x_i	data point
x_1	162.8822	x_{20}	123.4099
x_2	-227.8458	x_{21}	63.7109
x_3	64.9635	x_{22}	123.4099
x_4	123.4099	x_{23}	-187.1208
x_5	-187.1208	x_{24}	63.7109
x_6	63.7109	x_{25}	0
x_7	120.1083	x_{26}	0
x_8	121.9345	x_{27}	0
x_9	-242.0428	x_{28}	150.6946
x_{10}	-187.1208	x_{29}	-249.5113
x_{11}	123.4099	x_{30}	98.8167
x_{12}	63.7109	x_{31}	0
x_{13}	-251.8394	x_{32}	0
x_{14}	144.2360	x_{33}	0
x_{15}	107.6034	x_{34}	0
x_{16}	43.7724	x_{35}	0
x_{17}	-20.5434	x_{36}	0
x_{18}	-23.2290	x_{37}	2.1484
x_{19}	-187.1208	x_{38}	0.2053

Table 5.7

Data point of φAB, φBC ,φCA, $R_{01}$and R_{21}corresponding to

fault case: R22-Ra-FL5R90D-CG-9km, from t = 34.9965 s to t = 35.0235 s.

data point no.	time (s)	phase angle difference between line current			ratio sequence component of line current	
		$\varphi AB(^\circ)$	$\varphi BC(^\circ)$	$\varphi CA(^\circ)$	R_{01}	R_{21}
1	34.9965	121.9345	-242.0428	120.1083	0.0000	0.0002
2	34.9970	121.9912	-242.0084	120.0173	0.0000	0.0002
3	34.9975	122.0358	-241.9878	119.9520	0.0000	0.0002
4	34.9980	122.0682	-241.9612	119.8930	0.0000	0.0002
5	34.9985	122.0715	-241.9287	119.8572	0.0000	0.0002
6	34.9990	122.0617	-241.8779	119.8163	0.0000	0.0002
7	34.9995	122.0467	-241.8065	119.7597	0.0000	0.0002
8	35.0000	122.0372	-241.7163	119.6791	0.0000	0.0002
9	35.0005	122.0525	-241.5781	119.5256	0.0000	0.0002
10	35.0010	122.0996	-241.4742	119.3746	0.0000	0.0002
11	35.0015	122.1866	-241.3843	119.1977	0.0000	0.0002
12	35.0020	122.2656	-241.3189	119.0533	0.0000	0.0002
13	35.0025	122.1898	-241.2302	119.0403	0.0000	0.0002
14	35.0030	121.9300	-241.0009	119.0709	0.0000	0.0004
15	35.0035	122.0116	-241.1315	119.1199	0.0000	0.0004
16	35.0040	122.5784	-241.9528	119.3744	0.0001	0.0004
17	35.0045	123.5395	-243.1768	119.6373	0.0005	0.0005
18	35.0050	124.9063	-244.4683	119.5619	0.0016	0.0005
19	35.0055	127.6422	-246.3131	118.6710	0.0051	0.0005
20	35.0060	130.4095	-247.9222	117.5127	0.0098	0.0004
21	35.0065	133.5170	-249.4748	115.9578	0.0170	0.0007
22	35.0070	136.8505	-250.7191	113.8685	0.0273	0.0012
23	35.0075	140.1766	-251.5022	111.3256	0.0410	0.0017
24	35.0080	144.2360	-251.8394	107.6034	0.0648	0.0029
25	35.0085	146.9574	-251.6231	104.6657	0.0866	0.0042
26	35.0090	149.1961	-250.9288	101.7328	0.1115	0.0060
27	35.0095	150.6946	-249.5113	98.8167	0.1391	0.0081
28	35.0100	151.3047	-247.2579	95.9532	0.1688	0.0109
29	35.0105	150.5092	-242.7711	92.2619	0.2100	0.0155
30	35.0110	148.5941	-238.1950	89.6009	0.2410	0.0196
31	35.0115	145.7726	-232.7210	86.9485	0.2706	0.0240
32	35.0120	142.5343	-226.8386	84.3043	0.2977	0.0285
33	35.0125	139.1940	-220.9641	81.7700	0.3219	0.0332
34	35.0130	134.9090	-213.5742	78.6652	0.3496	0.0406
35	35.0135	133.1483	-209.5516	76.4033	0.3666	0.0457
36	35.0140	133.4626	-207.6693	74.2067	0.3810	0.0492
37	35.0145	135.7482	-207.8844	72.1362	0.3949	0.0509
38	35.0150	139.5045	-209.6533	70.1488	0.4113	0.0515
39	35.0155	146.8216	-214.5455	67.7240	0.4421	0.0500
40	35.0160	154.1417	-220.3767	66.2350	0.4760	0.0470

41	35.0165	162.8822	-227.8458	64.9635	0.5222	0.0435
42	35.0170	-187.1208	123.4099	63.7109	0.5825	0.0408
43	35.0175	-175.7107	113.2894	62.4212	0.6577	0.0394
44	35.0180	-157.8971	97.2968	60.6003	0.7800	0.0405
45	35.0185	-142.3964	83.2344	59.1620	0.8864	0.0438
46	35.0190	-125.3417	67.6671	57.6746	1.0032	0.0495
47	35.0195	-107.6930	51.5379	56.1551	1.1280	0.0576
48	35.0200	-90.8175	36.1973	54.6202	1.2580	0.0682
49	35.0205	-71.2718	18.6979	52.5739	1.4349	0.0858
50	35.0210	-59.1875	8.1340	51.0535	1.5667	0.1016
51	35.0215	-48.6639	-0.9679	49.6318	1.6975	0.1194
52	35.0220	-39.3879	-8.9290	48.3168	1.8253	0.1396
53	35.0225	-31.9868	-14.9838	46.9706	1.9404	0.1604
54	35.0230	-24.6662	-20.4590	45.1252	2.0696	0.1866
55	35.0235	-20.5434	-23.2290	43.7724	2.1484	0.2053

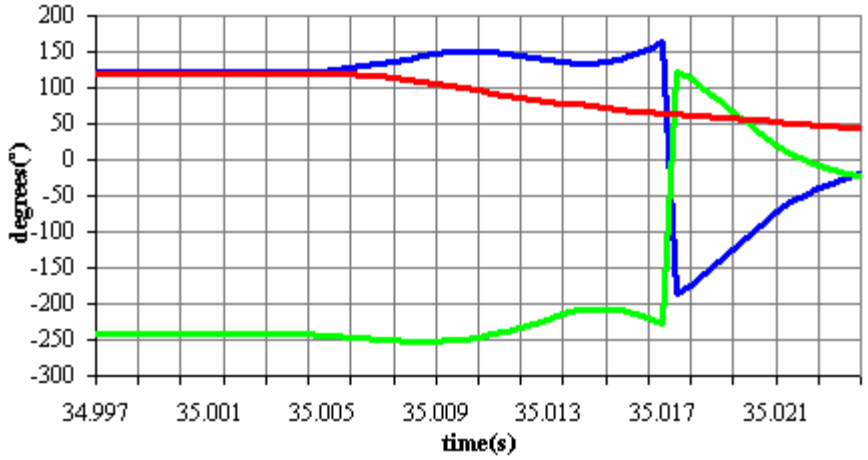

(a)

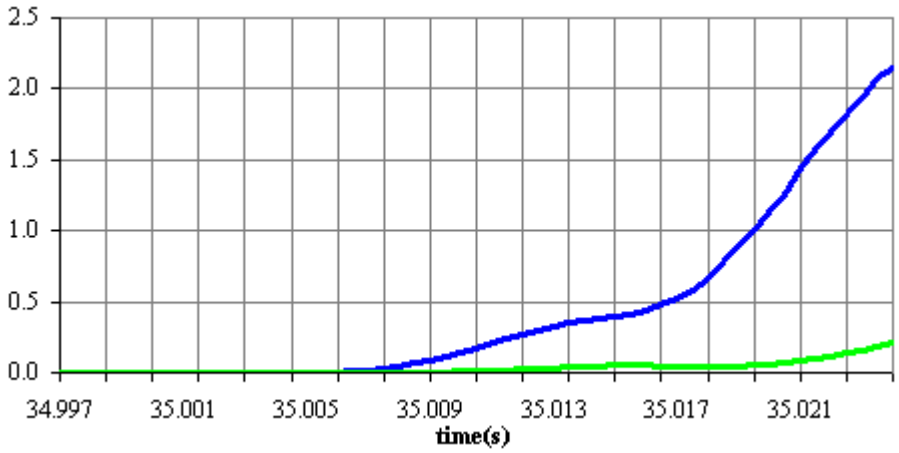

(b)

Figure 5.10 Variation of (a) φAB (blue waveform), φBC (green waveform) and φCA(red waveform) and (b) ratio R_{01}(blue waveform) and R_{21}(green waveform) of fault case: R22-Ra-FL5R90D-CG-9km from t = 34.9965 s to t = 35.0235 s.

In this research work, the fault data analysis process is carried out by a specifically developed C++ software module. The task of the whole fault data analysis processing, that includes retrieving each fault case from a folder called "Case Database A", followed by analyse of the fault data of that particular fault case, extracting the related elements of vector **X** and finally saving elements x_i, i = 1,2,3,….,38, corresponding to all fault cases under consideration in a file called "Case Database B". Vector **X** relating to all fault cases have been stored together in a single ".txt" file so that time can be efficiently used in the process of retrieving data from file "Case Database B" for subsequent optimisation process. The values of elements x_i of vector X of 2592 fault cases under investigation can be found in Appendix D. Note due to the space limitation, appendix D is stored in the attached CD-ROM.

5.5 Optimisation Process

The aim of the fault data optimization process is to determine the minimum number of elements of vector **X** that is sufficient to distinguish each fault case from the others in the total of 2592 fault cases. The application of an optimization process has resulted in an optimized vector $\mathbf{X_{optimise}}$ with 26 elements such that $\mathbf{X_{optimise}} = \{x_1, x_2, \ldots, x_k, \ldots, x_m\}$, k =1, 2, 3,…, m. x_k is the k^{th} feature and m = 26. Development of $\mathbf{X_{optimise}}$ is described in the following two sections.

5.5.1 Development Vector $\mathbf{X_c}$ based on the Elements of Vector X

The 38 elements of vector **X** related to any fault case are arranged to form a new vector called $\mathbf{X_c}$. This can be explained using Table 5.5 in section 5.4.2 and Table 5.8 below. A 13 elements vector $\mathbf{X_{cj}}$,where j = 1,2,3,….,13 elements has been formed from the 38 elements shown in Table 5.5. Each of the vector from element $\mathbf{X_{c1}}$ to $\mathbf{X_{c12}}$ contains those sequentially elements from Table 5.5, e.g., $\mathbf{X_{c1}} = \{x_1, x_2, x_3\}$, $\mathbf{X_{c2}} = \{x_4, x_5, x_6\}$ etc, where x_1, x_2, x_3 are the first three elements in Table 5.5 which are interrelated to each other. x_1 is the data point of φAB with a maximum value that occurred at the time instant, t within the investigated time interval. While x_2 and x_3 are the corresponding values of φBC and φCA at time instant, t. $\mathbf{X_{c13}}$ is the vector that is formed from the last two element x_i in vector **X** as shown in Table 5.5 where $\mathbf{X_{c13}} = \{x_{37}, x_{38}\}$. x_{37} and x_{38} are also interrelated to each other where both of

x_{37} and x_{38} are the only two variables within the 38 variables that have been selected base on the dominant criterion of ratios $R_{01}$and R_{21}.

Table 5.8

Vector $\mathbf{X_{cj}}$ and their corresponding element x_i.

$\mathbf{X_{cj}}$	element x_i
X_{c1}	x_1 , x_2 , x_3
X_{c2}	x_4 , x_5 , x_6
X_{c3}	x_7 , x_8 , x_9
X_{c4}	x_{10} , x_{11} , x_{12}
X_{c5}	x_{13} , x_{14} , x_{15}
X_{c6}	x_{16} , x_{17} , x_{18}
X_{c7}	x_{19} , x_{20} , x_{21}
X_{c8}	x_{22} , x_{23}, x_{24}
X_{c9}	x_{25} , x_{26}, x_{27}
X_{c10}	x_{28} , x_{29}, x_{30}
X_{c11}	x_{31} , x_{32}, x_{33}
X_{c12}	x_{34} , x_{35}, x_{36}
X_{c13}	x_{37}, x_{38}

5.5.2 Determination of an Optimised Vector $\mathbf{X_{optimise}}$ based on Vector $\mathbf{X_{cj}}$

The first two elements in vector X_{cj} in Table 5.8 in section 5.5.1, $\mathbf{X_{c1}}$ and $\mathbf{X_{c2}}$ are used to form another vector $\mathbf{X_{cc}}$ where $\mathbf{X_{cc}}$ ={X_{c1}, X_{c2}}. The X_{cc} = {X_{c1}, X_{c2}}of each fault case in "Case Database B" file is to be compared with the corresponding $\mathbf{X_{cc}}$ = {X_{c1}, X_{c2}} of the rest of 2591 fault cases stored in the same file. This can be explained as follows with reference to the following Table 5.9. In Table 5.9, X_{ccFN} refers to vector $\mathbf{X_{cc}}$ of N^{th} fault case, where N = 1, 2, 3,…., 2591. X_{ccF1} refers to the $\mathbf{X_{cc}}$ ={X_{c1}, X_{c2}}

corresponding to the 1st fault case, X_{ccF2} refers to the $\mathbf{X_{cc}}$ ={X_{c1}, X_{c2}} corresponding to the 2nd fault case etc. As shown in this table, X_{ccFN} is compared to $X_{ccF(N+1)}$, $X_{ccF(N+2)}$, $X_{ccF(N+3)}$, ….,$X_{ccF2592}$ e.g., X_{ccF1} compared to X_{ccF2}, X_{ccF3},…….. $X_{ccF2592}$, which means that $\mathbf{X_{cc}}$ = {X_{c1}, X_{c2}} of the 1st fault case compared to X_{cc} ={X_{c1}, X_{c2}} related to the 2nd fault case, 3rd fault case,…., 2592th fault case. Then, X_{ccF2} is compared to X_{ccF3}, X_{ccF4}, X_{ccF5},….,$X_{ccF2592}$, which means $\mathbf{X_{cc}}$ ={X_{c1}, X_{c2}}of the 2nd fault case is compared to $\mathbf{X_{cc}}$ ={X_{c1}, X_{c2}} related to the 3rd fault case, 4th fault case,…., 2592th fault. The comparison process is repeated until $X_{ccF2591}$ is compared to $X_{ccF2592}$ which means $\mathbf{X_{cc}}$ = {X_{c1}, X_{c2}} of the 2591th fault case is compared to $\mathbf{X_{cc}}$ = {X_{c1}, X_{c2}} of the 2592th fault case.

Table 5.9

The sequence of comparing $\mathbf{X_{cc}}$ of each of fault case with the corresponding $\mathbf{X_{cc}}$ of other fault cases under consideration.

N	X_{ccFN}	$X_{ccF(N+1)}$, $X_{ccF(N+2)}$,….,$X_{ccF(2592)}$
1	X_{ccF1}	X_{ccF2}, X_{ccF3},....,$X_{ccF2592}$
2	X_{ccF2}	X_{ccF3}, X_{ccF4},….,$X_{ccF2592}$
3	X_{ccF3}	X_{ccF4}, X_{ccF5},….,$X_{ccF2592}$
. . . .	. . . .	. . . .
2591	$X_{ccF2591}$	$X_{ccF2592}$

The vector $\mathbf{X_{optimise}}$ is formed based on $\mathbf{X_{c1}}$ and $\mathbf{X_{c2}}$ in $\mathbf{X_{cc}}$ = {X_{c1}, X_{c2}} if the pair $\mathbf{X_{c1}}$ and $\mathbf{X_{c2}}$ are found to successfully discriminate each of the fault case from all of other fault cases in the comparison process. Note that $\mathbf{X_{c1}}$ = {x_1 , x_2 , x_3} and $\mathbf{X_{c2}}$ = {x_4 , x_5 , x_6} as shown in Table 5.8 in the previous section 5.3.1 so $\mathbf{X_{cc}}$ = {X_{c1}, X_{c2}}= { x_1 , x_2 , x_3, x_4 , x_5 , x_6 }. Thus, if each of the fault cases from the 2592 fault cases can be uniquely distinguished using $\mathbf{X_{cc}}$ = {X_{c1}, X_{c2}}in the comparison process, then $\mathbf{X_{optimise}}$ = { x_1 , x_2 , x_3, x_4 , x_5 , x_6 } is formed. The comparison process can be explained as followed: if all the variables in $\mathbf{X_{cc}}$ = {x_1, x_2 , x_3, x_4 , x_5 , x_6}of a particular fault case are found to be identical to all variables in $\mathbf{X_{cc}}$ = {x_1 , x_2 , x_3, x_4 , x_5 , x_6}of any other fault cases under consideration, then X_{c1} and X_{c2} has unsuccessfully discriminated a fault case from the other fault case under

consideration. Otherwise the X_{c1} and X_{c2} has successfully discriminated a fault case from other fault cases under consideration. This can be explained as followed by demonstrating how $\mathbf{X_{c1}}$ and $\mathbf{X_{c2}}$ in $\mathbf{X_{cc}}$ of the two fault cases R22-Ra-FL5R90D-CG-9km and R22-Ri-HL5R0D-BG-7.5km are compared.

According to Table 5.6 in previous section 5.4.2 for fault case R22-Ra-FL5R90D-CG-9km, $\mathbf{X_{c1}}$ ={x_1, x_2, x_3}={162.8822, -227.8458 , 64.9635} and $\mathbf{X_{c2}}$ = {x_4, x_5, x_6}={123.4099, -187.1208, 63.7109} respectively. According to Table 5.10 below for fault case R22-Ri-HL5R0D-BG-7.5km, $\mathbf{X_{c1}}$ ={134.7765, -272.2805, 137.5040} and $\mathbf{X_{c2}}$ ={80.9110, -219.0675, 138.1565}respectively. Note that elements x_i and their corresponding data points shown in Table 5.10 are extracted from Table 1 in Appendix E. Table 1 consists of the data point of *φAB*, *φBC*, *φCA* and the ratio R_{01} and R_{21} within investigated time interval related to fault case R22-Ri-HL5R0D-BG-7.5km. Note that R22-Ri-HL5R0D-BG-7.5km refer to refers to b-g fault (based on line current measurement of relay R_{22} in Figure 5.1) assuming following fault and network operating conditions: $R_f = 5\Omega$, FIA = 0° (corresponding to the fault inception time of 34.998 s), fault location = 7.5km from the 2MW DFIG (within section 2), network configuration = ring network, loading condition = half load.

The values of $\mathbf{X_{c1}}$ and $\mathbf{X_{c2}}$ in $\mathbf{X_{cc}}$ of these two fault cases are summarised in the following Table 5.11. In this table, F1 referd to R22-Ra-FL5R90D-CG-9km and F2 refer to R22-Ri-HL5R0D-BG-7.5km. Each of the i^{th} element, x_i related to these fault cases have upper and lower tolerance limits of ± 5 e.g., as shown in Table 5.12, x_1 for fault case R22_CG_6KM_5R_90D_R_FL is 162.8822 , so the upper and lower tolerance limit are 167.8822 and 157.8822. Table 5.12 shows the upper and lower tolerance limits of all x_i elements of $\mathbf{X_{c1}}$ and $\mathbf{X_{c2}}$ in forming X_{cc} of these two fault cases. In this table, F1 refers to R22-Ra-FL5R90D-CG-9km and F2 refers to R22-Ri-HL5R0D-BG-7.5km. If the lower or upper limits of a particular x_i element corresponding to F1 overlaps with a particular x_i element corresponding to F2 then, both of these elements are said to be identical. It was found in this Table 5.12 that, -232.8458 < x_2 <-222.8458 corresponding to fault case F1 and -224.0675< x_5 <-214.0675 corresponding to fault case F2. It can be seen that, the upper tolerance limit of x_2 corresponding to fault case F1 is overlapping with lower tolerance limit of x_5 corresponding to fault case F2. Thus, the value of x_2 corresponding to the fault case

F1 are said to be identical to x_5 corresponding to fault case F2. In addition to that, it was found only x_2 in fault case F1 which is identical to x_5 in fault case F2. Thus, fault case F1 and F2 are said to be successfully distinguished.

Table 5.10

Elements of vector **X** for fault case R22-Ri-HL5R0D-BG-7.5km: element i^{th} x and the corresponding data point.

variable x	data point	variable x	data point
x_1	134.7765	x_{20}	80.9110
x_2	-272.2805	x_{21}	138.1565
x_3	137.5040	x_{22}	80.9110
x_4	80.9110	x_{23}	-219.0675
x_5	-219.0675	x_{24}	138.1565
x_6	138.1565	x_{25}	0
x_7	138.1565	x_{26}	0
x_8	80.9110	x_{27}	0
x_9	-219.0675	x_{28}	0
x_{10}	-219.0675	x_{29}	0
x_{11}	80.9110	x_{30}	0
x_{12}	138.1565	x_{31}	0
x_{13}	-272.2805	x_{32}	0
x_{14}	134.7765	x_{33}	0
x_{15}	137.5040	x_{34}	0
x_{16}	0.5548	x_{35}	0
x_{17}	-41.7975	x_{36}	0
x_{18}	41.2427	x_{37}	1.7564
x_{19}	-219.0675	x_{38}	0.8403

Table 5.11

Element i^{th} x and the corresponding data point related to the fault cases: R22-Ra-FL5R90D-CG-9km (F1) and R22-Ri-HL5R0D-BG-7.5km (F2).

x_i in X_{c1} and X_{c2}	fault case	
	F1	F2
x_1	162.8822	134.7765
x_2	-227.8458	-272.2805
x_3	64.9635	137.5040
x_4	123.4099	80.9110
x_5	-187.1208	-219.0675
x_6	63.7109	138.1565

Table 5.12

Lower limit and upper limit of element i^{th} x in $\mathbf{X_{c1}}$ and $\mathbf{X_{c2}}$ related to the fault cases: R22-Ra-FL5R90D-CG-9km (F1) and R22-Ri-HL5R0D-BG-7.5km (F2).

x_i in X_{c1} and X_{c2}	lower limit and upper limit of x_i	
	fault case F1	fault case F2
x_1	$157.8822 < x_1 < 167.8822$	$129.7765 < x_1 < 139.7765$
x_2	$-232.8458 < x_2 < -222.8458$	$-277.2805 < x_2 < -267.2805$
x_3	$59.9635 < x_3 < 69.9635$	$132.5040 < x_3 < 142.5040$
x_4	$118.4099 < x_4 < 128.4099$	$75.9110 < x_4 < 85.9110$
x_5	$-192.1208 < x_5 < -182.1208$	$-224.0675 < x_5 < -214.0675$
x_6	$58.7109 < x_6 < 68.7109$	$133.1565 < x_6 < 143.1565$

However if $\mathbf{X_{cc}} = \{X_{c1}, X_{c2}\}$ fails to discriminate a fault case from other fault cases under consideration, the comparison process will be repeated using different combinations to formed two $\mathbf{X_c}$. This can be explained with the following Table 5.13. In this table, X_{cN} refers to N^{th} of $\mathbf{X_c}$ shown in Table 5.8 in the previous section 5.5.1 where N =1,2,3,….,11 and $\{X_{cN}, X_{c(N+1)}\}$, $\{X_{cN}, X_{c(N+2)}\}$, $\{X_{cN}, X_{c(N+3)}\}$,….,$\{X_{cN}$,

$X_{c12}\}$ refer to possible combinations of $\mathbf{X_{cc}}$ beginning with X_{cN}, e.g., where N =1, $X_{cN} = X_{c1}$ and combination formed with two $\mathbf{X_c}$ where one of them is X_{c1} and the other are $X_{c(N+1)}$ and N = 1,2,3,….,11 are $\{X_{c1}, X_{c2}\}$, $\{X_{c1}, X_{c3}\}$….,$\{X_{c1}, X_{c12}\}$. When $\{X_{cN}, X_{c(N+1)}\}$ fails to discriminate a fault case from other fault cases under consideration, then $\{X_{cN}, X_{c(N+2)}\}$,….,$\{X_{cN}, X_{c12}\}$ will be used in the comparison process, e.g., if comparing $\mathbf{X_{c1}}$ and $\mathbf{X_{cc}} = \{X_{c1}, X_{c2}\}$ fails to discriminate a fault case from other fault cases under consideration, then each of $\{X_{c1}, X_{c3}\}$, $\{X_{c1}, X_{c4}\}$,...,$\{X_{c1}, X_{c12}\}$ is used in the comparison process. Then, the comparison process will be repeated if required with all possible combinations of $\mathbf{X_{cc}}$ beginning with $\mathbf{X_{c2}}$, $\mathbf{X_{c3}}$,.....,$\mathbf{X_{c11}}$. Note that only $\mathbf{X_{c1}}$ to $\mathbf{X_{c12}}$ have been involved in comparison process. The variables x_{37} and x_{38} in $\mathbf{X_{c13}}$ have to be included in $\mathbf{X_{optimise}}$ without going through the comparison process. This is because x_{37} and x_{38} are reflecting the characteristics of a network fault event which involves a ground connection. Consequently, both of these variables are necessary to be included as main data to construct the proposed fault identification algorithm in this research work.

Table 5.13

All possible combinations with two $\mathbf{X_c}$ to be used in comparison process.

N	X_{cN}	$\{X_{cN}, X_{c(N+1)}\}$, $\{X_{cN}, X_{c(N+2)}\}$,….,$\{X_{cN}, X_{c12}\}$
1	X_{c1}	$\{X_{c1}, X_{c2}\}$, $\{X_{c1}, X_{c3}\}$,….,$\{X_{c1}, X_{c12}\}$
2	X_{c2}	$\{X_{c2}, X_{c3}\}$, $\{X_{c2}, X_{c4}\}$,….,$\{X_{c2}, X_{c12}\}$
3	X_{c3}	$\{X_{c3}, X_{c4}\}$, $\{X_{c3}, X_{c5}\}$,…., $\{X_{c1}, X_{c12}\}$
. . . .	. . . .	. . . .
11	X_{c11}	$\{X_{cN}, X_{c12}\}$

If the above process fails to discriminate a fault case from the other fault cases under consideration, then the comparison process is repeated by forming vectors with three $\mathbf{X_c}$ if necessary. The worst condition is where the comparison process involves formation of vectors that contains all twelve $\mathbf{X_c}$ as shown in Table 5.8 of the section

5.5.1. The overall comparison process described in this section in order to obtain $\mathbf{X_{optimise}}$ can be summarised in flow chart shown in Figure 5.11.

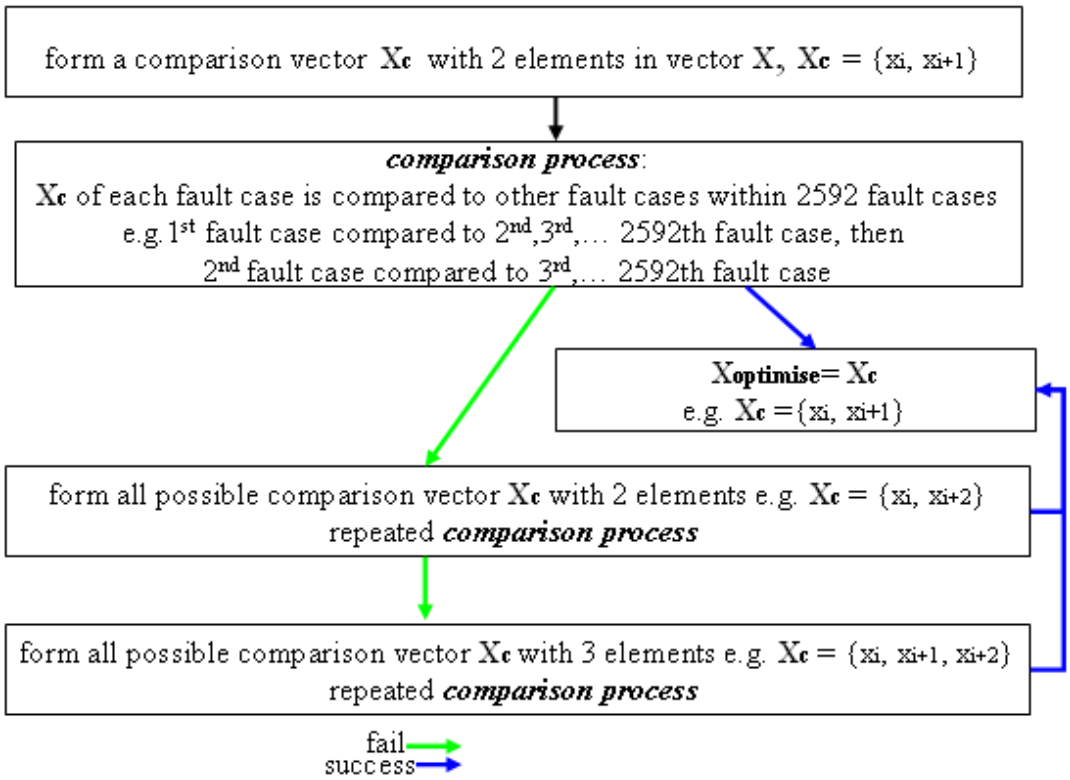

Figure 5.11 Flow chart illustrate the comparison process to obtain $\mathbf{X_{optimise}}$.

In this research work, it has been found that a vector X_{cc} with combination of eight $\mathbf{X_c}$ which is X_{cc}= {X_{c1}, X_{c2}, X_{c7}, X_{c8}, X_{c9}, X_{c10}, X_{c11}, X_{c12}} can successfully distinguish each of the fault case saved in folder "Case Database A". According to Table 5.8 in the section 5.5.1 $\mathbf{X_{c1}}$ = x_1, x_2, x_3, $\mathbf{X_{c2}}$ = x_4, x_5, x_6, $\mathbf{X_{c7}}$ = x_{19}, x_{20}, x_{21}, $\mathbf{X_{c8}}$ = x_{22}, x_{23}, x_{24}, $\mathbf{X_{c9}}$ = x_{25}, x_{26}, x_{27}, and $\mathbf{X_{c10}}$ = x_{28}, x_{29}, x_{30}, $\mathbf{X_{c11}}$ = x_{31}, x_{32}, x_{33}, $\mathbf{X_{c12}}$ = x_{34}, x_{35}, x_{36}. Thus, X_{cc} = {x_1, x_2, x_3, x_4, x_5, x_6, x_{19}, x_{20}, x_{21}, x_{22}, x_{23}, x_{24}, x_{25}, x_{26}, x_{27}, x_{28}, x_{29}, x_{30}, x_{31}, x_{32}, x_{33}, x_{34}, x_{35}, x_{36}} where the total number of elements x_k in X_{cc} is equals to 24. This vector therefore represents the optimised vector $\mathbf{X_{optimise}}$ but without including the effect of x_{37} and x_{38} which can be included in $\mathbf{X_{optimise}}$ to complete its formation. Thus, $\mathbf{X_{optimise}}$ ={ x_1, x_2, x_3, x_4, x_5, x_6, x_{19}, x_{20}, x_{21}, x_{22}, x_{23}, x_{24}, x_{25}, x_{26}, x_{27}, x_{28}, x_{29}, x_{30}, x_{31}, x_{32}, x_{33}, x_{34}, x_{35}, x_{36}, x_{37}, x_{38}}. The correspondence between elements of the optimised vector $\mathbf{X_{optimise}}$ and those in vector $\mathbf{X}$ is shown in Table 5.14.

Table 5.14

Elements x_k in parameter set of $\mathbf{X_{optimise}}$ and the corresponding x_i.

element x_k in $X_{optimise}$	element x_i corresponding to x_k in $X_{optimise}$
x_{k1}	x_1
x_{k2}	x_2
x_{k3}	x_3
x_{k4}	x_4
x_{k5}	x_5
x_{k6}	x_6
x_{k7}	x_{19}
x_{k8}	X_{20}
x_{k9}	X_{21}
x_{k10}	X_{22}
x_{k11}	X_{23}
x_{k12}	X_{24}
x_{k13}	X_{25}
x_{k14}	x_{26}
x_{k15}	x_{27}
x_{k16}	x_{28}
x_{k17}	x_{29}
x_{k18}	x_{30}
x_{k19}	x_{31}
x_{k20}	x_{32}
x_{k21}	x_{33}
x_{k22}	x_{34}
x_{k23}	x_{35}
x_{k24}	x_{36}
x_{k25}	x_{37}
x_{k26}	x_{38}

The optimisation process is complex and time consuming, it is almost impossible to carry out manually, which would probably lead to a wrong optimisation vector $\mathbf{X_{optimise}}$. Therefore it is concluded that computerization of the process is an essential. In this research work, the optimisation process is carried out with a specifically developed computer software module using C++. The task of the optimisation process includes retrieving elements x_i corresponding to each of fault case from "Case database B" followed by conducting comparison process to extract elements x_k of $X_{optimise}$ and finally saved these elements x_k in a file called "Case Database C". Elements x_k corresponding to all fault cases are saved together in a single txt. file in order to so that sufficient time can be reduced in process of retrieving data from Case Database C for the construction of fault identification algorithm subsequently.

The value of elements x_k of $X_{optimise}$ of 2592 fault cases under investigation can be found in Appendix F. The completed algorithm and graphical user interface (GUI) for fault data analysis and optimisation process can be found in Appendix G. Note that due to the space limitation, appendix F and G are stored in the attached CD-ROM.

5.6 Development of Rule-based Fault Identification

The elements, x_k in $\mathbf{X_{optimise}}$, corresponding to each of the fault case saved in "Case Database C" file have been used as the main data in the development of the rule-based fault identification algorithm proposed in this research work. This can be explained by demonstrating how the condition based-rules have been developed to identify R22-Ri-HL5R0D-BG-7.5km based on the following Table 5.15 that shows (i) elements x_k, (ii) dominant criterions of parameters φAB, φBC, φCA and ratios R_{01} and R_{21} corresponding to elements x_k and (iii) the data points corresponding to elements x_k for this fault case. The detailed description of each selected dominant criterion of parameters φAB, φBC, φCA and ratios R_{01} and R_{21} shown in Table 5.15 below can be found in Table 5.5 in previous section 5.4.2. Note that, the elements x_i of vector $\mathbf{X}$ for fault case R22-Ri-HL5R0D-BG-7.5km and their corresponding data points can be found in Table 5.10 in the previous section 5.5.2.

Table 5.15

Vector $\mathbf{X_{optimise}}$ of fault case R22-Ri-HL5R0D-BG-7.5km: dominant criterion and data points corresponding to x_k.

elements x_k in $X_{optimise}$	dominant criterion corresponding to x_k	data points corresponding to x_k in fault cases R22-Ri-HL5R0D-BG-7.5km
x_{k1}	$max\varphi AB$	134.7765
x_{k2}	$\varphi BC_{max\varphi AB}$	-272.2805
x_{k3}	$\varphi CA_{max\varphi AB}$	137.5040
x_{k4}	$max\varphi BC$	80.9110
x_{k5}	$\varphi AB_{max\varphi BC}$	-219.0675
x_{k6}	$\varphi CA_{max\varphi BC}$	138.1565
x_{k7}	$0\text{-}crossing\varphi AB$	-219.0675
x_{k8}	$\varphi BC_{0\text{-}crossing\varphi AB}$	80.9110
x_{k9}	$\varphi CA_{0\text{-}crossing\varphi AB}$	138.1565
x_{k10}	$0\text{-}crossing\varphi BC$	80.9110
x_{k11}	$\varphi AB_{0\text{-}crossing\varphi BC}$	-219.0675
x_{k12}	$\varphi CA_{0\text{-}crossing\varphi BC}$	138.1565
x_{k13}	$0\text{-}crossing\varphi CA$	0
x_{k14}	$\varphi AB_{0\text{-}crossing\varphi CA}$	0
x_{k15}	$\varphi BC_{0\text{-}crossing\varphi CA}$	0
x_{k16}	$150\text{-}crossing\varphi AB$	0
x_{k17}	$\varphi BC_{150\text{-}crossing\varphi AB}$	0
x_{k18}	$\varphi CA_{150\text{-}crossing\varphi AB}$	0
x_{k19}	$150\text{-}crossing\varphi BC$	0
x_{k20}	$\varphi AB_{150\text{-}crossing\varphi BC}$	0
x_{k21}	$\varphi CA_{150\text{-}crossing\varphi BC}$	0
x_{k22}	$150\text{-}crossing\varphi CA$	0
x_{k23}	$\varphi AB_{150\text{-}crossing\varphi CA}$	0
x_{k24}	$\varphi BC_{150\text{-}crossing\varphi CA}$	0
x_{k25}	$maxR_{01}$	1.7564
x_{k26}	$maxR_{21}$	0.8403

Table 5.16 shows the 'IF-THEN' condition-based rules that have been developed to identify fault case R22-Ri-HL5R0D-BG-7.5km. A total of 26 'IF-THEN' condition-based rules have been developed. The input to each statement in the 'IF-THEN' rules was fulfilled so that the final output statement can be executed. This can be outlined as followed : the statement in rule number 2 is executed after the statement in rule number 1 is fulfilled and the process is repeated until the statements in rule number 26 is fulfilled then, the final output statement (OUTPUT = R22-Ri-HL5R0D-BG-7.5km) will be executed. Each of the input statements in 'IF-THEN' condition rule is said to be fulfilled if the value of each dominant criterion of parameters φAB, φBC, φCA and ratios R_{01} and R_{21} is found to be within the upper and lower limits of variable x_k. This can be explained as follows: there are two conditions to be satisfied in the 'IF-THEN' statement of rule number 1. There are IF ($max\varphi AB$ >134.7765 -5) AND ($max\varphi AB$ < 134.7765 +5). With $max\varphi AB$,which is data point of φAB with maximum value of fault case R22-Ri-HL5R0D-BG-7.5km has been found to be 134.7765 (see Table 5.10 in section 5.5.2) which falls within the upper and lower limits of x_{k1} = 134.7765. Therefore, rule 1 is said to be fulfilled and consequently rule 2 will be executed. The condition-based rules shown in Table 5.16 are then transformed into a rule-based fault identification algorithm written with C++ source code.

Table 5.16

'IF-THEN' condition-based rules constructed based on Table 5.15 to identify fault case R22-Ri-HL5R0D-BG-7.5km.

number of rules	'IF-THEN' condition rules
1	IF ($max\varphi AB$ >134.7765 -5) AND ($max\varphi AB$ < 134.7765 +5) THEN
2	IF ($\varphi BC_{max\varphi AB}$ <-272.2805 -5) AND ($\varphi BC_{max\varphi AB}$ > -272.2805 +5) THEN
3	IF ($\varphi CA_{max\varphi AB}$ > 137.5040 -5) AND ($\varphi BC_{max\varphi AB}$ < 137.5040 +5) THEN

4	IF ($max\varphi BC$ >80.9110 -5) AND ($max\varphi BC$ <80.9110 +5) THEN
5	IF ($\varphi AB_{max\varphi BC}$ < -219.0675 -5) AND ($\varphi AB_{max\varphi BC}$ >-219.0675 +5) THEN
6	IF ($\varphi CA_{max\varphi BC}$ > 138.1565 -5) AND ($\varphi CA_{max\varphi BC}$ < 138.1565 +5) THEN
7	IF ($0\text{-}crossing\varphi AB$ <-219.0675 - 5) AND ($min\varphi AB$ > -219.0675+5) THEN
8	IF ($\varphi BC_{0\text{-}crossing\varphi AB}$ > 80.9110 -5) AND ($\varphi BC_{min\varphi AB}$ <80.9110 +5) THEN
9	IF ($\varphi CA_{0\text{-}crossing\varphi AB}$ > 138.1565 -5) AND ($\varphi CA_{max\varphi BC}$ < 138.1565 +5) THEN
10	IF ($0\text{-}crossing\varphi BC$ >80.9110 -5) AND ($max\varphi BC$ <80.9110 +5) THEN
11	IF ($\varphi AB_{0\text{-}crossing\varphi BC}$ <-219.0675 - 5) AND ($min\varphi AB$ > -219.0675+5) THEN
12	IF ($\varphi CA_{0\text{-}crossing\varphi BC}$ > 138.1565 -5) AND ($\varphi CA_{max\varphi BC}$ < 138.1565 +5) THEN
13	IF ($0\text{-}crossing\varphi CA$ = 0) THEN
14	IF ($\varphi AB_{0\text{-}crossing\varphi CA}$ = 0) THEN
15	IF ($\varphi BC_{0\text{-}crossing\varphi CA}$ = 0) THEN
16	IF ($150\text{-}crossing\varphi AB$ = 0) THEN

17	IF ($\varphi BC_{150\text{-}crossing\varphi AB}$ = 0) THEN
18	IF ($\varphi CA_{150\text{-}crossing\varphi AB}$ = 0) THEN
19	IF ($150\text{-}crossing\varphi BC$ = 0) THEN
20	IF ($\varphi AB_{150\text{-}crossing\varphi BC}$ = 0) THEN
21	IF ($\varphi CA_{150\text{-}crossing\varphi BC}$ = 0) THEN
22	IF ($150\text{-}crossing\varphi CA$ = 0) THEN
23	IF ($\varphi AB_{150\text{-}crossing\varphi CA}$ = 0) THEN
24	IF ($\varphi BC_{150\text{-}crossing\varphi CA}$ = 0) THEN
25	IF (R_{01} > 0.1) THEN
26	IF (R_{21} > 0.1) THEN OUTPUT = R22-Ri-HL5R0D-BG-7.5km

The example of condition-based rules shown in Table 5.16 above is used to indentify types of SLG faults. The following two condition- based rules with “IF-THEN” statements shown in the following Table 5.17 are added to the developed rule-based SLG fault identification algorithm to distinguish the normal network operating conditions and other network fault conditions. In this table, rule number 1 is used to identify normal network operating conditions and rule number 2 is used to identify the existence of a network fault condition. The input statements for both of rules 1

and 2 shown in Table 5.17 are developed based on the analysis of parameters φAB, φBC and φCA in normal network and fault conditions that have been reported in Chapter 4 section 4.3. The rules shown in Table 5.17 are evaluated before the rules in Table 5.16.

Table 5.17

'IF-THEN' condition-based rules constructed based on analysis reported in Chapter 4 section 4.3 to identify fault case normal network condition and fault condition.

number of rules	'IF-THEN' condition rules
1	IF (115 < φAB < 125) and (-245 < φBC < -235) and (115 < φCA < 125) THEN OUTPUT = NO FAULT
2	IF (φAB < 115 or φAB > 125) and (φBC <-245° or φBC > -235°) and (φCA <115 or φCA >125°) THEN OUTPUT = FAULT EXIST

In this research work, the process to develop a fault identification algorithm is carried out with a specifically developed computer software module using C++. The tasks of the whole process of constructing a fault identification algorithm include: retrieving elements x_k from "Case Database C" file and developments of 'IF-THEN' condition-based rules based on the elements x_k.

5.7 Development of Phase Selection Algorithm

As reported in Chapter 4, section 4.2.2, the DG feeder in the investigated power system is protected with a proposed zone protection approach. The feeder therefore is divided into protection zones such that when a fault occurs at a certain zone, it is cleared by the pair of circuit breakers that are located at the two ends of the considered section. For instance, it is shown in schematic diagram of the investigated system in Figure 5.1 that section 1 is protected with relays R_1 and R_{11} located at the two ends of this section. A fault that occurs at any location within section 1 e.g., either 1km, 2.5km or 4km from 33 kV grid within the section 1 will cause the tripping of the two circuit breakers associated with R_1 and R_{11} that contain a phase selector built with the proposed fault identification and phase selection algorithm.

The fault identification algorithm reported in the previous section 5.6 was developed mainly to indentify each of the SLG fault cases under consideration. The development of the phase selection algorithm elaborated in this section is for identifying the protection zone at which the fault occurs and also to indentify the faulty phase of a particular SLG fault case that has been detected. This applies if the fault case is an internal fault that may occur within section 1, 2 or 3 at the DG feeder (see Figure 5.1) so that the pair of relays protected that particular section can activate their associated circuit breakers to isolated the faulty phase within that protection section from the rest of the network under investigation. Note that the DG feeder is divided into three protection zones, sections 1, 2 and 3. Section 1 is protected with relays R_1 and R_{11} while section 2 is protected with relays R_2 and R_{22} and section 3 is protected with relays R_3 and R_{33}.

All fault cases under consideration are classified into nine categories that reflect (i) the type of SLG fault either a-g , b-g or c-g fault and (ii) the protected zone in terms of section 1, 2 or 3 at the DG feeder, as shown in Table 5.18 below. The fault case related to the fault event occurred at section 1 in the investigated system has been classified into one of the categories from C_1 to C_3 depending on fault type, e.g., fault case R11-Ri-HL5R0D-AG-12.5km will be classified into C_1 that indicates 'AG fault at section 1' which means the fault case is an a-g fault occurred at the section 1 of the protected zone. Note that, R11-Ri-HL5R0D-AG-12.5km refers to a-g fault (based on the line current measurement of relay R_{11} in Figure 5.1) assuming the following fault and network operating conditions: $R_f = 5\Omega$, FIA = 0° (corresponding to the fault inception time of 34.998 s), fault location = 12.5km from the 2MW DFIG (within section 1) , network configuration = ring network, loading condition = half load. The fault case related to the fault event occurred at section 2 in the investigated system has been classified into one of the category from C_4 to C_6. The fault case related to the fault event occurred at section 3 in the investigated system has been classified into one of the category from C_7 to C_9. The content in Table 5.18 is transformed into phase selection algorithm written in C++ source code. The completed fault identification and phase selection algorithm can be found in Appendix H in the attached CD-ROM.

Table 5.18

The nine fault categories of 2592 fault cases under consideration.

fault categories	description
C_1	AG at section 1
C_2	BG at section 1
C_3	CG at section 1
C_4	AG at section 2
C_5	BG at section 2
C_6	CG at section 2
C_7	AG at section 3
C_8	BG at section 3
C_9	CG at section 3

The phase selector of each the relays located at the DG feeder (see Figure 5.1 Chapter 5) is assumed to be installed with the standard completed set of rule-based fault identification and phase selection algorithms. Therefore, a user control interface is assumed on each of the relay units at the DG feeder to preset the relay location, e.g., R_1, before the installation to ensure correct discrimination of the faulty section. Only the pair of relays assigned to protect the faulty section responds to the results from fault identification and phase selection algorithm and consequently indicate the fault categories shown in Table 5.18. For instance, if an a-g fault occurs at 11km from the 2.0MW DFIG, after indentifying the fault case and fault category using the proposed fault identification and phase selection algorithm within the phase selector of each relays located at the DG feeder, only relays R_1 and R_{11}, located at both ends of section 1, will respond to the output results of the phase selector. Consequently, relay R_1 and R_{11} will issue a tripping signal to their corresponding circuit breakers to isolate phase “a” of section 1 at the DG feeder from the network.

5.8 Verification of Fault Identification and Phase Selection Algorithm

In the verification process, the five parameters φAB, φBC, φCA, ratios R_{01} and R_{21} of each fault case saved in the "Case Database A" folder are fed into a test module that contains the condition rule-based fault identification and phase selection algorithm, that has been developed in the previous section 5.6 and 5.7 to test the validity of the algorithm. The output signal from the test module that indicates (i) fault detection time and (ii) fault categories (see Table 5.18) are displayed graphically in the graphical user interface (GUI) of the test module which has been developed with Delphi source code [99-101]. The verification process can be summarised in flow chart shown in Figure 5.12 below.

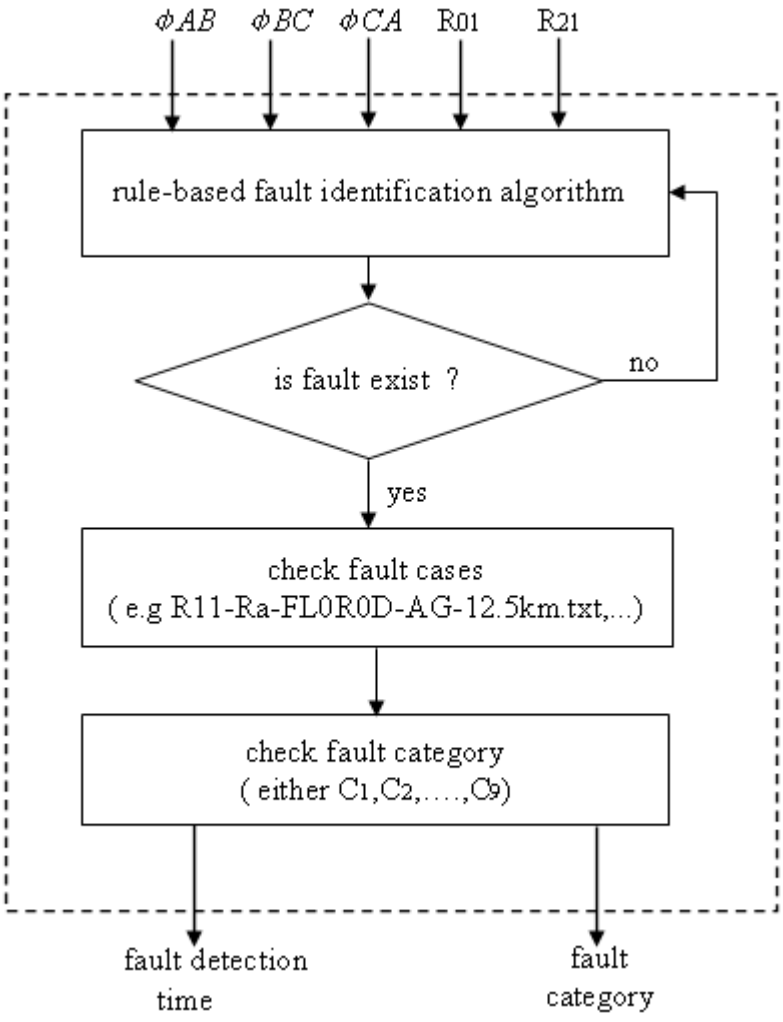

Figure 5.12 Flow chart illustrate the verification process of developed fault identification and phase selection algorithm.

In this research work, the verification process is carried out with a specifically developed computer software module using C++. The tasks in the process include: retrieving data from "Case Database A" folder, followed by feeding the five parameters φAB, φBC, φCA, R_{01} and R_{21} of each fault case into the test module and displaying the input signal and output signal of the test module in the GUI test panel. The completed verification test algorithm can be found in Appendix H. It is combined with the completed rule-based fault identification and phase selection algorithm in Appendix H. GUI test panel can also be found in Appendix H in the attached CD-ROM.

5.9 Graphical User Interface (GUI) Test Panel

Figure 5.13 shows the graphical user interface (GUI) of the test module which was developed using Delphi source code, for easy access of the end user to the verification process reported in section 5.6. There are three graphical windows in the developed GUI test panel. The top and middle graphical windows display the input signals to the test module and the bottom graphical window displays the output signal of the test module. The top graphical window displays input signals φAB (red waveform), φBC (blue waveform) and φCA (black waveform). The middle graphical window displays the ratios R_{01} (red waveform) and R_{21}(blue waveform). The bottom graphical window displays the output signal from the test module that indicates (i) fault detection time and (ii) fault category. In this particular figure, the top and middle graphical windows show variations of the five parameters obtained from fault case R22-Ri-HL5R0D-BG-7.5km. The bottom graphical window shows the output signal corresponding to this fault case. According to the verification process shown in Figure 5.10, the phase selection procedure can be outlined as follows: the rule based fault identification algorithm will firstly indentify a 'fault exist' or 'no fault' condition (see condition-based rules in Table 5.17) by issuing an output signal of '0' or '12' respectively. This is achieved by assessing φAB, φBC, φCA , R_{01} and R_{21} of the this fault cases. If the 'fault exist' condition is found, the output signal will turn from '12' down to '1', '2', '3', ….,'9' depending on the fault category which indentifies the faulty section and SLG fault type. Note that numerals '1' to '9', displayed in the bottom graphical window of the GUI test panel are corresponding to C_1 to C_9 in Table 5.18. The fault detection time refers to the time instant when the

output signal turns from ‘12’ corresponding to a ‘fault exists’ condition, to ‘1’ to ‘9’ that indicates the fault category.

In addition to the graphical windows, two text windows have been included in the GUI. The top test window display the file names of all 2592 fault cases under consideration, and the file name of a particular fault case that has been loaded for the verification test is highlighted in blue, i.e., R22-Ri-HL5R0D-BG-7.5km. The bottom text window displays a summary of the result obtained from the verification test. The information included in this text window are (i) the file name of each input fault case being verified. i.e., Tested Fault Case = R22-Ri-HL5R0D-BG-7.5km (ii) output results of test module that consisting of the fault detection time and the fault category i.e., Detected Fault Category = C5 (BG at section 2) and Fault Detection Time = 35.0185 s.

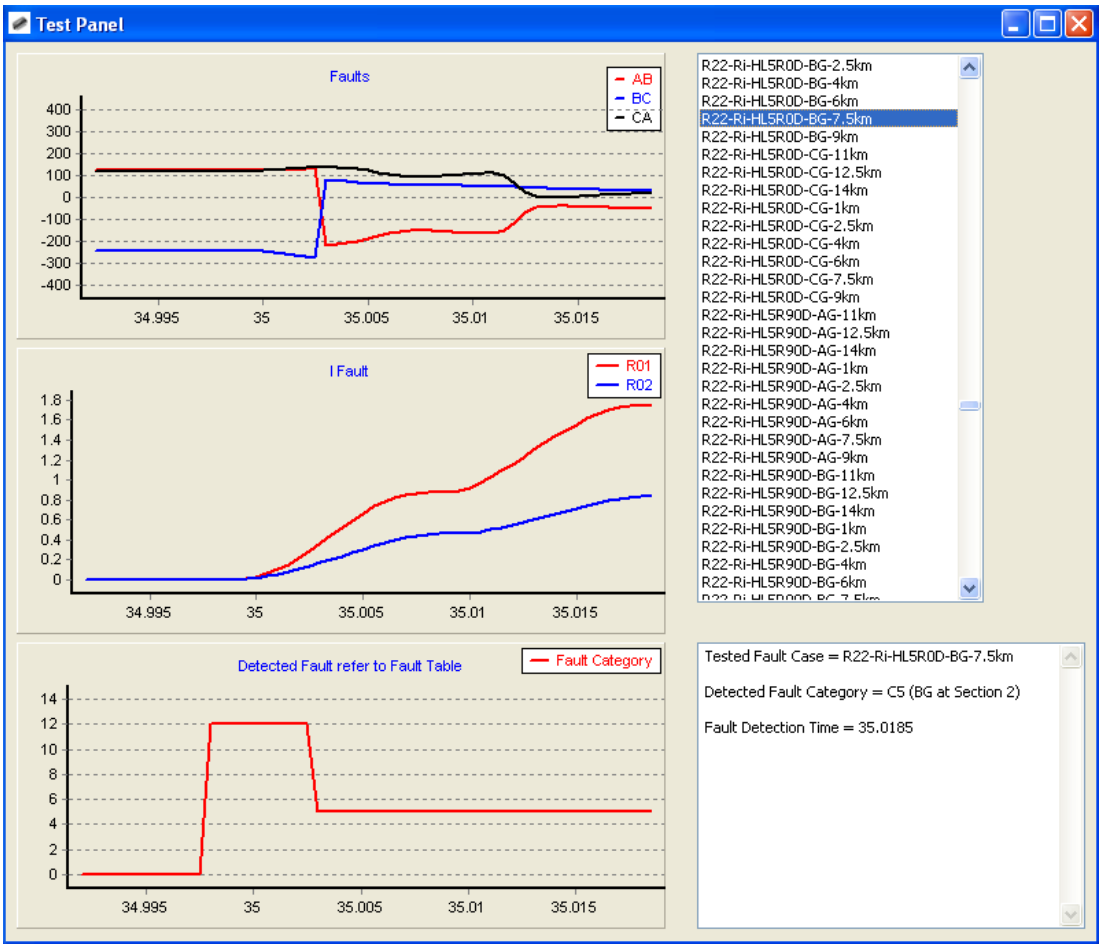

Figure 5.13 Display of output and input signal of test module in GUI test panel.

5.10 Verification Test Results

The complete verification test to indentify each of the fault cases, from the total of 2592, has been conducted. The proposed fault identification and phase selection algorithms have successfully indentified each of the fault cases and fault categories. Due to space limitation, the verification test results are shown in Appendix H in CD-ROM. Note that all fault cases under consideration have been loaded into the upper text window of the GUI test panel shown in Appendix G. The reader can assess the verification test result corresponding to a particular fault case by click on that file name displayed in the upper text window in the GUI test panel, so that the output test results will be displayed in the three graphical windows and bottom text window in the GUI test panel.The test results shown in following sections are used to demonstrate the effectiveness of the developed rule-based fault identification and phase selection algorithm operating over wide range of network operating condition and fault conditions. Note that the fault cases chosen for testing are picked randomly to reflect the different network scenarios e.g., different fault resistance and network loading levels that have been considered in this research work (see Table 4.4 ,section 4.5, Chapter 4).

5.10.1 Different Type of SLG Faults

Figure 5.14(a) to (c) show fault cases of three different SLG faults including AG, BG and CG fault. The network operating condition and network fault condition remain the same for all three fault cases where fault location = 9km from the 2MW DFIG (section 2), fault inception = 0°, fault resistance = 0Ω, network operating condition = radial network operating mode and network loading level = full loading.

5.10.2 SLG Faults occurred at different Fault Sections

Figure 5.15(a) to (c) show fault cases that occurs at the middle of three different sections: section 1(12.5km from the 2MW DFIG), section 2 (7.5km from the 2MW DFIG) and section 3(2.5km from the 2MG DFIG). The other network operating condition and network fault conditions remain the same for all three fault cases where fault type = BG fault, fault inception = 0°, fault resistance = 0Ω, network

operating condition = ring network operating mode and network loading level = half loading.

5.10.3 SLG Fault with different Fault Resistances

Figure 5.16(a) to (b) show fault cases with two different fault resistances of 0Ω and 5Ω. The other network operating condition and network fault condition remain the same for all three fault cases where fault type = CG fault, fault inception = 0°, fault location = 14km from 2MG DFIG (within section1), network operating condition= radial network operating mode and network loading level= full loading.

5.10.4 SLG Fault with different Fault Inception Angle

Figure 5.17(a) to (b) show fault cases that occur at two different fault inception angles 0° and 90°. The other network operating condition and network fault condition remain the same for all three fault cases where fault type = CG fault, fault resistance = 5Ω, fault location = 4km from the 2MW DFIG (within section 3), network operating condition= ring network operating mode and network loading level = half loading.

5.10.5 SLG Fault with different Network Operating Mode

Figure 5.18(a) to (b) show fault cases that are for two different network operating modes, i.e., radial and ring operating modes. The other network operating condition and network fault condition remain the same for all three fault cases where fault type = AG fault, fault inception = 90°, fault location = 7.5km from the 2MW DFIG (within section 2), fault resistance = 0Ω and network loading level = full loading.

5.10.6 SLG Fault with different Network Loading Level

Figure 5.19(a) to (b) show fault cases for two different network loading levels, i.e., load and half load. The other network operating condition and network fault conditions remain uniform for all three fault cases where fault type = BG fault, fault

inception = 0, fault location = 2.5km from the 2MW DFIG (within section 3), fault resistance = 5Ω, network operating condition = ring network operating mode.

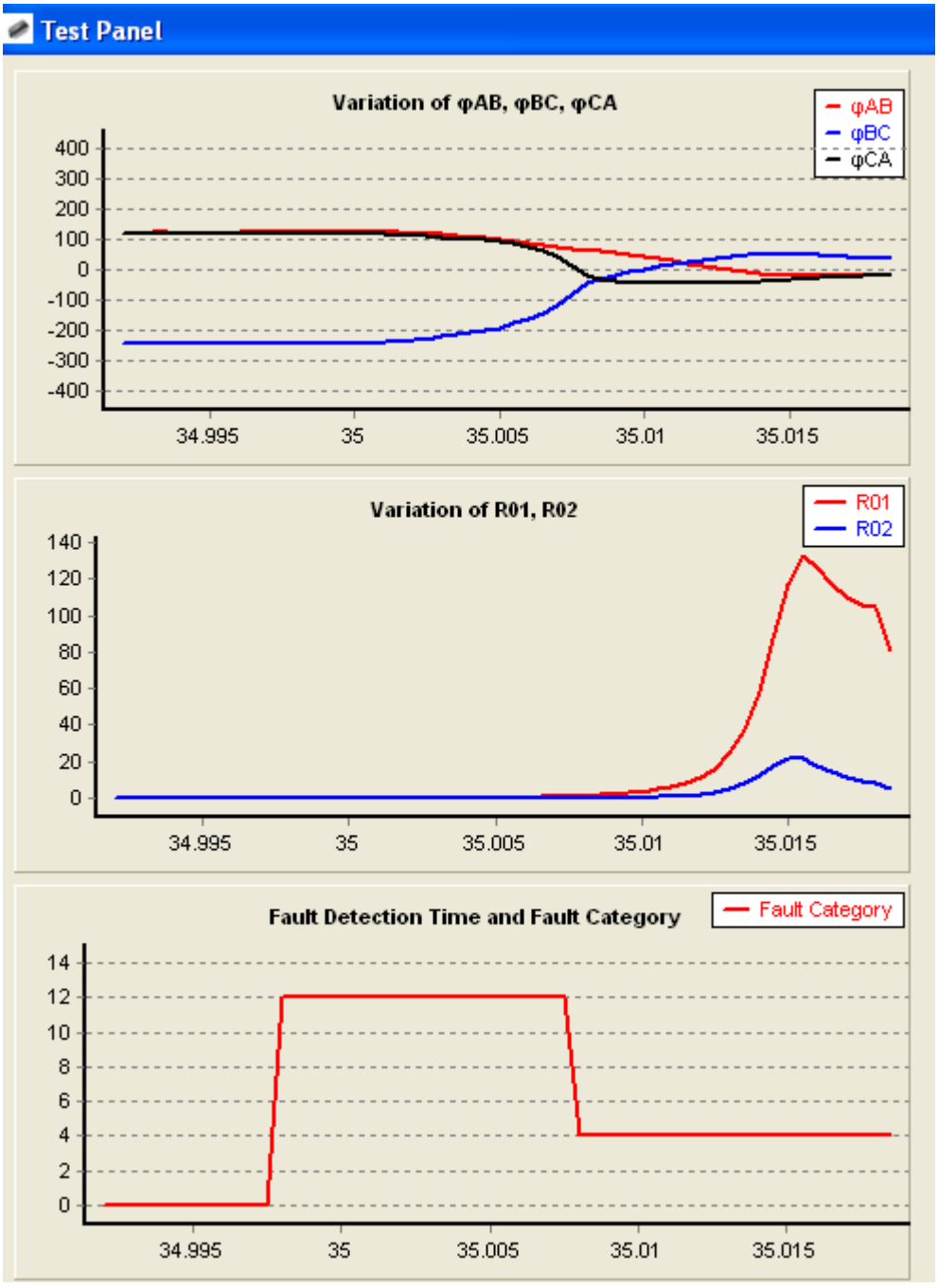

Figure 5.14(a) fault cases: R22-Ra-FL0R0D-AG-9km, fault detection time: 35.008 s fault categories: C4 (AG at section 2).

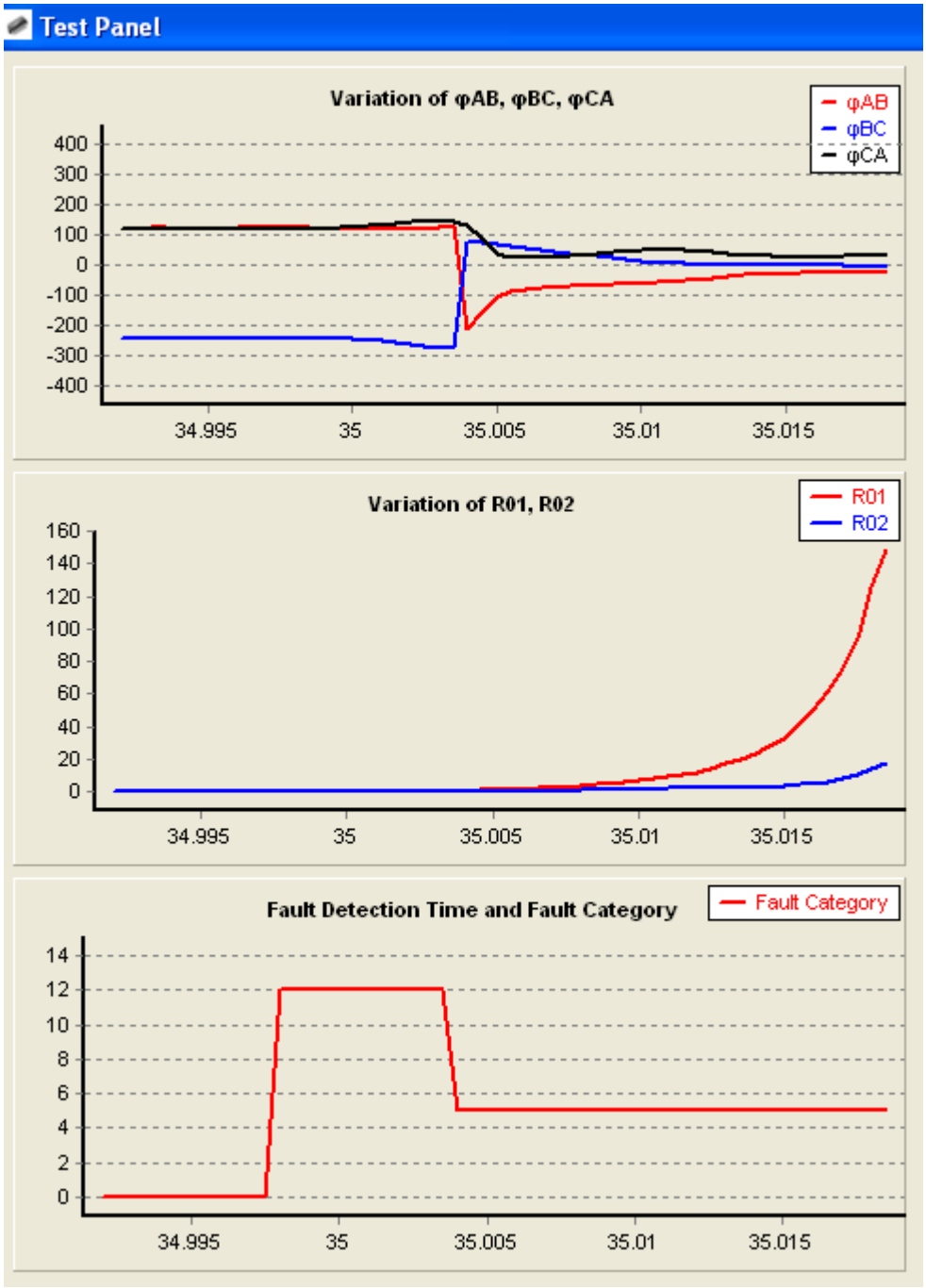

Figure 5.14(b) fault cases: R22-Ra-FL0R0D-BG-9km, fault detection time: 35.004 s fault categories: C5 (BG at section 2).

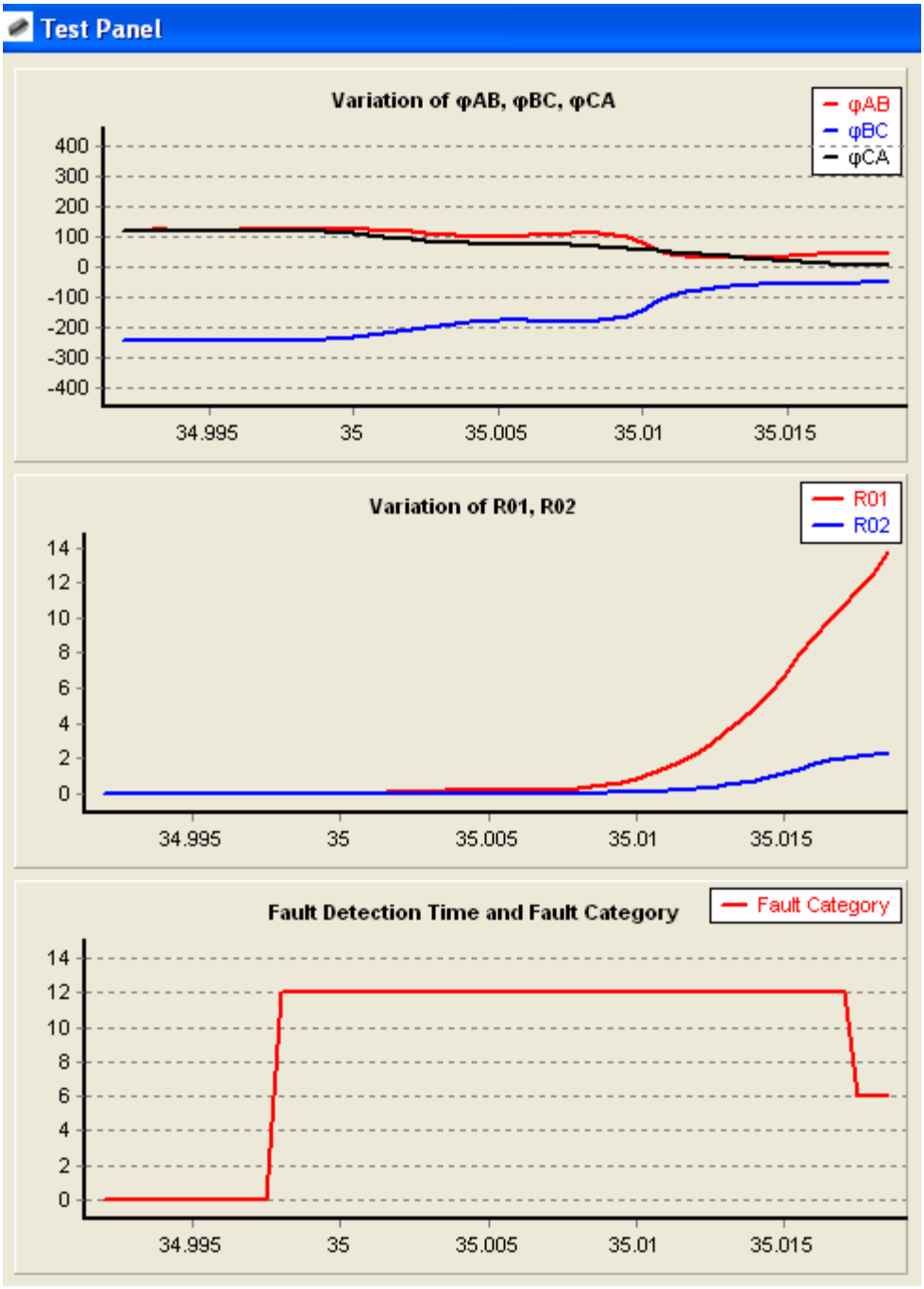

Figure 5.14(c) fault cases: R22-Ra-FL0R0D-CG-9km, fault detection time: 35.0175 s fault categories: C6 (CG at section 2).

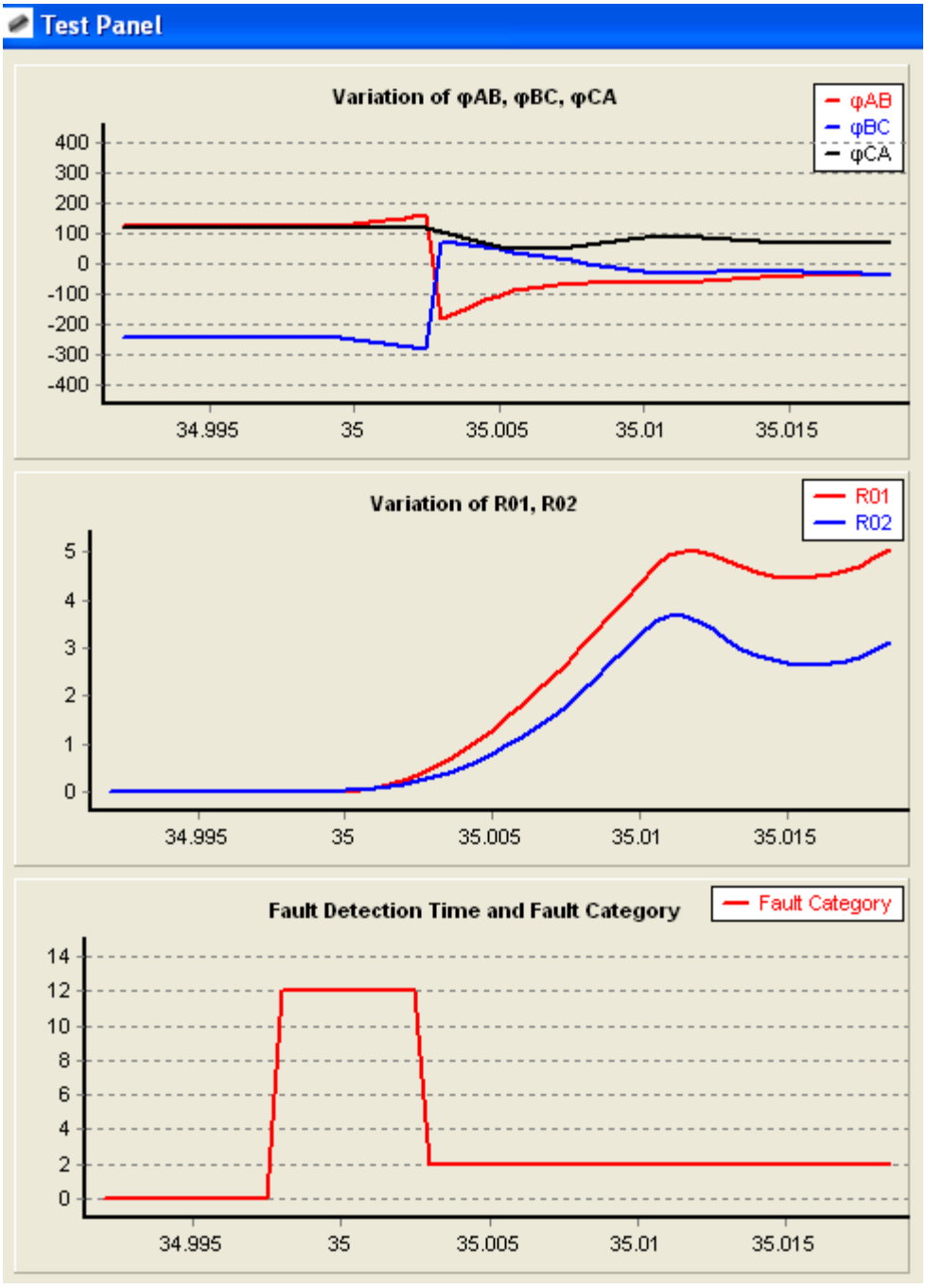

Figure 5.15(a) fault cases: R11-Ri-HL0R0D-BG-12.5km, fault detection time: 35.003 s fault categories: C2 (BG at section 1).

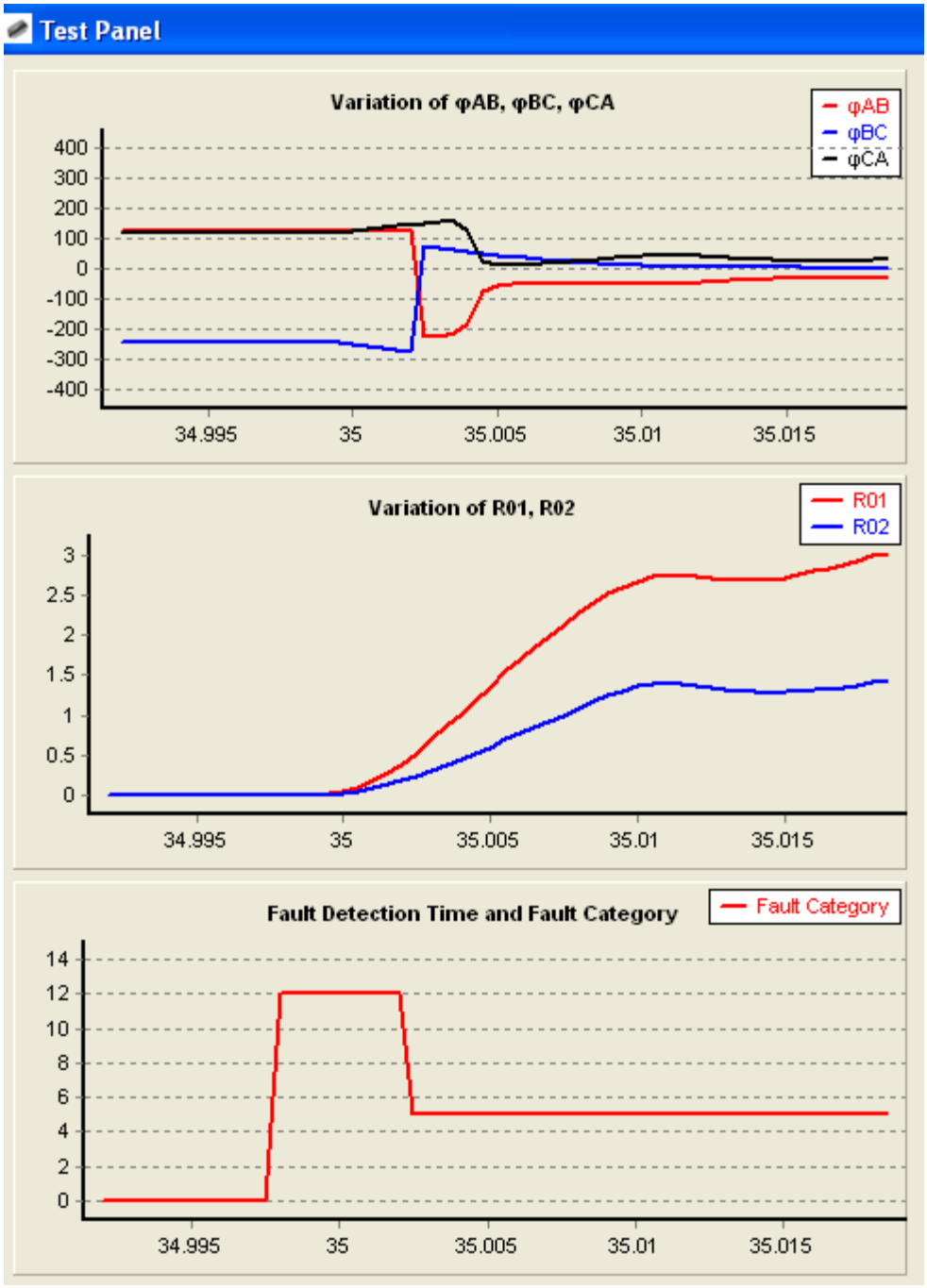

Figure 5.15(b) fault cases: R22-Ri-HL0R0D-BG-7.5km, fault detection time: 35.0025 s fault categories: C5 (BG at section 2).

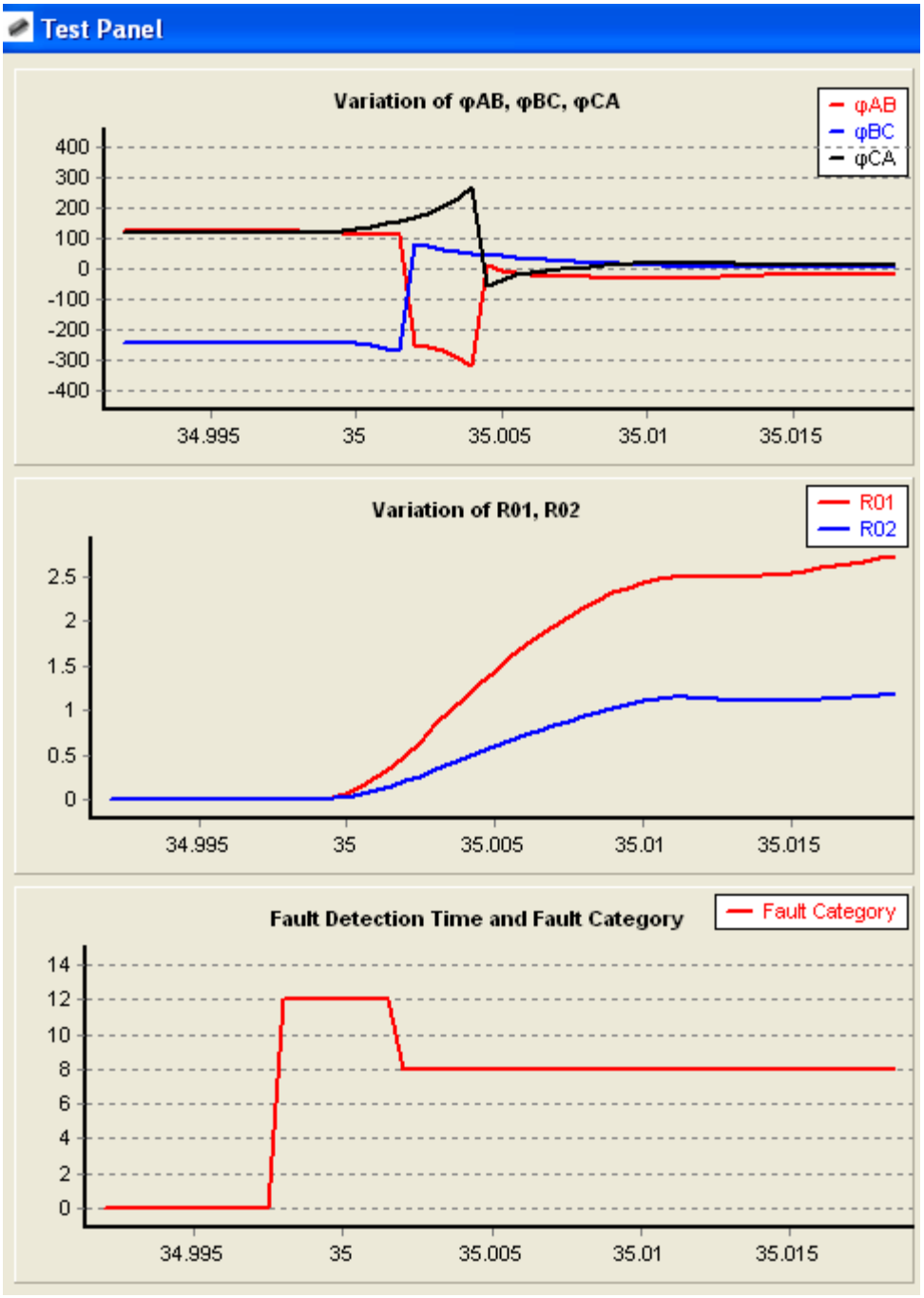

Figure 5.15(c) fault cases: R33-Ri-HL0R0D-BG-2.5km, fault detection time: 35.002 s fault categories: C8 (BG at section 3).

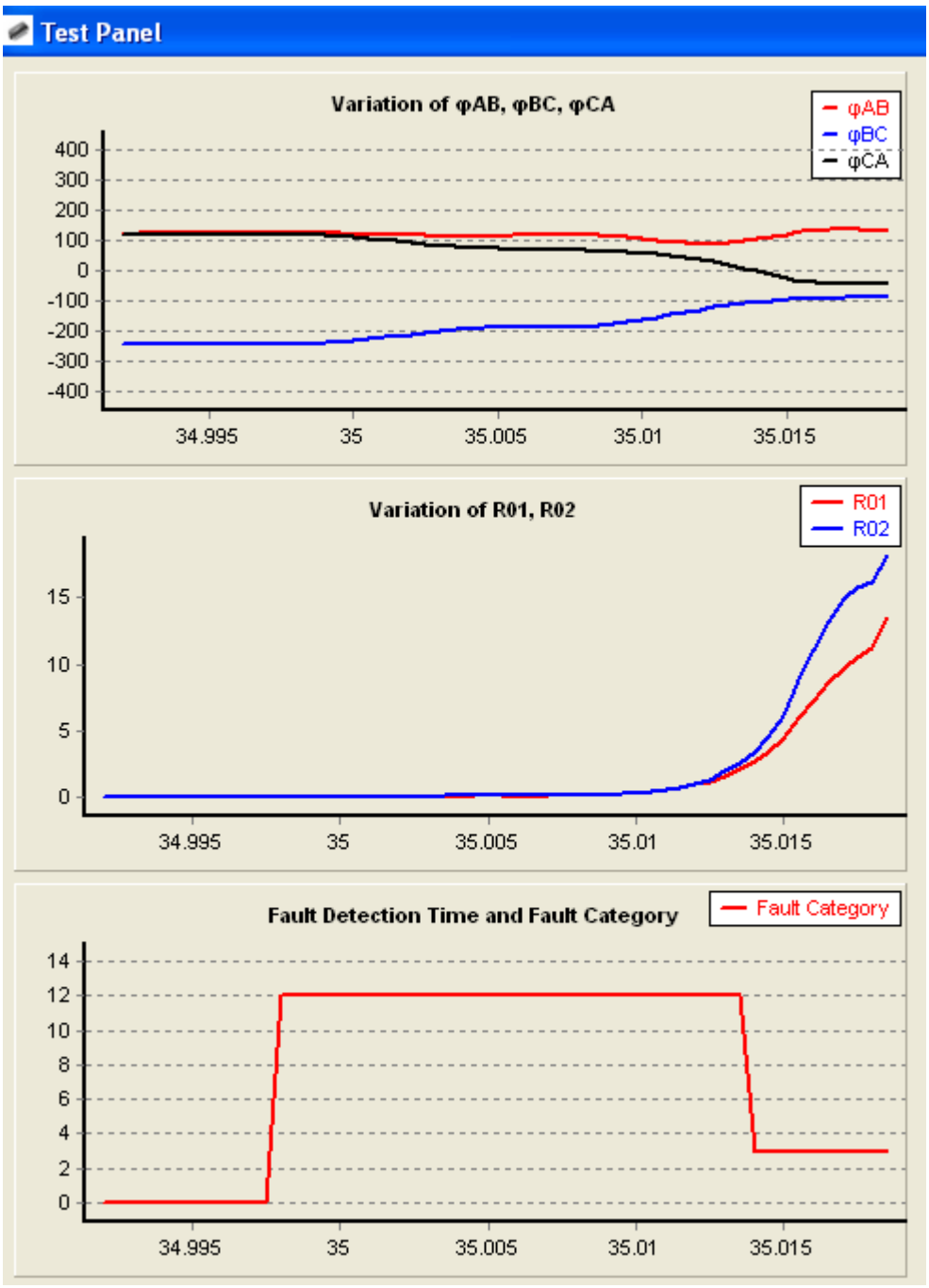

Figure 5.16(a) fault cases: R11-Ra-FL0R0D-CG-14km, fault detection time: 35.014 s fault categories: C3 (CG at section 1).

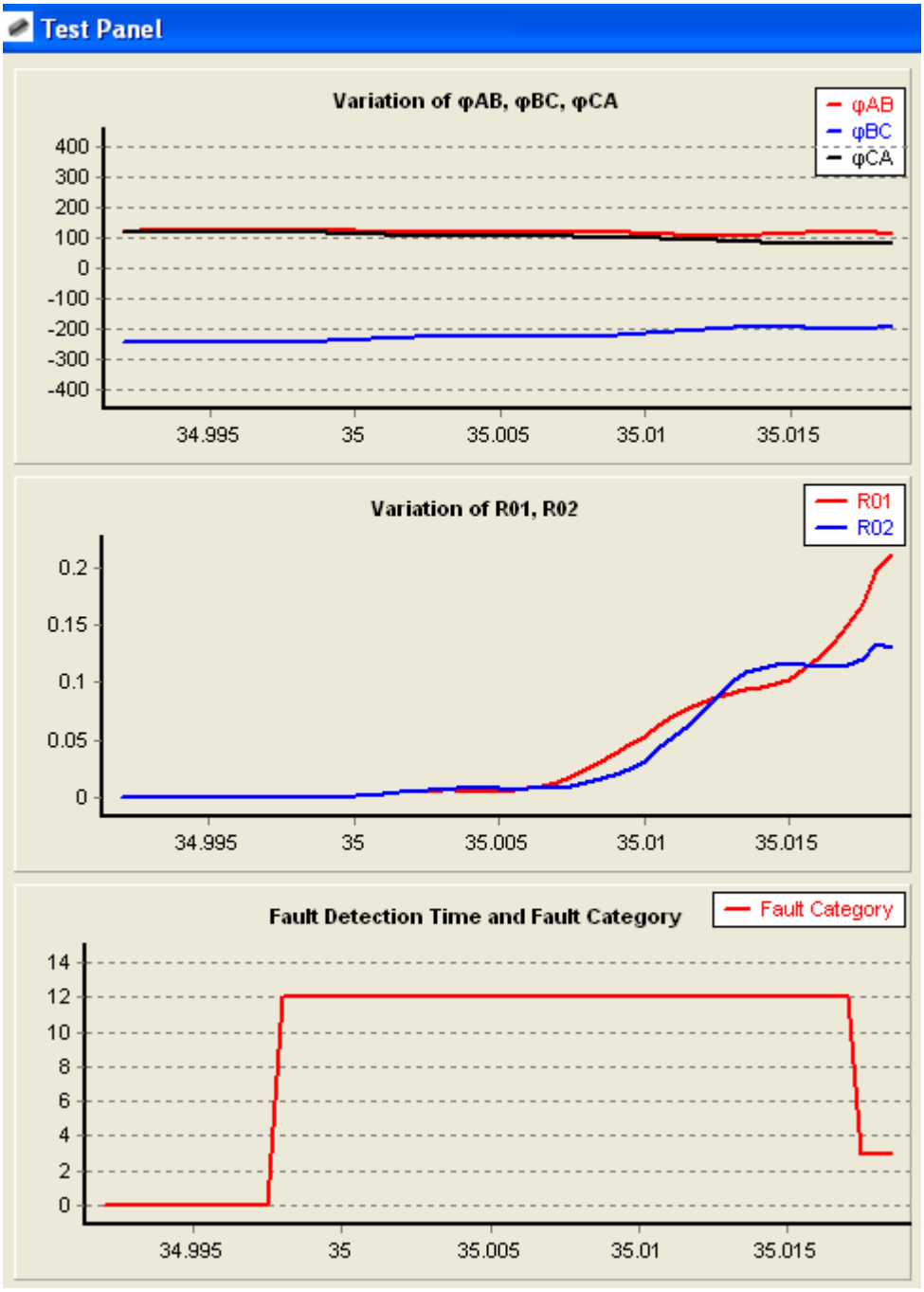

Figure 5.16(b) fault cases: R11-Ra-FL5R0D-CG-14km, fault detection time: 35.0175 s fault categories: C3 (CG at section 1).

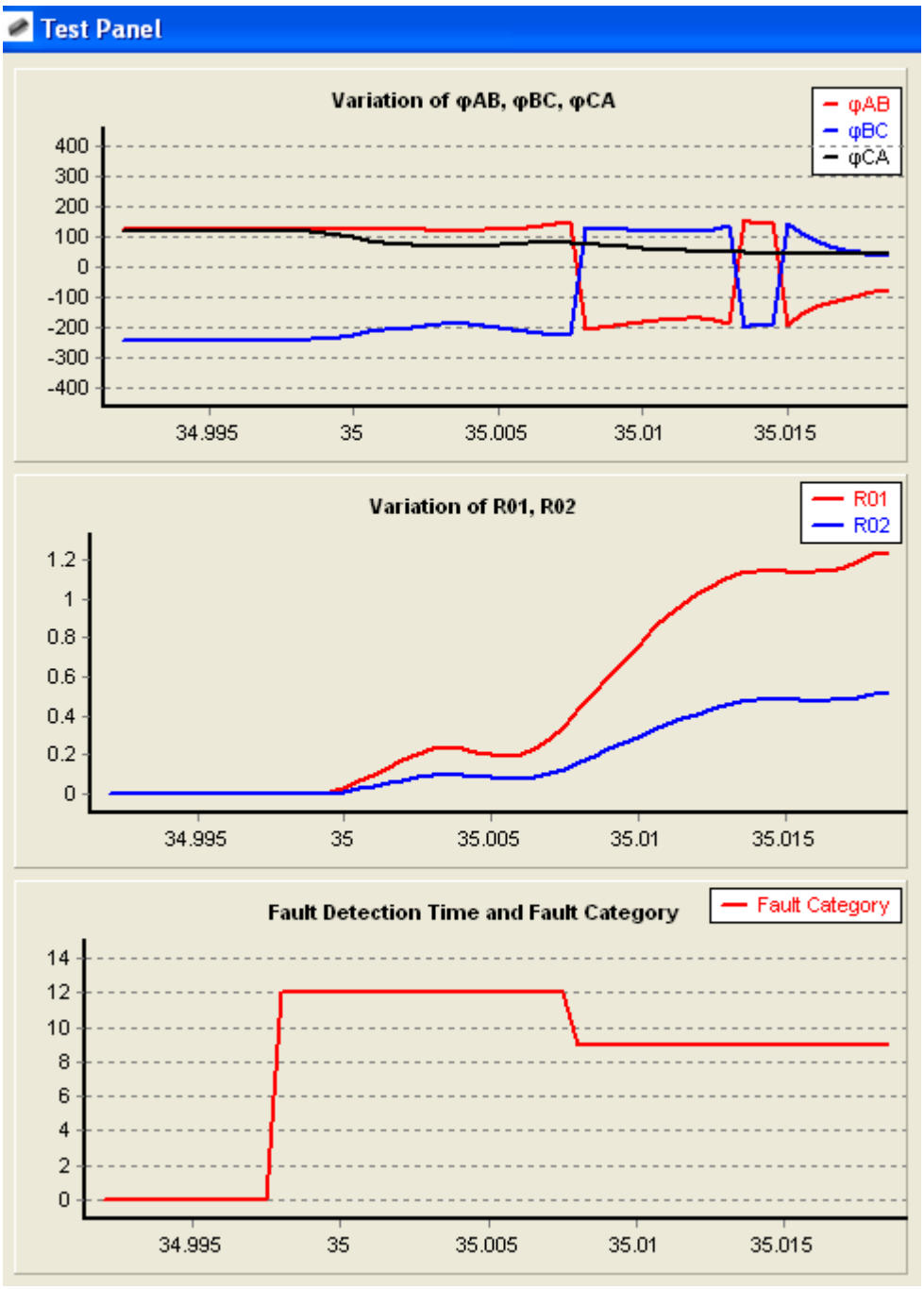

Figure 5.17(a) fault cases: R33-Ri-HL5R0D-CG-4km, fault detection time: 35.008 s fault categories: C9 (CG at section 3).

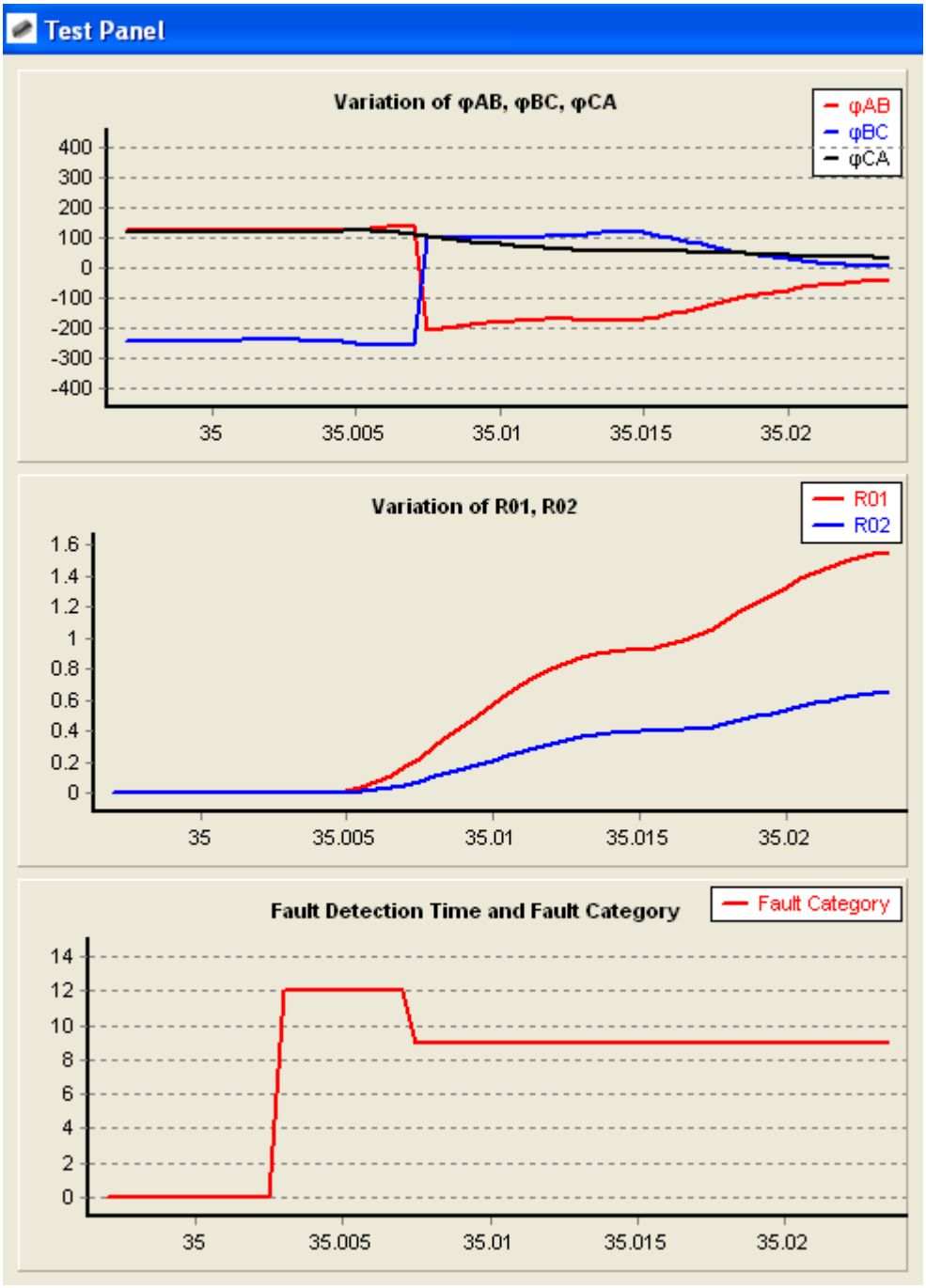

Figure 5.17(b) fault cases: R33-Ri-HL5R90D-CG-4km, fault detection time: 35.0075 s fault categories: C9 (CG at section 3).

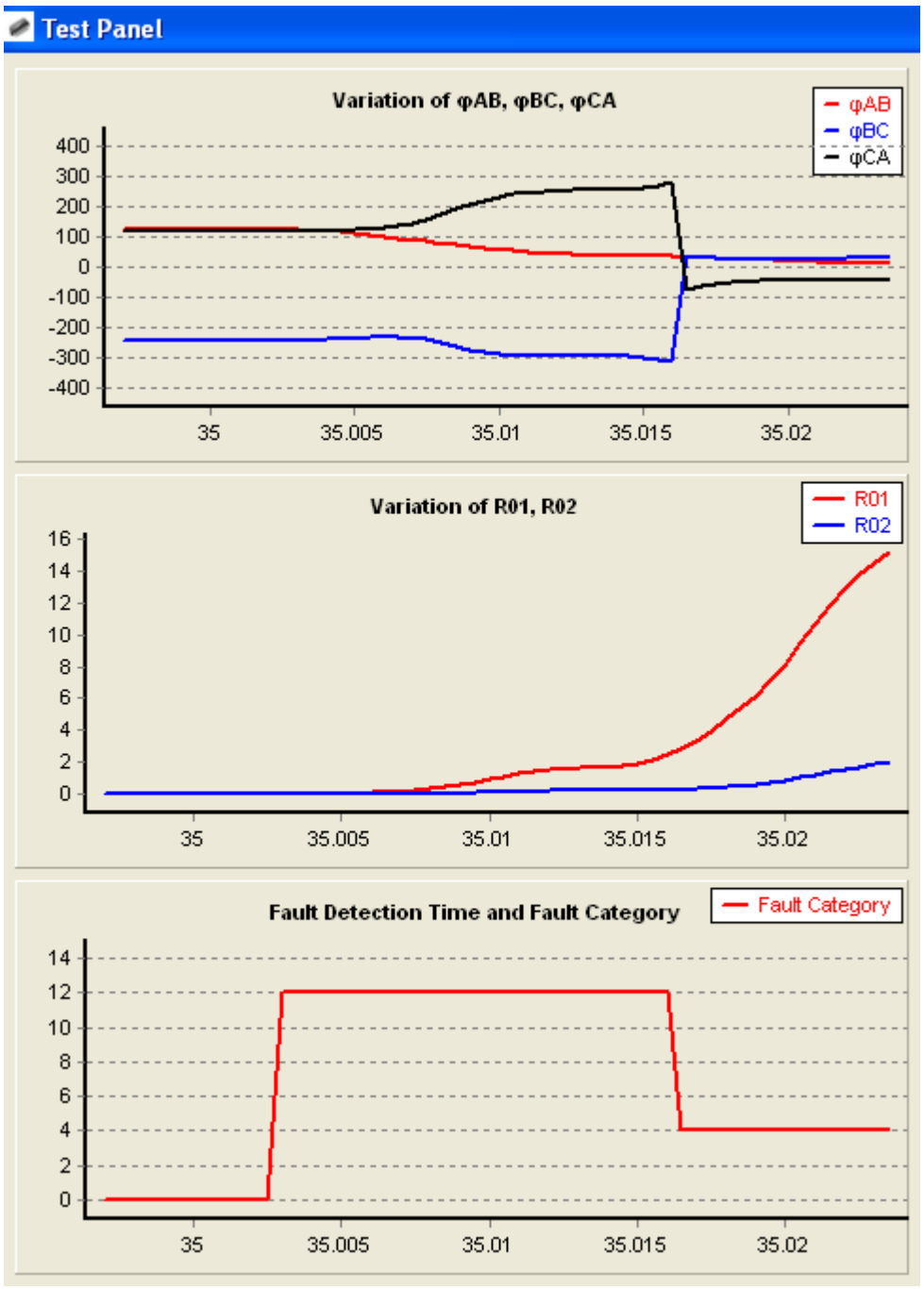

Figure 5.18(a) fault cases: R22-Ra-FL0R90D-AG-7.5km, fault detection time: 35.0165 s fault categories: C4 (AG at section 2).

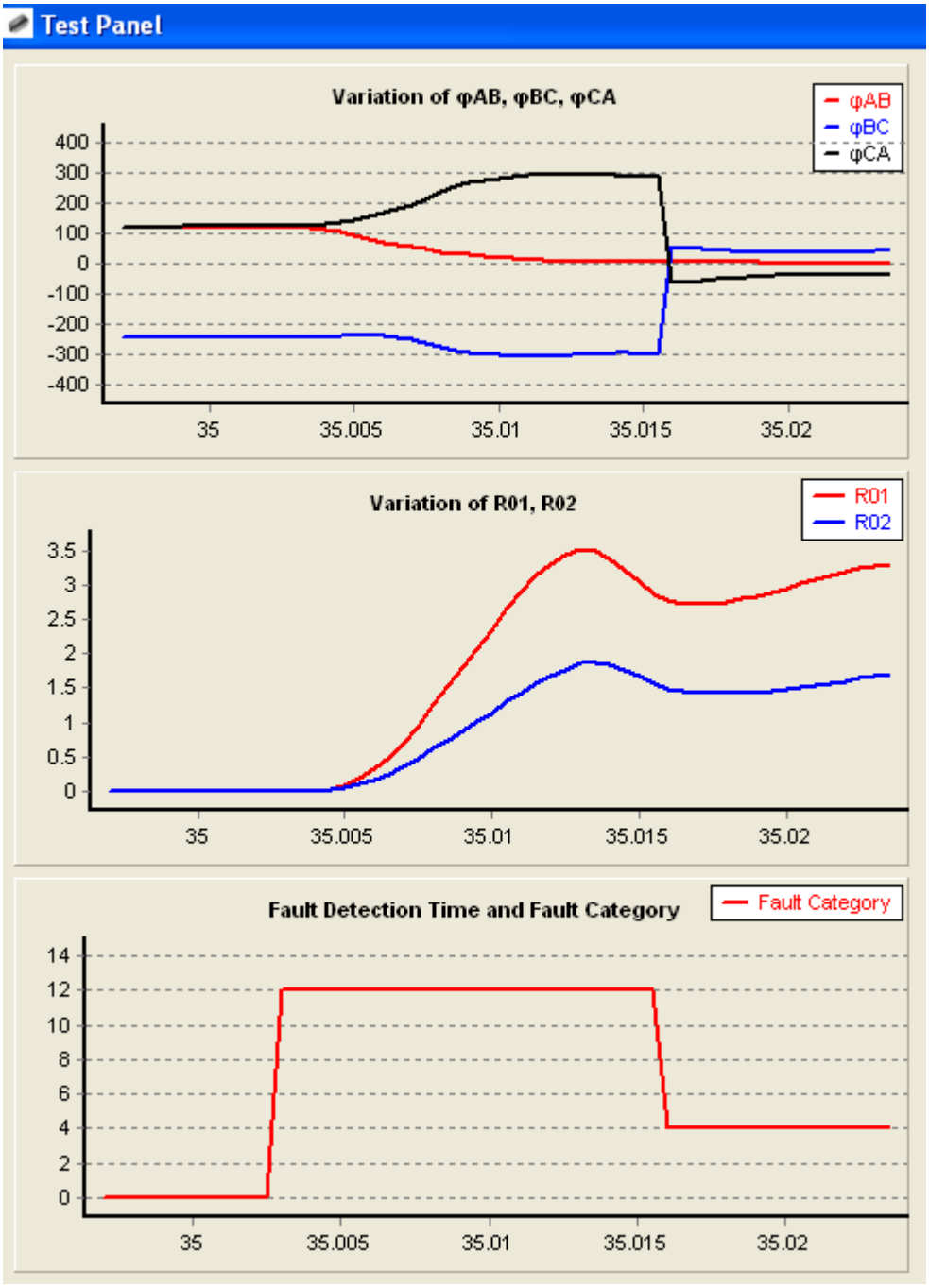

Figure 5.18(b) fault cases: R22-Ri-FL0R90D-AG-7.5km, fault detection time: 35.016 s fault categories: C4 (AG at section 2).

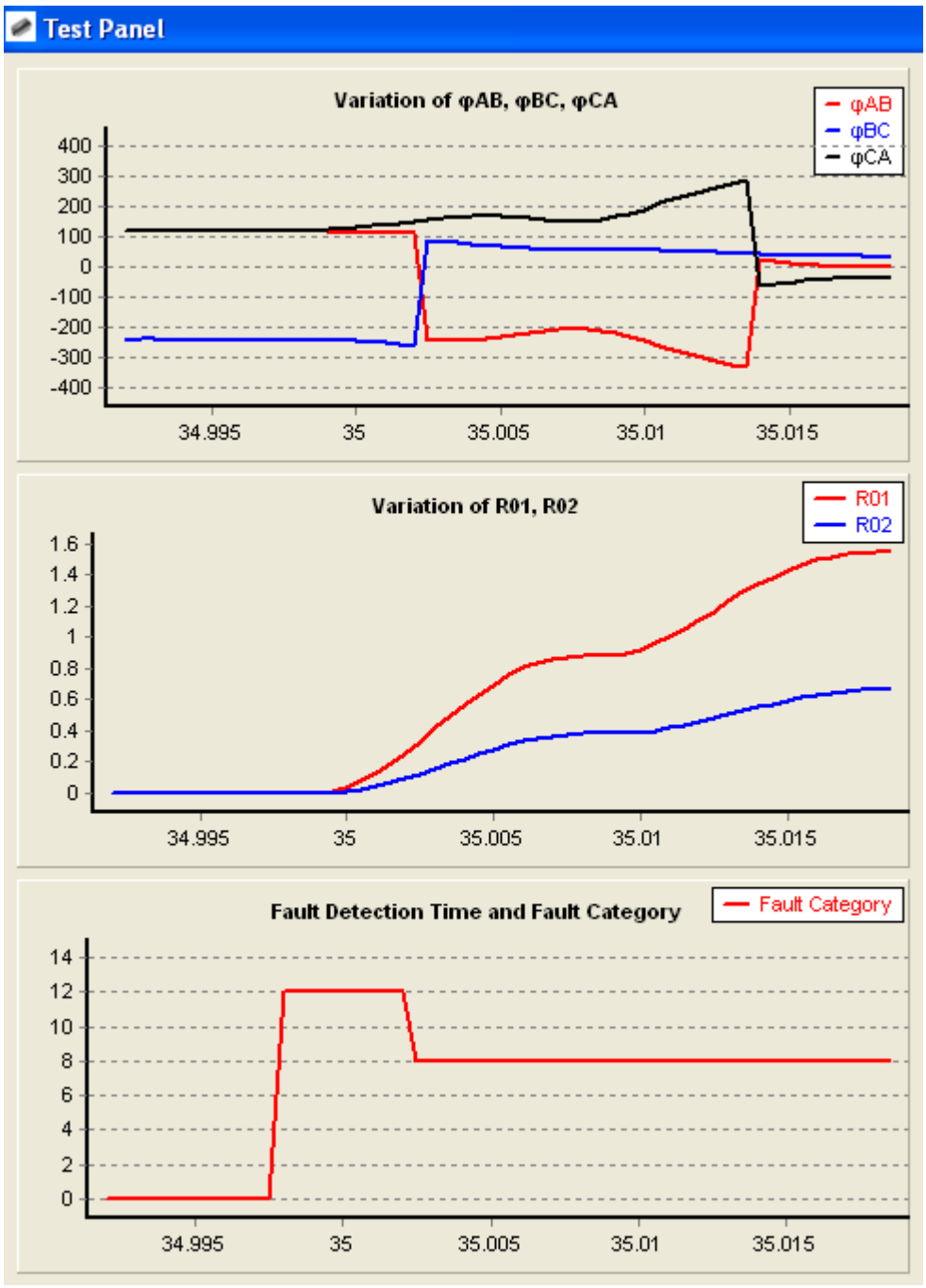

Figure 5.19(a) fault cases: R33-Ri-FL5R0D-BG-2.5km, fault detection time: 35.0025 s fault categories: C8 (BG at section 3).

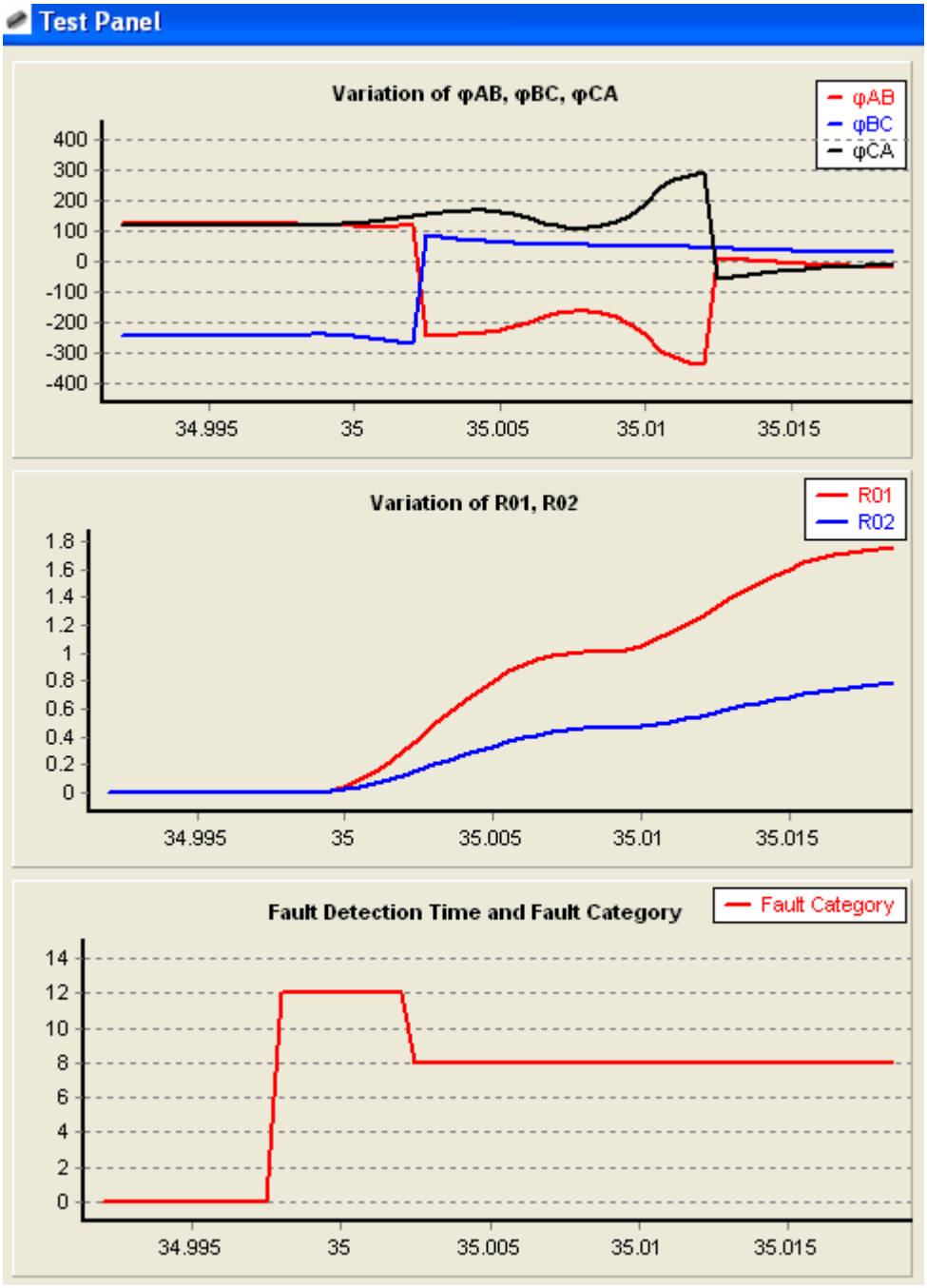

Figure 5.19(b) fault cases: R33-Ri-HL5R0D-BG-2.5km, fault detection time: 35.0025 s fault categories: C8 (BG at section 3).

5.9 Discussion

In this chapter, each stage of the digital data processing and analysing, algorithm construction and testing of the proposed rule-based fault identification and phase selection algorithm has been discussed in detail. The test results from the verification process have shown the following:

a. The proposed adaptive rule-based fault identification algorithm can successfully indentified all of the SLG fault cases under consideration.

b. The proposed phase selection algorithms can successfully indentifying the faulty phase and faulty section after a particular fault case is indentified.

c. The proposed method is effective over a wide range of network operating and fault conditions.

d. The fault detection time varies with fault cases. The speed of fault detection time is subjected to the criterions being used to construct the rule-based fault identification algorithm.

e. The proposed method has successfully indentified the faulty phase and faulty section within a period of one cycle after fault inception.

Chapter 6 Conclusions

6.1 Summary and Conclusions

6.1.1 Literature Review

Current protection arrangements in existing radial distribution networks that are based on a conventional overcurrent protection approach and three phase auto-reclosing scheme are becoming incompatible with the presence of DGs. Substantial research work has been carried out to find potential solutions for various DG protection issues. Examples include the application of an adaptive distance protection scheme to improve the transient performance of DGs during fault condition in cable distribution network. Another example involving the application of an ANN technique to detect LOM condition particularly where the DGs is islanded with a load of similar capacity, has been proposed.

The following issues have been indentified from continuous literature survey:

a. Current protection solutions that consider maintaining operation of DGs during fault condition are limited. In most proposed solutions, where the DGs are connected downstream of a feeder, protective devices need to ensure the disconnection of DGs before the 1st reclose action of the recloser takes place, to prevent islanding operation and disruption of the operation of conventional three phase auto reclosing schemes. Only a few research works that deal with solving the problem of maintaining the continued operation of DGs have been reported. Examples of such include the implementation of a zone protection scheme and an intensive communication medium in a distribution network with DGs to ensure continued operation of the DGs during fault conditions as far as possible.

b. With efficient DG placement and effective new adaption in both network voltage control and network protection, there is a possibility that future

distribution networks can be operated in ring, rather than radial mode, to increase the penetration of DGs. Although, general protection issues in ring operated networks have been addressed in the literature, further comprehensive research work is needed to identify the factors which influence the transient stability of DGs in a ring network. This is necessary to determine the new protection requirements needed to ensure continued operation of DGs during fault conditions in both radial and ring network modes of operation.

c. The adoption of a dynamic model of the DG is essential to thoroughly understand the transient response of DGs during network fault condition which in turn would help in facilitating the development of a potential protection solution for a particular protection issue due to grid connected DGs. However, the appropriate dynamic model of DGs, particularly FSIG and DFIG, which are the two popular types of DG, technologies in wind power generation, has not been considered in most of the research work has been conducted to investigate network protection issues related to DGs.

d. It has been recognised that 80% of faults which occur in existing distribution networks are temporary, and most of them are SLG. This should give a strong incentive to find ways for maintaining DGs in service during temporary SLG faults as far as possible, which would benefit utilities, DG developers and customers. It appears from the literature review that no research work has been carried out to investigate fault identification and phase selection algorithm in existing overhead distribution networks that takes into consideration the operation of DGs during fault conditions.

Thus, the work conducted in this research project has been focused on investigation of the following three topics in order to address the issues that have been identified above:

a. Investigation into the feeder protection requirements for continued operation of DGs in ring overhead distribution networks with DGs.

b. Investigation into the requirements of a new auto-reclosing scheme by assessing the sustainability of FSIG and DFIG during temporary SLG faults and observing the performance of both types of induction generator during recloser opening time.

c. Investigation into the development of fault identification and phase selection algorithms to be used in a novel SPAR scheme, specifically suitable to a distribution network with DGs.

The adoption of an appropriate dynamic model of both DFIG and FSIG based on wind power generation has been used in the investigations listed above.

6.1.2 Investigation into Factors affecting Transient Stability of DGs during Fault Condition in Distribution Network with Ring Operating Mode.

The literature review carried out in this research project shows that future distribution networks will be operated in ring operation mode, compared to radial, to increase the installation capacity of DGs. Thus, an investigation is presented in chapter 3 to indentify the generator's CCT for the FSIG and consequently the factors that affect the transient stability of integrated FSIG in a ring feeder in MV overhead distribution network during fault condition. The investigation is intended to identify the requirements for feeder protection in a ring network with DGs to ensure proper coordination between protective devices in a ring feeder, so that the fault clearing time does not exceed the generators' CCT, and operation of DGs can be continued after the faulted line section has been detected and isolated.

In this investigation, the investigated system is assumed to be configured in radial operation mode and then switches to ring operation mode. The considered FSIG is located at a feeder different from the faulty feeder. The following has been concluded from the simulation results obtained in this study:

a. Transient stability of DG is improved in ring compared to radial network operation. Thus, different relay time tripping setting are required to preserve the operation of DG that is located at an adjacent healthy feeder during fault condition in a ring network, compared to a radial network.

b. Other than that, it is reported in this investigation that longer tripping time can be allowed to maintain the stability of DGs if the faulty feeder is protected with zone protection scheme compared to a conventional time-graded overcurrent scheme. Under a zone protection scheme the faulty feeder is divided into several sections by installing additional protective devices. In such an arrangement the internal fault occurring within a particular section is isolated from the investigated system. In contrast, under a time graded overcurrent protection scheme, the whole faulty feeder is isolated from the investigated network, regardless of the fault location at the feeder.

c. Finally, simulation results revealed that an optimised generator location and tripping sequence of protective devices need to be taken into consideration when developing a novel protection in a ring network with DGs to maintain continued operation of DG at healthy feeders during fault conditions.

6.1.3 Investigation into the Sustainability of FSIG and DFIG during Temporary SLG fault

The literature survey shows that 80% of network faults occurring in overhead distribution networks are temporary and most of them are SLG fault. It is becoming increasingly important that DGs should remain in service during temporary SLG fault events as far possible for the benefits of customers, power utilities and DG

developers. Thus, investigation into the sustainability of both FSIG and DFIG during temporary SLG in MV overhead distribution networks has been presented in Chapter 3. The investigation is intended to determine the requirements for a new auto-reclosing scheme in a distribution network with DGs to ensure the continued operation of DGs during SLG fault condition. The following conclusions have been reached with respect to the sustainability of FSIG and DFIG during temporary SLG faults.

6.1.3.1 Comparison between Transient Performance of FSIG and DFIG in Radial and Ring Operated Distribution Network

a. The literature survey shows that it is important to adopt an appropriate dynamic model of DGs in research work related to DG protection issues in existing distribution networks. Thus, detailed dynamic models of both grid-connected FSIG and DFIG that are suitable for fault analysis have been used to compare and examine the transient performance of FSIG and DFIG in a network with radial and ring operating modes.

b. The simulation results revealed that for a fault event located at the DG feeder, the overall transient performance of both DFIG and FSIG is considerably improved in ring network compared to radial network operation. Moreover, longer fault clearance time can be allowed while maintaining the transient stability of both DFIG and FSIG in a ring network compared to a radial network.

c. In addition to that, DFIG has a better transient performance following a three-phase-to-ground fault, compared to FSIG in both radial and ring operated networks. The operation of DGs should be maintained in fault conditions to maximise the benefits of the DGs interconnection. In this context, operating FSIG in a radial network has been found as the worst case scenario in deciding the tripping time setting of the circuit breakers.

6.1.3.2 Effect of Unsymmetrical SLG Fault Event on the Transient Stability of DG and Operation of G59 Protection

a. The sustainability of both FSIG and DFIG during temporary single-phase-to-ground fault condition, while complying with the under/over voltage protection requirements of G59 have been determined in this investigation.

b. The simulation results revealed that SLG fault are not critical compared to symmetrical three-phase-to-ground faults. Both FSIG and DFIG remain stable during SLG fault conditions, although the voltage dip during fault conditions drops below the undervoltage limits specified in G59. Thus, if the operation of DG during fault conditions is permitted in the future, then the current voltage limits of under/over voltage protection specified in G59 needs to be justified.

c. Additionally, the action of the control scheme installed on the DFIG can improve the transient performance of DFIG compared to FSIG during the post fault period.

6.1.3.3 Impact of Operation of SPAR on the Transient Performance of DGs

a. The following two aspects related to the impact of the operation of SPAR on the transient performance of DG have been assessed in this investigation :

- Effect of recloser opening time (T_o) on dynamic behaviour of DG
- Effect of recloser opening time (T_o) on transient stability of DG

b. The effect of recloser opening time (T_o) on dynamic behaviour of FSIG is more significant compared to DFIG, particularly when the investigated system is operated in radial operating mode e.g., the terminal voltage of FSIG drops significantly during the recloser opening time when T_o settings of high speed reclosing attempts are increased from 0.5s to 2.0s.

c. The effect of recloser opening time (T_o) on the transient stability of DGs is determined by assessing the main machine parameters of DG which include generator terminal voltage, active power and rotor speed. If these parameters regain their prefault values during recloser opening time, after isolating the fault, the generator will be considered as stable, otherwise it is unstable.

d. The simulation results revealed that DFIG is more robust compared to FSIG. With the action of the control scheme installed at DFIG, it remains stable under different T_o settings for high speed and time delayed reclosing attempts. T_o settings of high speed attempts that have been considered in this simulation are 0.5 s, 1.0s and 2.0 s. T_o settings of time delayed attempt that have been considered in this simulation are 10 s, 30 s and 60 s.

e. If DGs are permitted to operate in SLG fault conditions in the future, the type of DG technology and network operation mode needs to be taken into consideration when deciding the recloser opening time. For instance, in the radial network with grid connected FSIG, if the faulty section is located far from the generator, a longer T_o setting can be applied.

6.1.4 Investigation into the Development of Adaptive Rule-based Fault Identification and Phase Selection Algorithm for Maintaining Continued Operation of DGs during Fault Condition

The development of an adaptive rule-based fault identification and phase selection algorithm to be used in SPAR scheme for a distribution network with DG has been presented in Chapters 4 and 5.

In Chapter 4, a comprehensive simulation analysis has been presented to demonstrate how types of SLG faults occurring in overhead 11 kV distribution networks with DFIG can be indentified and then isolated from the network with the proposed rule-based fault identification and phase selection algorithm. The SLG fault is assumed to occur at the DG feeder where the feeder is protected with a zone protection scheme incorporated with SPAR. Under the zone protection scheme with SPAR, only the faulty phase within the faulty section is isolated from the network to ensure the operation of the DG at the same feeder can continue in SLG fault conditions. The proposed fault identification strategy is based on the analysis of the phase angle between line currents, and the ratio of sequence components of the line currents that obtained from the relay point before fault condition and during the transient period that follows the fault condition.

The simulation results indicate that the proposed rule-based fault identification and phase selection algorithm can successfully identify the type of SLG fault, only using three line current measurements at the relay point. The type of SLG fault has been indentified within one cycle after fault inception. The fault detection speed depends on the criterions being used to construct the rule-based fault identification algorithm. The high speed of fault detection capability of the proposed technique can facilitate the operation of a high speed phase selector. Additionally, high speed fault detection is also one of the main requirements to maintain the transient stability of grid connected DGs.

A total of 2592 fault cases have been simulated using PSCAD/EMTDC transient analysis software packages to reproduce the possible SLG fault events assumed in a practical overhead MV distribution network with varying system operating and fault conditions. Consequently, a more effective manner is needed to analysis the fault data, so that the unique characteristics of each considered SLG fault case can be found and eventually the fault type of each fault case can be indentified correctly. In this context, several software programmes have been specifically developed using C++ to handle the process of data saving and analysing in order to effectively manage the large volume of collected fault data and extract the useful information required for the development of the proposed rule-based fault identification and phase selection algorithm.

The overall process of digital data processing, that includes fault data analysis and fault data optimisation, followed by the process of rule-based fault identification and phase selection algorithm construction and finally the verification process, have been presented in Chapter 5. The aim of the fault data analysis process is to determine common parameters of interest, e.g., max and min values, and to identify the features of each fault case. A total of 38 elements that represent the features of each fault case have been indentified. These elements are stored in a vector **X** where **X** = $\{x_1, x_2, \ldots, x_i, \ldots, x_m\}$, i = 1, 2, 3,…, m. x_i is the i^{th} element in vector **X** and m = 38. They are selected from a total of 275 data points which constitute the total collected data points within a window for a particular fault case. The aim of the fault data optimization process is to determine the minimum number of elements of vector **X** that is sufficient to distinguish each fault case from the others in the total of 2592

fault cases. Application of optimization process has resulted in an optimized vector $\mathbf{X_{optimise}}$ with 26 elements such that $\mathbf{X_{optimise}} = \{x_1, x_2, \ldots, x_k, \ldots, x_n\}$, k =1, 2, 3,…, n. x_k is the k^{th} element and n = 26. The input data used to develop the rule-based fault identification algorithm consists of the elements of $\mathbf{X_{optimise}}$. A phase selection algorithm is developed to further classify each of the fault cases that have been successfully indentified into 9 fault categories that reflect the information of fault section and fault phase corresponding to that fault case. The output result of the phase selection algorithm is used as an output tripping signal for the phase selector module that contains the proposed rule-based fault identification and phase selection algorithm.

Verification of the proposed rule-based fault identification and phase selection algorithm was achieved by feeding each fault case into the test module that contains developed rule-based fault identification and phase selection algorithm for testing the ability of the algorithms to correctly identify the considered fault case and fault category. In this context, a graphical user interface (GUI) of the test module has been developed using Delphi software, for easy access to the verification process.

The simulation test results from the verification process revealed that the proposed adaptive rule-based fault identification algorithm has successfully indentified each of the considered SLG fault cases. Additionally, it has been proved that the proposed rule-based fault identification and phase selection algorithms are effective over a wide range of network scenarios. It was also found that, the fault detection time varies with the fault cases. The speed of fault detection time is subjected to the criterions being used to construct the rule-based fault identification algorithm. Finally, the proposed phase selection algorithm has also successfully indentified the faulty phase and faulty section within a period of one cycle after fault inception.

6.2 Contribution to Knowledge

1. Appropriate dynamic models of FSIG and DFIG that are suitable for use in fault analysis have been adopted in all investigations carried out in this research project.

2. The factors affecting generator's CCT in a ring operated 11kV overhead distribution network with FSIG have been determined.

3. Transient response of both FSIG and DFIG in radial and ring operated 11kV overhead distribution networks have been investigated.

4. The effect of unsymmetrical SLG fault events on (i) the transient stability of both FSIG and DFIG and (ii) the under/over voltage limits specified in G59 protection have been determined.

5. The effect of recloser opening time (T_o) on the transient response of both FSIG and DFIG has been determined.

6. A proposal was made for the implementation of SPAR, incorporated with a zone protection scheme, to an existing MV overhead distribution network with DG, to ensure continued operation of DG during SLG faults.

7. Development of adaptive rule-based fault identification and phase selection algorithm to be used in SPAR stated in (6), for the SLG fault detection and isolation.

8. Development of several software modules in C++ to efficiently handle the process of data analysis followed by algorithm development and verification tests.

9. Development of a verification test panel with a GUI using Delphi for easy access to the verification process.

6.3 Future Work

The work presented in this research project can be further developed to enhance the final research output results if sufficient time is allowed to accomplish the work involved for further development as listed below:

6.3.1 Further Development on the Proposed Method to Indentify All Types of Fault Events

There are two aspects in relation to the objective of developing the proposed rule-based fault identification algorithm and phase selection technique. The first aspects is related to identifying the type of SLG fault event and faulty section within the DG feeder in the investigated network to ensure the correct isolation of the faulty phase, within the faulty section, from the network, so that the operation of DG can be continued during an SLG fault. The second aspect is related to identifying other types of fault event including DLG, LL and three phase symmetrical faults to ensure the tripping of all three phases of a faulty section when one of these fault types is indentified. Due to insufficient research time, only the first aspect of the main objective has been achieved and the verification test results show that the proposed method is very accurate. The second aspect of main objective is left to be accomplished subsequently, if the research project is to be continued.

The proposed method is essentially dependent on the analysis of the phase difference between the fault currents and the magnitude of the sequence component of the fault current at the fundamental frequency. According to the comprehensive analysis presented in Chapter 4, DLG, LL and three phase symmetrical fault types can be distinguished, based on the same principle that has been used in the proposed method. The process of fault data analysis presented in chapter 5 needs to be adapted to accommodate the large volume of the fault data that takes into consideration DLG, LL and three phase symmetrical fault cases.

6.3.2 Analysis to Distinguish between Fault Event and Other Network Transient Event

Network transient events such as load switching activities, will produce transient currents which are similar to fault events. For instance, in a distribution network, most of the industrial loads are squirrel cage induction motor and the transient current due to the starting of the squirrel cage induction motor is 8 to 10 times the full load current, which is similar to a fault event .

The proposed method basically dependents on the analysis of the significant variation of the phase angle between fault currents within the first cycle after fault inception, rather than the magnitude of the fault current (see Chapter 4 section 4.3.4). The variation of phase angle between line currents during the first cycle after starting of a motor may not be significantly different compared to those found in the first cycle after fault inception and needs to be checked. Thus, an analysis could be carried out to compare the variation of phase angle between line currents due to fault events and those due to the starting up of a squirrel cage motor in order to ensure that the proposed method can distinguish between these two network transient events.

6.3.3 Modification to the Existing Model of 11kV Overhead Distribution Network with DG Used in the Proposed Method

Several assumptions have been made in modelling the investigated 11kV overhead distribution network with DG used in the development of the proposed method. The following modifications could be made to improve the reliability of the output results of the proposed method.

a. As reported in Chapter 3 section 3.2.6, an assumption has been made in modelling the distribution line. In the absence of detailed information about the zero sequence impedance, Z_0 the ratio of $Z_0 / Z_1 = 2$ as suggested in the literature [84] has been adopted in the development of the proposed method. Due to the fact that Z_0 is important in determining unsymmetrical fault currents, the generated fault cases would be more reliable if real data for Z_0 is used compared to the assumed one. Thus, it is worth carrying out analysis to

compare the existing fault data, based on the assumed value of Z_0, with those based on its real value.

b. Only one type of system earthing arrangement has been considered in the proposed method, which is the solid neutral earthing arrangement. As reported in Chapter 2 section 2.3, it is one of the common earthing systems being used in 11kV distribution networks in the UK. The other earthing system arrangement in 11 kV distribution networks is an impedance neutral earthing system arrangement. The proposed method essentially depends on the phase difference between fault currents and the magnitude of the sequence components of the fault currents at the fundamental frequency. Thus, the magnitude of these sequence components would be varying. Thus, it is worth carrying out analysis to compare existing fault data with those obtained from an investigated network with an impedance neutral earthing system arrangement.

c. Inclusion of different types of DG model into the investigated network, such as wind turbine driven induction generator and synchronous generators. According to the literature review, different DG technologies have their own unique operational characteristic, which will affect their transient response during network faults. Thus, it is worth carrying out analysis to compare the existing fault data with those obtained from investigated networks with the wind power generator based on fixed speed induction machines and synchronous machines.

6.3.4 Development of Proposed Method Based on Fault Data Obtained from Real-World Overhead Distribution Network

The development of the proposed method is based on the simulation data. In order to check the reliability of the proposed method into a real-world power distribution network, an investigation into the development of the proposed method based on fault data obtained from a real-world power distribution network with DG could be carried out.

References

[1] E. Lakervi & E. J. Holmes, Electricity Distribution Network Design, 2nd ed., The Institution of Electrical Engineer, 1995.

[2] J.A.K. Douglas, N.J.L. Randles, D. Magee and H.D. Bailie, "Ranking of Design Criteria to Improvement Rural Network Perfomance", *IEE 2nd International Conference on the Reliability of Transmission and Distribution Equipment*, pp 145-150, March 1995.

[3] The Electricity Association, Power System Protection Vol. 3: Application, The Institution of Electrical Engineer, 1995.

[4] C. Ennis, R. Clarke and J.S. Stewart, "Automation of Overhead Line Distribution Systems", *4th International Conference on Trends in Distirbution Switchgear*, pp 90-94, November 1994.

[5] M. L. Hammond, A. J. Bower and T. Wade, "The Practical Implementation of 11kV Rural Distribution Automation Pilot Scheme", *IEE 6th International Conference on Development in Power System Protection*, vol.1, pp 247-250, March 1997.

[6] S. K. Salman, "Impact of Embedded Generation on Voltage Regulation and Losses of Distribution Networks". IEE Colloquium on the Impact of Embedded Generation on Distribution Network''. pp 2/1-2/5., Oct 1996

[7] Nick Jenkin, Ron Allan, Peter Crossley, Daniel Kirschen and Goran Strbac, Embedded Generation, The Institution of Electrical Engineer, 2000.

[8] Philip P. Barker and Robert W. De Mello, "Determining the Impact of Distributed Generation on Power Systems: Part1-Radial Distribution systems", *IEEE/PES 2000 Summer Meeting*, vol. 3, pp1645-4656, 2000.

[9] C.L. Masters, "Voltage Rise: the Big Issue when Connecting Embedded Generation to Long 11kV Overhead Lines", IEE *Power Engineering Journal*, vol.16, issue 1, pp5-12, February 2002.

[10] V. H. M. Quezada, J. R. Abbad, T.G.S. Roman, "Assessment of Energy Distribution Losses for Increasing Penetration of Distributed Generation", *IEEE Trans. on Power Systems*, vol.21, no.2, pp 533-540, May 2006.

[11] R.A. Walling R. Saint, R.C. Dugan, J. Burke, L.A. Kojovic, " Summary of Distributed Resources Impact on Power Delivery Systems", *IEEE Trans. Power Delivery*, vol.23, no.3, pp 1636 -1644, July 2008.

[12] R.C Dugan and T.E. McDermott, "Distributed Generation", *IEEE Industry Application Magazine*, pp 1077-2618, March/April 2002.

[13] M.T. Doyle, "Reviewing the Impacts of Distributed Generation on Distribution System Protection", *Proc*. *IEEE/PES 2002 Summer Meeting*, vol.1, pp 103-105, July 2002.

[14] S. M, Brahma, and A. A. Girgis, "Microprocessor Based Reclosing to Coordinate Fuse and Recloser in a System with High Penetration of Distributed Generation", *Proc. IEEE/PES 2002 Winter Meeting*, vol. 1, pp 453-458, 2002.

[15] K.J. Maki, S. Repo and P. Jarventausta, "Effect of Wind Power Based Distributed Generation on Protection of Distribution Network", *IEE 8th International Conference on Development in Power System Protection*, vol.1, pp 324-330, April 2004.

[16] L.K. Kumpulaineni, K.T. Kauhaniemi, Pekka Verho and Olavi Vahamaki, " New Requirements for System Protection caused by Distributed Generation", *CIRED 18th International Conference on Electricity Distribution*, June 2005
[17] L. K. Kumpulainen and K. T. Kauhaniemi, "Aspects of the Effects of Distributed Generation in Single-Line-to-Earth faults", *Proc. 2005 International Conference on Future Power Systems*, pp603-608, Nov. 2005.
[18] K.J. Maki, S. Repo and P. Jarventausta, "Impact of Distributed Generation on Earth Fault Protection in Distribution Network with Isolated Neutral", *CIRED 19th International Conference on Electricity Distribution*, May 2007.
[19] A. Dysko, G.M. Burt, S. Galloway, C. Booth and J.R. McDonald, "UK Distribution System Protection Issues", *IEE Proc. -Gener. Transm. Distrib*., vol.1, no. 4, pp 679-687, January 2007.
[20] Stefania Conti, "Analysis of Distirbution Network Protection Issues in Presence of Dispersed Generation", *Electric Power System Research*, vol.79, pp 49-56, 2009.
[21] W.Rojewski, Z.A. Styczynski and J.Izykowski, "Selected Problems of Protected Relaying for Distribution Network with Distributed Generation", *Proc. IEEE/PES 2009 General Meeting*, pp 1-6, July 2009.
[22] G.Chen, D.Jiang , Z.Lu and Z.Wu, "New proposal for Solid State Fault Current Limiter and Its Control Strategies", in *Proc. IEEE/PES 2004 General Meeting* vol.2, pp.1468-1473. June 2004
[23] S. M. Blair, N. K. Singh, C. D. Booth and G. M. Burt, "Operational Control and Protection Implications of Fault Current Limitation in Distribution Networks", *Proc. 44th International University Power Engineering Conference*, 2009, pp 1-5, Sept 2009.
[24] Z. Q. Bo, X.Z.Dong and B.R.J.Caunce, "Accelerated Protection of Distribution Systems with Tapped Off Loads", *IEE Proc.-Gener. Transm. Distrib.*, vol. 151, no 4, pp461-468, July 2004.
[25] H.Y. Li, P.A.Crossley and N.Jenkins, "Transient Directional Protection for Distribution Feeders with Embedded Generations," in *Proc. 14th Power System Computation Conference*, Session 03, Paper no.5, June 2002.
[26] I. Chilvers and P.A.Crossley, "Distance Relaying of 11kV Circuits to Increase the Installed Capacity of Distributed Generation", *IEE Proc. -Gener. Transm. Distrib*., vol.152, no. 1, pp40-46, January 2005.
[27] S. K. Salman and I. M. Rida, "Investigating the Impact of Embedded Generation on Relay Setting of Utilities' Electrical Feeders," *IEEE Trans on Power Delivery*, vol.16, no.2, pp 246-251, April 2001.
[28] S.M.Braham and A.A.Girgis, "Development of Adaptive Protection Scheme for Distribution Systems with High Penetration of Distributed Generation", IEEE *IEEE Trans. Power Delivery*, vol.19, No.1,pp56-63, January 2004.
[29] S. A. M. Javadian, and M.-R. Haghifam, "A Fault Location and Protection Scheme for Distribution Systems in Presence of DG Using MLP Neural Networks", *Proc. IEEE/PES 2009 General Meeting*, pp 1-8, July 2009.
[30] G.Celli, Fabrizio Pilo and Francesco Pilo, "An innovative transient-based protection scheme for MV distribution networks with distribution generation", *IEE 9th International Conference on Development in Power System Protection*, pp 285-290, March 2008.
[31] D.J.King "New Methods for the Protection of Embedded Generations against the Loss of Utility Network", PhD thesis, 1999, The Robert Gordon University.

[32] Ecconnet, Assessment of Islanded Operation of Distribution Networks and Measures for Protection, ETSU K/EL/00235/REP,2001
[33] Sami Repo, Ari Nikander, Hannu Laaksonen and Pertti Jarventausta, "A Method to Increase the Integration Capacity of Distributed Generation on Weak Distribution Networks", *CIRED 17th International Conference on Electricity Distribution*, 2003.
[34] G. Celli, F. Pilo, G. Pisano, V. Allegranza, R. Cicoria and A. Iaria, "Meshed vs Radial MV Distribution Network in Presence of Large Amount of DG," *Proc. IEEE PES Power Systems Conference& Exposition*, vol. 2,pp709–714, 2004.
[35] E.J. Coster, J.M.A. Myrzik, and W.L. Kling, "Transient Stability of Distributed Generation in MV-Ring Networks", *Proc. IEEE/PES 2008 Transmission& Distribution Conference and Exposition*, pp 1-7, Apr. 2008.
[36] K.J. Maki, S. Repo and P. Jarventausta, "Protection Issues Related to Distributed Generation in a Distribution Network Using Ring Operation Mode", *2004 Nordic Wind Power Conference*, Goterborg Sweden, March 2004.
[37] G. Celli, F. Pilo, G. Pisano, V. Allegranza and R. Cicoria, "Distribution Network Interconnecting for Facilitating the Diffusion of Distributed Generation", *CIRED 18th International Conference on Electricity Distribution*, 2005.
[38] World Wind Energy Association, "World Wind Energy Report 2009", June 2010, Turkey.
[39] European Wind Energy Assocation, "Wind Force 12", May 2004, Belgium.
[40] T.Burton, D.Sharpe, N.Jenkins, E.Bossanye, Wind Energy Hanbook, John Wiley &Sons, 2001.
[41] S.Muller, M.Deicke and R.W. De Doncker, " Doubly Fed Induction Generator Systems for Wind Turbines", *IEEE Industry Applications Magazine*, pp 26-33, May/June 2002
[42] Z.Lubosony, Wind Turbine Operation in Electric Power Systems, Springer Verlag, 2004.
[43] M.Godoy Simoes, F.A.Farret, Renewable Energy Systems: Design and Analysis with Induction Generators, London:CRC Press, 2004.
[44] T. Ackermann, Wind Power in Power Systems, Chochester: John Wiley 2005.
[45] L.Holadworth, X.G. Wu, J.B. Ekanayake and N.Jenkins, "Comparion of Fixed Speed and Doubly Fed Induction Wind Turbines during Power System Disturbance", *IEE Proc. Gener. Transm. Distrib.*, vol. 150, no.3, May 2003.
[46] Electricity Association, Recommendations for the Connection of Embedded Generation Plant to Public Electricity Suppliers' Distribution Systems, Engineering Recommendation G.59/1, 1991, London.
[47] GEC Measurement, Protective Relaying Application Guide, GEC, Alsthom Measurement Limited, 1987.
[48] IEEE Committee Report, Single Phase Tripping and Auto Reclosing of Transmission Lines, *IEEE Trans. Power Delivery*, vol.7, no.1, pp 182 -192, 1992.
[49] F. Calero and D.Hou, "Pratical Considerations for Single-Pole-Trip Line-Protection Schemes", *Proc IEEE 2006 Power Systems Conference: Advanced Metering, Protection, Control, Communication and Distributed Resource*, pp 299-315, March 2006.
[50] IEEE Std C37.104-2002 IEEE Guide for Automatic Reclosing of Line Circuit Breakers for AC Distribution and Transmission Lines, IEEE, 2003.

[51] M.A. Figueroa and E. Orduna, "Application of Single Pole Auto Reclosing in Medium Voltage Distribution Networks for Improving of Distributed Generation.", *Proc. IEEE/PES 2006 Transmission& Distribution Conference and Exposition: Latin America*, pp 1-6, Aug. 2006.
[52] Z.Q.Bo, R.K. Aggarwal, A.T. Johns, H.Y.Li and Y.H. Song, "A New Approach to Phase Selection Using Fault Generated Frequency Noise and Neural Network", *IEEE Trans. Power Delivery*, vol. 12, no.1, Jan. 1997.
[53] Omar A. S. Youseff, "A Novel Fuzzy Logic based Phase Selection Technique for Power System Relaying" *Electric Power System Research*, vol.68, pp 175-184, 2004.
[54] L. Zou, P. Liu and Q. Zhao, "Mathematical Morphology Based Phase Selection Scheme in Digital Relaying", *IEE Proc. Gener. Transm. Distrib.*, vol. 152, no.2, March 2005
[55] W.H.Chen, C.W.Liu and M.S.Tai, "Online Fault Diagnosis of Distribution Substations using Hybrid cause Effect Network and Fuzzy Rule Based Method", *IEEE Trans. Power Delivery*, vol.15, no.2, pp710 -717, Apr. 2000.
[56] Biswarup Das, "Fuzzy Logic-based fault-type Identification in Unbalanced Radial Power Distribution System", *IEEE Trans. Power Delivery*, vol.21, no.1, Jan. 2006.
[57] P. Dondi, D. Bayoumi, C. Haederli, D. Julian and M. Suter," Network Integration of Distributed Power Generation", *Journal of Power Sources*, vol. 106, pp 1-9, April 2002.
[58] W. El-Khattam and M.M.A. Salama, "Distributed generations technologies, definitions and benefits", *Electric Power System Research*, vol.71, pp 119-128, 2004.
[59] T. Ackermann, G. Anderson and L. Soder, "Distributed generation: a definition", *Electric Power Systems Research*, vol. 57, pp 195- 204, 2001.
[60] G. Pepermans, J. Driesen, D. Haeseldonckx, R. Belmans and W. D'haeseleer, "Distributed Generation: Definition, Benefits and Issues", *Energy Policy*, vol. 33, issue 6, pp 787-798, April 2005.
[61] J.A. Pecas Lopes, N. Hatziagyriou, J. Mutale, P. Djapic and N. Jenkins, "Integrating distributed generation into electric power systems: A review of drivers, challenges and opportunities", *Electric Power System Research*, vol.77, pp 1189-1203, 2007.
[62] IEEE Std 142, "Recommended Practice for Grounding of Industrial and Commercial Systems", IEEE, 1991.
[63] E.ON Central Network Manual Section E2 Earthing Guidance Notes, Sept 2007.
[64] United Utilities: System Earthing and Fault Level, [Online]. Available from http://www.unitedutilities.co.uk/1644.htm [accessed 16 June 2010]
[65] P.M.Anderson, Power System Protection, Wiley-IEEE Press,1998.
[66] L. K. Kumpulainen and K. T. Kauhaniemi, "Analysis of The Impact of Distributed Generation on Automatic Reclosing", *Proc. IEEE/PES Power Systems Conference & Exposition* , vol. 1, pp 603-608, 2004.
[67] C.M.Affonso, W.Feitaas, W.Xu and L.C.P. da Silva, "Perfomance of ROCOF Relays for Embedded Generation Applications", *IEE Proc. -Gener. Transm. Distrib.*, vol.152, no. 1, pp 109-114, January 2007
[68] Ari Nikander Sami Repo and Pertti Jarventausta, "Utilizing the Ring Operation Model of Medium Voltage Distribution Feeders", *17th International Conference on Electricity Distribution*, CIRED, May 2003.

[69] S. K.Salman & Anita L.J.Teo, "Windmill Modelling Consideration and Factors Influencing the Stability of a Grid Connected Wind Power based Embedded Generator", *IEEE Transc. on power systems*, vol.18, no.2, pp 793-802, May 2003.
[70] Walmir Freitas, Jose C.M.Vieira, Andre Morelato, Luiz C.P. da Silva, Vivaldo F.da Costa and Flavio A.B.Lemos, "Comparative Analysis Between Synchronous and Induction Machines for Distrihbuted Generation Applications", *IEEE Trans. Power Delivery* vol. 21, no.1, pp 301-311, Feb. 2006.
[71] Noja Power, Medium Voltage Auto Recloser : OSM Auto Circuit Recloser,[Online]. Available from http://www.nojapower.com.au/product/recloser.htm [accessed 12 June 2010].
[72] Schneider, Pole Mounted Switch / Recloser, [Online]. Available from http://www.schneider-electric.co.uk/sites/uk/en/products-services/electrical-distribution/products-offer/medium-voltage-secondary-distribution-products/polemounted-switch-recloser/u-series-n-series-w-series.page [accessed 12 June 2010]
[73] Liuchen Chang, Chris Diduch and Pinggang Song, "Development of Standards for Interconnecting Distributed Generators with Electric Power Systems", *Proc. IEEE 36th Conference in Power Electronic Specialists*, pp 2501-2507, June 2005.
[74] IEEE, *Standard 1547, Standard for Interconnecting Distributed Resources with Electric Power Systems*, June 2003.
[75] Standards Australia™, *Australian Standard AS 4777.1 – 2005 Grid Connection of Energy Systems via Inverters, Part 1: Installation*, 2005.
[76] EMTDC User's Guide, Manitoba HVDC Research Centre inc., Feb. 2002.
[77] N. R. Watson, "Power Systems Electromagnetic Transient Simulation", The Institution of Electrical Engineer, 2003.
[78] J. Mahseredjian, V. Dinavahi, and J.A. Martinez, "Simulation Tools for Electromagnetic Transients in Power Systems: Overview and Challenges", *IEEE Trans. Power Delivery* vol. 24, no.3, pp 1657-1669,July. 2009.
[79] PSCAD v4.0.3 Manual, Manitoba HVDC Research Centre inc., Jan. 2004.
[80] T.Lun, J.Eek, S.Uski and A.Perdana, "Dynamic Fault Simulation of Wind Turbines Using Commercial Simulation Tools", Proc. Fifth International Workshop on Large-Scale Integration of Wind Power and Transmission Networks for Offshore Wind, Galsgow, UK, April 2005.
[81] B.Badrazdeh. "Investigation into the Integration of Doubly Fed Induction Generator (DFIG) based Wind Farms into Electrical Power Systems" PhD thesis, 2006, The Robert Gordon University.
[82] William D.Stevenson, Elements of Power System Analysis, 4th end., New York:McGraw-Hill , 1982.
[83] J.J. Grainger and W.D. Stevenson, Power System Analysis, New York: McGraw-Hill, 1994.
[84] Juan M. Gers and Edward J.Holmes, Protection of Electricity Distribution Networks, 2nd end., The Institution of Electrical Engineer, 2005.
[85] M.S.Sarma, Electric Machines, Steady-State Theory and Dynamic Performance, USA; West Publishing Company, 1985.
[86] P.Kundar, Power System Stability and Control. New York: Mc Graw Hill, 1994.
[87] M. Alshamali and B. Fox, "Unsymmetrical Faults and Their Potential for Nuisance Tripping of Embedded Generators", *IEE 7th International Conference on Development in Power System Protection*, vol.1, pp 238-241, August, 2001.

[88] HuiSheng Wang and W.W.L.Keerthiapala, "Fuzzy-Neuro to Fault Classification for Transmission Line Protection", *IEEE Transc. on power delivery*, vol.13, no.4,pp 1093-1104, Oct 1998.
[89] T.Adu, "An Accurate Fault Indentification Technique for Power System Monitoring Devices", *IEEE Transc. on power delivery*, vol.17, no.3, pp 684-690, Jul. 2002.
[90] J SChlabbach, Short Circuit, The Institution of Electrical Engineer, 2005.
[91] A.T.Johns and S.K.Salman, "Digital Protection for Power Systems", Peter Peregrinus Ltd, 1995.
[92] Home of GNU Fortan, [Online]. Available from http://gcc.gnu.org/fortran/C++Fortan [accessed 12 June 2010]
[93] Larry R. Nyhoff, Sanford Leestma, Fortran 90 for engineers and scientists, Prentice-Hall Inc, 1997.
[94] Intel Fortan Programmer Reference, [online] http://www.intel.com/software/products/compilers/techtopics/for_prg.htm [accessed 12 June 2010].
[95] Cplusplus.com, [online]. Available from http://www.cplusplus.com/ [accessed 12 June 2010].
[96] Nicolai M. Josuttis, The C++ Standard Library: A Tutorial and Reference, Addison-Wesley Professional, 1999.
[97] C++ Reference, [Online]. Available from http://www.cppreference.com/wiki/ [accessed 12 June 2010].
[98] Scott Meyers, Effective C++: 55 Specific Ways to Improve Your Programs and Designs Third Edition, Addison-Wesley Professional, 2005.
[99] Delphi Basics, [Online]. Available from http://www.delphibasics.co.uk/ [accessed 12 June 2010].
[100] Freebyte's Guide to free Delphi Programming, [Online]. Available from http://www.freebyte.com/programming/delphi/ [accessed 12 June 2010].
[101] Expects Exchange, Delphi Zone,[Online]. Available from http://www.experts-exchange.com/Programming/Languages/Pascal/Delphi/Delphi [accessed 12 June 2010].

Appendix A.1

System Data for 0.6MW Wind Power based FSIG [69]

1. Wind Turbine Mechanical System Parameters:
   Generator moment of inertia = 0.5s
   Turbine moment of inertia = 3.2s
   Generator damping coefficient = 0 p.u
   Turbine damping coefficient = 0 p.u
   Turbine-generator mutual damping coefficient = 0 p.u
   Shaft stiffness = 55 p.u

2. Induction Generator Parameters :
   Stator resistance = 0.0092p.u
   First cage resistance = 0.0082p.u
   Second cage resistance = 10p.u
   Stator leakage reactance = 0.0945p.u
   Magnetising reactance = 4.0958p.u
   Rotor mutual reactance = 0.113p.u
   Rated frequency = 50Hz
   Synchronous speed = 1500r.p.m
   Number of poles = 4

Note: The per unit data are given based on corresponding full load voltage and active power of 0.6 MW squirrel cage induction machine.

Appendix A.2

System Data for 2.0 MW Wind Power based FSIG and DFIG Generator [81]

1. Wind Turbine Mechanical System Parameters:
   Generator moment of inertia = 1.4s
   Turbine moment of inertia = 6s
   Generator damping coefficient = 0.02p.u
   Turbine damping coefficient = 0.02p.u
   Turbine-generator mutual damping coefficient = 4.5p.u
   Shaft stiffness = 100p.u

2. Induction Generator Parameters:
   Stator resistance = 0.0175p.u
   Rotor resistance = 0.019p.u
   Stator leakage reactance = 0.2571p.u
   Rotor leakage reactance = 0.295p.u
   Magnetizing reactance = 6.921p.u
   Stator to rotor turn ratio = 0.4333
   Rated frequency = 50Hz
   Synchronous speed = 1500r.p.m
   Number of poles = 4

Note: the per unit data are given based on corresponding full load values of voltage and active power of 2.0MW wound rotor induction machine.

Appendix B

Table 1: Data points of φI_a, φI_b and φI_c corresponding to the a-g fault in Figure 4.2

Table 1 below shows the phase angle of line current a, b and c, φI_a, φI_b and φI_c that obtained from relay R_{11} in the investigated system shown in Chapter 4 Figure 4.1. The parameters φAB, φBC and φCA are derived from φI_a, φI_b and φI_c using the three equations B.1 to B.3 shown below:

$$\varphi AB = \varphi I_a - \varphi I_b \quad \text{(B.1)}$$

$$\varphi BC = \varphi I_b - \varphi I_c \quad \text{(B.2)}$$

$$\varphi CA = \varphi I_c - \varphi I_a \quad \text{(B.3)}$$

Table 1

The value of φI_a, φI_b and φI_c prior and following a-g fault corresponding to figure 4.2 from t = 34.996 s to t = 35.016 s.

Time (s)	Phase angle of line current I_a, I_b, and I_c		
	φI_a (°)	φI_b (°)	φI_c (°)
34.9960	-14.0570	-136.1375	106.2083
34.9965	-13.8800	-136.0587	106.2158
34.9970	-13.7347	-136.0115	106.2225
34.9975	-13.6255	-135.9892	106.2232
34.9980	-13.5332	-135.9868	106.2036
34.9985	-13.5819	-135.9968	106.1484
34.9990	-13.6993	-136.0176	106.0726
34.9995	-13.6750	-136.0695	106.0184
35.0000	-13.4886	-136.1683	105.9866
35.0005	-13.1623	-136.3782	105.9304
35.0010	-13.0842	-136.4466	105.7062
35.0015	-13.2440	-136.3923	105.2618
35.0020	-13.7143	-136.2746	104.5883
35.0025	-14.5742	-136.1850	103.7096
35.0030	-16.4898	-136.5343	102.2418
35.0035	-18.5565	-137.1445	101.1142
35.0040	-21.1113	-137.8823	100.1614
35.0045	-24.0959	-138.7393	99.5523
35.0050	-27.5279	-139.8730	99.5430
35.0055	-32.8547	-141.8226	101.1301

35.0060	-37.3408	-143.5310	104.2045
35.0065	-42.1321	-145.3541	109.7348
35.0070	-47.0646	-147.1367	118.6236
35.0075	-52.1589	-148.8563	131.0095
35.0080	-59.1655	-150.8052	149.4766
35.0085	-64.5169	-151.6305	160.7965
35.0090	-69.8992	-151.2830	168.4584
35.0095	-75.2697	-148.5195	172.9555
35.0100	-80.5897	-140.3460	175.1830
35.0105	-87.5476	-108.7990	175.8776
35.0110	-92.6244	-73.8178	175.3688
35.0115	-97.5357	-53.8101	174.4064
35.0120	-102.2311	-45.9375	173.2555
35.0125	-106.6507	-43.4769	172.1166
35.0130	-111.9515	-43.8342	171.0030
35.0135	-115.3660	-45.3361	170.6912
35.0140	-118.2673	-47.3637	170.9106
35.0145	-120.6517	-49.6943	171.7237
35.0150	-122.4536	-52.0966	173.2437
35.0155	-123.9554	-55.1688	176.3442
35.0160	-124.5081	-57.2638	179.2832

Appendix C

Data Points of 2592 Fault Cases under Consideration

Appendix C is stored in the attached CD-ROM. Appendix C shows the data points of 2592 fault in txt.form. The values of the data points of the 2592 fault cases under consideration have been generated using PSCAD/EMTDC.

Appendix D

Elements of Vector X of 2592 Fault Cases under Consideration

Appendix D is stored in the attached CD-ROM. Appendix D shows the values of elements of vector **X** of 2592 fault cases that have been investigated in the fault data analysis process of section 5.2, Chapter 5.

Appendix E

Table 1: Data point of φAB, φBC , φCA, $R_{01}$and R_{21}corresponding to fault case: R22-Ri-HL5R0D-BG-7.5km

Table 1

Data point of φAB, φBC , φCA, $R_{01}$and R_{21}corresponding to fault case: R22-Ri-HL5R0D-BG-7.5km, from investigated time interval t = 34.9915 s to t = 35.0185 s

Time (s)	Phase angle difference between line current			Ratio of magnitude of sequence component of line current	
	$\varphi AB(^\circ)$	$\varphi BC(^\circ)$	$\varphi CA(^\circ)$	R_{01}	R_{21}
34.9915	123.3140	-242.0193	118.7053	0.0000	0.0009
34.9920	123.1413	-242.0090	118.8678	0.0000	0.0009
34.9925	122.9590	-241.9527	118.9937	0.0000	0.0009
34.9930	123.0985	-242.0334	118.9349	0.0000	0.0009
34.9935	123.1695	-242.0825	118.9129	0.0000	0.0009
34.9940	123.0578	-241.9435	118.8857	0.0000	0.0009
34.9945	122.9072	-241.7119	118.8046	0.0000	0.0009
34.9950	122.9027	-241.7103	118.8076	0.0000	0.0009
34.9955	122.9357	-241.9100	118.9743	0.0000	0.0009
34.9960	122.9338	-241.8922	118.9583	0.0000	0.0009
34.9965	122.9660	-241.7905	118.8245	0.0000	0.0009
34.9970	123.0049	-241.7136	118.7086	0.0000	0.0009
34.9975	123.0399	-241.6544	118.6145	0.0000	0.0009
34.9980	123.0699	-241.5841	118.5142	0.0000	0.0010
34.9985	122.7951	-241.4437	118.6486	0.0001	0.0012
34.9990	122.2632	-241.8024	119.5391	0.0021	0.0032
34.9995	122.1035	-243.3164	121.2129	0.0097	0.0083
35.0000	122.4668	-245.9976	123.5308	0.0259	0.0175
35.0005	123.8450	-251.1255	127.2805	0.0642	0.0367
35.0010	125.5766	-255.9939	130.4173	0.1055	0.0555
35.0015	127.9787	-261.3532	133.3745	0.1568	0.0782
35.0020	131.0631	-266.8470	135.7839	0.2165	0.1048
35.0025	134.7765	-272.2805	137.5040	0.2826	0.1335
35.0030	-219.0675	80.9110	138.1565	0.3769	0.1738
35.0035	-213.2407	76.2931	136.9477	0.4495	0.2055
35.0040	-206.1558	72.1417	134.0141	0.5215	0.2377
35.0045	-197.5448	68.5248	129.0201	0.5919	0.2697
35.0050	-187.3829	65.4481	121.9348	0.6588	0.3013
35.0055	-173.3479	61.9710	111.3769	0.7384	0.3425
35.0060	-164.2627	59.8185	104.4442	0.7877	0.3716
35.0065	-157.3010	58.1077	99.1933	0.8260	0.3979

35.0070	-152.9198	56.7472	96.1726	0.8524	0.4204
35.0075	-150.7511	55.6950	95.0561	0.8680	0.4391
35.0080	-151.1245	54.6995	96.4250	0.8753	0.4547
35.0085	-153.2127	54.2078	99.0049	0.8770	0.4598
35.0090	-156.2175	53.8540	102.3634	0.8824	0.4615
35.0095	-159.3926	53.4530	105.9396	0.8967	0.4642
35.0100	-162.0572	52.8325	109.2247	0.9231	0.4704
35.0105	-163.2757	51.5205	111.7552	0.9779	0.4858
35.0110	-160.1076	50.1693	109.9383	1.0315	0.5025
35.0115	-147.4849	48.6602	98.8247	1.0914	0.5233
35.0120	-110.8990	47.0770	63.8219	1.1539	0.5480
35.0125	-67.3936	45.3306	22.0630	1.2193	0.5739
35.0130	-46.3822	42.9378	3.4444	1.3093	0.6084
35.0135	-41.7975	41.2427	0.5548	1.3755	0.6344
35.0140	-40.2717	39.6772	0.5944	1.4386	0.6604
35.0145	-40.1406	38.2620	1.8786	1.4980	0.6861
35.0150	-40.8785	37.0489	3.8296	1.5546	0.7115
35.0155	-42.6920	35.7180	6.9740	1.6232	0.7452
35.0160	-44.3797	34.8823	9.4975	1.6666	0.7698
35.0165	-46.0346	34.1132	11.9214	1.7011	0.7926
35.0170	-47.4735	33.4105	14.0630	1.7254	0.8118
35.0175	-48.5325	32.8011	15.7314	1.7395	0.8261
35.0180	-48.9861	32.1821	16.8040	1.7439	0.8361
35.0185	-48.4359	31.4798	16.9561	1.7564	0.8403

Appendix F

Elements of Vector $\mathbf{X}_{optimise}$ of 2592 Fault Cases under Consideration

Appendix F is stored in the attached CD-ROM. Appendix F shows the values of elements x_k of vector $\mathbf{X}_{optimise}$ of 2592 fault cases that have been investigated in the optimisation process of section 5.3, Chapter 5.

Appendix G

Algorithm and Graphical User Interface (GUI) for Fault Data Analysis Process and Optimisation Process

Appendix G is stored in the attached CD-ROM. Appendix G shows the algorithm and graphical user interface (GUI) for fault data analysis process and optimisation process to extract elements of vector $\mathbf{X}$ and $\mathbf{X}_{optimise}$ of 2592 fault cases under consideration.

Appendix H

Algorithm for Rule-based Fault Identification and Phase Selection and Graphical User Interface (GUI) for Verification Test.

Appendix H is stored in the attached CD-ROM. Appendix H shows the completed rule-based fault identification and phase selection algorithm and verification test algorithm that have been developed in this research project. This is followed by the GUI test panel that was used to verify the performance of the rule-based fault identification and phase selection algorithms proposed in this research project. Note that in order for the reader to access the verification result, all fault cases under consideration have been loaded into the upper text window of the GUI test panel. The reader can access the verification test results corresponding to a particular fault

case by clicking on that file name shown in the upper text window, so that the output result corresponding to that fault case will be displayed in the bottom graphical window and bottom text window in the GUI test panel. The input signal corresponding to that fault case will be displayed in the top and middle graphical windows.

Appendix I

List of Publications:

Journal:

1. S.K.Salman and S.F.Tan, "Development of Adaptive Rule-based Fault Identification and Phase Selection technique for Maintaining Continued Operation of DGs", prepared, to be submitted to IEEE Trans. on Power Delivery.

Conferences:

1. S.K.Salman and S.F Tan, "Digital Processing and Testing on an Adaptive-based Protection Scheme for Maintaining Continued Operation of Distributed Generation", Accepted for publication to 45th Universities Power engineering Conference, Cardiff, UK, Sept 2010.

2. S.K.Salman and S.F Tan, "Adaptive Single Phase Fault Identification and Selection Technique for Maintaining Continued Operation of Distributed Generation", in *Proc. IEE 10th International Conference on Development in Power System Protection Conference*, P82, Manchester, UK, March 2010.

3. S.K.Salman and S.F Tan, "Application of Single Pole Auto Reclosing in Distribution Network with High Penetration of DGs", in *Proc. 44th Universities Power engineering Conference*, paper ID:141, Glasgow, UK, Sept 2009.

4. S.K.Salman and S.F.Tan, "Investigation into the Implementation of Auto Re-closing Scheme in Distribution Networks with High Penetration of DGs", in *Proc. 43th Universities Power engineering Conference*, pp1-5, Padova, Italy, Sept 2008.

5. S.K.Salman and S.F.Tan, "Comparative Study of Protection Requirements of Active Distribution Networks using Radial and Ring Operations", in *Proc. 2007 Power Tech*, pp 1182-1186, Lausanne, Switzerland, July 2007.

6. S.K.Salman and S.F.Tan, "Investigation into System Protection of Active Distribution Network with High Penetration of Embedded Generations in Both Ring and Radial Operation Mode", in *Proc. 41th Universities Power engineering Conference*, pp841-845, Newcastle, UK, Sept 2006.

7. S.K.Salman and S.F Tan, "Investigation into Development of Future Active Distribution Network", in *Proc. 40th Universities Power engineering Conference*, paper ID:408, Cork, Ireland, Sept 2005.